NASA Contractor Report 4343

Hypervelocity Impact Physics

William P. Schonberg, Alan J. Bean,
and Kent Darzi

CONTRACT NAS8-36955
JANUARY 1991

NASA Contractor Report 4343

Hypervelocity Impact Physics

Willam P. Schonberg, Alan J. Bean,
and Kent Darzi
University of Alabama-Huntsville
Huntsville, Alabama

Prepared for
George C. Marshall Space Flight Center
under Contract NAS8-36955

National Aeronautics and
Space Administration
Office of Management
Scientific and Technical
Information Division

1991

Acknowledgments

The authors are grateful for support from the NASA/Marshall Space Flight Center under contract NAS8-36955/D.O.16. The authors would like to acknowledge the assistance and guidance provided by the NASA/MSFC Technical Contracting Officers, Mr. Roy Taylor and Dr. Ann Whitaker, and are grateful for the assistance of Mr. Russ Lakin during the data acquisition phase of this investigation. The authors would like to express their appreciation to Mssrs. Hubert Smith and Joe Lambert of the NASA/Marshall Space Flight Center Laboratory Support Branch, Mssrs. Phillip Petty and Robert Stowell of the Martin Marietta Corporation, and Mssrs. Ben Ramsey and Earl Shirley of the Boeing Corporation for conducting the impact testing that made this investigation possible. Finally, the authors are also grateful to Mr. Sherman Avans and Ms. Jennifer Horn of NASA/MSFC for reviewing this document in the various stages of its preparation and for making helpful suggestions and comments regarding its content.

Notation

d .... projectile diameter

d_h .... equivalent single hole diameter of pressure wall plate holes

d_1, d_2, d_3 ... corrugated bumper repeating element distances

h .... corrugation height in corrugated bumper

t_i .... inner-pane thickness in glass windows system

t_m .... mid-pane thickness in glass window system

t_o .... outer-pane thickness in glass window system

t_s .... bumper plate thickness

t_w .... pressure wall plate thickness; Lexgard panel thickness

t_1, t_2, t_3 ... corrugated bumper panel thicknesses

A_d .... damage area on pressure wall plate when $\theta=0^o$; internal Lexgard panel damage area

A_{d1}, A_{d2} .... normal, in-line pressure wall plate damage areas

A_p .... presented area of impacting projectile

A_s .... rear-side pressure wall plate spall area

C .... material speed of sound

D .... circular hole diameter

D_{min} .... elliptical hole minor diameter

D_{max} .... elliptical hole major diameter

E .... material modulus of elasticity

E_1, E_2 ...... uni-directional ply tensile moduli

G_{12} .... uni-directional ply shear modulus

S .... stand-off distance between bumper plate and pressure wall plate

S_i .... stand-off distance between inner and middle panes in a triple-pane glass test specimen

S_o .... stand-off distance between middle and outer panes in a triple-pane glass test specimen

V .... initial impact velocity

α .... corrugation rise angle

ϵ_{avg} .... average prediction error of regression equations

γ, γ_n .... secondary debris cloud cone angle when $\theta=0^o$

γ_1, γ_2 ...... normal, in-line debris cloud cone angles

ν .... material Poisson's ratio

$\nu_{12,21}$ ..... uni-directional ply Poisson's ratios

ρ .... material mass density

σ .... standard deviation of average regression equation prediction errors

θ .... initial impact trajectory obliquity

θ_1, θ_2 ...... normal, in-line debris cloud trajectory

θ_n .... debris cloud trajectory when $\theta=0^o$

Table of Contents

SECTION EIGHT -- HYPERVELOCITY IMPACT RESPONSE OF MULTI-BUMPER SYSTEMS

SECTION NINE -- CONCLUSIONS AND RECOMMENDATIONS

SECTION ONE -- INTRODUCTION

1.1 Background Information

All large spacecraft are susceptible to impacts by meteoroids and pieces of orbiting space debris. These impacts occur at extremely high speeds and can damage flight-critical systems, which can in turn lead to catastrophic failure of the spacecraft. To date twenty-six impact craters have been found on Space Shuttle Orbiter windows [1.1]. Other impact craters have been found on the Shuttle's heat resistant tiles. A preliminary examination of the recently recovered LDEF satellite revealed hundreds of craters, pits, and holes. While it is not precisely known how many of these are due to orbital debris impacts and how many are due to meteoroid impacts, the susceptibility of earth-orbiting spacecraft to high-speed impacts is clearly evident. Naturally, the susceptibility of such spacecraft increases with increased mission duration. Therefore, the design of a spacecraft for a long-duration mission must take into account the possibility of such impacts and their effects on the spacecraft structure and on all of its exposed subsystem components.

In order to successfully design a spacecraft for a mission into the meteoroid and space debris environment, it is necessary to be able to characterize the response of a variety of structural materials under such high speed impact loadings. With the advent of many new high-strength composite and ceramic materials and their proliferation in aircraft applications, it has become necessary to evaluate their potential for use in long-duration space and aerospace structural systems. In addition, with the installation of windows for viewing and scientific purposes, the suitability of various window materials for use in long-duration spacecraft must be evaluated. One aspect of this evaluation is the analysis of their response to hypervelocity projectile impact loadings.

A spacecraft developed for a mission into the meteoroid and space debris environment must include adequate protection against penetration of habitable spacecraft components by such impacts. Traditional penetration-resistant wall design for long-duration spacecraft consists of a bumper plate that is placed at a small distance away from the main pressure wall of the compartment or module. This concept was first proposed by Whipple [1.2] and has been studied extensively in the last three decades as a means of reducing the penetration threat of hypervelocity projectiles [1.3-1.18]. Dual-wall configurations were repeatedly shown to provide significant increases in protection against penetration by small high-speed projectiles over equivalent single-wall structures. However, the recent proliferation of large pieces of orbiting space debris has made it necessary to modify such systems so that they can resist penetration by projectiles with much higher impact energies. Novel design concepts that will possess increased levels of protection must be developed for spacecraft that are to be launched into the meteoroid and space debris environment. Design concepts that can increase the protection afforded a long-duration spacecraft include corrugated bumpers and multiple-bumper systems.

It has become evident that meteoroids and pieces of orbital space debris are far from spherical in shape. The densities of the various kinds of meteoroids (icy, stony, iron) are also significantly different from the densities of the various kind of orbital debris that exist in near-earth orbit (plastic, metallic, etc.). Additionally, the speeds at which meteoroids will impact a spacecraft (upward of 30 km/sec) are significantly different from the impact velocities of pieces of orbital debris (10 to 12 km/sec). Thus, the wall of a spacecraft destined for the meteoroid and space debris environment must be versatile and must be able to resist penetration under a wide variety of impact conditions.

1.2 Program Objectives

The work performed under the contract consisted of applied research in the area of Environmental Effects with specific regard to the effects of the particulate space environment on the candidate materials, design configurations, and support mechanisms of long-term space flight vehicles. Research was performed in the area of hypervelocity impact physics to analyze the damage that occurs when a space vehicle is impacted by a micro-meteoroid or a space debris particle.

Specifically, an impact analysis of over 500 test specimens was performed to generate a Hypervelocity Impact Damage Database. The analysis included the characterization of the effects of oblique impacts as compared to normal impacts, the characterization of rear-side pressure wall spall potential, the characterization of the effects of secondary debris generation, the characterization of the effects of non-spherical particle impacts, and, where possible, the development of regression equations based on the test data to predict hypervelocity impact damage. The Hypervelocity Impact Damage Database developed as a result of the analyses performed during the course of this investigation consists of the following information:

1. Test number;
2. Bumper plate hole dimensions;
3. Pressure wall penetrated? spalled?

4. Equivalent pressure wall single hole diameter (if applicable);
5. Diameter of the three largest penetrated holes in the pressure wall plate (if applicable);
6. Depth of the three deepest craters on the pressure wall plate and corresponding surface diameters;
7. Total area of front-surface pressure wall plate damage;
8. Total area of rear-side pressure wall spall (if applicable);
9. Magnitudes of penetrating and ricochet debris cloud angles.

A complete print-out of the Hypervelocity Impact Damage Database can be found in the Appendix at the end of this report.

It is noted that the Hypervelocity Impact Damage Database developed in this study must be used in conjunction with the MSFC/Boeing Phase B Test Parameter Database. The MSFC/Boeing Database contains the material, geometric, and impact parameters for each test in the Hypervelocity Impact Damage Database. Specifically, the MSFC/Boeing Database contains the following parameter information:

1. Test number and date performed;
2. Particle velocity, diameter, material, and shape;
3. Angle of obliquity (impact angle);
4. Bumper plate material and thickness;
5. Pressure wall plate material and thickness;
6. Presence of MLI;
7. Stand-off distance.

This Final Report is divided into several sections. The next section, Section Two, gives an overview of hypervelocity impact testing that has been done at NASA/MSFC. Section Three discusses the phenomena associated with the hypervelocity impact of dual-wall structures. A comparison of the effects of hypervelocity impact on dual-wall structures made from different materials is discussed in Section Four. In Section Five, the response of spacecraft window materials to hypervelocity impact is considered. Section Six deals with the response of dual-wall systems with corrugated bumpers, while Section Seven considers the effects of projectile shape and materials on hypervelocity impact response. The response of multi-bumper systems is discussed in Section Eight. Conclusions and recommendations for future work are presented in Section Nine. Finally, the Appendix at the end of this report contains a discussion and a print-out of the Hypervelocity Impact Damage Database developed during the course of this investigation.

1.3 References

1.1 K. Edelstein, Orbiter Windshield Impact Testing and Analysis Meeting, NASA/Johnson Space Center, July 11, 1989.

1.2 F.L. Whipple, "Meteorites and Space Travel", Astonomical Journal, Vol. 52, p. 137 (1947).

1.3 R.F. Rolsten, H.H. Hunt, and J.N. Wellnitz, Study of Principles of Meteoroid Protection, General Dynamics, Report No. AE62-0413, Contract NAS8-875, April (1962).

1.4 C.J. Maiden, J.W. Gehring, and A.R. McMillan, Investigation of Fundamental Mechanism of Damage to Thin Targets by Hypervelocity Projectiles, General Motors Defense Research Laboratory, Report No. TR63-225, Santa Barbara, California, September (1963).

1.5 C.J. Maiden, A.R. McMillan, R.E. Sennett, and J.W. Gehring, Experimental Investigation of Simulated Meteoroid Damage to Various Spacecraft Structures, General Motors Defense Research Laboratory, Report No. TR65-48, Sanata Barabara, California, July (1965).

1.6 A.R. McMillan, Experimental Investigations of Simulated Meteoroid Damage to Various Spacecraft Structures, NASA CR-915, Washington, D.C., January (1965).

1.7 D.P. Hickey, An Experimental Study of High Velocity Impact at Normal and Oblique Incidence on Multiple Space 2024-T3 Aluminum Plates, Douglas Aircraft Company, Inc., Missile and Space Systems Division, Report No. SM-47873, Santa Monica, California, June (1965).

1.8 J.F. Lundeberg, P.H. Stern, and J.R. Bristow, Meteoroid Protection for Spacecraft Structures, NASA CR-54201, Washington, D.C., October (1965).

1.9 W.H. Friend, C.L. Murphy, and I. Shanfield, Review of Meteoroid-Bumper Interaction Studies at McGill University, NASA CR-54847, Washington, D.C., August (1966).

1.10 G.T. Burch, Multiplate Damage Study, Air Force Armament Laboratory, Report No. AFATL-TR-67-116, Eglin AFB, Florida, September (1967).

1.11 J.R. Powers, Structural Design for Meteoroid Protection, Brown Engineering Company, Report No. TD-C1-SAA-054, Contract NAS8-20073, March (1967).

1.12 D.W. Cornett, and W.H. Armstrong, Study of Structural-Thermal Insulation-Meteoroid Protection Integration, The Boeing Company, Aerospace Group, Report No. D5-17525, Contract NAS8-21430, May (1969).

1.13 A.P. Fraas, Protection of Spacecraft from Meteoroids and Orbital Debris, Oak Ridge National Laboratory, Report No. TM-9904, Knoxville, Tennessee, March (1986).

1.14 A.R. Coronado, M.N. Gibbins, M.A. Wright, and P.H. Stern, Space Station Integrated Wall Design and Penetration Damage Control, Boeing Aerospace Company, Report No. D180-30550-4, Final Report, Contract NAS8-36426, Seattle, Washington, May (1987).

1.15 E. Christiansen, Evaluation of Space Station Meteoroid/Debris Shielding Materials, Eagle Engineering, Report No.87-163, Contract NAS9-15800, September (1987).

1.16 E.D. Brewer, W.R. Hendrich, D.G. Thomas, and J.E. Smith, Effects of Oblique Impact on Hypervelocity Shield Performance, Oak Ridge National Laboratory, Report No. TM-11390, Knoxville, Tennessee, January (1990).

1.17 E.D. Brewer, W.R. Hendrich, D.G. Thomas, and J.E. Smith, Shield Design, Analysis, and Testing to Survice Stainless Steel Projectiles, Oak Ridge National Laboratory, Report No. TM-11381, Knoxville, Tennessee, January (1990).

1.18 E.D. Brewer, W.R. Hendrich, D.G. Thomas, and J.E. Smith, Shield Design, Analysis, and Testing Against a 3 km/sec Projectile, Oak Ridge National Laboratory, Report No. TM-11382, Knoxville, Tennessee, January (1990).

SECTION TWO -- AN OVERVIEW OF THE HYPERVELOCITY IMPACT TESTING AT THE NASA/MARSHALL SPACE FLIGHT CENTER

2.1 NASA/MSFC Hypervelocity Impact Testing

Hypervelocity impact testing began at the NASA/Marshall Space Flight Center in 1964 with the installation of a light gas gun in what is now known as the Materials and Processes Laboratory. The initial need and function of the facility was to provide a means of simulating meteoroid impacts on spacecraft and to provide the data required to determine the penetration probability of candidate spacecraft wall designs by such impacts. In the 1970's, the interest in testing for protection against meteoroid impacts declined. However, because of increased launch activity in recent years, a new threat to the safety of earth-orbiting spacecraft has arisen -- the threat of orbital debris impact.

Orbital debris impact testing began at NASA/MSFC in July, 1985 at the Space Debris Simulation Facility of the Materials and Processes Laboratory at the NASA/Marshall Space Flight Center. The facility consists of an instrumented two-stage light gas gun capable of launching 2.5 mm to 12.7 mm projectiles at velocities of 2 to 8 km/sec. Projectile velocity measurements are accomplished via pulsed X-ray, laser diode detectors, and a Hall photographic station. For a detailed description of the gun and its instrumentation, the reader is referred to Reference 2.1.

As of March 2, 1989, over 500 impact tests have been performed using the NASA/MSFC light gas gun. Testing has been focused primarily on multiple wall structures consisting of 'bumper', 'pressure wall', and 'witness' plates that were designed to simulate possible Space Station wall configurations. Projectiles of aluminum, steel, lexan, and cadmium ranging in diameter from 3.175 mm to 12.7 mm have been fired at velocities ranging from 2 to 8 km/sec. Test sample configurations have included single and multiple bumper specimens employing a variety of engineering materials, including aluminum, Kevlar, graphite/epoxy, cadmium, and alumina, of various thicknesses and spaced at various distances apart. Tests were performed with and without multi-layer insulation (MLI) within the spacing between the sacrificial bumper plates and the pressure wall plates in the test specimens. Hypervelocity impact testing of window materials, such as Lexgard and glass, and testing of simulated pressure bottles have also been performed. Although the majority of the testing has been performed normal to the plane of the test specimen, a significant number of oblique impact tests have been performed as well.

This Section contains a series of tables and charts that summarize the orbital debris impact testing performed at NASA/MSFC since 1985. The information contained in these tables and charts is based on the MSFC/Boeing Hypervelocity Impact Test Database dated March 2, 1989. This database contains a detailed summary of test parameters and results for 540 hypervelocity impact test firings. The parameters of the 540 test shots in the database are presented in Section 2.5.1. A review of the NASA/MSFC Database revealed that there were several errors in the values of certain impact and geometric parameters. These errors are summarized in Table 2.1. The summary tables and charts are presented in Sections 2.5.2 through 2.5.4 and are described in the following Section.

2.2 MSFC/Boeing Hypervelocity Impact Test Database Summaries

A general summary according to impact test and configuration parameters is presented in Section 2.5.2. The test shots are grouped in broad categories such as Impact Obliquity, Configuration, and Stand-off Distance. Examination of these tables reveals several interesting features about NASA/MSFC hypervelocity impact testing through March, 1989.

1) Very few shots have been fired above 7 km/sec. While this velocity is near the upper limit of the velocities attainable by the light gas gun, it is clear that more testing must be performed at these high velocities in order to be able to even come close to duplicating the anticipated on-orbit speeds of impact.

2) Only a few shots have been fired using very large projectiles. Although impacts by smaller pieces of orbital debris are more probable than impacts by excessively large pieces, the effects of large particle impact must be fully understood in order to decide whether or not such impacts can be withstood by existing or newly-developed protective measures.

3) Of the 540 test shots in the MSFC/Boeing database, approximately two-thirds were fired normal to the plane of the test specimen. With the increasing concern for the pollution of the orbital environment by the secondary ricochet debris particles that are formed in an oblique hypervelocity impact, additional oblique impact testing is necessary, especially in the high obliquity regime (ie. obliquities greater than 60^{o}), to fully understand the damage potential of these secondary debris particles.

4) Nearly three-quarters of previous impact testing has been performed on dual-wall (ie. single bumper) specimens with different kinds of aluminum as the bumper and pressure wall plate materials. With the recent development of many new high-strength materials, it is imperative that additional test-

ing be performed with bumper plates made from materials other than aluminum. Additionally, alternative configurations, such as double or triple bumpers at stand-off distances other than 4 inches, should be performed in combination with bumper plates made from these new materials. The results from these tests should aid in the selection of the materials and the geometric configuration for the final Space Station structural wall design.

5) With the desire to install windows for viewing as well as for scientific purposes in the Space Station Freedom, the need has arisen to conduct more hypervelocity impact testing of window materials. Although some preliminary testing of Lexgard and glass has been performed, more tests are needed in order to fully understand the response of a variety of window materials to hypervelocity impact loadings. This information can be used to determine the protection level required to ensure the safe operation of the windows that are installed in the Space Station Freedom.

6) Although a large number of tests have been performed with MLI between the bumper and pressure wall plate, there still exists an uncertainty as to whether or not the advantages of using MLI outweigh the disadvantages, from a hypervelocity impact response viewpoint. Additional tests must be performed to determine the effects of MLI under the full range of particle sizes and impact velocities.

7) All but thirteen of the tests listed in the MSFC/Boeing Database have been performed using spherical projectiles. While this has been done mainly for reasons of consistency and repeatability, it is clear that orbital debris particles are not round, but are rather jagged with varying length-to-diameter ratios. Additional testing must be performed using non-

spherical projectiles in order to be able to extrapolate the response of a structure under spherical projectile impact to a structure that is impacted by a non-spherical projectile.

Section 2.5.3 contains a series of charts that detail the distribution of the single bumper test shots. Only single bumper testing was considered in the development of these charts and tables because of the relative scarcity of multi-bumper testing and the increased number and complexity of test parameters that describe such test shots. The test and configuration parameters for the single bumper shots are defined on the first page of Section 2.5.3. Any deviations from these baseline parameters are signified with a footnote. A footnote legend is provided on the first page in Section 2.5.3.

The charts categorize the test shots according to the presence of MLI, the projectile diameter D, the impact velocity V, and the thickness of the bumper plate. The number in the upper right hand corner of these charts is a number that identifies the impact obliquity, velocity range, and spacing for the test shots in a particular chart. For example, the number 45V23S4 implies that the test shots in that chart were all fired at 45 degrees with velocities between 2 and 3 km/sec and that the target was a single bumper specimen with a stand-off distance of 4 inches. A series of tables that summarize the gaps in the hypervelocity impact testing of single bumper specimens is presented in Section 2.5.4 D based on the detailed charts in Section 2.5.3.

The information provided in these charts and tables is intended as a guide in the selection of impact parameters for future hypervelocity impact test firings. From Sections 2.5.3 and 2.5.4, it is evident that a large number of test shots are required to close the gaps in the existing test database. The suggestions made earlier in this section should serve to fill in a number of these gaps and greatly improve the practical applicability of the existing test database.

2.3 Summary and Conclusions

An extensive program of spacecraft materials testing and evaluation under hypervelocity projectile impact has been underway at the NASA/Marshall Space Flight Center since its inception over two decades ago. Recent efforts have focused on the evaluation of structural wall configurations for the Space Station Freedom. Although an extensive test database has been established, additional testing is still required to fully understand the phenomena associated with the hypervelocity impact response of the metallic and non-metallic materials that will be exposed to the meteoroid and space debris environment. Specifically, the following recommendations are made for inclusion in a future test program to address this need.

1) Perform additional testing at higher impact velocities.
2) Perform additional testing using larger projectiles.
3) Perform additional testing at higher impact obliquities.
4) Perform additional testing of alternate bumper plate materials and alternate wall configurations.
5) Perform additional testing of different types of glass.
6) Perform additional testing to determine the effects of MLI under the full range of particle sizes and impact velocities.
7) Perform additional tests using non-spherical projectiles.
8) Perform additional tests with different density projectiles.

9) Perform tests to determine the effects of internal pressure and wall curvature on module wall response.

10) Perform tests to define the conditions for pressure wall spallation without penetration.

The test data produced by such a test program will complement the existing test database and, together with the existing data, will serve to establish a new, more comprehensive, more versatile hypervelocity impact test database.

2.4 References

2.1 Taylor, R.A., "A Space Debris Simulation Facility for Spacecraft Materials Evaluation", SAMPE Quarterly, Vol. 18, No. 2, 1987, pp. 28-34.

Table 3.1 Corrections to MSFC/Boeing Hypervelocity Impact Test Database

Test No.	Parameter	Current Value	Correct Value
EH4B	MLI?	No	Yes
107 107A 107B	Back Wall Thickness	0.125 0.125 0.125	0.175 0.200 0.225
121-1	Velocity	6.82	6.04
144A 144B 144C	Back Wall Thickness	0.250 0.250 0.250	0.125 0.125 0.125
145A 145B 145C	Test Article Type	COMP-BMPR COMP-BMPR COMP-BMPR	CORR-BMPR CORR-BMPR CORR-BMPR
148A 148B 148C	BMPR 1 Material	6061-T6 6061-T6 6061-T6	CPR CPR CPR
158A	Impact Angle	65^o	0^o
163A 163B	BMPR 1 Standoff	4 4	7 7
163A 163B	BMPR 2 Standoff	1 1	4 4
167B	BMPR 1 Standoff	8	6
178A 178B	Test Article Type	COMP-BMPR	BOTTLE
190B	Test Article Type	SNGL-BMPR	TRPL-BMPR
190B	BMPR 1 Standoff	4	12
190B	BMPR 2 Material	N/A	6061-T6
190B	BMPR 2 Thickness	N/A	0.040

190B	BMPR 2 Standoff	N/A	8
190B	BMPR 3 Material	N/A	6061-T6
190B	BMPR 3 Material	N/A	0.040
190B	BMPR 3 Material	N/A	4
214A 214B 214C 214D	BMPR 1 Standoff	4 4 4 4	8 8 8 8
301	Back Wall Thickness	0.125	0.160
303A	Back Wall Thickness	0.125	0.160
P18-5	Projectile Diameter	0.150	0.125
P33B P33B1 P33C	MLI?	No	Yes
P34 P34B P34C P34C1 P34C2	Back Wall Thickness	0.125 0.125 0.125 0.125 0.125	0.100 0.100 0.100 0.100 0.100
P34 P34C P34C1	BMPR 1 Thickness	0.040 0.040 0.040	0.063 0.063 0.063
P35C	BMPR 1 Thickness	0.080	0.063

Section 2.5.1

MSFC/Boeing Hypervelocity Impact Test Database as of March 2, 1989

SPACE STATION METEOROID/DEBRIS TEST DATABASE

TEST NUMBER	DATA SOURCE	TEST DATE	TEST ARTICLE TYPE	BMPR 1 MATERIAL	BMPR 1 THICKNESS (IN.)	BMPR 1 STANDOFF (IN.)	BMPR 2 MATERIAL	BMPR 2 THICKNESS (IN.)	BMPR 2 STANDOFF (IN.)	BMPR 3 MATERIAL	BMPR 3 THICKNESS (IN.)	BMPR 3 STANDOFF (IN.)	MLI (Y/N)	BACK WALL MATERIAL	BACK WALL THICKNESS (IN.)	PROJECTILE MATERIAL	PROJECTILE DIAMETER (IN.)	PROJECTILE L/D RATIO	IMPACT ANGLE (DEG)	AVERAGE VELOCITY (KM/SEC)
PT-1	MSFC	10/20/86	SNGL-BMPR	2219-T87	0.125	36.00	N/A			N/A			NO	PLEXIGLAS	0.125	1100-AL	0.313		0.00	5.50
CD-132B	MSFC	08/13/86	SNGL-BMPR	CADMIUM	0.040	4.00	N/A			N/A			NO	2219-T87	0.125	CADMIUM	0.257		0.00	6.50
CD-132C	MSFC	08/14/86	SNGL-BMPR	CADMIUM	0.040	4.00	N/A			N/A			NO	2219-T87	0.125	CADMIUM	0.257		0.00	6.00
CD-133A	MSFC	08/15/86	SNGL-BMPR	CADMIUM	0.040	4.00	N/A			N/A			NO	2219-T87	0.125	CADMIUM	0.239		0.00	3.45
CD-133B	MSFC	08/15/86	SNGL-BMPR	CADMIUM	0.040	4.00	N/A			N/A			NO	2219-T87	0.125	CADMIUM	0.238		0.00	4.63
CD-133C	MSFC	08/18/86	SNGL-BMPR	CADMIUM	0.040	4.00	N/A			N/A			NO	2219-T87	0.125	CADMIUM	0.238		0.00	5.01
CD-134A	MSFC	08/19/86	SNGL-BMPR	CADMIUM	0.040	4.00	N/A			N/A			NO	2219-T87	0.125	CADMIUM	0.216		0.00	4.60
CD-134B	MSFC	08/20/86	SNGL-BMPR	CADMIUM	0.040	4.00	N/A			N/A			NO	2219-T87	0.125	CADMIUM	0.216		0.00	3.69
CD-134C	MSFC	08/21/86	SNGL-BMPR	CADMIUM	0.040	4.00	N/A			N/A			NO	2219-T87	0.125	CADMIUM	0.216		0.00	4.82
CD-134D	MSFC	08/21/86	SNGL-BMPR	CADMIUM	0.040	4.00	N/A			N/A			NO	2219-T87	0.125	CADMIUM	0.238		0.00	2.76
CD-1366	MSFC	08/12/86	SNGL-BMPR	CADMIUM	0.040	4.00	N/A			N/A			NO	2219-T87	0.125	CADMIUM	0.257		0.00	7.00
CS-141B	MSFC	10/07/86	SNGL-BMPR	6061-T6	0.063	7.00	N/A			N/A			NO	2219-T87	0.125	1100-AL	0.313		0.00	4.97
EH2-A	MSFC	08/05/87	SNGL-BMPR	6061-T6	0.063	4.00	N/A			N/A			YES	2219-T87	0.125	1100-AL	0.313		0.00	7.06
EH2-B	MSFC	08/14/87	SNGL-BMPR	6061-T6	0.063	4.00	N/A			N/A			YES	2219-T87	0.125	1100-AL	0.313		0.00	6.67
EH2-C	MSFC	08/25/87	SNGL-BMPR	6061-T6	0.063	4.00	N/A			N/A			YES	2219-T87	0.125	1100-AL	0.313		0.00	6.64
EH2-D	MSFC	08/26/87	SNGL-BMPR	6061-T6	0.063	4.00	N/A			N/A			YES	2219-T87	0.125	1100-AL	0.313		0.00	6.66
EH2-E	MSFC	08/27/87	SNGL-BMPR	6061-T6	0.063	4.00	N/A			N/A			YES	2219-T87	0.125	1100-AL	0.313		0.00	6.79
EH3-A	MSFC	09/21/87	SNGL-BMPR	6061-T6	0.063	4.00	N/A			N/A			NO	2219-T87	0.125	1100-AL	0.313		0.00	6.64
EH4-A	MSFC	12/01/87	SNGL-BMPR	6061-T6	0.063	4.00	N/A			N/A			YES	2219-T87	0.125	1100-AL	0.313		0.00	6.13
EH4-B	MSFC	12/11/87	SNGL-BMPR	6061-T6	0.063	4.00	N/A			N/A			NO	2219-T87	0.125	1100-AL	0.313		0.00	6.76
EHMP-1	MSFC	06/28/88	SNGL-BMPR	6061-T6	0.063	4.00	N/A			N/A			NO	5456	0.125	1100-AL	0.313		60.00	6.93
EHMP-2	MSFC	06/29/88	SNGL-BMPR	6061-T6	0.063	4.00	N/A			N/A			NO	5456	0.125	1100-AL	0.313		65.00	6.85
EHMP-3	MSFC	06/30/88	SNGL-BMPR	6061-T6	0.063	4.00	N/A			N/A			NO	5456	0.125	1100-AL	0.313		45.00	6.83
EHMP-4	MSFC	07/15/88	SNGL-BMPR	6061-T6	0.063	4.00	N/A			N/A			NO	5456	0.125	1100-AL	0.250		60.00	7.71
EHMP-5	MSFC	07/18/88	SNGL-BMPR	6061-T6	0.063	4.00	N/A			N/A			NO	5456	0.125	1100-AL	0.250		65.00	7.56
EHMP-6	MSFC	07/19/88	SNGL-BMPR	6061-T6	0.063	4.00	N/A			N/A			NO	5456	0.125	1100-AL	0.250		45.00	7.63
EHMP-7	MSFC	07/25/88	SNGL-BMPR	6061-T6	0.063	4.00	N/A			N/A			NO	2219-T87	0.125	1100-AL	0.187		60.00	8.04
EHMP-8	MSFC	07/28/88	SNGL-BMPR	6061-T6	0.063	4.00	N/A			N/A			NO	2219-T87	0.125	1100-AL	0.187		45.00	7.39
EHMP-9	MSFC	07/29/88	SNGL-BMPR	6061-T6	0.063	4.00	N/A			N/A			NO	2219-T87	0.125	1100-AL	0.187		65.00	7.34
EHSS-1A	MSFC	02/18/88	SNGL-BMPR	6061-T6	0.063	4.00	N/A			N/A			NO	5456	0.125	1100-AL	0.250		0.00	5.88
EHSS-1B	MSFC	02/22/88	SNGL-BMPR	6061-T6	0.063	4.00	N/A			N/A			NO	5456	0.125	1100-AL	0.250		0.00	6.02
EHSS-1C	MSFC	02/24/88	SNGL-BMPR	6061-T6	0.063	4.00	N/A			N/A			NO	5456	0.125	1100-AL	0.250		0.00	6.40
EHSS-2A	MSFC	03/02/88	SNGL-BMPR	6061-T6	0.063	4.00	N/A			N/A			NO	2219-T87	0.125	1100-AL	0.250		0.00	6.36
EHSS-2B	MSFC	03/04/88	SNGL-BMPR	6061-T6	0.063	4.00	N/A			N/A			NO	2219-T87	0.125	1100-AL	0.250		0.00	5.88
EHSS-3A	MSFC	03/17/88	SNGL-BMPR	6061-T6	0.063	4.00	N/A			N/A			NO	5456	0.125	1100-AL	0.250		30.00	6.79
EHSS-3B	MSFC	03/30/88	SNGL-BMPR	6061-T6	0.063	4.00	N/A			N/A			NO	5456	0.125	1100-AL	0.250		30.00	7.06
EHSS-3C	MSFC	04/15/88	SNGL-BMPR	6061-T6	0.063	4.00	N/A			N/A			NO	2219-T87	0.125	1100-AL	0.250		30.00	6.81
EHSS-4A	MSFC	04/01/88	SNGL-BMPR	6061-T6	0.063	4.00	N/A			N/A			NO	5456	0.125	1100-AL	0.250		45.00	6.78
EHSS-4B	MSFC	04/04/88	SNGL-BMPR	6061-T6	0.063	4.00	N/A			N/A			NO	5456	0.125	1100-AL	0.250		45.00	6.97
EHSS-4C	MSFC	07/14/88	SNGL-BMPR	6061-T6	0.063	4.00	N/A			N/A			NO	5456	0.125	1100-AL	0.250		45.00	5.58
EHSS-5A	MSFC	04/07/88	SNGL-BMPR	6061-T6	0.063	4.00	N/A			N/A			NO	5456	0.125	1100-AL	0.250		45.00	4.08
EHSS-5B	MSFC	04/12/88	SNGL-BMPR	6061-T6	0.063	4.00	N/A			N/A			NO	5456	0.125	1100-AL	0.250		25.00	4.95
EHSS-5C	MSFC	04/20/88	SNGL-BMPR	6061-T6	0.063	4.00	N/A			N/A			NO	5456	0.125	1100-AL	0.250		65.00	5.26
EHSS-5D	MSFC	04/23/88	SNGL-BMPR	6061-T6	0.063	4.00	N/A			N/A			NO	5456	0.125	1100-AL	0.250		65.00	4.28
EHSS-6A	MSFC	05/02/88	SNGL-BMPR	6061-T6	0.063	4.00	N/A			N/A			NO	5456	0.125	1100-AL	0.313		0.00	6.55
EHSS-6B	MSFC	05/09/88	SNGL-BMPR	6061-T6	0.063	4.00	N/A			N/A			NO	5456	0.125	1100-AL	0.313		0.00	6.63
EHSS-6C	MSFC	06/09/88	SNGL-BMPR	6061-T6	0.063	4.00	N/A			N/A			NO	2219-T87	0.125	1100-AL	0.313		0.00	6.64
EHSS-7A	MSFC	05/11/88	SNGL-BMPR	6061-T6	0.063	4.00	N/A			N/A			NO	5456	0.125	1100-AL	0.313		45.00	6.60
EHSS-7B	MSFC	05/17/88	SNGL-BMPR	6061-T6	0.063	4.00	N/A			N/A			NO	5456	0.125	1100-AL	0.313		45.00	7.03
EHSS-8A	MSFC	05/26/88	SNGL-BMPR	6061-T6	0.063	4.00	N/A			N/A			NO	5456	0.125	1100-AL	0.313		75.00	7.09
Gr-Al-1	MSFC	04/03/87	COMP-BMPR	Gr-Al	0.040	4.00	N/A			N/A			NO	Gr-Al	0.040	1100-AL	0.125		0.00	2.15
HDAC-9	MSFC	11/19/87	P-BOTTLE	N/A			N/A			N/A			NO	GR-EP	0.313	1100-AL	0.313		0.00	2.93

DATE: 02-Mar-89

SPACE STATION METEOROID/DEBRIS TEST DATABASE

TEST NUMBER	DATA SOURCE	TEST DATE	TEST ARTICLE TYPE	BMPR 1 MATERIAL	BMPR 1 THICKNESS (IN.)	BMPR 1 STANDOFF (IN.)	BMPR 2 MATERIAL	BMPR 2 THICKNESS (IN.)	BMPR 2 STANDOFF (IN.)	BMPR 3 MATERIAL	BMPR 3 THICKNESS (IN.)	BMPR 3 STANDOFF (IN.)	MLI (Y/N)	BACK WALL MATERIAL	BACK WALL THICKNESS (IN.)	PROJECTILE MATERIAL	PROJECTILE DIAMETER (IN.)	PROJECTILE L/D RATIO	IMPACT ANGLE (DEG)	AVERAGE VELOCITY (KM/SEC)
MDAC-10	MSFC	11/20/87	P-BOTTLE	N/A			N/A			N/A			NO	GR-EP	0.000	1100-AL	0.313		0.00	5.76
MDAC-11A	MSFC	11/17/87	P-BOTTLE	6061-T6	0.060	6.00	N/A			N/A			NO	GR-EP-AL	0.112	1100-AL	0.375		0.00	6.52
MDAC-11B	MSFC	11/18/87	P-BOTTLE	6061-T6	0.060	4.00	N/A			N/A			NO	GR-EP-AL	0.112	1100-AL	0.375		0.00	6.59
MDAC-11C	MSFC	11/18/87	P-BOTTLE	6061-T6	0.040	6.00	N/A			N/A			NO	GR-EP	0.000	1100-AL	0.375		0.00	6.58
MDAC-12	MSFC	11/24/87	P-BOTTLE	6061-T6	0.063	4.00	N/A			N/A			NO	GR-EP-PR	0.000	1100-AL	0.313		0.00	2.82
MD-TEST-A	MSFC	01/29/87	SNGL-BMPR	6061-T6	0.063	4.00	N/A			N/A			YES	2219-T87	0.125	1100-AL	0.187		0.00	2.15
MD-TEST-B	MSFC	01/29/87	SNGL-BMPR	6061-T6	0.063	4.00	N/A			N/A			YES	2219-T87	0.125	1100-AL	0.187		0.00	2.45
MD-TEST-D	MSFC	03/03/87	SNGL-BMPR	6061-T6	0.063	4.00	N/A			N/A			YES	2219-T87	0.125	1100-AL	0.313		0.00	5.63
PR-EH1	MSFC	05/20/87	SNGL-BMPR	2219-T87	0.063	4.00	N/A			N/A			YES	2219-T87	0.125	1100-AL	0.313		0.00	7.04
PR-EH2	MSFC	05/20/87	SNGL-BMPR	2219-T87	0.063	4.00	N/A			N/A			YES	2219-T87	0.125	1100-AL	0.313		0.00	6.92
SS-001A	MSFC	02/10/87	SNGL-BMPR	6061-T6	0.080	4.00	N/A			N/A			NO	2219-T87	0.125	1100-AL	0.313		45.00	6.62
SS-001B	MSFC	02/10/87	SNGL-BMPR	6061-T6	0.080	4.00	N/A			N/A			YES	2219-T87	0.125	1100-AL	0.313		45.00	6.53
SS-002A	MSFC	02/12/87	SNGL-BMPR	6061-T6	0.063	4.00	N/A			N/A			NO	2219-T87	0.125	1100-AL	0.313		45.00	6.50
SS-002B	MSFC	02/12/87	SNGL-BMPR	6061-T6	0.063	4.00	N/A			N/A			YES	2219-T87	0.125	1100-AL	0.313		45.00	6.45
SS-003A	MSFC	03/25/87	SNGL-BMPR	6061-T6	0.040	4.00	N/A			N/A			YES	2219-T87	0.125	1100-AL	0.313		45.00	6.54
SS-004A	MSFC	03/26/87	SNGL-BMPR	6061-T6	0.080	4.00	N/A			N/A			YES	2219-T87	0.125	1100-AL	0.313		65.00	6.28
SS-101	MARTIN	01/16/86	SNGL-BMPR	6061-T6	0.080	4.00	N/A			N/A			NO	2219-T87	0.125	1100-AL	0.187		0.00	3.09
SS-101A	MARTIN	01/17/86	SNGL-BMPR	6061-T6	0.080	4.00	N/A			N/A			NO	2219-T87	0.125	1100-AL	0.187		0.00	3.70
SS-101B	MARTIN	01/21/86	SNGL-BMPR	6061-T6	0.080	4.00	N/A			N/A			NO	2219-T87	0.125	1100-AL	0.187		0.00	4.27
SS-102	MARTIN	01/21/86	SNGL-BMPR	6061-T6	0.080	4.00	N/A			N/A			NO	2219-T87	0.125	1100-AL	0.300		0.00	7.20
SS-102A	MARTIN	01/22/86	SNGL-BMPR	6061-T6	0.080	4.00	N/A			N/A			YES	2219-T87	0.125	1100-AL	0.300		0.00	5.35
SS-102B	MARTIN	01/23/86	SNGL-BMPR	6061-T6	0.080	4.00	N/A			N/A			YES	2219-T87	0.125	1100-AL	0.300		0.00	5.96
SS-102C	MARTIN	01/23/86	SNGL-BMPR	6061-T6	0.080	4.00	N/A			N/A			YES	2219-T87	0.125	1100-AL	0.300		0.00	4.74
SS-102D	MARTIN	01/24/86	SNGL-BMPR	6061-T6	0.080	4.00	N/A			N/A			YES	2219-T87	0.125	1100-AL	0.300		0.00	3.83
SS-103	MARTIN	01/24/86	COMP-BMPR	KEVLAR	0.080	4.00	N/A			N/A			NO	2219-T87	0.125	1100-AL	0.187		0.00	4.62
SS-103A	MARTIN	01/28/86	COMP-BMPR	KEVLAR	0.150	4.00	N/A			N/A			NO	2219-T87	0.125	1100-AL	0.187		0.00	3.52
SS-103B	MARTIN	02/03/86	COMP-BMPR	KEVLAR	0.150	4.00	N/A			N/A			NO	2219-T87	0.125	1100-AL	0.187		0.00	3.43
SS-103C	MARTIN	02/04/86	COMP-BMPR	KEVLAR	0.150	4.00	N/A			N/A			NO	2219-T87	0.125	1100-AL	0.187		0.00	3.84
SS-103-1	MARTIN	01/27/86	COMP-BMPR	KEVLAR	0.150	4.00	N/A			N/A			NO	2219-T87	0.125	1100-AL	0.187		0.00	4.24
SS-104	MARTIN	02/04/86	COMP-BMPR	KEVLAR	0.150	4.00	N/A			N/A			NO	2219-T87	0.125	1100-AL	0.300		0.00	6.74
SS-104A	MARTIN	02/06/86	COMP-BMPR	KEVLAR	0.150	4.00	N/A			N/A			NO	2219-T87	0.125	1100-AL	0.300		0.00	6.65
SS-104B	MARTIN	03/05/86	COMP-BMPR	KEVLAR	0.150	4.00	N/A			N/A			NO	2219-T87	0.125	1100-AL	0.300		0.00	7.01
SS-105	MARTIN	02/06/86	SNGL-BMPR	6061-T6	0.080	4.00	N/A			N/A			NO	2219-T87	0.125	1100-AL	0.350		45.00	3.51
SS-105A	MARTIN	02/07/86	SNGL-BMPR	6061-T6	0.080	4.00	N/A			N/A			NO	2219-T87	0.125	1100-AL	0.350		60.00	4.05
SS-105B	MARTIN	02/11/86	SNGL-BMPR	6061-T6	0.080	4.00	N/A			N/A			NO	2219-T87	0.125	1100-AL	0.350		75.00	3.89
SS-106	MARTIN	02/21/86	SNGL-BMPR	6061-T6	0.080	4.00	N/A			N/A			NO	2219-T87	0.125	1100-AL	0.350		45.00	6.84
SS-106A	MARTIN	02/26/86	SNGL-BMPR	6061-T6	0.080	4.00	N/A			N/A			NO	2219-T87	0.125	1100-AL	0.375		60.00	6.66
SS-106B	MARTIN	02/27/86	SNGL-BMPR	6061-T6	0.080	4.00	N/A			N/A			NO	2219-T87	0.125	1100-AL	0.375		75.00	6.73
SS-106-1	MARTIN	02/24/86	SNGL-BMPR	6061-T6	0.080	4.00	N/A			N/A			NO	2219-T87	0.125	1100-AL	0.350		60.00	6.80
SS-106-2	MARTIN	02/25/86	SNGL-BMPR	6061-T6	0.080	4.00	N/A			N/A			NO	2219-T87	0.125	1100-AL	0.350		75.00	6.65
SS-107	MARTIN	02/19/86	SNGL-BMPR	6061-T6	0.080	4.00	N/A			N/A			NO	2219-T87	0.125	1100-AL	0.350		0.00	6.80
SS-107A	MARTIN	02/20/86	SNGL-BMPR	6061-T6	0.080	4.00	N/A			N/A			NO	2219-T87	0.125	1100-AL	0.350		0.00	6.74
SS-107B	MARTIN	02/20/86	SNGL-BMPR	6061-T6	0.080	4.00	N/A			N/A			NO	2219-T87	0.125	1100-AL	0.350		0.00	6.82
SS-108	MARTIN	02/18/86	SNGL-BMPR	6061-T6	0.080	12.00	N/A			N/A			NO	2219-T87	0.125	1100-AL	0.350		0.00	6.85
SS-109	MARTIN	01/14/86	SNGL-BMPR	6061-T6	0.080	4.00	N/A			N/A			NO	2219-T87	0.125	1100-AL	0.187		0.00	7.39
SS-109A	MARTIN	03/03/86	SNGL-BMPR	6061-T6	0.080	4.00	N/A			N/A			NO	2219-T87	0.125	1100-AL	0.187		0.00	4.06
SS-109B	MARTIN	03/03/86	SNGL-BMPR	6061-T6	0.080	4.00	N/A			N/A			NO	2219-T87	0.125	1100-AL	0.187		0.00	3.61
SS-109C	MARTIN	03/04/86	SNGL-BMPR	6061-T6	0.080	4.00	N/A			N/A			NO	2219-T87	0.125	1100-AL	0.187		0.00	2.56
SS-109D	MARTIN	03/04/86	SNGL-BMPR	6061-T6	0.080	4.00	N/A			N/A			NO	2219-T87	0.125	1100-AL	0.187		0.00	2.00
SS-110	MARTIN	02/12/86	SNGL-BMPR	6061-T6	0.080	4.00	N/A			N/A			NO	2219-T87	0.125	6061-T6	0.300		0.00	7.13
SS-113	MARTIN	03/10/86	SNGL-BMPR	6061-T6	0.063	4.00	N/A			N/A			NO	2219-T87	0.125	6061-T6	0.250		60.00	3.18
SS-113A	MARTIN	03/10/86	SNGL-BMPR	6061-T6	0.063	4.00	N/A			N/A			NO	2219-T87	0.125	6061-T6	0.250		45.00	3.20

ORIGINAL PAGE IS
OF POOR QUALITY

DATE: 02-Mar-89

SPACE STATION METEOROID/DEBRIS TEST DATABASE

TEST NUMBER	DATA SOURCE	TEST DATE	TEST ARTICLE TYPE	BMPR 1 MATERIAL	BMPR 1 THICKNESS (IN.)	BMPR 1 STANDOFF (IN.)	BMPR 2 MATERIAL	BMPR 2 THICKNESS (IN.)	BMPR 2 STANDOFF (IN.)	BMPR 3 MATERIAL	BMPR 3 THICKNESS (IN.)	BMPR 3 STANDOFF (IN.)	MLI (Y/N)	BACK WALL MATERIAL	BACK WALL THICKNESS (IN.)	PROJECTILE MATERIAL	PROJECTILE DIAMETER (IN.)	PROJECTILE L/D RATIO	IMPACT ANGLE (DEG)	AVERAGE VELOCITY (KM/SEC)
SS-114	MARTIN	03/11/86	SNGL-BMPR	6061-T6	0.063	4.00	N/A			N/A			NO	2219-T87	0.125	6061-T6	0.300		60.00	3.34
SS-114A	MARTIN	?????	SNGL-BMPR	6061-T6	0.063	4.00	N/A			N/A			NO	2219-T87	0.125	6061-T6	0.300		45.00	3.51
SS-114B	MARTIN	03/12/86	SNGL-BMPR	6061-T6	0.032	4.00	N/A			N/A			NO	2219-T87	0.125	1100-AL	0.300		45.00	3.51
SS-115-1	MARTIN	04/29/86	DBL-BMPR	6061-T6	0.032	4.00	6061-T6	0.032	3.00	N/A			NO	2219-T87	0.125	1100-AL	0.250		0.00	4.40
SS-115-2	MARTIN	04/30/86	DBL-BMPR	6061-T6	0.032	4.00	6061-T6	0.032	3.00	N/A			NO	2219-T87	0.125	1100-AL	0.250		0.00	4.06
SS-115-3	MARTIN	05/01/86	DBL-BMPR	6061-T6	0.032	4.00	6061-T6	0.032	3.00	N/A			NO	2219-T87	0.125	1100-AL	0.250		0.00	3.82
SS-116-1	MARTIN	05/14/86	DBL-BMPR	6061-T6	0.032	4.00	6061-T6	0.032	3.00	N/A			NO	2219-T87	0.125	1100-AL	0.187		0.00	3.01
SS-116-2	MARTIN	05/15/86	DBL-BMPR	6061-T6	0.032	4.00	6061-T6	0.032	3.00	N/A			NO	2219-T87	0.125	1100-AL	0.187		0.00	2.57
SS-117-1	MARTIN	05/02/86	DBL-BMPR	6061-T6	0.032	4.00	6061-T6	0.032	2.00	N/A			NO	2219-T87	0.125	1100-AL	0.250		0.00	4.09
SS-117-2	MARTIN	05/02/86	DBL-BMPR	6061-T6	0.032	4.00	6061-T6	0.032	2.00	N/A			NO	2219-T87	0.125	1100-AL	0.250		0.00	4.17
SS-118-1	MARTIN	05/05/86	DBL-BMPR	6061-T6	0.032	4.00	6061-T6	0.032	1.00	N/A			NO	2219-T87	0.125	1100-AL	0.250		0.00	4.40
SS-118-2	MARTIN	05/05/86	DBL-BMPR	6061-T6	0.032	4.00	6061-T6	0.032	1.00	N/A			NO	2219-T87	0.125	1100-AL	0.250		0.00	4.49
SS-118-3	MARTIN	05/06/86	DBL-BMPR	6061-T6	0.032	4.00	6061-T6	0.032	1.00	N/A			NO	2219-T87	0.125	1100-AL	0.250		0.00	4.52
SS-119-1	MARTIN	05/07/86	DBL-BMPR	6061-T6	0.032	4.00	6061-T6	0.032	1.00	N/A			NO	2219-T87	0.080	1100-AL	0.250		0.00	4.76
SS-119-2	MARTIN	05/08/86	DBL-BMPR	6061-T6	0.063	4.00	6061-T6	0.032	1.00	N/A			NO	2219-T87	0.080	1100-AL	0.250		0.00	5.32
SS-119-3	MARTIN	05/08/86	DBL-BMPR	6061-T6	0.032	4.00	6061-T6	0.032	1.00	N/A			NO	2219-T87	0.080	1100-AL	0.250		0.00	5.55
SS-120-1	MARTIN	05/12/86	COMP-BMPR	6061-T6	0.063	4.00	KEVLAR	0.080	1.00	N/A			NO	2219-T87	0.080	1100-AL	0.250		0.00	4.46
SS-120-2	MARTIN	05/13/86	COMP-BMPR	6061-T6	0.063	4.00	KEVLAR	0.080	1.00	N/A			NO	2219-T87	0.080	1100-AL	0.250		0.00	3.44
SS-120-3	MARTIN	05/14/86	COMP-BMPR	6061-T6	0.063	4.00	KEVLAR	0.080	1.00	N/A			NO	2219-T87	0.080	1100-AL	0.250		0.00	2.84
SS-121-1	MARTIN	05/21/86	SNGL-BMPR	6061-T6	0.080	6.00	N/A			N/A			NO	2219-T87	0.125	1100-AL	0.300		0.00	6.82
SS-121-2	MARTIN	05/22/86	SNGL-BMPR	6061-T6	0.080	6.00	N/A			N/A			NO	2219-T87	0.125	1100-AL	0.300		0.00	6.55
SS-122-1	MARTIN	05/28/86	COMP-BMPR	KEV49/EP	0.115	6.00	N/A			N/A			NO	2219-T87	0.125	1100-AL	0.300		0.00	7.15
SS-122-2	MARTIN	05/28/86	COMP-BMPR	KEV49/EP	0.115	6.00	N/A			N/A			NO	2219-T87	0.125	1100-AL	0.300		0.00	7.29
SS-123-1	MARTIN	05/30/86	WINDOW	N/A			N/A			N/A			NO	LEXIGARD	0.750	1100-AL	0.125		0.00	5.40
SS-123-2	MARTIN	06/02/86	WINDOW	N/A			N/A			N/A			NO	LEXIGARD	0.750	1100-AL	0.125		0.00	5.80
SS-123-3	MARTIN	06/02/86	WINDOW	N/A			N/A			N/A			NO	LEXIGARD	0.750	1100-AL	0.125		0.00	6.40
SS-124-1	MARTIN	06/03/86	WINDOW	N/A			N/A			N/A			NO	LEXIGARD	0.750	1100-AL	0.187		0.00	6.30
SS-124-2	MARTIN	06/04/86	WINDOW	N/A			N/A			N/A			NO	LEXIGARD	0.750	1100-AL	0.187		0.00	5.86
SS-124-3	MARTIN	06/06/86	WINDOW	N/A			N/A			N/A			NO	LEXIGARD	0.750	1100-AL	0.187		0.00	5.46
SS-124-4	MARTIN	06/10/86	WINDOW	N/A			N/A			N/A			NO	LEXIGARD	0.750	1100-AL	0.187		0.00	4.66
SS-125A	MARTIN	06/11/86	WINDOW	N/A			N/A			N/A			NO	LEXIGARD	0.750	1100-AL	0.250		0.00	5.27
SS-125B	MARTIN	06/11/86	WINDOW	N/A			N/A			N/A			NO	LEXIGARD	0.750	1100-AL	0.250		0.00	3.78
SS-125C	MARTIN	06/12/86	WINDOW	N/A			N/A			N/A			NO	LEXIGARD	0.750	1100-AL	0.250		0.00	3.23
SS-126A	MARTIN	06/18/86	WINDOW	N/A			N/A			N/A			NO	LEXIGARD	1.250	1100-AL	0.187		0.00	7.08
SS-126B	MARTIN	06/19/86	WINDOW	N/A			N/A			N/A			NO	LEXIGARD	1.250	1100-AL	0.187		0.00	7.47
SS-127A	MARTIN	06/20/86	WINDOW	N/A			N/A			N/A			NO	LEXIGARD	1.250	1100-AL	0.250		0.00	7.05
SS-127B	MARTIN	06/23/86	WINDOW	N/A			N/A			N/A			NO	LEXIGARD	1.250	1100-AL	0.250		0.00	7.46
SS-128A	MARTIN	06/27/86	DBL-BMPR	6061-T6	0.032	4.00	6061-T6	0.032	3.00	N/A			YES	2219-T87	0.125	1100-AL	0.250		0.00	4.10
SS-128B	MARTIN	06/30/86	DBL-BMPR	6061-T6	0.032	4.00	6061-T6	0.032	3.00	N/A			YES	2219-T87	0.125	1100-AL	0.250		0.00	3.53
SS-129A	MARTIN	07/03/86	WINDOW	N/A			N/A			N/A			NO	LEXIGARD	1.250	1100-AL	0.300		0.00	6.76
SS-129B	MARTIN	07/07/86	WINDOW	N/A			N/A			N/A			NO	LEXIGARD	1.250	1100-AL	0.300		0.00	6.39
SS-129C	MARTIN	07/07/86	WINDOW	N/A			N/A			N/A			NO	LEXIGARD	1.250	1100-AL	0.300		0.00	5.92
SS-130A	MARTIN	07/10/86	DBL-BMPR	6061-T6	0.032	4.00	6061-T6	0.032	3.00	N/A			NO	2219-T87	0.125	1100-AL	0.300		0.00	3.60
SS-130B	MARTIN	07/10/86	DBL-BMPR	6061-T6	0.032	4.00	6061-T6	0.032	3.00	N/A			NO	2219-T87	0.125	1100-AL	0.300		0.00	4.85
SS-130C	MARTIN	07/11/86	DBL-BMPR	6061-T6	0.032	4.00	6061-T6	0.032	3.00	N/A			NO	2219-T87	0.125	1100-AL	0.300		0.00	5.25
SS-131A	MARTIN	07/11/86	DBL-BMPR	6061-T6	0.063	4.00	6061-T6	0.032	1.00	N/A			NO	2219-T87	0.125	1100-AL	0.250		0.00	4.60
SS-131B	MARTIN	08/25/86	DBL-BMPR	6061-T6	0.063	4.00	6061-T6	0.032	1.00	N/A			NO	2219-T87	0.125	1100-AL	0.250		0.00	4.31
SS-131C	MARTIN	08/26/86	DBL-BMPR	6061-T6	0.063	4.00	6061-T6	0.032	1.00	N/A			NO	2219-T87	0.125	1100-AL	0.250		0.00	4.64
SS-135A	MARTIN	08/26/86	SNGL-BMPR	6061-T6	0.063	4.00	N/A			N/A			NO	2219-T87	0.125	1100-AL	0.250		30.00	5.95
SS-135B	MARTIN	08/27/86	SNGL-BMPR	6061-T6	0.063	4.00	N/A			N/A			NO	2219-T87	0.125	1100-AL	0.250		30.00	7.18
SS-135C	MARTIN	08/27/86	SNGL-BMPR	6061-T6	0.063	4.00	N/A			N/A			NO	2219-T87	0.125	1100-AL	0.250		30.00	6.67
SS-135D	MARTIN	08/28/86	SNGL-BMPR	6061-T6	0.063	4.00	N/A			N/A			NO	2219-T87	0.125	1100-AL	0.250		30.00	6.85

DATE: 02-Mar-89

SPACE STATION METEOROID/DEBRIS TEST DATABASE

TEST NUMBER	DATA SOURCE	TEST DATE	TEST ARTICLE TYPE	BMPR 1 MATERIAL	BMPR 1 THICKNESS (IN.)	BMPR 1 STANDOFF (IN.)	BMPR 2 MATERIAL	BMPR 2 THICKNESS (IN.)	BMPR 2 STANDOFF (IN.)	BMPR 3 MATERIAL	BMPR 3 THICKNESS (IN.)	BMPR 3 STANDOFF (IN.)	MLI (Y/N)	BACK WALL MATERIAL	BACK WALL THICKNESS (IN.)	PROJECTILE MATERIAL	PROJECTILE DIAMETER (IN.)	PROJECTILE L/D RATIO	IMPACT ANGLE (DEG)	AVERAGE VELOCITY (KM/SEC)
SS-135E	MARTIN	08/29/86	SNGL-BMPR	6061-T6	0.063	4.00	N/A			N/A			NO	2219-T87	0.125	1100-AL	0.250		30.00	7.21
SS-136A	MARTIN	08/29/86	SNGL-BMPR	6061-T6	0.063	4.00	N/A			N/A			NO	2219-T87	0.125	1100-AL	0.250		55.00	6.25
SS-136B	MARTIN	09/02/86	SNGL-BMPR	6061-T6	0.063	4.00	N/A			N/A			NO	2219-T87	0.125	1100-AL	0.250		55.00	7.24
SS-136C	MARTIN	09/02/86	SNGL-BMPR	6061-T6	0.063	4.00	N/A			N/A			NO	2219-T87	0.125	1100-AL	0.250		55.00	6.67
SS-137A	MSFC	09/09/86	DBL-BMPR	6061-T6	0.032	4.00	6061-T6	0.032	3.00	N/A			NO	2219-T87	0.125	1100-AL	0.250		45.00	4.86
SS-137B	MSFC	09/09/86	DBL-BMPR	6061-T6	0.032	4.00	6061-T6	0.032	3.00	N/A			NO	2219-T87	0.125	1100-AL	0.250		45.00	5.65
SS-137C	MSFC	09/10/86	DBL-BMPR	6061-T6	0.032	4.00	6061-T6	0.032	3.00	N/A			NO	2219-T87	0.125	1100-AL	0.250		45.00	6.16
SS-137D	MSFC	02/09/87	DBL-BMPR	6061-T6	0.032	4.00	6061-T6	0.032	3.00	N/A			NO	2219-T87	0.125	1100-AL	0.250		45.00	7.03
SS-138A	MSFC	09/12/86	DBL-BMPR	6061-T6	0.032	4.00	6061-T6	0.032	3.00	N/A			NO	2219-T87	0.125	1100-AL	0.250		45.00	6.52
SS-138B	MSFC	09/15/86	DBL-BMPR	6061-T6	0.032	4.00	6061-T6	0.032	3.00	N/A			NO	2219-T87	0.125	1100-AL	0.300		45.00	7.15
SS-139A	MSFC	09/24/86	SNGL-BMPR	2219-T87	0.125	4.00	N/A			N/A			NO	2219-T87	0.125	1100-AL	0.300		0.00	5.04
SS-139B	MSFC	09/24/86	SNGL-BMPR	2219-T87	0.125	4.00	N/A			N/A			NO	2219-T87	0.125	1100-AL	0.250		0.00	4.43
SS-140A	MSFC	10/01/86	COMP-BMPR	AL203	0.075	4.00	AL203	0.075	?????	AL203	0.075	?????	NO	2219-T87	0.125	1100-AL	0.250		0.00	6.26
SS-140B	MSFC	10/01/86	COMP-BMPR	AL203	0.075	4.00	AL203	0.075	?????	AL203	0.075	?????	NO	2219-T87	0.125	1100-AL	0.250		0.00	7.13
SS-140C	MSFC	10/02/86	COMP-BMPR	AL203	0.075	4.00	AL203	0.075	?????	AL203	0.075	?????	NO	2219-T87	0.125	1100-AL	0.250		0.00	6.82
SS-141A	MSFC	10/06/86	DBL-BMPR	6061-T6	0.063	7.00	6061-T6	0.063	1.00	N/A			NO	2219-T87	0.125	1100-AL	0.250		0.00	5.43
SS-141B	MSFC	10/07/86	DBL-BMPR	6061-T6	0.063	7.00	6061-T6	0.063	1.00	N/A			NO	2219-T87	0.125	1100-AL	0.313		0.00	4.29
SS-141C	MSFC	10/07/86	DBL-BMPR	6061-T6	0.063	7.00	6061-T6	0.063	1.00	N/A			NO	2219-T87	0.125	1100-AL	0.313		0.00	4.93
SS-141D	MSFC	10/08/86	DBL-BMPR	6061-T6	0.063	7.00	6061-T6	0.063	1.00	N/A			NO	2219-T87	0.125	1100-AL	0.313		0.00	6.33
SS-142A	MSFC	10/09/86	SNGL-BMPR	2219-T87	0.125	8.00	N/A			N/A			NO	2219-T87	0.125	1100-AL	0.313		0.00	3.40
SS-143A	MSFC	10/10/86	SNGL-BMPR	2219-T87	0.125	8.00	N/A			N/A			NO	2219-T87	0.250	1100-AL	0.250		0.00	3.84
SS-143B	MSFC	10/10/86	SNGL-BMPR	2219-T87	0.125	8.00	N/A			N/A			NO	2219-T87	0.250	1100-AL	0.313		0.00	2.85
SS-144A	MSFC	10/22/86	SNGL-BMPR	2219-T87	0.125	4.00	N/A			N/A			NO	2219-T87	0.250	1100-AL	0.313		0.00	4.93
SS-144B	MSFC	10/23/86	SNGL-BMPR	2219-T87	0.125	4.00	N/A			N/A			NO	2219-T87	0.250	1100-AL	0.250		0.00	4.52
SS-144C	MSFC	10/23/86	SNGL-BMPR	2219-T87	0.125	4.00	N/A			N/A			NO	2219-T87	0.250	1100-AL	0.250		0.00	3.97
SS-145A	MSFC	11/03/86	COMP-BMPR	2024-T3	0.750	4.00	•			•			NO	2219-T87	0.250	1100-AL	0.250		0.00	5.47
SS-145B	MSFC	11/03/86	COMP-BMPR	2024-T3	0.750	4.00	•			•			NO	2219-T87	0.250	1100-AL	0.250		0.00	4.38
SS-145C	MSFC	11/04/86	COMP-BMPR	2024-T3	0.750	4.00	•			•			NO	2219-T87	0.250	1100-AL	0.250		0.00	3.79
SS-146A	MSFC	11/07/86	SNGL-BMPR	6061-T6	0.063	4.00	N/A			N/A			NO	2219-T87	0.250	1100-AL	0.250		0.00	5.95
SS-146B	MSFC	11/07/86	SNGL-BMPR	6061-T6	0.063	4.00	N/A			N/A			NO	2219-T87	0.125	STEEL	0.125		0.00	7.75
SS-147A	MSFC	12/16/86	COMP-BMPR	CPR400	1.000	0.00	N/A			N/A			NO	2219-T87	0.125	STEEL	0.125		0.00	5.53
SS-147B	MSFC	12/17/86	COMP-BMPR	CPR400	1.000	0.00	N/A			N/A			NO	2219-T87	0.125	1100-AL	0.125		0.00	3.38
SS-147C	MSFC	12/18/86	COMP-BMPR	CPR400	1.000	0.00	N/A			N/A			NO	2219-T87	0.125	1100-AL	0.125		0.00	6.95
SS-148A	MSFC	12/22/86	SNGL-BMPR	6061-T6	0.063	4.00	N/A			N/A			NO	2219-T87	0.125	1100-AL	0.125		0.00	5.74
SS-148B	MSFC	01/05/87	SNGL-BMPR	6061-T6	0.063	4.00	N/A			N/A			NO	2219-T87	0.125	1100-AL	0.250		0.00	4.59
SS-148C	MSFC	01/06/87	SNGL-BMPR	6061-T6	0.063	4.00	N/A			N/A			NO	2219-T87	0.125	1100-AL	0.250		0.00	3.63
SS-149A	MSFC	01/07/87	COMP-BMPR	CPR400	1.000	0.00	N/A			N/A			NO	2219-T87	0.125	1100-AL	0.250		0.00	5.15
SS-149B	MSFC	01/07/87	COMP-BMPR	CPR400	1.000	0.00	N/A			N/A			NO	2219-T87	0.125	1100-AL	0.125		45.00	5.60
SS-149C	MSFC	01/08/87	COMP-BMPR	CPR400	1.000	0.00	N/A			N/A			NO	2219-T87	0.125	1100-AL	0.125		45.00	6.65
SS-150A	MSFC	01/27/87	SNGL-BMPR	6061-T6	0.063	4.00	N/A			N/A			NO	2219-T87	0.125	1100-AL	0.125		45.00	7.00
SS-151A	MSFC	02/09/87	SNGL-BMPR	6061-T6	0.080	4.00	N/A			N/A			NO	2219-T87	0.125	1100-AL	0.250		45.00	6.68
SS-152A	MSFC	02/13/87	DBL-BMPR	6061-T6	0.040	4.00	6061-T6	0.020	2.00	N/A			NO	2219-T87	0.125	1100-AL	0.250		45.00	4.62
SS-152B	MSFC	02/17/87	DBL-BMPR	6061-T6	0.040	4.00	6061-T6	0.020	2.00	N/A			NO	2219-T87	0.125	1100-AL	0.250		0.00	3.63
SS-153A	MSFC	03/31/87	DBL-BMPR	6061-T6	0.080	4.00	6061-T6	0.063	0.00	N/A			NO	2219-T87	0.125	1100-AL	0.250		0.00	5.58
SS-153B	MSFC	04/01/87	DBL-BMPR	6061-T6	0.080	4.00	6061-T6	0.063	0.00	N/A			NO	2219-T87	0.125	1100-AL	0.375		0.00	6.92
SS-154A	MSFC	04/02/87	SNGL-BMPR	6061-T6	0.040	4.00	N/A			N/A			NO	2219-T87	0.125	1100-AL	0.350		0.00	6.83
SS-154B	MSFC	04/02/87	SNGL-BMPR	6061-T6	0.040	4.00	N/A			N/A			NO	2219-T87	0.125	1100-AL	0.187		45.00	5.95
SS-155A	MSFC	04/09/87	SNGL-BMPR	6061-T6	0.063	4.00	N/A			N/A			NO	2219-T87	0.125	1100-AL	0.187		45.00	7.02
SS-156A	MSFC	04/15/87	SNGL-BMPR	6061-T6	0.063	4.00	N/A			N/A			NO	2219-T87	0.125	1100-AL	0.187		45.00	7.10
SS-156B	MSFC	04/15/87	SNGL-BMPR	6061-T6	0.063	4.00	N/A			N/A			NO	2219-T87	0.125	1100-AL	0.187		65.00	5.95
SS-156C	MSFC	04/16/87	SNGL-BMPR	6061-T6	0.063	4.00	N/A			N/A			NO	2219-T87	0.125	1100-AL	0.187		65.00	4.15
SS-157A	MSFC	04/16/87	SNGL-BMPR	6061-T6	0.063	4.00	N/A			N/A			NO	2219-T87	0.125	1100-AL	0.187		50.00	7.40

SPACE STATION METEOROID/DEBRIS TEST DATABASE

TEST NUMBER	DATA SOURCE	TEST DATE	TEST ARTICLE TYPE	BMPR 1 MATERIAL	BMPR 1 THICKNESS (IN.)	BMPR 1 STANDOFF (IN.)	BMPR 2 MATERIAL	BMPR 2 THICKNESS (IN.)	BMPR 2 STANDOFF (IN.)	BMPR 3 MATERIAL	BMPR 3 THICKNESS (IN.)	BMPR 3 STANDOFF (IN.)	MLI (Y/N)	BACK WALL MATERIAL	BACK WALL THICKNESS (IN.)	PROJECTILE MATERIAL	PROJECTILE DIAMETER (IN.)	PROJECTILE L/D RATIO	IMPACT ANGLE (DEG)	AVERAGE VELOCITY (KM/SEC)
SS-158A	MSFC	04/17/87	DBL-BMPR	6061-T6	0.032	4.00	6061-T6	0.032	3.00	N/A			NO	2219-T87	0.125	1100-AL	0.250		65.00	3.20
SS-158B	MSFC	04/20/87	DBL-BMPR	6061-T6	0.032	6.00	6061-T6	0.032	5.00	N/A			NO	2219-T87	0.125	1100-AL	0.250		0.00	3.21
SS-159A	MSFC	04/21/87	DBL-BMPR	6061-T6	0.032	6.00	6061-T6	0.032	5.00	N/A			NO	2219-T87	0.125	1100-AL	0.313		0.00	6.13
SS-159B	MSFC	04/22/87	DBL-BMPR	6061-T6	0.032	6.00	6061-T6	0.032	5.00	N/A			NO	2219-T87	0.125	1100-AL	0.313		0.00	6.18
SS-160	MSFC	04/23/87	DBL-BMPR	6061-T6	0.032	6.00	6061-T6	0.032	5.00	N/A			NO	2219-T87	0.125	1100-AL	0.375		0.00	6.50
SS-162A	MSFC	05/26/87	SNGL-BMPR	6061-T6	0.063	4.00	N/A			N/A			NO	2219-T87	0.125	1100-AL	0.187		30.00	6.53
SS-162B	MSFC	05/27/87	SNGL-BMPR	6061-T6	0.063	4.00	N/A			N/A			NO	2219-T87	0.125	1100-AL	0.187		30.00	5.11
SS-163A	MSFC	05/27/87	DBL-BMPR	6061-T6	0.080	4.00	6061-T6	0.080	1.00	N/A			NO	2219-T87	0.125	1100-AL	0.313		0.00	5.60
SS-163B	MSFC	05/28/87	DBL-BMPR	6061-T6	0.080	4.00	6061-T6	0.080	1.00	N/A			NO	2219-T87	0.125	1100-AL	0.313		0.00	4.39
SS-167A	MSFC	08/06/87	DBL-BMPR	6061-T6	0.063	8.00	6061-T6	0.063	4.00	N/A			NO	2219-T87	0.125	1100-AL	0.375		0.00	6.58
SS-167B	MSFC	08/07/87	DBL-BMPR	6061-T6	0.063	8.00	6061-T6	0.063	4.00	N/A			NO	2219-T87	0.125	1100-AL	0.375		0.00	6.65
SS-168A	MSFC	08/10/87	DBL-BMPR	6061-T6	0.032	4.00	6061-T6	0.032	3.718	N/A			NO	2219-T87	0.125	1100-AL	0.250		45.00	5.54
SS-168B	MSFC	08/11/87	DBL-BMPR	6061-T6	0.032	4.00	6061-T6	0.032	3.718	N/A			NO	2219-T87	0.125	1100-AL	0.250		45.00	5.98
SS-168C	MSFC	08/12/87	DBL-BMPR	6061-T6	0.032	4.00	6061-T6	0.032	3.718	N/A			NO	2219-T87	0.125	1100-AL	0.250		45.00	6.67
SS-168D	MSFC	08/13/87	DBL-BMPR	6061-T6	0.032	4.00	6061-T6	0.032	3.718	N/A			NO	2219-T87	0.125	1100-AL	0.250		45.00	7.02
SS-169A	MSFC	08/17/87	DBL-BMPR	6061-T6	0.032	4.00	6061-T6	0.032	3.843	N/A			NO	2219-T87	0.125	1100-AL	0.250		45.00	6.87
SS-169B	MSFC	08/18/87	DBL-BMPR	6061-T6	0.032	4.00	6061-T6	0.032	3.843	N/A			NO	2219-T87	0.125	1100-AL	0.250		45.00	6.55
SS-170A	MSFC	08/20/87	DBL-BMPR	6061-T6	0.032	4.00	6061-T6	0.032	3.468	N/A			NO	2219-T87	0.125	1100-AL	0.250		45.00	6.52
SS-170B	MSFC	08/24/87	DBL-BMPR	6061-T6	0.032	4.00	6061-T6	0.032	3.468	N/A			NO	2219-T87	0.125	1100-AL	0.250		45.00	6.85
SS-171A	MSFC	08/28/87	WINDOW	N/A			N/A			N/A			NO	LEXIGARD	1.300	1100-AL	0.375		45.00	6.61
SS-172A	MSFC	08/31/87	WINDOW	N/A			N/A			N/A			NO	LEXIGARD	1.300	1100-AL	0.375		65.00	6.71
SS-173A	MSFC	09/01/87	WINDOW	N/A			N/A			N/A			NO	LEXIGARD	0.750	1100-AL	0.313		45.00	6.99
SS-174A	MSFC	09/02/87	WINDOW	N/A			N/A			N/A			NO	LEXIGARD	0.750	1100-AL	0.313		65.00	6.92
SS-175A	MSFC	09/03/87	DBL-BMPR	6061-T6	0.032	4.00	6061-T6	0.032	3.468	N/A			NO	2219-T87	0.125	1100-AL	0.250		0.00	6.99
SS-175B	MSFC	09/04/87	DBL-BMPR	6061-T6	0.032	4.00	6061-T6	0.032	3.468	N/A			NO	2219-T87	0.125	1100-AL	0.250		0.00	7.34
SS-175C	MSFC	09/08/87	DBL-BMPR	6061-T6	0.032	4.00	6061-T6	0.032	3.468	N/A			NO	2219-T87	0.125	1100-AL	0.250		0.00	7.30
SS-176A	MSFC	09/09/87	DBL-BMPR	6061-T6	0.032	5.00	6061-T6	0.032	3.000	N/A			NO	2219-T87	0.125	1100-AL	0.250		0.00	6.61
SS-176B	MSFC	09/10/87	DBL-BMPR	6061-T6	0.032	5.00	6061-T6	0.032	3.000	N/A			NO	2219-T87	0.125	1100-AL	0.250		0.00	5.89
SS-176C	MSFC	09/11/87	DBL-BMPR	6061-T6	0.032	5.00	6061-T6	0.032	3.000	N/A			NO	2219-T87	0.125	1100-AL	0.250		0.00	5.07
SS-176D	MSFC	09/14/87	DBL-BMPR	6061-T6	0.032	5.00	6061-T6	0.032	3.000	N/A			NO	2219-T87	0.125	1100-AL	0.250		0.00	4.33
SS-177A	MSFC	09/15/87	COMP-BMPR	GR-EP	0.150	4.00	N/A			N/A			NO	2219-T87	0.125	1100-AL	0.250		0.00	6.92
SS-177B	MSFC	09/16/87	COMP-BMPR	GR-EP	0.150	4.00	N/A			N/A			NO	2219-T87	0.125	1100-AL	0.250		0.00	7.59
SS-178A	MSFC	09/17/87	COMP-BMPR	GR-AL	0.315	16.00	N/A			N/A			NO	2219-T87	0.080	1100-AL	0.375		0.00	6.69
SS-178B	MSFC	09/18/87	COMP-BMPR	GR-AL	0.315	16.00	N/A			N/A			NO	2219-T87	0.080	1100-AL	0.313		0.00	3.15
SS-179A	MSFC	09/22/87	DBL-BMPR	6061-T6	0.040	7.00	6061-T6	0.040	4.00	N/A			NO	2219-T87	0.125	1100-AL	0.375		0.00	6.46
SS-179B	MSFC	09/23/87	DBL-BMPR	6061-T6	0.040	7.00	6061-T6	0.040	4.00	N/A			NO	2219-T87	0.125	1100-AL	0.375		0.00	6.70
SS-180A	MSFC	09/24/87	QUAD-BMPR	6061-T6	0.040	7.00	6061-T6	0.040	6.00	6061-T6	0.040	5.00	NO	2219-T87	0.125	1100-AL	0.375		0.00	6.41
SS-180B	MSFC	09/25/87	QUAD-BMPR	6061-T6	0.040	7.00	6061-T6	0.040	6.00	6061-T6	0.040	5.00	NO	2219-T87	0.125	1100-AL	0.375		0.00	5.53
SS-181A	MSFC	09/28/87	DBL-BMPR	2219-T87	0.125	7.00	6061-T6	0.040	4.00	N/A			NO	2219-T87	0.125	1100-AL	0.375		0.00	6.32
SS-181B	MSFC	09/29/87	DBL-BMPR	2219-T87	0.125	7.00	6061-T6	0.040	4.00	N/A			NO	2219-T87	0.125	1100-AL	0.375		0.00	5.52
SS-182A	MSFC	09/30/87	QUAD-BMPR	6061-T6	0.040	7.00	6061-T6	0.040	5.00	6061-T6	0.04	3.00	NO	2219-T87	0.125	1100-AL	0.375		0.00	6.30
SS-183A	MSFC	10/01/87	DBL-BMPR	6061-T6	0.032	4.00	6061-T6	0.032	3.00	N/A			NO	2219-T87	0.125	STEEL	0.125		0.00	7.53
SS-183B	MSFC	10/02/87	DBL-BMPR	6061-T6	0.032	4.00	6061-T6	0.032	3.00	N/A			NO	2219-T87	0.125	STEEL	0.125		0.00	5.54
SS-184A	MSFC	10/07/87	SNGL-BMPR	2219-T87	0.187	12.00	N/A			N/A			NO	2219-T87	0.187	6061-AL	0.500		0.00	5.70
SS-184B	MSFC	10/08/87	SNGL-BMPR	2219-T87	0.187	12.00	N/A			N/A			NO	2219-T87	0.187	6061-AL	0.500		0.00	5.28
SS-185A	MSFC	10/14/87	SNGL-BMPR	2219-T87	0.187	6.00	N/A			N/A			NO	2219-T87	0.187	6061-AL	0.500		0.00	5.99
SS-186A	MSFC	10/15/87	DBL-BMPR	2219-T87	0.125	12.00	6061-T6	0.080	8.00	N/A			NO	2219-T87	0.125	6061-T6	0.500		0.00	5.07
SS-186B	MSFC	10/16/87	DBL-BMPR	2219-T87	0.125	12.00	6061-T6	0.080	8.00	N/A			NO	2219-T87	0.125	6061-T6	0.500		0.00	5.36
SS-187A	MSFC	10/19/87	DBL-BMPR	2219-T87	0.125	8.00	6061-T6	0.080	4.00	N/A			NO	2219-T87	0.125	6061-T6	0.500		0.00	6.36
SS-187B	MSFC	10/20/87	DBL-BMPR	2219-T87	0.125	8.00	6061-T6	0.080	4.00	N/A			NO	2219-T87	0.125	6061-T6	0.500		0.00	6.02
SS-188A	MSFC	10/21/87	DBL-BMPR	2219-T87	0.125	12.00	6061-T6	0.080	4.00	N/A			NO	2219-T87	0.125	6061-T6	0.500		0.00	5.72
SS-188B	MSFC	10/22/87	DBL-BMPR	6061-T6	0.080	12.00	6061-T6	0.080	4.00	N/A			NO	2219-T87	0.125	6061-T6	0.500		0.00	6.21

ORIGINAL PAGE IS
OF POOR QUALITY

DATE: 02-Mar-89

SPACE STATION METEOROID/DEBRIS TEST DATABASE

TEST NUMBER	DATA SOURCE	TEST DATE	TEST ARTICLE TYPE	BMPR 1 MATERIAL	BMPR 1 THICKNESS (IN.)	BMPR 1 STANDOFF (IN.)	BMPR 2 MATERIAL	BMPR 2 THICKNESS (IN.)	BMPR 2 STANDOFF (IN.)	BMPR 3 MATERIAL	BMPR 3 THICKNESS (IN.)	BMPR 3 STANDOFF (IN.)	MLI (Y/N)	BACK WALL MATERIAL	BACK WALL THICKNESS (IN.)	PROJECTILE MATERIAL	PROJECTILE DIAMETER (IN.)	PROJECTILE L/D RATIO	IMPACT ANGLE (DEG)	AVERAGE VELOCITY (KM/SEC)
SS-188C	MSFC	10/23/87	DBL-BMPR	2219-T87	0.125	*****	6061-T6	0.040	*****	N/A			NO	2219-T87	0.125	1100-AL	0.500		0.00	6.06
SS-188D	MSFC	10/28/87	TRPL-BMPR	6061-T6	0.040	12.00	6061-T6	0.040	8.00	6061-T6	0.040	4.00	NO	2219-T87	0.125	1100-AL	0.500		0.00	6.12
SS-188E	MSFC	10/29/87	DBL-BMPR	6061-T6	0.080	12.00	6061-T6	0.040	4.00	N/A			NO	2219-T87	0.125	1100-AL	0.500		0.00	6.12
SS-189A	MSFC	10/30/87	SNGL-BMPR	2219-T87	0.125	12.00	N/A			N/A			NO	2219-T87	0.125	1100-AL	0.500		0.00	6.13
SS-189B	MSFC	11/02/87	SNGL-BMPR	2219-T87	0.125	12.00	N/A			N/A			NO	2219-T87	0.125	1100-AL	0.500		0.00	6.10
SS-189C	MSFC	11/04/87	SII-BMPR	2024-T3	0.020	12.00	2024-T3	0.020	10.00	2024-T3	0.020	8.00	NO	2219-T87	0.125	1100-AL	0.500		0.00	5.87
SS-189D	MSFC	11/05/87	TRPL-BMPR	6061-T6	0.040	12.00	6061-T6	0.040	8.00	6061-T6	0.040	4.00	NO	2219-T87	0.125	1100-AL	0.500		0.00	4.98
SS-190A	MSFC	11/10/87	TRPL-BMPR	6061-T6	0.040	12.00	6061-T6	0.040	8.00	6061-T6	0.040	4.00	NO	2219-T87	0.125	1100-AL	0.375		0.00	3.20
SS-190B	MSFC	11/12/87	SNGL-BMPR	6061-T6	0.040	4.00	N/A			N/A			NO	2219-T87	0.125	1100-AL	0.375		0.00	4.47
SS-191A	MSFC	11/13/87	DBL-BMPR	6061-T6	0.040	8.00	6061-T6	0.040	4.00	N/A			NO	2219-T87	0.125	1100-AL	0.375		0.00	6.57
SS-192A	MSFC	11/30/87	DBL-BMPR	6061-T6	0.080	7.00	6061-T6	0.080	4.00	N/A			NO	2219-T87	0.125	1100-AL	0.313		0.00	3.20
SS-201A	IWALL	07/17/86	SNGL-BMPR	6061-T6	0.040	4.00	N/A			N/A			YES	2219-T87	0.125	1100-AL	0.250		45.00	4.33
SS-201B	IWALL	07/17/86	SNGL-BMPR	6061-T6	0.040	4.00	N/A			N/A			YES	2219-T87	0.125	1100-AL	0.250		45.00	5.51
SS-201C	IWALL	07/18/86	SNGL-BMPR	6061-T6	0.040	4.00	N/A			N/A			YES	2219-T87	0.125	1100-AL	0.250		45.00	7.21
SS-201D	IWALL	07/21/86	SNGL-BMPR	6061-T6	0.040	4.00	N/A			N/A			YES	2219-T87	0.125	1100-AL	0.250		45.00	7.59
SS-202A	IWALL	06/05/86	SNGL-BMPR	6061-T6	0.040	4.00	N/A			N/A			NO	2219-T87	0.125	1100-AL	0.187		45.00	3.52
SS-202B	IWALL	06/05/86	SNGL-BMPR	6061-T6	0.040	4.00	N/A			N/A			NO	2219-T87	0.125	1100-AL	0.187		45.00	3.24
SS-202C	IWALL	07/14/86	SNGL-BMPR	6061-T6	0.040	4.00	N/A			N/A			NO	2219-T87	0.125	1100-AL	0.187		45.00	5.25
SS-202D	IWALL	07/14/86	SNGL-BMPR	6061-T6	0.040	4.00	N/A			N/A			NO	2219-T87	0.125	1100-AL	0.187		45.00	6.44
SS-202E	IWALL	07/15/86	SNGL-BMPR	6061-T6	0.040	4.00	N/A			N/A			NO	2219-T87	0.125	1100-AL	0.187		45.00	7.19
SS-202F	IWALL	07/15/86	SNGL-BMPR	6061-T6	0.040	4.00	N/A			N/A			NO	2219-T87	0.125	1100-AL	0.187		45.00	7.51
SS-203A	IWALL	07/08/86	SNGL-BMPR	6061-T6	0.040	4.00	N/A			N/A			YES	2219-T87	0.125	1100-AL	0.300		65.00	4.79
SS-203B	IWALL	07/08/86	SNGL-BMPR	6061-T6	0.040	4.00	N/A			N/A			YES	2219-T87	0.125	1100-AL	0.300		65.00	3.65
SS-203C	IWALL	07/09/86	SNGL-BMPR	6061-T6	0.040	4.00	N/A			N/A			YES	2219-T87	0.125	1100-AL	0.300		65.00	2.72
SS-203D	IWALL	07/09/86	SNGL-BMPR	6061-T6	0.040	4.00	N/A			N/A			YES	2219-T87	0.125	1100-AL	0.300		65.00	5.59
SS-203E	IWALL	07/21/86	SNGL-BMPR	6061-T6	0.040	4.00	N/A			N/A			YES	2219-T87	0.125	1100-AL	0.300		65.00	6.72
SS-203F	IWALL	08/01/86	SNGL-BMPR	6061-T6	0.040	4.00	N/A			N/A			YES	2219-T87	0.125	1100-AL	0.350		65.00	3.05
SS-203G	IWALL	08/01/86	SNGL-BMPR	6061-T6	0.040	4.00	N/A			N/A			YES	2219-T87	0.125	1100-AL	0.350		65.00	4.64
SS-204A	IWALL	06/30/86	SNGL-BMPR	6061-T6	0.040	4.00	N/A			N/A			NO	2219-T87	0.125	1100-AL	0.250		65.00	4.77
SS-204B	IWALL	07/01/86	SNGL-BMPR	6061-T6	0.040	4.00	N/A			N/A			NO	2219-T87	0.125	1100-AL	0.250		65.00	5.86
SS-204C	IWALL	07/01/86	SNGL-BMPR	6061-T6	0.040	4.00	N/A			N/A			NO	2219-T87	0.125	1100-AL	0.250		65.00	4.25
SS-204D	IWALL	07/16/86	SNGL-BMPR	6061-T6	0.040	4.00	N/A			N/A			NO	2219-T87	0.125	1100-AL	0.250		65.00	3.18
SS-205A	IWALL	06/24/86	SNGL-BMPR	6061-T6	0.063	4.00	N/A			N/A			YES	2219-T87	0.125	1100-AL	0.250		45.00	4.16
SS-205B	IWALL	06/25/86	SNGL-BMPR	6061-T6	0.063	4.00	N/A			N/A			YES	2219-T87	0.125	1100-AL	0.250		45.00	4.61
SS-205C	IWALL	06/25/86	SNGL-BMPR	6061-T6	0.063	4.00	N/A			N/A			YES	2219-T87	0.125	1100-AL	0.250		45.00	5.30
SS-205D	IWALL	06/26/86	SNGL-BMPR	6061-T6	0.063	4.00	N/A			N/A			YES	2219-T87	0.125	1100-AL	0.250		45.00	6.30
SS-205E	IWALL	06/27/86	SNGL-BMPR	6061-T6	0.063	4.00	N/A			N/A			YES	2219-T87	0.125	1100-AL	0.250		45.00	3.15
SS-206A	IWALL	06/06/86	SNGL-BMPR	6061-T6	0.063	4.00	N/A			N/A			NO	2219-T87	0.125	1100-AL	0.187		45.00	4.77
SS-206B	IWALL	06/09/86	SNGL-BMPR	6061-T6	0.063	4.00	N/A			N/A			NO	2219-T87	0.125	1100-AL	0.187		45.00	5.09
SS-206C	IWALL	06/09/86	SNGL-BMPR	6061-T6	0.063	4.00	N/A			N/A			NO	2219-T87	0.125	1100-AL	0.187		45.00	5.40
SS-206D	IWALL	06/10/86	SNGL-BMPR	6061-T6	0.063	4.00	N/A			N/A			NO	2219-T87	0.125	1100-AL	0.187		45.00	3.69
SS-206E	IWALL	06/17/86	SNGL-BMPR	6061-T6	0.063	4.00	N/A			N/A			NO	2219-T87	0.125	1100-AL	0.187		45.00	3.24
SS-206F	IWALL	06/18/86	SNGL-BMPR	6061-T6	0.063	4.00	N/A			N/A			NO	2219-T87	0.125	1100-AL	0.187		45.00	6.15
SS-207A	IWALL	07/03/86	SNGL-BMPR	6061-T6	0.063	4.00	N/A			N/A			YES	2219-T87	0.125	1100-AL	0.300		65.00	5.74
SS-207B	IWALL	07/23/86	SNGL-BMPR	6061-T6	0.063	4.00	N/A			N/A			YES	2219-T87	0.125	1100-AL	0.300		65.00	6.25
SS-207C	IWALL	07/24/86	SNGL-BMPR	6061-T6	0.063	4.00	N/A			N/A			YES	2219-T87	0.125	1100-AL	0.300		65.00	7.03
SS-208A	IWALL	06/13/86	SNGL-BMPR	6061-T6	0.063	4.00	N/A			N/A			NO	2219-T87	0.125	1100-AL	0.250		65.00	4.98
SS-208B	IWALL	06/13/86	SNGL-BMPR	6061-T6	0.063	4.00	N/A			N/A			NO	2219-T87	0.125	1100-AL	0.250		65.00	4.29
SS-208C	IWALL	06/16/86	SNGL-BMPR	6061-T6	0.063	4.00	N/A			N/A			NO	2219-T87	0.125	1100-AL	0.250		55.00	3.32
SS-208D	IWALL	06/17/86	SNGL-BMPR	6061-T6	0.063	4.00	N/A			N/A			NO	2219-T87	0.125	1100-AL	0.250		65.00	5.63
SS-208E	IWALL	07/16/86	SNGL-BMPR	6061-T6	0.063	4.00	N/A			N/A			NO	2219-T87	0.125	1100-AL	0.250		65.00	6.47
SS-209A	IWALL	07/25/86	SNGL-BMPR	6061-T6	0.063	4.00	N/A			N/A			YES	2219-T87	0.125	1100-AL	0.250		65.00	4.29

SPACE STATION METEOROID/DEBRIS TEST DATABASE

TEST NUMBER	DATA SOURCE	TEST DATE	TEST ARTICLE TYPE	BMPR 1 MATERIAL	BMPR 1 THICKNESS (IN.)	BMPR 1 STANDOFF (IN.)	BMPR 2 MATERIAL	BMPR 2 THICKNESS (IN.)	BMPR 2 STANDOFF (IN.)	BMPR 3 MATERIAL	BMPR 3 THICKNESS (IN.)	BMPR 3 STANDOFF (IN.)	MLI (Y/N)	BACK WALL MATERIAL	BACK WALL THICKNESS (IN.)	PROJECTILE MATERIAL	PROJECTILE DIAMETER (IN.)	PROJECTILE L/D RATIO	IMPACT ANGLE (DEG)	AVERAGE VELOCITY (KM/SEC)
SS-209B	IWALL	07/31/86	SNGL-BMPR	6061-T6	0.063	4.00	N/A			N/A			YES	2219-T87	0.125	1100-AL	0.250		65.00	6.35
SS-209D	IWALL	07/31/86	SNGL-BMPR	6061-T6	0.063	4.00	N/A			N/A			YES	2219-T87	0.125	1100-AL	0.250		65.00	7.34
SS-210B	IWALL	08/04/86	SNGL-BMPR	6061-T6	0.063	4.00	N/A			N/A			YES	2219-T87	0.125	1100-AL	0.350		65.00	5.69
SS-210D	IWALL	08/05/86	SNGL-BMPR	6061-T6	0.063	4.00	N/A			N/A			YES	2219-T87	0.125	1100-AL	0.350		65.00	6.93
SS-211B	IWALL	08/05/86	SNGL-BMPR	6061-T6	0.063	4.00	N/A			N/A			YES	2219-T87	0.125	1100-AL	0.350		45.00	5.87
SS-211D	IWALL	08/06/86	SNGL-BMPR	6061-T6	0.063	4.00	N/A			N/A			YES	2219-T87	0.125	1100-AL	0.350		45.00	6.97
SS-212B	IWALL	08/06/86	SNGL-BMPR	6061-T6	0.063	4.00	N/A			N/A			YES	2219-T87	0.125	1100-AL	0.300		45.00	6.27
SS-213A	IWALL	09/25/86	SNGL-BMPR	6061-T6	0.080	4.00	N/A			N/A			NO	2219-T87	0.188	1100-AL	0.313		0.00	4.94
SS-213B	IWALL	09/25/86	SNGL-BMPR	6061-T6	0.080	4.00	N/A			N/A			NO	2219-T87	0.188	1100-AL	0.313		0.00	5.82
SS-213C	IWALL	01/16/87	SNGL-BMPR	6061-T6	0.080	4.00	N/A			N/A			NO	2219-T87	0.188	1100-AL	0.250		0.00	4.43
SS-213D	IWALL	01/20/87	SNGL-BMPR	6061-T6	0.080	4.00	N/A			N/A			NO	2219-T87	0.188	1100-AL	0.250		0.00	5.13
SS-214A	IWALL	09/03/86	SNGL-BMPR	6061-T6	0.040	4.00	N/A			N/A			NO	2219-T87	0.188	1100-AL	0.250		0.00	5.61
SS-214B	IWALL	09/03/86	SNGL-BMPR	6061-T6	0.040	4.00	N/A			N/A			NO	2219-T87	0.188	1100-AL	0.250		15.00	4.94
SS-214C	IWALL	09/04/86	SNGL-BMPR	6061-T6	0.040	4.00	N/A			N/A			NO	2219-T87	0.188	1100-AL	0.250		0.00	4.78
SS-214D	IWALL	09/05/86	SNGL-BMPR	6061-T6	0.040	4.00	N/A			N/A			NO	2219-T87	0.188	1100-AL	0.250		0.00	4.51
SS-215A	IWALL	09/04/86	SNGL-BMPR	6061-T6	0.040	4.00	N/A			N/A			YES	2219-T87	0.188	1100-AL	0.350		0.00	4.61
SS-215B	IWALL	09/05/86	SNGL-BMPR	6061-T6	0.040	4.00	N/A			N/A			YES	2219-T87	0.188	1100-AL	0.350		0.00	5.48
SS-215C	IWALL	09/16/86	SNGL-BMPR	6061-T6	0.040	4.00	N/A			N/A			YES	2219-T87	0.188	1100-AL	0.350		0.00	6.21
SS-215D	IWALL	09/16/86	SNGL-BMPR	6061-T6	0.040	4.00	N/A			N/A			YES	2219-T87	0.188	1100-AL	0.350		0.00	6.13
SS-216A	IWALL	09/08/86	SNGL-BMPR	6061-T6	0.080	4.00	N/A			N/A			NO	2219-T87	0.188	1100-AL	0.350		45.00	5.99
SS-216B	IWALL	09/08/86	SNGL-BMPR	6061-T6	0.080	4.00	N/A			N/A			NO	2219-T87	0.188	1100-AL	0.350		45.00	6.54
SS-216C	IWALL	02/11/86	SNGL-BMPR	6061-T6	0.080	4.00	N/A			N/A			NO	2219-T87	0.188	1100-AL	0.313		45.00	6.91
SS-217A	IWALL	09/22/86	SNGL-BMPR	6061-T6	0.040	4.00	N/A			N/A			NO	2219-T87	0.188	1100-AL	0.313		45.00	6.59
SS-217B	IWALL	09/23/86	SNGL-BMPR	6061-T6	0.040	4.00	N/A			N/A			NO	2219-T87	0.188	1100-AL	0.313		45.00	7.10
SS-217C	IWALL	01/21/87	SNGL-BMPR	6061-T6	0.040	4.00	N/A			N/A			NO	2219-T87	0.188	1100-AL	0.250		45.00	6.05
SS-217D	IWALL	01/22/87	SNGL-BMPR	6061-T6	0.040	4.00	N/A			N/A			NO	2219-T87	0.188	1100-AL	0.250		45.00	6.47
SS-217E	IWALL	01/23/87	SNGL-BMPR	6061-T6	0.040	4.00	N/A			N/A			NO	2219-T87	0.188	1100-AL	0.250		45.00	7.14
SS-218A	IWALL	????	SNGL-BMPR	6061-T6	0.040	4.00	N/A			N/A			YES	2219-T87	0.188	1100-AL	0.350		45.00	5.82
SS-218B	IWALL	09/19/86	SNGL-BMPR	6061-T6	0.040	4.00	N/A			N/A			YES	2219-T87	0.188	1100-AL	0.350		45.00	6.30
SS-218C	IWALL	09/22/86	SNGL-BMPR	6061-T6	0.040	4.00	N/A			N/A			YES	2219-T87	0.188	1100-AL	0.350		45.00	6.82
SS-219A	IWALL	10/15/86	COMP-BMPR	AL-LI	0.063	4.00	N/A			N/A			NO	2219-T87	0.125	1100-AL	0.313		0.00	3.45
SS-219B	IWALL	10/16/86	COMP-BMPR	AL-LI	0.063	4.00	N/A			N/A			NO	2219-T87	0.125	1100-AL	0.313		0.00	5.58
SS-219C	IWALL	10/16/86	COMP-BMPR	AL-LI	0.063	4.00	N/A			N/A			NO	2219-T87	0.125	1100-AL	0.313		0.00	7.27
SS-219D	IWALL	10/17/86	COMP-BMPR	AL-LI	0.063	4.00	N/A			N/A			NO	2219-T87	0.125	1100-AL	0.313		0.00	6.99
SS-220A	IWALL	10/21/86	COMP-BMPR	DSIC	0.063	4.00	N/A			N/A			NO	2219-T87	0.125	1100-AL	0.313		0.00	6.65
SS-220B	IWALL	10/22/86	COMP-BMPR	DSIC	0.063	4.00	N/A			N/A			NO	2219-T87	0.125	1100-AL	0.313		0.00	7.30
SS-221A	IWALL	10/02/86	SNGL-BMPR	6061-T6	0.040	4.00	N/A			N/A			YES	2219-T87	0.125	1100-AL	0.187		45.00	6.42
SS-221B	IWALL	10/03/86	SNGL-BMPR	6061-T6	0.040	4.00	N/A			N/A			YES	2219-T87	0.125	1100-AL	0.187		45.00	5.93
SS-221C	IWALL	10/03/86	SNGL-BMPR	6061-T6	0.040	4.00	N/A			N/A			YES	2219-T87	0.125	1100-AL	0.187		45.00	4.60
SS-221D	IWALL	10/06/86	SNGL-BMPR	6061-T6	0.040	4.00	N/A			N/A			YES	2219-T87	0.125	1100-AL	0.187		45.00	4.08
SS-222A	IWALL	10/14/86	SNGL-BMPR	6061-T6	0.040	4.00	N/A			N/A			NO	2219-T87	0.125	1100-AL	0.125		45.00	5.60
SS-222B	IWALL	10/14/86	SNGL-BMPR	6061-T6	0.040	4.00	N/A			N/A			NO	2219-T87	0.125	1100-AL	0.125		45.00	5.03
SS-222C	IWALL	10/15/86	SNGL-BMPR	6061-T6	0.040	4.00	N/A			N/A			NO	2219-T87	0.125	1100-AL	0.125		45.00	3.33
SS-223A	IWALL	10/24/86	SNGL-BMPR	6061-T6	0.040	4.00	N/A			N/A			YES	2219-T87	0.125	6061-T6	0.262	1.00	45.00	6.58
SS-223B	IWALL	10/24/86	SNGL-BMPR	6061-T6	0.040	4.00	N/A			N/A			YES	2219-T87	0.125	6061-T6	0.262	1.00	45.00	6.75
SS-223C	IWALL	10/27/86	SNGL-BMPR	6061-T6	0.040	4.00	N/A			N/A			YES	2219-T87	0.125	6061-T6	0.262	1.00	45.00	5.67
SS-224A	IWALL	10/28/86	SNGL-BMPR	6061-T6	0.040	4.00	N/A			N/A			YES	2219-T87	0.125	6061-T6	0.262	1.00	65.00	6.49
SS-224B	IWALL	10/28.86	SNGL-BMPR	6061-T6	0.040	4.00	N/A			N/A			YES	2219-T87	0.125	6061-T6	0.262	1.00	65.00	4.86
SS-224C	IWALL	10/29/86	SNGL-BMPR	6061-T6	0.040	4.00	N/A			N/A			YES	2219-T87	0.125	6061-T6	0.262	1.00	65.00	3.70
SS-225A	IWALL	10/31/86	SNGL-BMPR	6061-T6	0.040	4.00	N/A			N/A			NO	2219-T87	0.125	LEXAN	0.350		0.00	5.80
SS-225B	IWALL	11/04/86	SNGL-BMPR	6061-T6	0.040	4.00	N/A			N/A			NO	2219-T87	0.125	LEXAN	0.350		0.00	4.85
SS-225C	IWALL	11/05/86	SNGL-BMPR	6061-T6	0.040	4.00	N/A			N/A			NO	2219-T87	0.125	LEXAN	0.350		0.00	4.28

DATE: 02-Mar-89

SPACE STATION METEOROID/DEBRIS TEST DATABASE

TEST NUMBER	DATA SOURCE	TEST DATE	TEST ARTICLE TYPE	BMPR 1 MATERIAL	BMPR 1 THICKNESS (IN.)	BMPR 1 STANDOFF (IN.)	BMPR 2 MATERIAL	BMPR 2 THICKNESS (IN.)	BMPR 2 STANDOFF (IN.)	BMPR 3 MATERIAL	BMPR 3 THICKNESS (IN.)	BMPR 3 STANDOFF (IN.)	MLI (Y/N)	BACK WALL MATERIAL	BACK WALL THICKNESS (IN.)	PROJECTILE MATERIAL	PROJECTILE DIAMETER (IN.)	PROJECTILE L/D RATIO	IMPACT ANGLE (DEG)	AVERAGE VELOCITY (KM/SEC)
SS-225B-1	IWALL	11/06/86	SNGL-BMPR	6061-T6	0.040	4.00	N/A			N/A			NO	2219-T87	0.125	LEXAN	0.375	1.00	0.00	6.41
SS-226A	IWALL	11/24/86	SNGL-BMPR	6061-T6	0.032	4.00	N/A			N/A			YES	2219-T87	0.100	1100-AL	0.250		45.00	4.45
SS-226B	IWALL	12/01/86	SNGL-BMPR	6061-T6	0.032	4.00	N/A			N/A			YES	2219-T87	0.100	1100-AL	0.250		45.00	5.49
SS-226C	IWALL	12/03/86	SNGL-BMPR	6061-T6	0.032	4.00	N/A			N/A			YES	2219-T87	0.100	1100-AL	0.250		45.00	6.73
SS-227A	IWALL	12/04/86	SNGL-BMPR	6061-T6	0.032	4.00	N/A			N/A			YES	2219-T87	0.063	1100-AL	0.250		45.00	5.58
SS-227B	IWALL	12/12/86	SNGL-BMPR	6061-T6	0.032	4.00	N/A			N/A			YES	2219-T87	0.063	1100-AL	0.250		45.00	7.19
SS-228A	IWALL	12/11/86	SNGL-BMPR	6061-T6	0.032	4.00	N/A			N/A			NO	2219-T87	0.063	1100-AL	0.313		0.00	5.99
SS-228B	IWALL	12/11/86	SNGL-BMPR	6061-T6	0.032	4.00	N/A			N/A			NO	2219-T87	0.063	1100-AL	0.313		0.00	6.75
SS-228C	IWALL	03/27/87	SNGL-BMPR	6061-T6	0.032	4.00	N/A			N/A			NO	2219-T87	0.188	1100-AL	0.250		0.00	6.96
SS-228D	IWALL	03/30/87	SNGL-BMPR	6061-T6	0.032	4.00	N/A			N/A			NO	2219-T87	0.188	1100-AL	0.250		0.00	6.58
SS-229A	IWALL	12/18/86	SNGL-BMPR	6061-T6	0.080	4.00	N/A			N/A			YES	2219-T87	0.188	1100-AL	0.313		0.00	5.30
SS-229B	IWALL	12/19/86	SNGL-BMPR	6061-T6	0.080	4.00	N/A			N/A			YES	2219-T87	0.188	1100-AL	0.313		0.00	3.07
SS-229C	IWALL	12/19/86	SNGL-BMPR	6061-T6	0.080	4.00	N/A			N/A			YES	2219-T87	0.188	1100-AL	0.313		0.00	3.56
SS-230A	IWALL	11/05/86	SNGL-BMPR	6061-T6	0.063	4.00	N/A			N/A			YES	2219-T87	0.125	1100-AL	0.187		45.00	4.41
SS-230B	IWALL	11/06/86	SNGL-BMPR	6061-T6	0.063	4.00	N/A			N/A			YES	2219-T87	0.125	1100-AL	0.187		45.00	3.23
SS-230C	IWALL	02/03/87	SNGL-BMPR	6061-T6	0.063	4.00	N/A			N/A			NO	2219-T87	0.125	1100-AL	0.250		45.00	5.18
SS-230D	IWALL	02/11/87	SNGL-BMPR	6061-T6	0.063	4.00	N/A			N/A			NO	2219-T87	0.125	1100-AL	0.250		45.00	5.55
SS-230E	IWALL	02/05/87	SNGL-BMPR	6061-T6	0.063	4.00	N/A			N/A			NO	2219-T87	0.125	1100-AL	0.250		45.00	6.57
SS-231A	IWALL	04/08/87	SNGL-BMPR	6061-T6	0.063	4.00	N/A			N/A			NO	2219-T87	0.125	1100-AL	0.187		65.00	3.34
SS-231B	IWALL	04/09/87	SNGL-BMPR	6061-T6	0.063	4.00	N/A			N/A			NO	2219-T87	0.125	1100-AL	0.187		65.00	2.44
SS-231C	IWALL	04/10/87	SNGL-BMPR	6061-T6	0.063	4.00	N/A			N/A			NO	2219-T87	0.125	1100-AL	0.313		65.00	6.59
SS-231D	IWALL	04/13/87	SNGL-BMPR	6061-T6	0.063	4.00	N/A			N/A			NO	2219-T87	0.125	1100-AL	0.313		65.00	7.26
SS-301	MSFC	07/03/87	SNGL-BMPR	6061-T6	0.063	4.00	N/A			N/A			YES	2219-T87	0.125	1100-AL	0.250		45.00	2.94
SS-303	MSFC	07/22/87	SNGL-BMPR	6061-T6	0.063	4.00	N/A			N/A			YES	2219-T87	0.160	1100-AL	0.313		45.00	4.65
SS-303A	MSFC	07/27/87	SNGL-BMPR	6061-T6	0.063	4.00	N/A			N/A			YES	2219-T87	0.125	1100-AL	0.313		45.00	3.72
SS-303B	MSFC	07/31/87	SNGL-BMPR	6061-T6	0.063	4.00	N/A			N/A			YES	2219-T87	0.160	1100-AL	0.313		45.00	4.42
SS-306	MSFC	07/24/87	SNGL-BMPR	6061-T6	0.063	4.00	N/A			N/A			YES	2219-T87	0.160	1100-AL	0.375		45.00	6.35
SS-307	MSFC	07/15/87	CORR-BMPR	6061-T6	0.032	4.00	6061-T5	6061-T5	1.00	N/A			YES	2219-T87	0.125	1100-AL	0.250		45.00	3.00
SS-308	MSFC	07/16/87	CORR-BMPR	6061-T6	0.032	4.00	6061-T6	6061-T6	1.00	N/A			YES	2219-T87	0.125	1100-AL	0.250		45.00	4.47
SS-309	MSFC	07/16/87	CORR-BMPR	6061-T6	0.032	4.00	6061-T6	6061-T6	1.00	N/A			YES	2219-T87	0.125	1100-AL	0.313		45.00	4.63
SS-309-1	MSFC	07/30/87	CORR-BMPR	6061-T6	0.032	4.00	6061-T6	6061-T6	1.00	N/A			YES	2219-T87	0.125	1100-AL	0.313		65.00	4.74
SS-309B	MSFC	07/29/87	CORR-BMPR	6061-T6	0.032	4.00	6061-T6	6061-T6	1.00	N/A			YES	2219-T87	0.125	1100-AL	0.313		45.00	4.87
SS-309R	MSFC	07/28/87	CORR-BMPR	6061-T6	0.020	4.00	6061-T6	6061-T6	1.00	N/A			YES	2219-T87	0.125	1100-AL	0.313		45.00	4.62
SS-310	MSFC	07/17/87	CORR-BMPR	6061-T6	0.032	4.00	6061-T6	6061-T6	1.00	N/A			YES	2219-T87	0.125	1100-AL	0.313		45.00	5.80
SS-310A	MSFC	07/29/87	CORR-BMPR	6061-T6	0.020	4.00	6061-T6	6061-T6	1.00	N/A			YES	2219-T87	0.125	1100-AL	0.313		45.00	5.84
SS-311	MSFC	07/20/87	CORR-BMPR	6061-T6	0.032	4.00	6061-T6	6061-T6	1.00	N/A			YES	2219-T87	0.125	1100-AL	0.375		45.00	5.35
SS-312	MSFC	07/20/87	CORR-BMPR	6061-T6	0.032	4.00	6061-T6	6061-T6	1.00	N/A			YES	2219-T87	0.125	1100-AL	0.375		45.00	6.10
SS-312B	MSFC	07/21/87	CORR-BMPR	6061-T6	0.032	4.00	6061-T6	6061-T6	1.00	N/A			YES	2219-T87	0.125	1100-AL	0.375		45.00	6.52
SS-319	MSFC	04/24/87	SNGL-BMPR	6061-T6	0.040	4.00	N/A			N/A			YES	2219-T87	0.125	1100-AL	0.313		45.00	2.99
SS-320	MSFC	04/28/87	SNGL-BMPR	6061-T6	0.063	4.00	N/A			N/A			YES	2219-T87	0.125	1100-AL	0.313		45.00	3.08
SS-321	MSFC	04/28/87	SNGL-BMPR	6061-T6	0.080	4.00	N/A			N/A			YES	2219-T87	0.125	1100-AL	0.313		45.00	3.01
SS-324	MSFC	04/29/87	SNGL-BMPR	6061-T6	0.040	4.00	N/A			N/A			YES	2219-T87	0.125	1100-AL	0.313		45.00	4.12
SS-325	MSFC	05/01/87	SNGL-BMPR	6061-T6	0.063	4.00	N/A			N/A			YES	2219-T87	0.125	1100-AL	0.313		45.00	4.25
SS-326	MSFC	05/01/87	SNGL-BMPR	6061-T6	0.080	4.00	N/A			N/A			YES	2219-T87	0.125	1100-AL	0.313		45.00	4.25
SS-333	MSFC	05/11/87	SNGL-BMPR	6061-T6	0.040	4.00	N/A			N/A			YES	2219-T87	0.125	1100-AL	0.187		45.00	2.93
SS-334	MSFC	05/07/87	SNGL-BMPR	6061-T6	0.040	4.00	N/A			N/A			YES	2219-T87	0.125	1100-AL	0.187		45.00	3.66
SS-335	MSFC	05/05/87	SNGL-BMPR	6061-T6	0.040	4.00	N/A			N/A			YES	2219-T87	0.125	1100-AL	0.250		45.00	4.12
SS-336	MSFC	05/06/87	SNGL-BMPR	6061-T6	0.040	4.00	N/A			N/A			YES	2219-T87	0.125	1100-AL	0.250		45.00	4.54
SS-336A	MSFC	05/13/87	SNGL-BMPR	6061-T6	0.040	4.00	N/A			N/A			YES	2219-T87	0.125	1100-AL	0.250		45.00	5.76
SS-337	MSFC	05/18/87	SNGL-BMPR	6061-T6	0.040	4.00	N/A			N/A			YES	2219-T87	0.125	1100-AL	0.313		45.00	6.90
SS-338	MSFC	05/14/87	SNGL-BMPR	6061-T6	0.040	4.00	N/A			N/A			YES	2219-T87	0.125	1100-AL	0.313		45.00	7.02
SS-339	MSFC	05/21/87	SNGL-BMPR	6061-T6	0.040	4.00	N/A			N/A			YES	2219-T87	0.125	1100-AL	0.375		45.00	6.55

SPACE STATION METEOROID/DEBRIS TEST DATABASE

TEST NUMBER	DATA SOURCE	TEST DATE	TEST ARTICLE TYPE	BMPR 1 MATERIAL	BMPR 1 THICKNESS (IN.)	BMPR 1 STANDOFF (IN.)	BMPR 2 MATERIAL	BMPR 2 THICKNESS (IN.)	BMPR 2 STANDOFF (IN.)	BMPR 3 MATERIAL	BMPR 3 THICKNESS (IN.)	BMPR 3 STANDOFF (IN.)	MLI (Y/N)	BACK WALL MATERIAL	BACK WALL THICKNESS (IN.)	PROJECTILE MATERIAL	PROJECTILE DIAMETER (IN.)	PROJECTILE L/D RATIO	IMPACT ANGLE (DEG)	AVERAGE VELOCITY (KM/SEC)
SS-EH1A	MSFC	09/26/86	SNGL-BMPR	6061-T6	0.063	4.00	N/A			N/A			NO	2219-T87	0.125	1100-AL	0.313		30.00	7.11
SS-EH1B	MSFC	09/26/86	SNGL-BMPR	6061-T6	0.063	4.00	N/A			N/A			NO	2219-T87	0.125	1100-AL	0.313		45.00	7.01
SS-EH1C	MSFC	09/29/86	SNGL-BMPR	6061-T6	0.063	4.00	N/A			N/A			NO	2219-T87	0.125	1100-AL	0.313		60.00	7.17
SS-EH1D	MSFC	09/30/86	SNGL-BMPR	6061-T6	0.063	4.00	N/A			N/A			NO	2219-T87	0.125	1100-AL	0.313		75.00	7.16
SS-PT12A	MSFC	12/05/86	NO BMPR	N/A			N/A			N/A			NO	2219-T87	0.125	1100-AL	0.250		0.00	4.59
SS-PT4A	MSFC	11/25/86	SNGL-BMPR	6061-T6	0.063	4.00	N/A			N/A			NO	2219-T87	0.125	1100-AL	0.250		0.00	3.64
SS-PT4B	MSFC	11/26/86	SNGL-BMPR	6061-T6	0.063	4.00	N/A			N/A			NO	2219-T87	0.125	1100-AL	0.250		0.00	4.26
SS-PT6A	MSFC	11/19/86	SNGL-BMPR	6061-T6	0.040	4.00	N/A			N/A			NO	2219-T87	0.125	1100-AL	0.313		0.00	4.29
SS-PT8A	MSFC	11/20/86	SNGL-BMPR	6061-T6	0.063	4.00	N/A			N/A			NO	2219-T87	0.125	1100-AL	0.313		0.00	4.35
SS-PT8B	MSFC	11/21/86	SNGL-BMPR	6061-T6	0.063	4.00	N/A			N/A			NO	2219-T87	0.125	1100-AL	0.313		0.00	4.37
SS-P-001	ADP SMI	08/19/85	SNGL-BMPR	6061-T6	0.063	4.00	N/A			N/A			NO	2219-T87	0.125	1100-AL	0.250		0.00	2.75
SS-P-002	ADP SMI	08/20/85	SNGL-BMPR	6061-T6	0.063	4.00	N/A			N/A			NO	2219-T87	0.125	1100-AL	0.250		0.00	2.99
SS-P-003	ADP SMI	08/23/85	SNGL-BMPR	6061-T6	0.063	4.00	N/A			N/A			NO	2219-T87	0.125	1100-AL	0.250		0.00	4.90
SS-P-004	ADP SMI	08/26/85	SNGL-BMPR	6061-T6	0.063	4.00	N/A			N/A			NO	2219-T87	0.125	1100-AL	0.250		0.00	4.95
SS-P-005	ADP SMI	08/28/85	SNGL-BMPR	6061-T6	0.063	4.00	N/A			N/A			NO	2219-T87	0.125	1100-AL	0.250		0.00	6.90
SS-P-006A	ADP SMI	08/30/85	SNGL-BMPR	6061-T6	0.063	4.00	N/A			N/A			NO	2219-T87	0.125	1100-AL	0.250		0.00	6.95
SS-P-007	ADP SMI	09/07/85	SNGL-BMPR	6061-T6	0.063	4.00	N/A			N/A			YES	2219-T87	0.125	1100-AL	0.250		0.00	2.93
SS-P-008	ADP SMI	09/05/85	SNGL-BMPR	6061-T6	0.063	4.00	N/A			N/A			YES	2219-T87	0.125	1100-AL	0.250		0.00	2.96
SS-P-009	ADP SMI	09/06/85	SNGL-BMPR	6061-T6	0.063	4.00	N/A			N/A			YES	2219-T87	0.125	1100-AL	0.250		0.00	5.25
SS-P-010	ADP SMI	09/09/85	SNGL-BMPR	6061-T6	0.063	4.00	N/A			N/A			YES	2219-T87	0.125	1100-AL	0.250		0.00	5.04
SS-P-011	ADP SMI	09/11/85	SNGL-BMPR	6061-T6	0.063	4.00	N/A			N/A			YES	2219-T87	0.125	1100-AL	0.250		0.00	6.63
SS-P-012B	ADP SMI	09/11/85	SNGL-BMPR	6061-T6	0.063	4.00	N/A			N/A			YES	2219-T87	0.125	1100-AL	0.250		0.00	6.83
SS-P-012C	ADP SMI	01/02/86	SNGL-BMPR	6061-T6	0.063	4.00	N/A			N/A			YES	2219-T87	0.125	1100-AL	0.250		0.00	4.33
SS-P-012D	ADP SMI	01/03/86	SNGL-BMPR	6061-T6	0.063	4.00	N/A			N/A			YES	2219-T87	0.125	1100-AL	0.250		0.00	3.96
SS-P-013	ADP SMI	09/17/85	SNGL-BMPR	6061-T6	0.063	6.00	N/A			N/A			NO	2219-T87	0.125	1100-AL	0.250		0.00	4.77
SS-P-013B	ADP SMI	09/18/85	SNGL-BMPR	6061-T6	0.063	6.00	N/A			N/A			NO	2219-T87	0.125	1100-AL	0.250		0.00	6.15
SS-P-013C	ADP SMI	09/19/85	SNGL-BMPR	6061-T6	0.063	6.00	N/A			N/A			NO	2219-T87	0.125	1100-AL	0.250		0.00	5.79
SS-P-013D	ADP SMI	09/20/85	SNGL-BMPR	6061-T6	0.063	6.00	N/A			N/A			YES	2219-T87	0.125	1100-AL	0.250		0.00	5.98
SS-P-013E	ADP SMI	12/03/85	SNGL-BMPR	6061-T6	0.063	6.00	N/A			N/A			YES	2219-T87	0.125	1100-AL	0.250		0.00	3.94
SS-P-014	ADP SMI	09/23/85	SNGL-BMPR	6061-T6	0.063	6.00	N/A			N/A			NO	2219-T87	0.125	1100-AL	0.187		0.00	3.72
SS-P-014A	ADP SMI	09/24/85	SNGL-BMPR	6061-T6	0.063	6.00	N/A			N/A			NO	2219-T87	0.125	1100-AL	0.187		0.00	4.18
SS-P-014B	ADP SMI	09/25/85	SNGL-BMPR	6061-T6	0.063	6.00	N/A			N/A			NO	2219-T87	0.125	1100-AL	0.187		0.00	3.71
SS-P-014C	ADP SMI	09/26/85	SNGL-BMPR	6061-T6	0.063	6.00	N/A			N/A			YES	2219-T87	0.125	1100-AL	0.187		0.00	3.74
SS-P-014D	ADP SMI	10/03/85	SNGL-BMPR	6061-T6	0.063	6.00	N/A			N/A			NO	2219-T87	0.125	1100-AL	0.187		0.00	3.26
SS-P-014E	ADP SMI	12/02/85	SNGL-BMPR	6061-T6	0.063	6.00	N/A			N/A			YES	2219-T87	0.125	1100-AL	0.187		0.00	2.77
SS-P-014F	ADP SMI	12/02/85	SNGL-BMPR	6061-T6	0.063	6.00	N/A			N/A			YES	2219-T87	0.125	1100-AL	0.187		0.00	2.95
SS-P-015	ADP SMI	09/27/85	SNGL-BMPR	6061-T6	0.063	6.00	N/A			N/A			NO	2219-T87	0.125	1100-AL	0.125		0.00	2.85
SS-P-015B	ADP SMI	10/01/85	SNGL-BMPR	6061-T6	0.063	6.00	N/A			N/A			YES	2219-T87	0.125	1100-AL	0.125		0.00	2.11
SS-P-015C	ADP SMI	10/02/85	SNGL-BMPR	6061-T6	0.063	6.00	N/A			N/A			NO	2219-T87	0.125	1100-AL	0.125		0.00	3.01
SS-P-016	ADP SMI	10/04/85	SNGL-BMPR	6061-T6	0.063	6.00	N/A			N/A			NO	2219-T87	0.125	6061-T6	0.300		0.00	5.14
SS-P-016A	ADP SMI	10/04/85	SNGL-BMPR	6061-T6	0.063	6.00	N/A			N/A			NO	2219-T87	0.125	6061-T6	0.300		0.00	6.04
SS-P-016B	ADP SMI	10/07/85	SNGL-BMPR	6061-T6	0.063	6.00	N/A			N/A			NO	2219-T87	0.125	6061-T6	0.300		0.00	6.33
SS-P-016C	ADP SMI	10/08/85	SNGL-BMPR	6061-T6	0.063	6.00	N/A			N/A			NO	2219-T87	0.125	6061-T6	0.300		0.00	6.63
SS-P-016E	ADP SMI	10/10/85	SNGL-BMPR	6061-T6	0.063	6.00	N/A			N/A			NO	2219-T87	0.125	6061-T6	0.300		0.00	6.78
SS-P-016G	ADP SMI	10/15/85	SNGL-BMPR	6061-T6	0.063	6.00	N/A			N/A			NO	2219-T87	0.125	6061-T6	0.300		0.00	7.18
SS-P-016H	ADP SMI	10/16/85	SNGL-BMPR	6061-T6	0.063	6.00	N/A			N/A			YES	2219-T87	0.125	6061-T6	0.300		0.00	7.13
SS-P-016J	ADP SMI	10/22/85	SNGL-BMPR	6061-T6	0.063	6.00	N/A			N/A			YES	2219-T87	0.125	6061-T6	0.300		0.00	6.73
SS-P-016K	ADP SMI	10/25/86	SNGL-BMPR	6061-T6	0.063	6.00	N/A			N/A			YES	2219-T87	0.125	6061-T6	0.300		0.00	6.73
SS-P-016L	ADP SMI	12/03/85	SNGL-BMPR	6061-T6	0.063	6.00	N/A			N/A			YES	2219-T87	0.125	6061-T6	0.300		0.00	4.82
SS-P-016M	ADP SMI	12/04/85	SNGL-BMPR	6061-T6	0.063	6.00	N/A			N/A			YES	2219-T87	0.125	6061-T6	0.300		0.00	3.37
SS-P-016N	ADP SMI	12/10/85	SNGL-BMPR	6061-T6	0.063	6.00	N/A			N/A			YES	2219-T87	0.125	6061-T6	0.300		0.00	3.76
SS-P-016P	ADP SMI	12/11/85	SNGL-BMPR	6061-T6	0.063	6.00	N/A			N/A			YES	2219-T87	0.125	6061-T6	0.300		0.00	4.23

DATE: 02-Mar-89

SPACE STATION METEOROID/DEBRIS TEST DATABASE

TEST NUMBER	DATA SOURCE	TEST DATE	TEST ARTICLE TYPE	BMPR 1 MATERIAL	BMPR 1 THICKNESS (IN.)	BMPR 1 STANDOFF (IN.)	BMPR 2 MATERIAL	BMPR 2 THICKNESS (IN.)	BMPR 2 STANDOFF (IN.)	BMPR 3 MATERIAL	BMPR 3 THICKNESS (IN.)	BMPR 3 STANDOFF (IN.)	MLI (Y/N)	BACK WALL MATERIAL	BACK WALL THICKNESS (IN.)	PROJECTILE MATERIAL	PROJECTILE DIAMETER (IN.)	PROJECTILE L/D RATIO	IMPACT ANGLE (DEG)	AVERAGE VELOCITY (KM/SEC)
SS-P-017	ADP SMI	10/17/85	SNGL-BMPR	6061-T6	0.063	4.00	N/A			N/A			NO	2219-T87	0.125	6061-T6	0.300		0.00	7.01
SS-P-018RV	ADP SMI	10/18/85	SNGL-BMPR	6061-T6	0.063	6.00	N/A			N/A			NO	2219-T87	0.125	6061-T6	0.262	1.00	0.00	7.12
SS-P-018-1	ADP SMI	03/17/86	WINDOW	N/A			N/A			N/A			NO	GLASS	1.500	1100-AL	0.125		0.00	6.50
SS-P-018-2	ADP SMI	03/25/86	WINDOW	N/A			N/A			N/A			NO	GLASS	1.500	1100-AL	0.125		0.00	6.33
SS-P-018-3	ADP SMI	03/27/86	WINDOW	N/A			N/A			N/A			NO	GLASS	1.870	1100-AL	0.125		0.00	6.50
SS-P-018-4	ADP SMI	03/27/86	WINDOW	N/A			N/A			N/A			NO	GLASS	1.870	1100-AL	0.125		0.00	5.63
SS-P-018-5	ADP SMI	03/28/86	WINDOW	N/A			N/A			N/A			NO	GLASS	1.500	1100-AL	0.150		0.00	6.50
SS-P-020B	ADP SMI	10/30/85	SNGL-BMPR	6061-T6	0.063	6.00	N/A			N/A			NO	2219-T87	0.125	1100-AL	0.300		0.00	6.98
SS-P-020C	ADP SMI	11/01/85	SNGL-BMPR	6061-T6	0.063	6.00	N/A			N/A			NO	2219-T87	0.125	1100-AL	0.300		0.00	6.63
SS-P-020F	ADP SMI	11/05/85	SNGL-BMPR	6061-T6	0.063	6.00	N/A			N/A			YES	2219-T87	0.125	1100-AL	0.300		0.00	4.96
SS-P-020G	ADP SMI	11/06/85	SNGL-BMPR	6061-T6	0.063	6.00	N/A			N/A			YES	2219-T87	0.125	1100-AL	0.300		0.00	4.25
SS-P-020H	ADP SMI	12/12/85	SNGL-BMPR	6061-T6	0.063	6.00	N/A			N/A			YES	2219-T87	0.125	1100-AL	0.300		0.00	4.68
SS-P-021	ADP SMI	01/09/86	SNGL-BMPR	6061-T6	0.063	4.00	N/A			N/A			NO	2219-T87	0.125	1100-AL	0.300		0.00	6.63
SS-P-021A	ADP SMI	01/09/86	SNGL-BMPR	6061-T6	0.063	4.00	N/A			N/A			NO	2219-T87	0.125	1100-AL	0.300		0.00	6.47
SS-P-021B	ADP SMI	01/10/86	SNGL-BMPR	6061-T6	0.063	4.00	N/A			N/A			YES	2219-T87	0.125	1100-AL	0.300		0.00	6.89
SS-P-021C	ADP SMI	01/10/86	SNGL-BMPR	6061-T6	0.063	4.00	N/A			N/A			YES	2219-T87	0.125	1100-AL	0.300		0.00	6.60
SS-P-021D	ADP SMI	01/13/86	SNGL-BMPR	6061-T6	0.063	4.00	N/A			N/A			YES	2219-T87	0.125	1100-AL	0.300		0.00	5.85
SS-P-022	ADP SMI	01/14/86	SNGL-BMPR	6061-T6	0.063	4.00	N/A			N/A			NO	2219-T87	0.125	1100-AL	0.262	1.00	0.00	5.09
SS-P-022A	ADP SMI	01/15/86	SNGL-BMPR	6061-T6	0.063	4.00	N/A			N/A			YES	2219-T87	0.125	1100-AL	0.262	1.00	0.00	6.16
SS-P-022B	ADP SMI	01/15/86	SNGL-BMPR	6061-T6	0.063	4.00	N/A			N/A			NO	2219-T87	0.125	1100-AL	0.262	1.00	0.00	6.89
SS-P-024C	ADP SMI	11/13/85	SNGL-BMPR	6061-T6	0.063	4.00	N/A			N/A			NO	2219-T87	0.125	6061-T6	0.250		0.00	5.80
SS-P-024F	ADP SMI	11/20/85	SNGL-BMPR	6061-T6	0.063	6.00	N/A			N/A			NO	2219-T87	0.125	6061-T6	0.250		0.00	5.88
SS-P-024G	ADP SMI	11/21/85	SNGL-BMPR	6061-T6	0.063	6.00	N/A			N/A			YES	2219-T87	0.125	6061-T6	0.250		0.00	4.31
SS-P-025	ADP SMI	11/21/85	SNGL-BMPR	6061-T6	0.063	6.00	N/A			N/A			NO	2219-T87	0.125	6061-T6	0.187		0.00	3.71
SS-P-025A	ADP SMI	11/22/85	SNGL-BMPR	6061-T6	0.063	6.00	N/A			N/A			NO	2219-T87	0.125	6061-T6	0.187		0.00	3.27
SS-P-025B	ADP SMI	11/22/85	SNGL-BMPR	6061-T6	0.063	6.00	N/A			N/A			NO	2219-T87	0.125	6061-T6	0.187		0.00	2.25
SS-P-025C	ADP SMI	11/25/85	SNGL-BMPR	6061-T6	0.063	6.00	N/A			N/A			NO	2219-T87	0.125	6061-T6	0.187		0.00	2.59
SS-P-025D	ADP SMI	11/26/85	SNGL-BMPR	6061-T6	0.063	6.00	N/A			N/A			YES	2219-T87	0.125	6061-T6	0.187		0.00	1.62
SS-P-027	ADP SMI	12/12/85	SNGL-BMPR	6061-T6	0.063	4.00	N/A			N/A			NO	2219-T87	0.125	1100-AL	0.187		0.00	4.53
SS-P-027A	ADP SMI	12/13/85	SNGL-BMPR	6061-T6	0.063	4.00	N/A			N/A			NO	2219-T87	0.125	1100-AL	0.187		0.00	3.87
SS-P-027B	ADP SMI	12/16/85	SNGL-BMPR	6061-T6	0.063	4.00	N/A			N/A			NO	2219-T87	0.125	1100-AL	0.187		0.00	4.15
SS-P-027C	ADP SMI	12/16/85	SNGL-BMPR	6061-T6	0.063	4.00	N/A			N/A			YES	2219-T87	0.125	1100-AL	0.187		0.00	3.68
SS-P-027D	ADP SMI	12/17/85	SNGL-BMPR	6061-T6	0.063	4.00	N/A			N/A			YES	2219-T87	0.125	1100-AL	0.187		0.00	3.08
SS-P-027E	ADP SMI	12/18/85	SNGL-BMPR	6061-T6	0.063	4.00	N/A			N/A			YES	2219-T87	0.125	1100-AL	0.187		0.00	2.83
SS-P-027F	ADP SMI	01/06/86	SNGL-BMPR	6061-T6	0.063	4.00	N/A			N/A			YES	2219-T87	0.125	1100-AL	0.187		0.00	2.54
SS-P-028	ADP SMI	12/18/85	SNGL-BMPR	6061-T6	0.063	4.00	N/A			N/A			NO	2219-T87	0.125	1100-AL	0.125		0.00	3.00
SS-P-033	ADP SMI	03/17/86	SNGL-BMPR	6061-T6	0.040	4.00	N/A			N/A			NO	2219-T87	0.125	1100-AL	0.250		0.00	7.21
SS-P-033B	ADP SMI	03/20/86	SNGL-BMPR	6061-T6	0.040	4.00	N/A			N/A			NO	2219-T87	0.125	1100-AL	0.250		0.00	4.85
SS-P-033B-1	ADP SMI	03/24/86	SNGL-BMPR	6061-T6	0.040	4.00	N/A			N/A			NO	2219-T87	0.125	1100-AL	0.250		0.00	5.26
SS-P-033C	ADP SMI	03/24/86	SNGL-BMPR	6061-T6	0.040	4.00	N/A			N/A			NO	2219-T87	0.125	1100-AL	0.250		0.00	5.53
SS-P-034	ADP SMI	03/12/86	SNGL-BMPR	6061-T6	0.040	4.00	N/A			N/A			NO	2219-T87	0.125	1100-AL	0.250		0.00	5.80
SS-P-034B	ADP SMI	03/13/86	SNGL-BMPR	6061-T6	0.063	4.00	N/A			N/A			NO	2219-T87	0.125	1100-AL	0.250		0.00	7.06
SS-P-034C	ADP SMI	03/13/86	SNGL-BMPR	6061-T6	0.040	4.00	N/A			N/A			YES	2219-T87	0.125	1100-AL	0.250		0.00	5.49
SS-P-034C-1	ADP SMI	03/14/86	SNGL-BMPR	6061-T6	0.040	4.00	N/A			N/A			YES	2219-T87	0.125	1100-AL	0.250		0.00	4.41
SS-P-034C-2	ADP SMI	03/14/86	SNGL-BMPR	6061-T6	0.063	4.00	N/A			N/A			YES	2219-T87	0.125	1100-AL	0.250		0.00	5.17
SS-P-035	ADP SMI	03/06/86	SNGL-BMPR	6061-T6	0.063	6.00	N/A			N/A			NO	2219-T87	0.125	1100-AL	0.350		0.00	6.69
SS-P-035B	ADP SMI	03/07/86	SNGL-BMPR	6061-T6	0.063	6.00	N/A			N/A			YES	2219-T87	0.125	1100-AL	0.350		0.00	6.30
SS-P-035C	ADP SMI	03/11/86	SNGL-BMPR	6061-T6	0.080	6.00	N/A			N/A			YES	2219-T87	0.125	1100-AL	0.350		0.00	5.72
SS-T2-1	MSFC	03/02/87	SNGL-BMPR	6061-T6	0.040	4.00	N/A			N/A			YES	2219-T87	0.125	1100-AL	0.187		0.00	2.54
SS-T2-10	MSFC	02/20/87	NO BMPR	N/A			N/A			N/A			NO	2219-T87	0.125	1100-AL	0.125		0.00	3.65
SS-T2-11	MSFC	02/19/87	NO BMPR	N/A			N/A			N/A			YES	2219-T87	0.125	1100-AL	0.250		0.00	3.55
SS-T2-12	MSFC	02/19/87	NO BMPR	N/A			N/A			N/A			NO	2219-T87	0.125	1100-AL	0.250		0.00	3.57

SPACE STATION METEOROID/DEBRIS TEST DATABASE

TEST NUMBER	DATA SOURCE	TEST DATE	TEST ARTICLE TYPE	BMPR 1 MATERIAL	BMPR 1 THICKNESS (IN.)	BMPR 1 STANDOFF (IN.)	BMPR 2 MATERIAL	BMPR 2 THICKNESS (IN.)	BMPR 2 STANDOFF (IN.)	BMPR 3 MATERIAL	BMPR 3 THICKNESS (IN.)	BMPR 3 STANDOFF (IN.)	ML1 (Y/N)	BACK WALL MATERIAL	BACK WALL THICKNESS (IN.)	PROJECTILE MATERIAL	PROJECTILE DIAMETER (IN.)	PROJECTILE L/D RATIO	IMPACT ANGLE (DEG)	AVERAGE VELOCITY (KM/SEC)
SS-T2-13	MSFC	03/09/87	SNGL-BMPR	6061-T6	0.063	4.00	N/A			N/A			YES	2219-T87	0.125	1100-AL	0.200	1.00	0.00	3.05
SS-T2-14	MSFC	03/10/87	SNGL-BMPR	6061-T6	0.040	4.00	N/A			N/A			YES	2219-T87	0.125	1100-AL	0.200	1.00	0.00	3.89
SS-T2-15	MSFC	03/10/87	SNGL-BMPR	6061-T6	0.040	4.00	N/A			N/A			YES	2219-T87	0.125	1100-AL	0.375		0.00	5.02
SS-T2-16	MSFC	03/11/87	SNGL-BMPR	6061-T6	0.040	4.00	N/A			N/A			NO	2219-T87	0.125	1100-AL	0.375		0.00	5.41
SS-T2-17	MSFC	03/09/87	SNGL-BMPR	6061-T6	0.063	4.00	N/A			N/A			YES	2219-T87	0.125	1100-AL	0.375		0.00	4.63
SS-T2-18	MSFC	03/04/87	SNGL-BMPR	6061-T6	0.063	4.00	N/A			N/A			NO	2219-T87	0.125	1100-AL	0.375		0.00	5.05
SS-T2-19	MSFC	03/04/87	SNGL-BMPR	6061-T6	0.063	6.00	N/A			N/A			YES	2219-T87	0.125	1100-AL	0.313		0.00	4.09
SS-T2-19A	MSFC	03/06/87	SNGL-BMPR	6061-T6	0.063	6.00	N/A			N/A			YES	2219-T87	0.125	1100-AL	0.313		0.00	3.00
SS-T2-19B	MSFC	03/11/87	SNGL-BMPR	6061-T6	0.063	6.00	N/A			N/A			YES	2219-T87	0.125	1100-AL	0.313		0.00	2.92
SS-T2-2	MSFC	02/26/87	SNGL-BMPR	6061-T6	0.040	4.00	N/A			N/A			NO	2219-T87	0.125	1100-AL	0.187		0.00	3.30
SS-T2-20	MSFC	03/06/87	SNGL-BMPR	6061-T6	0.063	6.00	N/A			N/A			NO	2219-T87	0.125	1100-AL	0.313		0.00	4.73
SS-T2-3	MSFC	02/25/87	SNGL-BMPR	6061-T6	0.063	4.00	N/A			N/A			YES	2219-T87	0.125	1100-AL	0.250		0.00	3.00
SS-T2-4	MSFC	02/25/87	SNGL-BMPR	6061-T6	0.063	4.00	N/A			N/A			YES	2219-T87	0.125	1100-AL	0.250		0.00	4.32
SS-T2-5	MSFC	02/23/87	SNGL-BMPR	6061-T6	0.040	4.00	N/A			N/A			YES	2219-T87	0.125	1100-AL	0.313		0.00	3.95
SS-T2-6	MSFC	02/23/87	SNGL-BMPR	6061-T6	0.040	4.00	N/A			N/A			NO	2219-T87	0.125	1100-AL	0.313		0.00	4.62
SS-T2-6A	MSFC	03/03/87	SNGL-BMPR	6061-T6	0.063	4.00	N/A			N/A			NO	2219-T87	0.125	1100-AL	0.313		0.00	4.64
SS-T2-7	MSFC	02/24/87	SNGL-BMPR	6061-T6	0.063	4.00	N/A			N/A			YES	2219-T87	0.125	1100-AL	0.313		0.00	3.26
SS-T2-7A	MSFC	03/05/87	SNGL-BMPR	6061-T6	0.063	4.00	N/A			N/A			YES	2219-T87	0.125	1100-AL	0.313		0.00	3.26
SS-T2-8	MSFC	02/24/87	SNGL-BMPR	6061-T6	0.063	4.00	N/A			N/A			NO	2219-T87	0.125	1100-AL	0.313		0.00	3.39
SS-T2-9	MSFC	02/20/87	NO BMPR	N/A			N/A			N/A			YES	2219-T87	0.125	1100-AL	0.125		0.00	3.69

ORIGINAL PAGE IS
OF POOR QUALITY

Section 2.5.2

Summary of NASA/MSFC Hypervelocity Impact Test Shot Distribution

as of March 2, 1989

DATA SUMMARY
Date: March 2,1989
Total number of shots: 540

Velocity (km/sec)	$7.0 \leq V < 8.0^{+}$	61
	$6.0 \leq V < 7.0$	165
	$5.0 \leq V < 6.0$	94
	$4.0 \leq V < 5.0$	103
	$3.0 \leq V < 4.0$	85
	$2.0 \leq V < 3.0$	31
	$1.0 \leq V < 2.0$	1
		540

Diameter (in.)	$0.4 \leq D \leq 0.5$	16
	$0.3 \leq D < 0.4$	218
	$0.2 \leq D < 0.3$	200
	$0.1 \leq D < 0.2$	106
		540

Obliquity (deg.)	0^{o}	337
	15^{o}	1
	25^{o}	1
	30^{o}	11
	45^{o}	128
	55^{o}	3
	60^{o}	10
	65^{o}	44
	75^{o}	5
		540

Configuration	Single Wall	11
	1 Bumper	396
	2 Bumpers	89
	3 Bumpers	6
	4 Bumpers	3
	6 Bumpers	1
	Windows	26
	Bottles	8
		540

Stand-Off Distance (Single Bumper)	4 inches	334
	6 inches	52
	7 inches	1
	8 inches	3
	12 inches	5
	16 inches	1
		396

Miscellaneous	Cadmium Bumpers	10
	Cadmium Projectiles	10
	Composite Bumpers	27
	Corrugated Bumpers	11
	Non-1100 Projectiles	34
	Cylindrical Projectiles	11
	Non-2219 Walls	31

Section 2.5.3

Detailed NASA/MSFC Hypervelocity Impact Test Shot Distribution

as of March 2, 1989

BASELINE PARAMETERS

Pressure Wall Thickness ... 0.125 in.

Stand-Off Distance .... 4.0 in.

Number of Bumper Plates ... 1

Projectile Shape .... Sphere

Projectile Material .... Al 1100

Bumper Plate Material ..... Al 6061-T6

Pressure Wall Material .... Al 2219-T87

Footnotes

[1]Pressure Wall Material ... Al 5456-H116

[2]Projectile Material ...... Al 6061-T6

[3]Backwall Thickness .... 0.188 in.

[4]Projectile Material ...... Al 6061-T6; L/D = 1.0

[5]Bumper Plate Material .... Al 2219-T87

[6]Stand-Off Distance .... 12 in.

[7]Stand-Off Distance .... 6 in.

[8]Projectile Material ...... Steel

[9]Projectile Material ...... Lexan

[10]Stand-Off Distance ...... 8 in.

[11]Cylindrical Projectile

[12]Backwall Thickness ...... 0.175 in.

[13]Backwall Thickness ...... 0.200 in.

[14]Backwall Thickness ...... 0.225 in.

[15]Backwall Thickness ...... 0.160 in.

[16]Backwall Thickness ...... 0.100 in.

[17]Backwall Thickness ...... 0.063 in.

		t_B = 0.080	t_B = 0.063	t_B = 0.040	t_B = 0.032
0.3 < D < 0.4	w/MLI		T2-19B[7]		
	w/o MLI				
0.2 < D < 0.3	w/MLI		P-007 P-008		
	w/o MLI		P-001 P-002 T2-13[11]		
0.1 < D < 0.2	w/MLI		MD-TEST-A MD-TEST-B P-014E[7] P-014F[7] P-015B[7] P-027E P-027F	T2-1	
	w/o MLI	109C 109D	P-015[7] P-025B[2,7] P-025C[2,7]		

		t_B = 0.080	t_B = 0.063	t_B = 0.040	t_B = 0.032
0.3 < D < 0.4	w/MLI			319	
	w/o MLI				
0.2 < D < 0.3	w/MLI		301[15]		
	w/o MLI				
0.1 < D < 0.2	w/MLI			333	
	w/o MLI				

		$t_B = 0.080$	$t_B = 0.063$	$t_B = 0.040$	$t_B = 0.032$
$0.3 < D < 0.4$	w/MLI			203C	
	w/o MLI				
$0.2 < D < 0.3$	w/MLI				
	w/o MLI				
$0.1 < D < 0.2$	w/MLI				
	w/o MLI		231B		

		$t_B = 0.080$	$t_B = 0.063$	$t_B = 0.040$	$t_B = 0.032$
$0.3 < D < 0.4$	w/MLI	102D 229B[3] 229C[3]	P-016M[7] P-016N[7] T2-19A[7] T2-7 T2-7A	T2-5	
$0.3 < D < 0.4$	w/o MLI		T2-8		
$0.2 < D < 0.3$	w/MLI		P-012D P-013E[7] T2-3	T2-14[11]	
$0.2 < D < 0.3$	w/o MLI		PT4A		
$0.1 < D < 0.2$	w/MLI		P-014C[7] P-027C P-027D		
$0.1 < D < 0.2$	w/o MLI	101 101A 109B	P-014[7] P-014B[7] P-014D[7] P-015C[7] P-025[2,7] P-025A[2,7] P-027A P-028	T2-2	

		$t_B = 0.080$	$t_B = 0.063$	$t_B = 0.040$	$t_B = 0.032$
$0.3 < D < 0.4$	w/MLI	321	303A[15] 320		
	w/o MLI	105	114A[2]		114B
$0.2 < D < 0.3$	w/MLI		205E		
	w/o MLI		113A[2]		
$0.1 < D < 0.2$	w/MLI		230B	334	
	w/o MLI		206D 206E	202A 202B 222C	

		$t_B = 0.080$	$t_B = 0.063$	$t_B = 0.040$	$t_B = 0.032$
$0.3 < D < 0.4$	w/MLI				
	w/o MLI		114[2]		
$0.2 < D < 0.3$	w/MLI				
	w/o MLI		113[2]		
$0.1 < D < 0.2$	w/MLI				
	w/o MLI				

		t_B = 0.080	t_B = 0.063	t_B = 0.040	t_B = 0.032
$0.3 < D < 0.4$	w/MLI			203B 203F	
	w/o MLI				
$0.2 < D < 0.3$	w/MLI			224C[4]	
	w/o MLI		208C	204D	
$0.1 < D < 0.2$	w/MLI				
	w/o MLI		231A		

	$t_B = 0.080$	$t_B = 0.063$	$t_B = 0.040$	$t_B = 0.032$	
$0.3 < D < 0.4$					w/MLI
	105B				w/o MLI
$0.2 < D < 0.3$					w/MLI
					w/o MLI
$0.1 < D < 0.2$					w/MLI
					w/o MLI

		$t_B = 0.080$	$t_B = 0.063$	$t_B = 0.040$	$t_B = 0.032$
0.3 < D < 0.4	w/MLI	102C	P-016L[7] P-016P[7] P-020F[7] P-020G[7] p-020H[7] T2-17 T2-19[7]	215A[3]	
0.3 < D < 0.4	w/o MLI	213A[3]	PT8A PT8B T2-20[7] T2-6A	225B[7] 225C[7] PT6A T2-6	
0.2 < D < 0.3	w/MLI		P-012C P-024G[2,7] T2-4 P-034C-1[16]	P-033B	
0.2 < D < 0.3	w/o MLI	213C[3]	PT4B P-003 P-004 P-013[7]	214C[10,3] 214D[10,3]	
0.1 < D < 0.2	w/MLI				
0.1 < D < 0.2	w/o MLI	101B 109A	P-014A P-027 P-027B		

D	MLI	t_B = 0.080	t_B = 0.063	t_B = 0.040	t_B = 0.032
0.3 < D < 0.4	w/MLI	326	303[15] 303B[15] 325	324	
0.3 < D < 0.4	w/o MLI				
0.2 < D < 0.3	w/MLI		205A 205B	201A 335 336	226A[16]
0.2 < D < 0.3	w/o MLI		EHSS-5A[1]		
0.1 < D < 0.2	w/MLI		230A	221C 221D	
0.1 < D < 0.2	w/o MLI		206A		

		t_B = 0.080	t_B = 0.063	t_B = 0.040	t_B = 0.032
0.3 < D < 0.4	w/MLI				
	w/o MLI	105A			
0.2 < D < 0.3	w/MLI				
	w/o MLI				
0.1 < D < 0.2	w/MLI				
	w/o MLI				

		$t_B = 0.080$	$t_B = 0.063$	$t_B = 0.040$	$t_B = 0.032$
$0.3 < D < 0.4$	w/MLI			203A 203G	
	w/o MLI				
$0.2 < D < 0.3$	w/MLI		209A	224B[4]	
	w/o MLI		EHSS-5D[1] 208A 208B	204A 204C	
$0.1 < D < 0.2$	w/MLI				
	w/o MLI		156C		

D	MLI	$t_B = 0.080$	$t_B = 0.063$	$t_B = 0.040$	$t_B = 0.032$
$0.3 < D < 0.4$	w/MLI	102A 102B 229A[3]	MD-TEST-D P-021D P-035C[7]	215B[3] T2-15	
	w/o MLI	213B[3]	P-016[7] T2-18	225A[9] T2-16	228A[3]
$0.2 < D < 0.3$	w/MLI		P-009 P-010 P-013D[7] P-034C-2[16] P-034C[16]	P-033B-1 P-033C	
	w/o MLI	213D[3]	EHSS-2B P-013C[7] P-022[11] P-024C[2,7] P-024F[2,7]	214A[10,3]	
$0.1 < D < 0.2$	w/MLI				
	w/o MLI				

		$t_B = 0.080$	$t_B = 0.063$	$t_B = 0.040$	$t_B = 0.032$
$0.3 < D < 0.4$	w/MLI				
	w/o MLI				
$0.2 < D < 0.3$	w/MLI				
	w/o MLI		135A		
$0.1 < D < 0.2$	w/MLI				
	w/o MLI		162B		

		t_B = 0.080	t_B = 0.063	t_B = 0.040	t_B = 0.032
0.3 < D < 0.4	w/MLI		211B	218A[3]	
	w/o MLI	216A[3]			
0.2 < D < 0.3	w/MLI		205C	201B 223C[4] 336A	226B[16] 227A[17]
	w/o MLI		EHSS-4C[1] 230C 230D		
0.1 < D < 0.2	w/MLI			221B	
	w/o MLI		206B 206C	154B 202C 222A 222B	

		$t_B = 0.080$	$t_B = 0.063$	$t_B = 0.040$	$t_B = 0.032$
$0.3 < D < 0.4$	w/MLI		207A 210B	203D	
	w/o MLI				
$0.2 < D < 0.3$	w/MLI				
	w/o MLI		EHSS-5C[1] 208D	204B	
$0.1 < D < 0.2$	w/MLI				
	w/o MLI		156B		

		t_B = 0.080	t_B = 0.063	t_B = 0.040	t_B = 0.032
0.3 < D < 0.4	w/MLI		EH2-B EH2-C EH2-D EH2-E EH4-A PR-EH2[5] P-016J[7] P-016K[7] P-021B P-021C P-035B[7] EH4-B	215C[3] 215D[3]	
0.3 < D < 0.4	w/o MLI	107[12] 107A[13] 107B[14] 108[6] 121-1[7] 121-2[7]	EH3-A EHSS-6A[1] EHSS-6B[1] EHSS-6C P-016A[7] P-016B[7] P-016C[7] P-016E[7] P-020B[7] P-020C[7] P-021 P-021A P-035[7]	225D-1[9,11]	228B[3]
0.2 < D < 0.3	w/MLI		P-011 P-012B P-022A[11]		
0.2 < D < 0.3	w/o MLI		EHSS-1A[1] EHSS-1B[1] EHSS-1C[1] EHSS-2A P-005 P-006A P-013B[7] P-022B[11] P-034[16]		228C[3] 228D[3]
0.1 < D < 0.2	w/MLI				
0.1 < D < 0.2	w/o MLI		146A[8]		

		t_B = 0.080	t_B = 0.063	t_B = 0.040	t_B = 0.032
$0.3 < D < 0.4$	w/MLI				
	w/o MLI				
$0.2 < D < 0.3$	w/MLI				
	w/o MLI		EHSS-3A[1] EHSS-3C 135C 135D		
$0.1 < D < 0.2$	w/MLI				
	w/o MLI		162A		

		$t_B = 0.080$	$t_B = 0.063$	$t_B = 0.040$	$t_B = 0.032$
$0.3 < D < 0.4$	w/MLI	001B	002B 211D 212B 306[15]	003A 218B[3] 218C[3] 337 339	
	w/o MLI	106 216B[3] 216C[3]	EHRP-3[1] EHSS-7A[1] 002A	217A[3]	
$0.2 < D < 0.3$	w/MLI		205D	223A[4] 223B[4]	226C[16]
	w/o MLI	151A	EHSS-4A[1] EHSS-4B[1] 230E	217C[3] 217D[3]	
$0.1 < D < 0.2$	w/MLI			221A	
	w/o MLI		206F	154A 202D	

		$t_B = 0.080$	$t_B = 0.063$	$t_B = 0.040$	$t_B = 0.032$
$0.3 < D < 0.4$	w/MLI				
$0.3 < D < 0.4$	w/o MLI	106A 106-1	EHRP-1[1]		
$0.2 < D < 0.3$	w/MLI				
$0.2 < D < 0.3$	w/o MLI				
$0.1 < D < 0.2$	w/MLI				
$0.1 < D < 0.2$	w/o MLI				

		$t_B = 0.080$	$t_B = 0.063$	$t_B = 0.040$	$t_B = 0.032$
$0.3 < D < 0.4$	w/MLI	004A	207B 210D	203E	
	w/o MLI		EHRP-2[1] 231C		
$0.2 < D < 0.3$	w/MLI		209B	224A[4]	
	w/o MLI		208E		
$0.1 < D < 0.2$	w/MLI				
	w/o MLI				

		$t_B = 0.080$	$t_B = 0.063$	$t_B = 0.040$	$t_B = 0.032$
$0.3 < D < 0.4$	w/MLI				
	w/o MLI	106B 106-2			
$0.2 < D < 0.3$	w/MLI				
	w/o MLI				
$0.1 < D < 0.2$	w/MLI				
	w/o MLI				

		$t_B = 0.080$	$t_B = 0.063$	$t_B = 0.040$	$t_B = 0.032$
$0.3 < D < 0.4$	w/MLI		EH2-A PR-EH1[5] P-016H[7]		
	w/o MLI	102 110	P-016G[7] P-017		
$0.2 < D < 0.3$	w/MLI				
	w/o MLI		P-018RV[7] P-034B[16]	P-033	
$0.1 < D < 0.2$	w/MLI				
	w/o MLI	109	146B[8]		

		$t_B = 0.080$	$t_B = 0.063$	$t_B = 0.040$	$t_B = 0.032$
$0.3 < D < 0.4$	w/MLI				
	w/o MLI		EH1A		
$0.2 < D < 0.3$	w/MLI				
	w/o MLI		EHSS-3B[1] 135B 135E		
$0.1 < D < 0.2$	w/MLI				
	w/o MLI				

		t_B = 0.080	t_B = 0.063	t_B = 0.040	t_B = 0.032
0.3 < D < 0.4	w/MLI			338	
0.3 < D < 0.4	w/o MLI		EHSS-7B[1] EH1B	217B[3]	
0.2 < D < 0.3	w/MLI			201C 201D	227B[17]
0.2 < D < 0.3	w/o MLI		EHRP-6[1] 150A	217E[3]	
0.1 < D < 0.2	w/MLI				
0.1 < D < 0.2	w/o MLI		EHRP-8 155A	202E 202F	

		$t_B = 0.080$	$t_B = 0.063$	$t_B = 0.040$	$t_B = 0.032$
$0.3 < D < 0.4$	w/MLI				
	w/o MLI		EH1C		
$0.2 < D < 0.3$	w/MLI				
	w/o MLI		EHRP-4[1]		
$0.1 < D < 0.2$	w/MLI				
	w/o MLI		EHRP-7 157A		

		$t_B = 0.080$	$t_B = 0.063$	$t_B = 0.040$	$t_B = 0.032$
$0.3 < D < 0.4$	w/MLI		207C		
	w/o MLI		231D		
$0.2 < D < 0.3$	w/MLI		209D		
	w/o MLI		EHRP-5[1]		
$0.1 < D < 0.2$	w/MLI				
	w/o MLI		EHRP-9 156A		

		$t_B = 0.080$	$t_B = 0.063$	$t_B = 0.040$	$t_B = 0.032$
$0.3 < D < 0.4$	w/MLI				
	w/o MLI		EHSS-8A[1] EH1D		
$0.2 < D < 0.3$	w/MLI				
	w/o MLI				
$0.1 < D < 0.2$	w/MLI				
	w/o MLI				

Section 2.5.4

Gaps in NASA/MSFC Hypervelocity Impact Test Database

as of March 2, 1989

NOTATION KEY

L) ... $0.3 < D < 0.4$
M) ... $0.2 < D < 0.3$
S) ... $0.1 < D < 0.2$

VEL .... impact velocity range in km/sec

NO SHOTS ... no tests have been performed in that velocity range at any bumper thickness

X SHOTS AT t = .yyy .... x tests have been performed at bumper thickness t = .yyy in.; no other tests in that velocity range have been performed at any other bumper thickness

NO SHOTS AT t = .yyy ... no tests have been performed at bumper thickness t = .yyy in.; other thicknesses have been used in testing

XXXXX ... full range of testing performed in this velocity range for this projectile size

NORMAL SHOTS		
VEL	W/MLI	W/O MLI
2-3	L)1 SHOT AT t = .063 M)2 SHOTS AT t = .063 S)NO SHOTS AT t= .080 & 0.32	L)NO SHOTS M)2 SHOTS AT t = .063 S)NO SHOTS AT t = .040 & .032
3-4	L)NO SHOTS AT t = .032 M)NO SHOTS AT t = .080 & .032 S)3 SHOTS AT t = .063	L)1 SHOT AT t = .063 M)2 SHOTS AT t = .063 S)NO SHOTS AT t = .032
4-5	L)NO SHOTS AT t = .032 M)NO SHOTS AT t = .080 & .032 S)NO SHOTS	L)NO SHOTS AT t = .032 M)NO SHOTS AT t = .032 S)NO SHOTS AT t = .040 & .032
5-6	L)NO SHOTS AT t = .032 M)NO SHOTS AT t = .80 & .032 S)NO SHOTS	L) XXXXX M)NO SHOTS AT t = .032 S)NO SHOTS
6-7	L)NO SHOTS AT t = .080 & .032 M)3 SHOTS AT t = .063 S)NO SHOTS	L) XXXXX M)NO SHOTS AT t = .080 S)1 SHOT AT t = .063
7-8	L)3 SHOTS AT t = .063 M)NO SHOTS S)NO SHOTS	L)NO SHOTS AT t = .040 & .032 M)NO SHOTS AT t = .080 & .032 S)NO SHOTS AT t = .040 & .032

OBLIQUE SHOTS 30 DEG		
VEL	W/MLI	W/O MLI
2-3	L)NO SHOTS M)NO SHOTS S)NO SHOTS	L)NO SHOTS M)NO SHOTS S)NO SHOTS
3-4	L)NO SHOTS M)NO SHOTS S)NO SHOTS	L)NO SHOTS M)NO SHOTS S)NO SHOTS
4-5	L)NO SHOTS M)NO SHOTS S)NO SHOTS	L)NO SHOTS M)NO SHOTS S)NO SHOTS
5-6	L)NO SHOTS M)NO SHOTS S)NO SHOTS	L)NO SHOTS M)1 SHOT AT t = .063 S)1 SHOT AT t = .063
6-7	L)NO SHOTS M)NO SHOTS S)NO SHOTS	L)NO SHOTS M)4 SHOTS AT t = .063 S)1 SHOT At t = .063
7-8	L)NO SHOTS M)NO SHOTS S)NO SHOTS	L)1 SHOT AT t = .063 M)3 SHOTS AT t = .063 S)NO SHOTS

OBLIQUE SHOTS 45 DEG		
VEL	W/MLI	W/O MLI
2-3	L)1 SHOT AT t = .040 M)1 SHOT AT t = .063 S)1 SHOT AT t = .040	L)NO SHOTS M)NO SHOTS S)NO SHOTS
3-4	L)NO SHOTS AT t = .040 & .032 M)1 SHOT AT t = .063 S)NO SHOTS AT t = .080 & .032	L)NO SHOTS AT t = .040 M)1 SHOT AT t = .063 S)NO SHOTS AT t = .080 & .032
4-5	L)NO SHOTS AT t = .032 M)NO SHOTS AT t = .080 S)NO SHOTS AT t = .080 & .032	L)NO SHOTS M)1 SHOT AT t = .063 S)1 SHOT AT t = .063
5-6	L)NO SHOTS AT t = .080 & .032 M)NO SHOTS AT t = .080 S)1 SHOT AT t = .040	L)1 SHOT AT t = .063 M)3 SHOTS AT t = .063 S)NO SHOTS AT t = .080 & .032
6-7	L)NO SHOTS AT t = .032 M)NO SHOTS AT t = .080 S)1 SHOT AT t = .040	L)NO SHOTS AT t = .032 M)NO SHOTS AT t = .032 S)NO SHOTS AT t = .080 & .032
7-8	L)1 SHOT AT t = .040 M)NO SHOTS AT t = .080 & .063 S)NO SHOTS	L)NO SHOTS AT t = .080 & .032 M)NO SHOTS AT t = .080 & .032 S)NO SHOTS AT t = .080 & .032

OBLIQUE SHOTS 60 DEG		
VEL	W/MLI	W/O MLI
2-3	L)NO SHOTS M)NO SHOTS S)NO SHOTS	L)NO SHOTS M)NO SHOTS S)NO SHOTS
3-4	L)NO SHOTS M)NO SHOTS S)NO SHOTS	L)1 SHOT AT t = .063 M)1 SHOT AT t = .063 S)NO SHOTS
4-5	L)NO SHOTS M)NO SHOTS S)NO SHOTS	L)1 SHOT AT t = .080 M)NO SHOTS S)NO SHOTS
5-6	L)NO SHOTS M)NO SHOTS S)NO SHOTS	L)NO SHOTS M)NO SHOTS S)NO SHOTS
6-7	L)NO SHOTS M)NO SHOTS S)NO SHOTS	L)NO SHOTS AT t = .040 & .032 M)NO SHOTS S)NO SHOTS
7-8	L)NO SHOTS M)NO SHOTS S)NO SHOTS	L)1 SHOT AT t = .063 M)1 SHOT AT t = .063 S)2 SHOTS AT t = .063

OBLIQUE SHOTS 65 DEG		
VEL	W/MLI	W/O MLI
2-3	L)1 SHOT AT t = .040 M)NO SHOTS S)NO SHOTS	L)NO SHOTS M)NO SHOTS S)1 SHOT AT t = .063
3-4	L)2 SHOTS AT t = .040 M)1 SHOT AT t = .040 S)NO SHOTS	L)NO SHOTS M)NO SHOTS AT t = .080 & .032 S)1 SHOT AT t = .063
4-5	L)2 SHOTS AT t = .040 M)NO SHOTS AT t = .080 & .032 S)NO SHOTS	L)NO SHOTS M)NO SHOTS AT t = .080 & .032 S)1 SHOT AT t = .063
5-6	L)NO SHOTS AT t = .080 & .032 M)NO SHOTS S)NO SHOTS	L)NO SHOTS M)NO SHOTS AT t = .080 & .032 S)1 SHOT AT t = .063
6-7	L)NO SHOTS AT t = .032 M)NO SHOTS AT t = .080 & .032 S)NO SHOTS	L)2 SHOTS AT t = .063 M)1 SHOT AT t = .063 S)NO SHOTS
7-8	L)1 SHOT AT t = .063 M)1 SHOT AT t = .063 S)NO SHOTS	L)1 SHOT AT t = .063 M)1 SHOT AT t = .063 S)2 SHOTS AT t = .063

OBLIQUE SHOTS 75 DEG		
VEL	W/MLI	W/O MLI
2-3	L)NO SHOTS M)NO SHOTS S)NO SHOTS	L)NO SHOTS M)NO SHOTS S)NO SHOTS
3-4	L)NO SHOTS M)NO SHOTS S)NO SHOTS	L)1 SHOT AT t = .080 M)NO SHOTS S)NO SHOTS
4-5	L)NO SHOTS M)NO SHOTS S)NO SHOTS	L)NO SHOTS M)NO SHOTS S)NO SHOTS
5-6	L)NO SHOTS M)NO SHOTS S)NO SHOTS	L)NO SHOTS M)NO SHOTS S)NO SHOTS
6-7	L)NO SHOTS M)NO SHOTS S)NO SHOTS	L)2 SHOTS AT t = .080 M)NO SHOTS S)NO SHOTS
7-8	L)NO SHOTS M)NO SHOTS S)NO SHOTS	L)2 SHOTS AT t = .063 M)NO SHOTS S)NO SHOTS

SECTION THREE -- HYPERVELOCITY IMPACT OF DUAL-WALL STRUCTURES

3.1 Introduction

In this Section, an overview of the various processes associated with the normal and oblique hypervelocity impact of dual-wall structures is presented and discussed. Included in this discussion are the results of an in-depth investigation of the effects of geometric (e.g. plate thicknesses, and spacing) and impact (e.g. projectile diameter, trajectory, and velocity) parameters on the penetration resistance of dual-wall structures under high-speed projectile impact. This investigation was performed using the information contained in the Damage Mechanism Database described in the previous Section. For additional information on the effects of bumper thickness, spacing, pressure wall thickness, bumper material, pressure wall material, etc., the reader is referred to the References in Sections 1.3 and 3.4.

A total of 396 test specimens were analyzed in the study of dual-wall structures under normal and oblique hypervelocity impact. In all of the tests, the bumper plate and pressure wall plate materials were aluminum 6061-T6 and 2219-T87, respectively; projectile materials used in the testing were aluminum 1100-0 and 6061-T6. Projectile diameters ranged from 3.175 to 12.7 mm; impact velocities ranged from 2 to 8 km/sec. The thicknesses of the bumper plates used in the test program were 0.8, 1.016, 1.6, and 2.032 mm; the pressure wall thicknesses were 1.6, 2.54, 3.175, 4.064, and 4.775 mm. Two stand-off distances were used: 10.16 and 15.24 cm. In the oblique impact tests, projectiles were fired at trajectory obliquities of 30^{o}, 45^{o}, 55^{o}, 60^{o}, 65^{o}, and 75^{o}.

The results of the analyses performed are presented in two forms: penetration and spall functions, and empirical predictor equations that were derived through a linear multiple regression analysis of the damage data. Figures 3.2 through 3.5, and Figures 3.6, 3.7 present penetration and spall functions, respectively, for dual-wall structures under normal hypervelocity impact. Figures 3.9 through 3.13 and Figures 3.14, 3.15 present penetration and spall functions, respectively, for oblique impacts. Finally, Figures 3.16 through 3.21 present a comparison of the predictions of the empirical equations with the experimental data.

While hypervelocity impact tests were performed with a variety of geometric and impact parameters, occasionally an insufficient number of tests were performed for a necessary range of parameter values. For example, if a series of tests was performed using a certain bumper thickness, stand-off distance, pressure wall thickness, and trajectory obliquity, and if the pressure walls were perforated in all of the tests in the series over the range of projectile diameters and velocities considered, then, because it is not known what projectile diameter-velocity combinations would not perforate the pressure walls, it would be impossible to draw a penetration function for that test series. A specific example is Test Series No. 216 (t_s=1.6 mm, t_w=3.175 mm, S=10.16 cm, θ=45^o) in which all three tests had perforated pressure wall plates. As a result, a complete set of penetration and spall functions for all the geometric configurations used during the test program could not be constructed; penetration and spall functions are presented only for data sets for which such curves could legitimately be drawn. In those cases where penetration and/or spall functions could not be drawn, test-by-test comparisons had to be performed. Although it would be impractical to present the details of each comparative analysis, observations made from such analyses of the data are included in the discussions of hypervelocity impact phenomena that follow in this Section.

Regression analyses were performed on the following dual-wall system damage data: bumper plate hole dimensions, debris cloud trajectory angles, debris cloud cone angles, pressure wall front surface damage area, pressure wall rear surface spall area (in the event of spall), and pressure wall hole diameter (in the event of perforation). Empirical predictor equations are presented in this Section for these quantities for aluminum dual-wall systems under high-speed spherical projectile impact. The results of additional regression analyses for dual-wall systems with composite bumpers, window systems, dual-wall structures under cylindrical projectile impact, and impact of multi-bumper systems are presented in subsequent Sections of this Final Report. Furthermore, since normal impact is a special case of oblique impact, no equations were derived purely for normal impact. Equations for normal impact can be obtained simply by setting $\theta=0^{\circ}$ in the oblique impact equations. As such, all of the regression equations are presented in the sub-section on oblique hypervelocity impact phenomena.

3.2 Penetration Phenomena Associated With Normal Hypervelocity Impacts

Consider the normal hypervelocity impact of a spherical projectile on the structure shown in Figure 3.1. The structure consists of two walls: a 'pressure wall plate', which is the main wall of the structure, and a protective 'bumper plate', which is traditionally a relatively thin layer of material that is placed at a relatively small distance away from the pressure wall plate. The protection of the pressure wall against perforation is afforded by the bumper plate through the disintegration of the impacting projectile and the creation of a diffuse debris particle cloud which, in the velocity range tested, imparts a significantly lower impulse to the pressure wall. Previous investigations (see References in Section 1.3) have shown that the combined mass of the bumper plate and the pressure wall required to prevent pressure wall perforation is typically much less than that required for a pressure wall without a bumper plate. Although not shown in Figure 3.1, a blanket of multi-layer insulation is often placed on the pressure wall of the dual-wall structure for thermal protection purposes. Under certain impact conditions, this multi-layer insulation (MLI) can increase the protection afforded to the pressure wall plate by absorbing the kinetic energy of the smaller and slower particles of the debris particle cloud. However, for very large particles traveling at high speeds which the bumper is unable to shatter completely, the presence of MLI on the pressure wall can prove to be disastrous and can result in severe petalling of the pressure wall plate.

In the case of space debris particles and meteoroids, impact velocities are on the order of 10 and 20 km/sec, respectively. Upon impact at these velocities, strong shock waves are propagated through both the impacting particle and the impacted bumper plate. The pressures associated with these shocks typically exceed the strengths of the projectile and bumper plate materials, which causes them to fragment, melt, or vaporize, depending on material properties, geometric parameters, and the impact velocity. Geometric factors that can affect the response of a projectile/target system include the size and shape of the impacting projectile, the thickness of the bumper plate, and the angle of impact relative to the bumper plate surface normal. For each set of particle impact parameters, there exists an ideal bumper design that will efficiently break up the particle to prevent penetration of the pressure wall. Because of the intense pressures generated in a hypervelocity impact, material strength ceases to be an important factor in determining material response. The resulting hole in the bumper plate is typically several times larger than the diameter of the impacting projectile.

As the shock waves propagate, the projectile and target materials are heated adiabatically and non-isentropically. However, the release of the shock pressures occurs isentropically through the action of rarefaction waves that are created as the shock waves interact with projectile and target free surfaces. This process leaves the projectile and target materials in high energy states which can cause either or both to melt or vaporize, partially or completely. As the velocity increases, the shock heating increases and, in turn, improves the performance of the bumper plate. This partially explains why micro-meteoroid impacts that occur at very high velocities (on the order of 20 to 50 km/sec) are potentially less lethal from a penetration standpoint than the space debris particle impacts, which occur at lower velocities (on the order of 10 to 12 km/sec). The lower average density of meteoroid particles also contributes to their lesser lethality (0.5 gm/cm^3 as compared to 2.8 gm/cm^3 for orbital debris particles).

When the projectile and a portion of the bumper shield are fragmented, melted, or vaporized, a secondary debris cloud is created. This debris cloud travels towards and impacts the pressure wall plate. However, the impacts of the debris particles will be distributed over a large area of the pressure wall which will result in a reduction of the pressure impulse on the pressure wall plate. The area over which the load impulse is distributed on the pressure wall is governed by the manner in which the projectile and bumper plate fragment, melt, or vaporize, and by the spacing between the bumper plate and the pressure wall.

It is important to note that spallation of the rear surface of the pressure wall may occur with or without pressure wall penetration if the rarefaction stress near the rear surface exceeds the dynamic tensile fracture strength of the pressure wall material. This spallation could result in ejecta that can travel at high velocities and can damage internal spacecraft mission systems as well as life support systems. Although the depth of spall can be, theoretically, up to 50% of the plate thickness, the depths of spall in thin plates such as those used in dual-wall systems are typically 10% to 25% of the plate thickness.

In the following sub-sections, the effects of individual dual-wall system parameters on the response of the system under hypervelocity projectile impact are discussed in more detail. Unless otherwise noted, the MLI was taped to the side of the pressure wall facing the bumper plate and consisted of 30 layers of 0.5 mil kapton aluminized on one side and 29 layers of Dacron mesh, one layer between each kapton layer. Additionally, 1 layer of beta-cloth (coated s-glass) was added on the side nearest the bumper plate for durability. The areal density of this combination was calculated to be approximately 0.107 gm/cm^2 [3.38]. It is also noted that in Figures 3.2 through 3.7 and 3.9 through 3.15, the penetration and spall functions are simply lines of demarcation between regions of penetration or spall (above) and regions of no-penetration or no-spall (below). In addition, while penetrations functions are presented for dual-wall systems with and without MLI, spall functions are presented only for systems without MLI. It was found that placing MLI on the side of the pressure wall facing the bumper plate significantly reduced the tendency for rear-side spallation to occur. Out of the approximately 200 hypervelocity impact tests performed with MLI, rear-side spallation of the pressure wall plate was observed in only 9 of these tests.

3.2.1 Effect of Bumper Thickness

Under normal impact, dual-wall systems with thinner bumper plates (t_s=1.016 mm or t_s=0.8 mm) exhibited more frequent and more severe pressure wall plate perforations (ie. larger hole sizes) than did dual-wall systems with thicker bumper plates (ie. t_s=1.6 mm or t_s = 2.032 mm). However, by comparing the penetration functions in Figure 3.2 and 3.3, it can be seen that changing the thickness of the bumper plate from 1.6 mm to 2.032 mm while keeping all other geometric parameters constant did not significantly affect the penetration function or level of protection afforded to the pressure wall plate. An examination of the spall functions in Figure 3.6 reveals that, for a spacing of 10.16 cm and a pressure wall thickness of 3.175 mm, the likelihood of rear-side spallation of dual-wall systems with a bumper thickness of 1.6 mm is very similar to that of dual-wall systems with bumper thickness of 1.016 mm.

3.2.2 Effect of Pressure Wall Thickness

As expected, increasing the thickness of the pressure wall while keeping all other geometric parameters constant increased the penetration resistance of the dual-wall structure. This can be seen by noting the relative positions of the penetration functions in Figure 3.5 for the different pressure wall thicknesses. The higher position of the penetration function for the thicker pressure wall plate indicates resistance to perforation by projectile diameter-velocity combinations that would perforate the thinner pressure wall. However, increasing the pressure wall thickness was found to increase the tendency of the rear side of the pressure wall to undergo spallation. As the pressure wall plate thickness is increased, past a certain thickness the debris cloud particles cannot penetrate deep enough into the pressure wall and connect with the rear-side spallations to cause perforation of the plate. As a result, the plate is cratered on the front surface and remains spalled on the rear surface. Naturally, if the pressure wall thickness were to continue to increase, the amount of rear-side spallation would decrease until only a dimple would remain on the rear surface of the plate.

3.2.3 Effect of Stand-Off Distance

It was found that increasing the stand-off distance resulted in an increase in the penetration resistance of the dual-wall structure (compare Figure 3.4 with Figure 3.3). This is also to be expected because the larger the stand-off distance, the more spread out the secondary debris cloud will become before it impacts the pressure wall plate. As a result, the impulsive loading it delivers to the pressure wall will be more diffuse and less likely to cause perforation. In the dual-wall systems without MLI, increasing the stand-off distance also increased the frequency with which pressure wall plates exhibited rear-side spallation with and without penetration. However, by comparing the spall function for t_s=1.6 mm in Figure 3.7 with that for t_s=1.6 mm in Figure 3.6 reveals that increasing the stand-off distance from 10.16 cm to 15.24 cm did not significantly affect the likelihood of rear-side spallation. This implies that there are certain bumper thicknesses that possess similar levels of efficiency in fragmenting an impacting projectile and in creating secondary debris particles whose impacts on the pressure wall cannot induce significant damage in the way of rear-side spallation.

3.2.4 Effect of MLI

In dual-wall structures without MLI, the craters are contained in a circular area on the pressure wall plate directly below the hole in the bumper plate. Perforation of the pressure wall plate is usually in the form of a single central hole or several small holes scattered throughout the damage area. In the systems with MLI on the pressure wall in which pressure wall plate perforation does not occur, the pressure wall contains a central bulge with only a minimal amount of cratering. If perforation of the pressure wall does occur, it is usually in the form of a single hole that is accompanied by petals which, depending on the impact parameters, can be anywhere from 2 cm to 15 cm long.

The penetration functions for dual-wall systems with MLI always lay above those for dual-wall structures without MLI (see Figures 3.2 and 3.4). The area between the two curves represents those diameter-velocity combinations that would penetrate the pressure wall plates of dual-wall systems without MLI but not those of similar dual-wall systems with MLI. However, under normal impact, the holes in perforated pressure wall plates in dual-wall systems with MLI against the pressure wall were often much larger than those in similar systems without MLI. This was found to be especially true in normal impacts by projectile with diameters exceeding 0.795 cm and traveling at speeds faster than 6.5 km/sec.

3.3 Penetration Phenomena Associated With Oblique Hypervelocity Impacts

It has become increasingly evident that most meteoroid or space debris impacts will not occur normal to the surface of a spacecraft [3.8]. The response of a dual-wall structure to oblique hypervelocity projectile impact can be significantly different from its response to normal hypervelocity impact. Unlike normal high-speed impacts, oblique impacts can produce a tremendous volume of ricochet debris particles. These ricochet particles can severely damage panels of instrumentation units located on the exterior of a structure. Obliquity effects, therefore, must be considered in the design of any space or aerospace structure structure that will be exposed to a hazardous debris environment.

Naturally, some of the response characteristics described in the previous sub-Section on normal hypervelocity impact apply to the case of oblique impact as well. These include the fragmentation, melt, or vaporization of the projectile and the bumper shield upon impact, the creation of secondary projectile and bumper fragments, the impact and possible perforation of the pressure wall by debris clouds containing these fragments, and the possibility of spallation occurring on the rear surface of the pressure wall plate. However, there are certain response characteristics that appear in an oblique impact that do not exist in a normal impact. For example, in the oblique impact of a dual-wall structure, some of the secondary debris fragments that are created during the impact of the projectile on the bumper are sprayed on the pressure wall while some fragments ricochet and travel away from the dual-wall structure. In Figure 3.8, the angles θ_1 and θ_2 denote the trajectories of the centers-of-mass of the 'normal' and 'in-line' penetration fragments, respectively; the angles γ_1 and γ_2 represent the spread of these fragments. The angle α_c and α_{99} characterize the trajectory of the center-of-mass of the ricochet debris fragments and the spread of these fragments, respectively. The impacts of the secondary debris particles created 'normal' and 'in-line' damage areas A_{d1} and A_{d2}, respectively, on the front surface of the pressure wall. Occasionally, the impacts of the secondary bumper and projectile fragments resulted in the creation of thin spall fragments that are ejected from the rear side of the pressure wall plate. In these cases, the total area of rear-side spall is denoted by A_s. The following paragraphs summarize trends that were observed during the analysis of damaged and perforated dual-wall systems under oblique high-speed impact.

3.3.1 Response of Bumper Plate Under Oblique Impact

Consider a dual-wall structure that is impacted by a projectile that is traveling along a trajectory that is inclined with respect to the outward normal of the outer wall (Figure 3.8). As in the case of normal impact, the projectile and a portion of the bumper are shattered upon impact which creates a hole in the bumper plate. The size of the hole depends on the material and geometric parameters of the projectile and the bumper as well as the impact velocity and the trajectory obliquity. As the trajectory obliquity is increased from 0^o (normal impact) to 90^o (grazing impact), the hole in the bumper plate becomes increasingly elliptical. The major axis of the elliptical hole lies along the projection of the particle trajectory on the bumper plate. As the trajectory is increased above 60^o or 65^o, the leading edge of the hole becomes jagged. This indicates that some tearing and cracking of the bumper plate occurs at large trajectory obliquities.

3.3.2 Response of Pressure Wall Under Oblique Impact

3.3.2.1 Effect of Impact Obliquity

In the case of normal impacts, ie. when the impact obliquity was 0°, the 'normal' and 'in-line' debris clouds overlapped to form a single damage area on the pressure wall. As the trajectory obliquity began to deviate from 0°, three distinct impact regimes became apparent. In the 'low obliquity regime' (ie. $0^{\circ}<\theta<45^{\circ}$), there was extensive damage to the pressure wall; only a minimal amount of ricochet debris was created in this impact regime. The pressure wall penetration and crater damage strongly resembled that which results from a normal impact, and the trajectories of the debris cloud fragments were very close to the original impact trajectory.

In the 'medium obliquity regime' (ie. $45^{\circ}<\theta<60^{\circ}$), two distinct areas of damage became discernible on the pressure wall. The 'normal' damage area consisted of round holes and craters caused by bumper fragment impact and lay fairly close to the inward-pointing normal drawn from the center of impact to the pressure wall. The 'in-line' damage area contained oval holes and craters caused by projectile fragment impact and lay near the point of intersection of the original impact trajectory and the pressure wall plate. As the obliquity was increased, the locations of both damage areas moved closer to the inward-pointing bumper normal. Up to a certain 'critical angle of impact obliquity', the pressure wall exhibited significant penetration and perforation damage and a relatively small amount of ricochet debris was created. However, as the impact trajectory obliquity was increased past the critical angle, an increasing amount of ricochet debris was formed while the amount of damage sustained by the pressure wall decreased dramatically. This critical angle is estimated to have a value between 60° and 65°; it signifies the onset of the 'high obliquity regime'.

In the 'high obliquity regime' (ie. $65^{\circ}<\theta<90^{\circ}$), a tremendous amount of ricochet debris was created while only a relatively small quantity of penetration debris was formed. It is also noted that there was a much lower tendency for rear-side spall of the pressure wall plate in this regime than in all the others. This can be seen by comparing the location of the spall function for t_s=1.6mm in Figure 3.15 ($\theta=65^{\circ}$) with the location of the corresponding spall functions in Figure 3.14 ($\theta=45^{\circ}$) and in Figure 3.6 ($\theta=0^{\circ}$). It is seen that the location of the spall function for $\theta=65^{\circ}$ is 'higher' than the other two, indicating an marked decrease in the occurrence of rear-side spallation at high impact obliquities.

Finally, below 30° and above 65° there was significant overlapping of the 'normal' and 'in-line' secondary debris clouds. At intermediate obliquities, whether or not there was any separation of the debris clouds depended on the original impact parameters and the material and geometric parameters of the bumper plate. It is interesting to note that in the case of low trajectory obliquity, the overlapping of the debris clouds concentrated the debris into a much smaller volume and thereby increased the damage potential of the secondary debris particles. However, in the high obliquity regime, because so few penetration debris particles were created, the overlapping of the debris clouds did not contribute significantly to their damage potential.

3.3.2.2 Effect of Bumper Thickness

Examination of Figures 3.10 and 3.11 reveals that in the low obliquity impact regime, a thinner bumper plate (e.g. t_s=1.016 mm) provided less protection to the pressure wall of the dual-wall systems than did a thicker bumper plate (e.g. t_s=1.6 mm). In contrast, in the high obliquity regime, thinner bumper plates provided more protection to the pressure wall of a dual-wall system than did thicker plates. Thus, it would appear that thicker bumper plates provide better perforation resistance at low impact angles (ie. $\theta<60^o$) while thinner bumper plates provide better perforation resistance at high impact angles (ie. $\theta>65^o$). It is interesting to note that the change in bumper thickness required for optimum performance of the bumper also occurs at the 'critical angle of impact obliquity', that is, between 60^o and 65^o.

The difference in the bumper thicknesses required for optimum performance at different impact angles is due to the fact that the phenomena involved in a hypervelocity impact are governed by the normal component of the particle impact velocity. For a given impact velocity, at a low impact angle, the normal component of the impact velocity is higher than that at a high impact angle. Therefore, for a given projectile diameter and impact velocity, the shock pressures generated at a low impact angle will be higher than those generated at a high impact angle. This implies that, at a low impact angle, the projectile must interact with the bumper plate for a longer period of time than at a high impact angle in order for it to be completely destroyed. At a low impact angle, if the bumper were too thin, then the projectile would pass through the bumper relatively unscathed. Conversely, at a high impact angle, if the bumper were too thick (but not thick enough to prevent perforation by the projectile), then it would simply fragment into several relatively large, slow moving fragments. These large, low-speed fragments pose more of a threat to the pressure wall plate than do the small, high-speed particles that are created in a high-obliquity impact.

3.3.2.3 Effect of Pressure Wall Thickness

As in the case of normal impact, increasing the thickness of the pressure wall while keeping all other geometric parameters constant increased the penetration resistance of the dual-wall structure. This can be seen by noting the relative positions of the penetration functions in Figure 3.13 for the different pressure wall thicknesses. The higher position of the penetration function for the thicker pressure wall plate indicates resistance to perforation by projectile diameter-velocity combinations that would perforate the thinner pressure wall.

3.3.2.4 Effect of Stand-Off Distance

Unfortunately, no oblique impact tests were conducted at stand-off distances other than 10.16 cm. However, it is expected that as in the case of normal impact, increasing the stand-off distance would result in an increase in the penetration resistance of a dual-wall structure.

3.3.2.5 Effect of MLI

An analysis of the obliquely-impact damaged dual-wall systems revealed that, as in the case of normal impact, placing MLI on the pressure wall plate increased the penetration resistance of the dual-wall structures (note and compare the penetration functions in Figure 3.10 and 3.11). This was found to be true for all three impact regimes. However, unlike normal impact, severe petalling did not accompany perforation of the pressure wall plate, even at velocities above 6.5 km/sec.

3.3.3 Analysis of Ricochet Debris

A statistical analysis of the extent of the damage on the ricochet witness plates in the impacted dual-wall specimens revealed that, regardless of original projectile size, speed, and obliquity, 99% of the damage to the ricochet witness plates occurred within an angle of 30^{o} with respect to the plane of the bumper plate, that is, $\alpha_{99} = 30^{o}$. The trajectory of the center-of-mass of the ricochet debris cloud was typically at an angle of 8^{o} with respect to the plane of the bumper plate, that is, $\alpha_c = 8^{o}$. This indicates that the majority of the ricochet debris fragments are concentrated within an angle of approximately 15^{o} with respect to the plane of the bumper plate. Such a strong concentration of high speed particles is extremely dangerous if critical external spacecraft subsystems happen to be located in the path of the ricochet debris cloud.

An analysis of ricochet witness plate crater damage revealed several interesting features of ricochet debris particles. First, high obliquity impacts and impacts by large projectiles produce larger ricochet debris particles than do impacts at low obliquities or impacts by spall projectiles. In other words, the severity of the ricochet damage is directly related to the trajectory obliquity and size of the original projectile. Second, an average ricochet debris particle can have a diameter as large as 40% of the original projectile diameter and can travel at speeds up to 36% of the original impact velocity. The details of the analyses performed to arrive at these conclusions may be found in Reference 3.39.

3.4 Regression Analysis of Damage Data

3.4.1 Bumper Plate Hole Dimensions

In order to be able to predict the damage potential of the secondary debris fragments, it is necessary to know the total volume of secondary debris that is generated by the high-speed impact of a projectile on the bumper plate of a dual-wall structure. A good estimate of the volume of bumper plate fragments can be obtained by calculating the volume of the elliptical hole created in the bumper plate by the impact. For the case of spherical projectiles (cylindrical projectile impact is addressed in another Section of this Report), a regression analysis of the bumper plate hole dimensions resulted in the following pair of equations for the minimum and maximum hole dimensions:

$$D_{min}/d = 2.698(V/C)^{0.689}(t_s/d)^{0.708}\cos^{0.021}\theta + 0.93 \tag{3.1}$$

$$D_{max}/d = 2.252(V/C)^{0.622}(t_s/d)^{0.667}e^{0.815\theta} + 1.00 \tag{3.2}$$

where $C = \sqrt{E/\rho}$ is the speed of sound in the bumper plate material, and θ is in radians. The averages and standard deviations of the prediction errors of these equations are presented in the first and second columns, respectively, of Table 3.1. A measure of the 'goodness of fit' of the regression equations, the correlation coefficient, is presented for each equation in the third column of Table 3.1. From the data in Table 3.1, it can be seen that equations (3.1) and (3.2) represent a good fit to the experimental bumper plate hole dimension data. The relatively large spread of the prediction errors for equation (3.2) is due to an inherent physical uncertainty in the maximum hole dimension, especially in holes produced by high obliquity impacts. As discussed previously, high obliquity impacts can tear, as well as perforate, the bumper plate. A set of curves comparing the predictions of equations (3.1) and (3.2) with experimental results is shown in Figure 3.16. From the close agreement between the predicted and experimental values seen in Figure 3.16, it is again concluded that equations (3.1) and (3.2) are a good fit to the experimental hole dimensions data. However, it is noted that these equations are valid only for aluminum projectiles impacting thin aluminum plates, and for $0.064<t_s/d<0.684$, for $0^o<\theta<75^o$, and for $2<V<8$ km/sec.

3.4.2 Debris Cloud Trajectories and Cone Angles

A regression analysis of the debris cloud trajectory and cone angle data obtained from an analysis of the test specimens without MLI resulted in the following empirical equations for θ_1, θ_2, and for γ_1, γ_2:

$$\theta_1/\theta = 0.471(V/C)^{-0.049}(t_s/d)^{-0.054}\cos^{1.134}\theta \;, \quad 30^o < \theta < 75^o \qquad (3.3)$$

$$\theta_2/\theta = 0.532(V/C)^{-0.086}(t_s/d)^{-0.478}\cos^{0.586}\theta \;, \quad 30^o < \theta < 75^o \qquad (3.4)$$

$$\tan\gamma_1 = 1.318(V/C)^{0.907}(t_s/d)^{0.195}\cos^{0.394}\theta \;, \quad 0^o < \theta < 75^o \qquad (3.5)$$

$$\tan\gamma_2 = 1.556(V/C)^{1.096}(t_s/d)^{0.345}\cos^{0.738}\theta \;, \quad 0^o < \theta < 75^o \qquad (3.6)$$

These equations were derived using data only from damaged test specimens without MLI because the MLI often absorbed a substantial portion of the debris cloud particles which, in some cases, resulted in smaller damage areas. Thus, using the data from the tests with MLI to develop equations to predict debris cloud cone angles would have resulted in equations that would under-estimate the size of the debris clouds.

The averages and standard deviations of the prediction errors and the correlation coefficients for each equation are presented in Table 3.2. The relatively large spread of the prediction errors and the low correlation coefficients for equations (3.5) and (3.6) is due to the fact that is was often difficult to determine the exact boundaries of the pressure wall plate damage areas. The actual values of the debris cloud cone angles are therefore seen to be dependent on the person performing the analyses. In addition to the angular limitations already imposed, it is noted that these equations are valid only for aluminum projectiles impacting aluminum dual-wall structures, and for $0.064<t_s/d<0.684$, and $2<V<8$ km/sec.

Typical plots of θ_1 and θ_2 as functions of θ are presented and compared against experimental values in Figure 3.17. It is seen that the 'in-line' trajectory angle, θ_2, is not a single-valued function of trajectory obliquity. In fact, θ_2 varies directly with θ up to a critical value between 60^o and 65^o, and then decreases with further increases in θ. This reversal at the critical value of trajectory obliquity also corresponds to the sudden decrease in the penetration potential of an obliquely incident high speed projectile. This behavior is also seen in the plot of θ_1, although to a lesser degree. Typical plots of the γ_1 and γ_2 as functions of θ are presented in Figure 3.18. From the agreement between the predicted and the experimental values seen in Figures 3.17 and 3.18, it is concluded that equations (3.5)-(3.8) are a fairly good fit to the experimental angle data.

3.4.3 Pressure Wall Damage Areas

A regression analysis of the pressure wall plate damage areas and the rear-surface spall areas was also performed. The following empirical predictor equations for total pressure wall damage area $A_d = A_{d1} + A_{d2}$ and rear-side spall area A_s were obtained:

Without MLI:

$$A_d/A_p = 39.91(V/C)^{0.828}(t_s/d)^{0.294}(S/d)^{0.814}\cos^{0.127}\theta \quad (3.7)$$

$$A_s/A_p = 201.48(V/C)^{0.714}(t_s/d)^{-0.609}(S/d)^{-1.248}(t_w/d)^{0.619}\cos^{3.188}\theta \quad (3.8)$$

With MLI:

$$A_d/A_p = 25.66(V/C)^{0.713}(t_s/d)^{-0.351}(S/d)^{0.327}\cos^{0.423}\theta \quad (3.9)$$

No equation is provided for spall prediction in dual-wall specimens with MLI because of the scarcity with which rear-side spall occured in such systems. The averages and standard deviations of the prediction errors and the correlation coefficients for equations (3.7)-(3.9) are presented in Table 3.3. As in the regression of the cone angle data, the relatively large spread of the errors for the damage area predictor equations is due to the fact that is was often difficult to determine the exact boundaries of the pressure wall damage areas. Typical plots of A_d as a function of θ for dual-wall systems with and without MLI are presented and compared against experimental results in Figure 3.19; a plot of A_s as a function of θ for dual-wall systems without MLI is shown in Figure 3.20. As is expected, Figure 3.19 shows that the damage areas on the front surfaces of the pressure wall plates are smaller in systems with MLI than in those systems without MLI. The agreement between the experimental results and the predicted values seen in Figures 3.19 and 3.20 indicates that equations (3.7)-(3.9) are a fairly good fit to the experimental data. It is again noted that these equations are valid for aluminum projectiles impacting aluminum dual-wall structures, and for $0.064<t_s/d<0.684$, for $0^o<\theta<75^o$, and for $2<V<8$ km/sec.

3.4.4 Pressure Wall Hole Diameters

Finally, empirical predictor equations were obtained for the equivalent single hole diameter in the event of pressure wall plate perforation:

Without MLI:

$$d_h/d = 2.820(V/C)^{0.490}(t_s/d)^{-0.421}(S/d)^{-0.457}(t_w/d)^{-0.726}\cos^{1.245}\theta \quad (3.10)$$

With MLI:

$$d_h/d = 1.464(V/C)^{0.093}(t_s/d)^{-0.973}(S/d)^{-0.575}(t_w/d)^{-0.772}\cos^{1.701}\theta \quad (3.11)$$

The averages and standard deviations of the prediction errors and the correlation coefficients for equations (3.10) and (3.11) are presented in Table 3.3. Typical plots of the hole diameters in perforated pressure wall plates in dual-wall systems with and without MLI under low energy (d=0.795 cm, V=6.5 km/sec) and and high energy (d=1.27 cm, V=7.0 km/sec) projectile impacts are shown and compared against experimental results in Figure 3.21. The most notable feature of Figure 3.21 is that for high energy impacts, the hole in the perforated pressure wall plate in a dual-all system with MLI can, for impact obliquities less than 45°, significantly exceed the hole in the perforated pressure wall plate of a similar dual-wall system without MLI. However, as the trajectory obliquity is increased beyond 45°, the hole size in the system with MLI gets smaller, and eventually becomes smaller than those in similar systems without MLI.

3.4.5 Additional Comments

It is noted that before equations (3.8) and (3.10),(3.11) are used to estimate rear-side spall areas and equivalent single-hole diameters in a dual-wall system under the impact of a spherical projectile with a particular diameter, velocity, and obliquity, it must first be determined whether or not rear-side spall or pressure wall perforation will occur in the system under the specified impact conditions. This can be determined using the appropriate penetration and spall functions for the particular geometric configuration of the dual-wall system and the specified conditions of impact. In addition, caution is urged when using equation (3.8) to predict rear-side spall areas in dual-wall configurations under impact conditions that lie close a spall function. In these 'border-line' cases, it was found that equation (3.8) has a tendency to over-predict the area of rear-side spall. Likewise, caution is urged when applying equation (3.11) to predict the single-hole diameter in perforated pressure wall plates of dual-wall systems with MLI that are impacted normally by large, high-speed projectiles (ie. diameter greater than 0.75 cm, velocity greater than 6.5 km/sec). In these cases, pressure wall penetration was accompanied by severe petalling which tremendously increased the size of the hole. Thus, in these cases of high energy impacts, while qualitative agreement will exist, equation (3.11) will under-predict the actual size of the pressure wall hole in the event of a perforation.

3.5 References

3.1 C.E. Anderson, T.G. Trucano, and S.A. Mullin, "Debris Cloud Dynamics", Int. J. Impact Engng., Vol. 9, No. 1, pp. 89-113 (1990).

3.2 R.W. Watson, "The Perforation of Thin Plates by High Velocity Fragments", Proc. Fifth Hypervelocity Impact Symp., Vol. I, Pt. 2, pp. 581-592, Col. School of Mines, Denver, Col. (1961).

3.3 K.N. Kreyenhagen and L. Zernow, "Penetration of Thin Plates", Proc. Fifth Hypervelocity Impact Symp., Vol. I, Pt. 2, pp. 611-624, Col. School of Mines, Denver, Col. (1961).

3.4 E. Schneider, "Velocity Dependencies of Some Impact Phenomena", Proc. Comet Halley Micrometeoroid Hazard Workshop, Longdon, N., ed., pp. 101-107, ESA SP-153, Paris, France (1979).

3.5 R.J. Arenz, "Projectile Size and Density Effects on Hypervelocity Penetration", J. Spacecraft, Vol. 6, No. 11, pp. 1319-1321, (1969).

3.6 B.G. Cour-Palais, "Space Vehicle Meteoroid Shielding Design", Proc.

Comet Halley Micrometeoroid Hazard Workshop, Longdon, N., ed., pp. 85-92, ESA SP-153, Paris, France (1979).

3.7 B.G. Cour-Palais, "Meteoroid Protection by Multiwall Structures", Paper No. 69-372, Proc. AIAA Hypervelocity Impact Conference, Cincinnati (1969).

3.8 B.G. Cour-Palais, "Hypervelocity Impact Investigations and Meteoroid Shielding Experience Related to Apollo and Skylab", Orbital Debris, NASA CP-2360 (1982).

3.9 P.J. D'Anna, "A Combined System Concept for Control of the Meteoroid Hazard to Space Vehicles", J. Spacecraft, Vol. 2, No. 1, pp. 33-37 (1965).

3.10 A.M. Rajendran and N. Elfer, "Debris-Impact Protection of Space Structures", pp. 41-78, Structural Failure, J. Wierzbicki, ed., John Wiley and Sons (1989).

3.11 J.W. Gehring, D.R. Christman, and A.R. McMillan, "Experimental Studies Concerning the Meteoroid Hazard to Aerospace Materials and Structures", J. Spacecraft, Vol. 2, No. 5, pp. 731-737 (1965).

3.12 D. Humes, "Meteoroid Protection for the Comet Halley Probe", Proc. Comet Halley Micrometeoroid Hazard Workshop, Longdon, N., ed., pp. 73-76, ESA SP-153, Paris, France (1979).

3.13 D. Humes, R.N. Hopko, and W.H. Kinard, "An Experimental Investigation of Single Aluminum 'Meteor Bumpers'", Proc. Fifth Hypervelocity Impact Symp., Vol. I, Pt. 2, pp. 567-580, Col. School of Mines, Denver, Col. (1961).

3.14 R.R. Wallace, J.R. Vinson, and M. Kornhauser, "Effects of Hypervelocity Particles on Shielded Structures", ARS Journal, Vol. 32, No. 8, pp. 1231-1237 (1962).

3.15 A.J. Laderman and C.H. Lewis, "Particle Cloud Impingement Damage", J. Spacecraft, Vol. 6, No. 11, pp. 1327-1328 (1969).

3.16 C.H. Lewis and A.J. Laderman, "Effect of Debris Shielding on Energy Partition", J. Spacecraft, Vol. 6, No. 12, pp. 1470-1472 (1969).

3.17 L.L. Long and R.L. Hammitt, "Meteoroid Perforation Effects on Space Cabin Design", Paper No. 69-365, Proc. AIAA Hypervelocity Impact Conference, Cincinnati, Ohio (1969).

3.18 J.F. Lundeberg, D.H. Lee, and G.T. Burch Jr., "Impact Penetration of Manned Space Stations", J. Spacecraft, Vol. 3, No. 2, pp. 182-187 (1966).

3.19 J. F. Lundeberg, "Meteoroid Design Criteria", Paper No. 65-0786, Proc. Natl. Aero. and Space Engrng. and Mfrng. Mtg., Los Angeles, CA (1965).

3.20 C.J. Maiden and A.R. McMillan, " An Investigation of the Protection Afforded a Spacecraft by a Thin Shield", AIAA Journal, Vol. 2, No. 11, pp. 1992-1998 (1964).

3.21 C. R. Nysmith, "An Experimental Impact Investigation of Aluminum Double-Sheet Structures", Paper No. 69-375, AIAA Hypervelocity Impact Conference, Cincinnati, Ohio (1969).

3.22 F.C. Posever, F.L. Rish, and C.N. Scully, "Impact Effects on Meteoroid Shielding Configurations for Velocities up to 60,000 fps", J. Spacecraft, Vol. 2, No. 5, pp. 738-741 (1965).

3.23 W.G. Reinecke, "Debris Shielding during High-Speed Erosion", AIAA Journal, Vol. 12, No. 11, pp. 1592-1594 (1974).

3.24 A.J. Richardson and J.P. Sanders, "Development of Dual Bumper Wall Construction for Advanced Spacecraft", J. Spacecraft, Vol. 9, No. 6, pp. 448-451 (1972).

3.25 A.J. Richardson, "Theoretical Penetration Mechanics of Multisheet Structures Based on Discrete Debris Particle Modeling", J. Spacecraft, Vol. 7, No. 4, pp. 486-489 (1970).

3.26 T.D. Riney and E.J. Halda, "Effectiveness of Meteoroid Bumpers Composed of Two Layers of Distinct Materials", AIAA Journal, Vol. 6, No. 2, pp. 338-344 (1968).

3.27 D. Rodriguez, "Meteoroid Shielding for Space Vehicles", Aerospace Engineering, pp.20-23, 55-66, December (1960).

3.28 R.F. Rolsten, J.N. Wellnitz, and H.H. Hunt, "An Example of Hole Diameter in Thin Plates Due to Hypervelocity Impact", J. Applied Physics, Vol. 33, No. 3, Pt. 1, pp. 556-559 (1964).

3.29 D.R. Sawle, "Hypervelocity Impact in Thin Sheets and Semi-Infinite Targets at 15 km/sec", AIAA Journal, Vol. 8, No. 7, pp. 1240-1244, (1970).

3.30 R.E. Sennett, "Effectiveness of Multisheet Structures for Meteoroid Impact Protection", AIAA Journal, Vol. 6, No. 5, pp. 942-944 (1968).

3.31 E. Schneider, A. Stilp, R. Bureo, and M. Lambert, "Micrometeorite and Space Debris Simulation for Columbus Hull Components", Int. J. Impact Engng., Vol. 10, in press (1990).

3.32 H. F. Swift, "Summary of Discussions in Group B (High Velocity Impacts/ Shield Design)", Proc. Comet Halley Micrometeoroid Hazard Workshop, Longdon, N., ed, ESA SP-153, pp. 141-142, Paris, France (1979).

3.33 A.K. Hopkins, T.W. Lee, and H.F. Swift, "Material Phase Transformation Effects upon Performance of Spaced Bumper Systems", J. Spacecraft, Vol. 9, No. 5, pp. 342-345 (1972).

3.34 H.F. Swift, D.D. Preonas, W.C. Turpin, and J.M. Carson, "Debris Clouds behind Plates Impacted by Hypervelocity Pellets", J. Spacecraft, Vol. 7, No. 3, pp. 313-318 (1970).

3.35 H.F. Swift and A.K. Hopkins, "Effects of Bumper Material Properties on the Operation of Spaced Meteoroid Shields", J. Spacecraft, Vol. 7, No. 1, pp. 73-77 (1970).

3.36 H.F. Swift and A.K. Hopkins, "The Effects of Bumper Plate Material Properties on the Operation of Spaced Hypervelocity Particle Shields", Paper No. 69-379, Proc. AIAA Hypervelocity Impact Conference, Cincinnati, Ohio (1969).

3.37 D.J. Weidman, "A Simplified Procedure for Determining the Perforation Limits for Thin Plates", AIAA Journal, Vol. 6, No. 8, pp. 1622-1623 (1968).

3.38 A.R. Coronado, M.N. Gibbins, M.A. Wright, and P.H. Stern, Space Station Integrated Wall Design and Penetration Damage Control, Boeing Aerospace Company, Report No. D180-30550-4, Final Report, Contract NAS8-36426, Seattle, Washington, May (1987).

3.39 W.P. Schonberg, "Characterizing the Damage Potential of Ricochet Debric Due to an Oblique Hypervelocity Impact", Paper No. 89-1410, Proc. 30th AIAA/ASME/ASCE/AHS/ASC SDM Conference, Mobile, Alabama (1989).

Table 3.1 Regression Analysis of Bumper Plate Dimension Data, Error Summary

Regression Function	$\%\epsilon_{avg}$	$\sigma(\%)$	$100R^2$
D_{min}/d	-0.148	6.35	83.0
D_{max}/d	0.079	9.48	87.7

Table 3.2 Regression Analysis of Cone Angle Data, Error Summary

Regression Function	$\%\epsilon_{avg}$	$\sigma(\%)$	$100R^2$
θ_1/θ	4.793	29.82	54.5
θ_2/θ	1.385	17.02	61.6
$\tan \gamma_1$	7.704	40.10	30.3
$\tan \gamma_2$	9.729	43.89	40.9

Table 3.3 Regression Analysis of Pressure Wall Damage Area and Hole Diameter Data, Error Summary

Regression Function	$\%\epsilon_{avg}$	$\sigma(\%)$	$100R^2$
	Without MLI		
A_d/A_p	6.974	38.08	38.7
A_s/A_p	16.250	67.67	73.1
d_h/d	6.706	38.78	64.9
	With MLI		
A_d/A_p	9.801	43.77	21.0
d_h/d	12.13	52.38	51.1

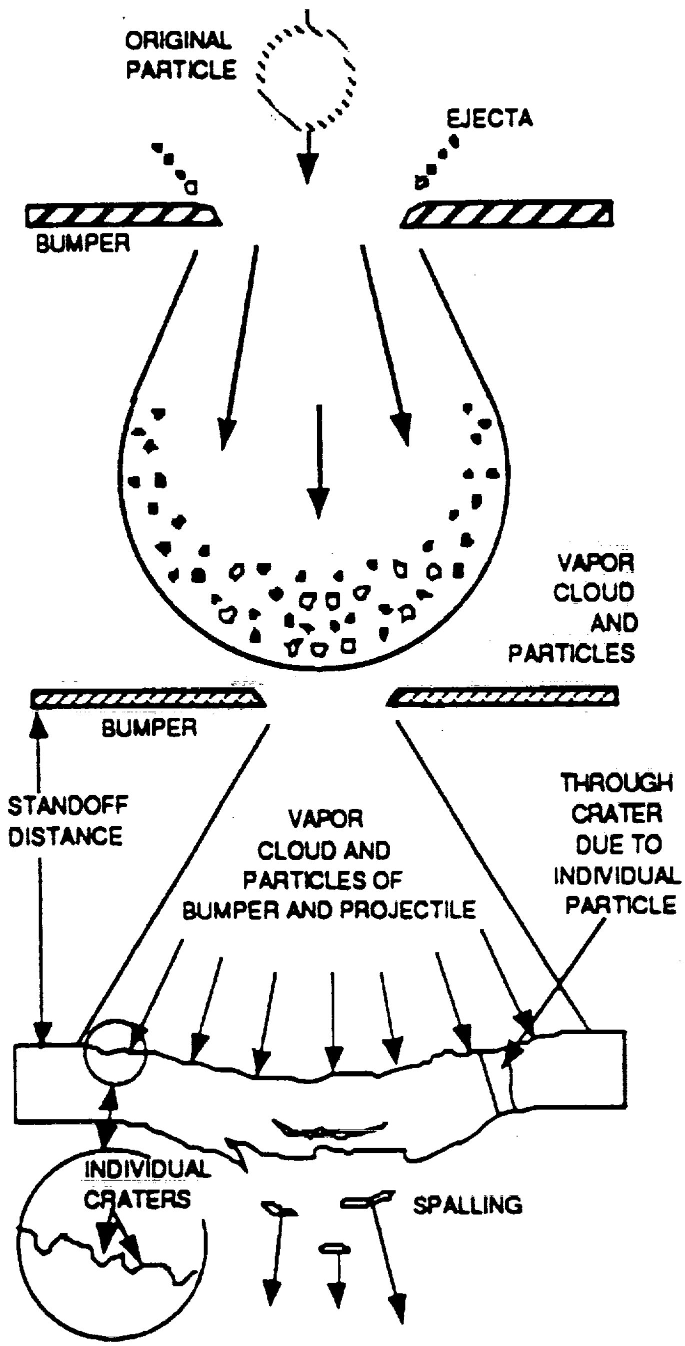

Figure 3.1 Normal Impact of a Dual-Wall Structure [2.1]

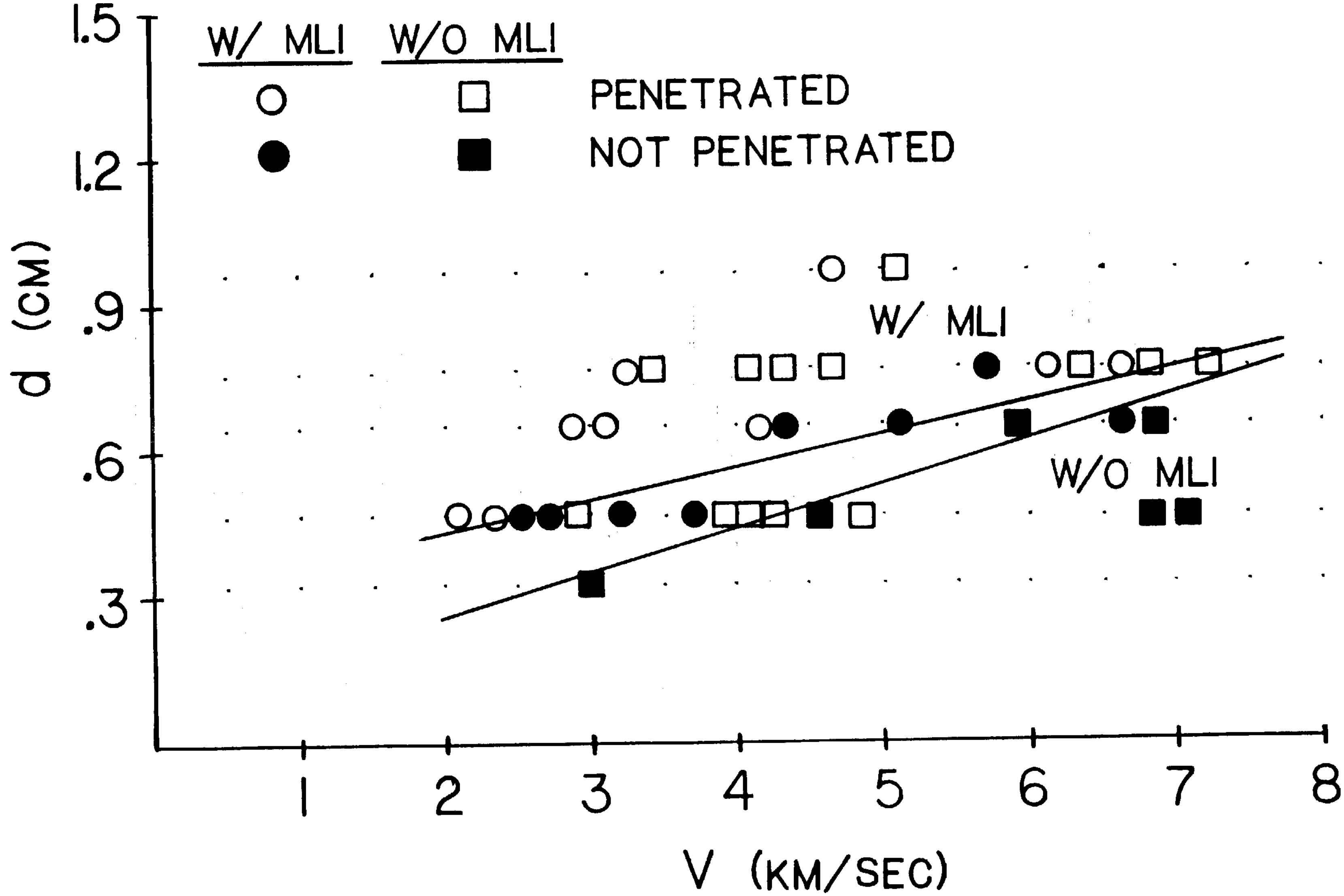

Figure 3.2 Penetration Function, t_s=1.6 mm, t_w=3.175 mm, θ=0°, S=10.16 cm, With and Without MLI

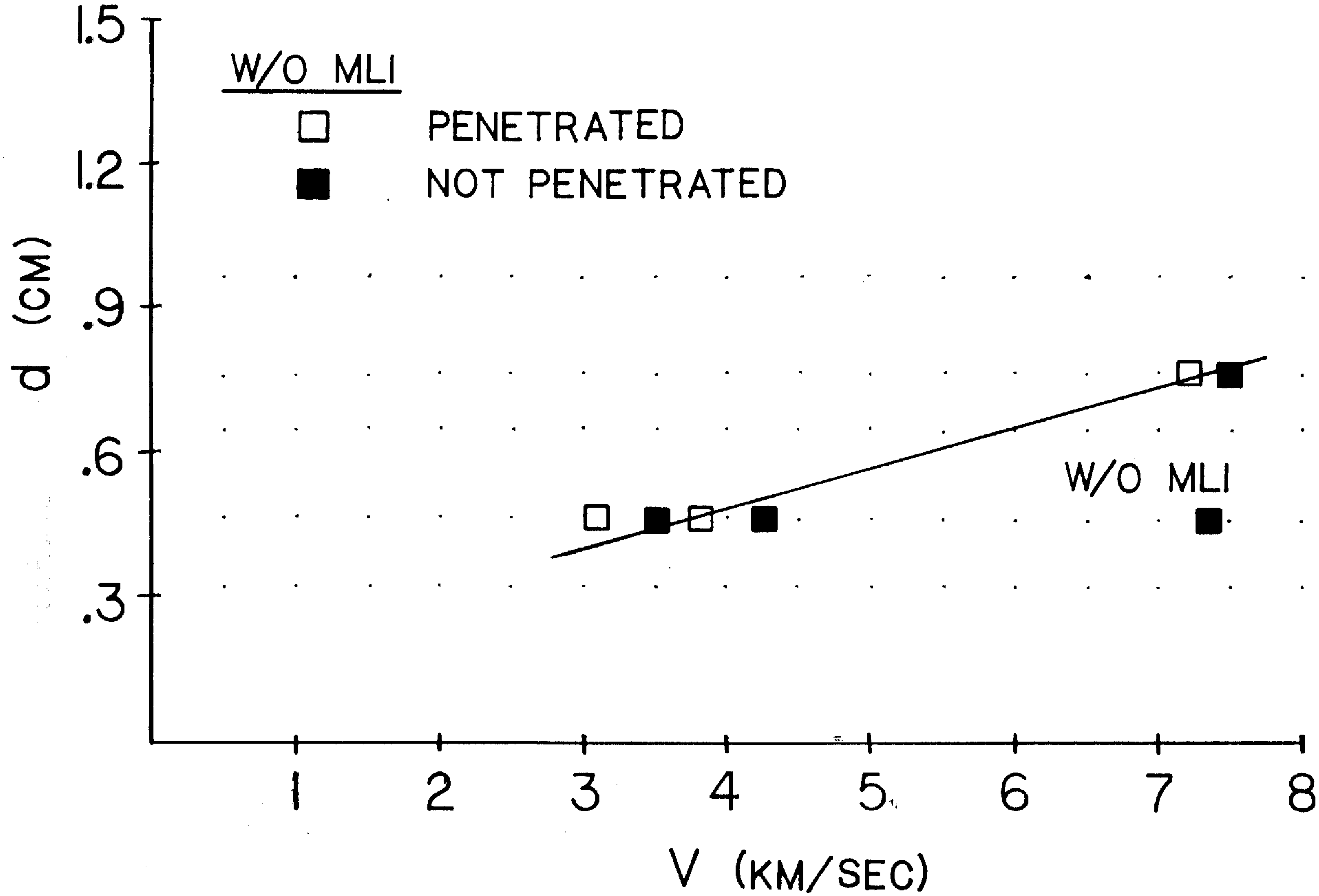

Figure 3.3 Penetration Function, t_s=2.032 mm, t_w=3.175 mm, θ=0^o, S=10.16 cm, Without MLI

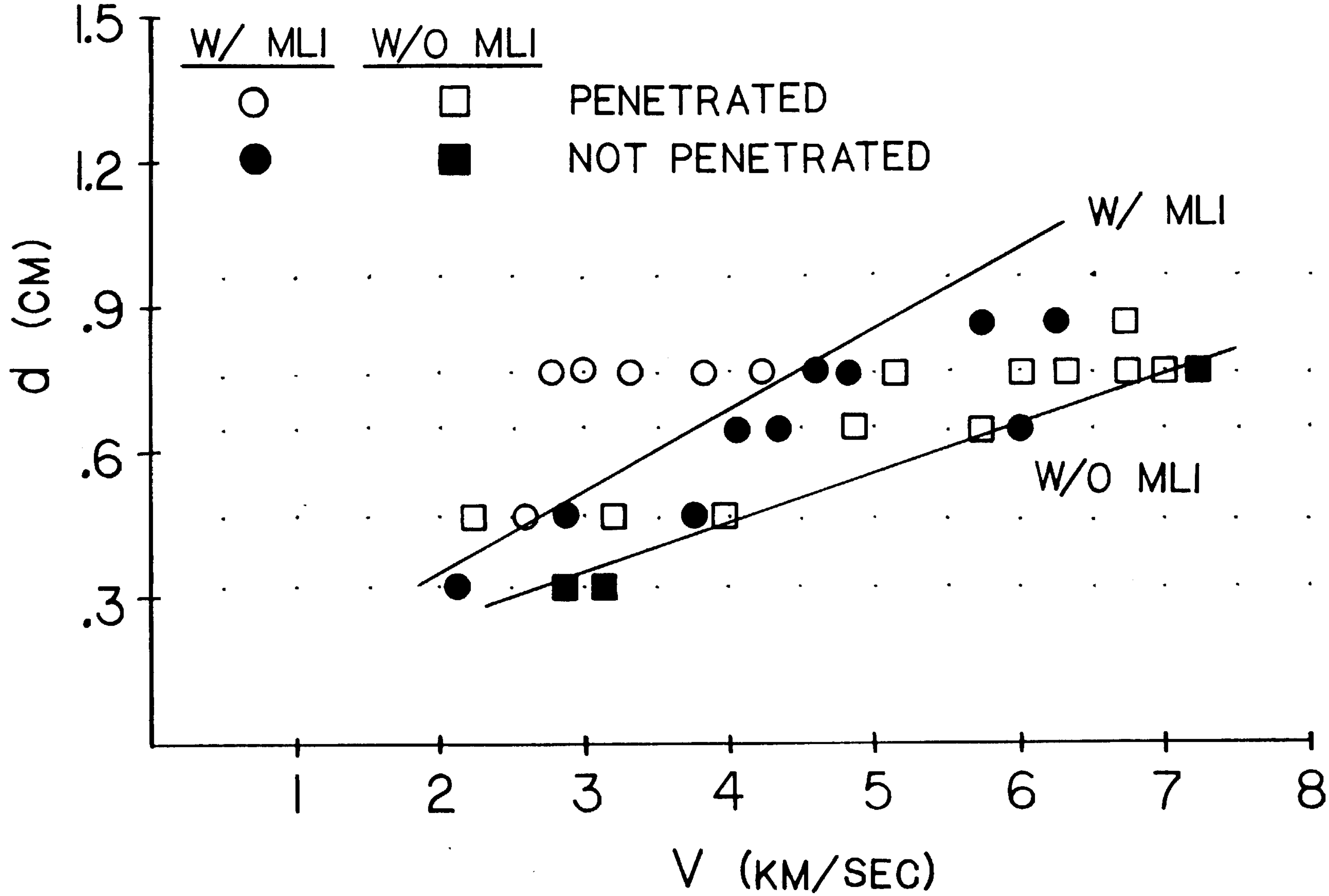

Figure 3.4 Penetration Function, t_s=1.6 mm, t_w=3.175 mm, $\theta=0^{\circ}$, S=15.24 cm, With and Without MLI

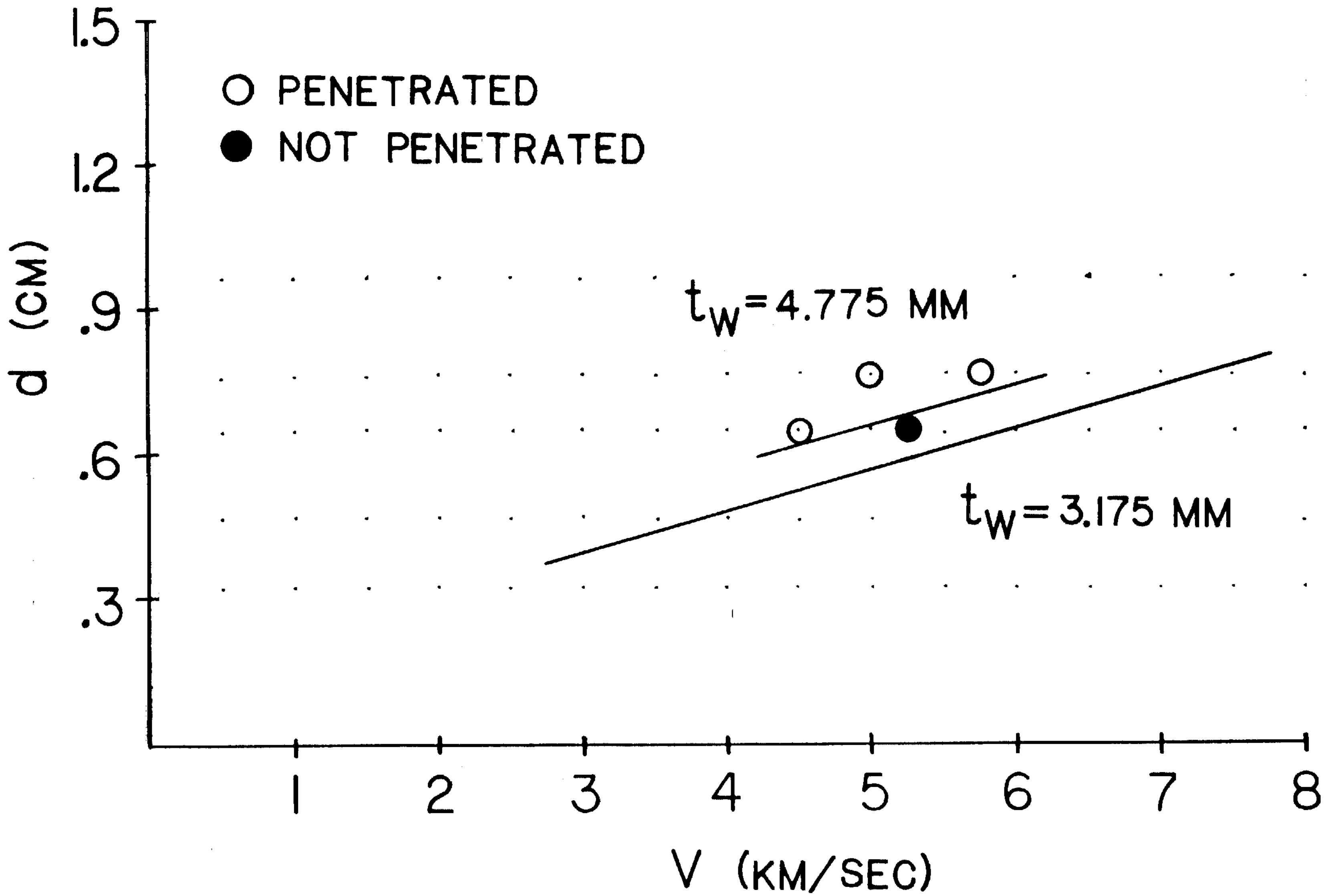

Figure 3.5 Penetration Function, t_s=2.032 mm, θ=0°, S=10.16 cm Without MLI, t_w=4.775 mm and t_w=3.175 mm

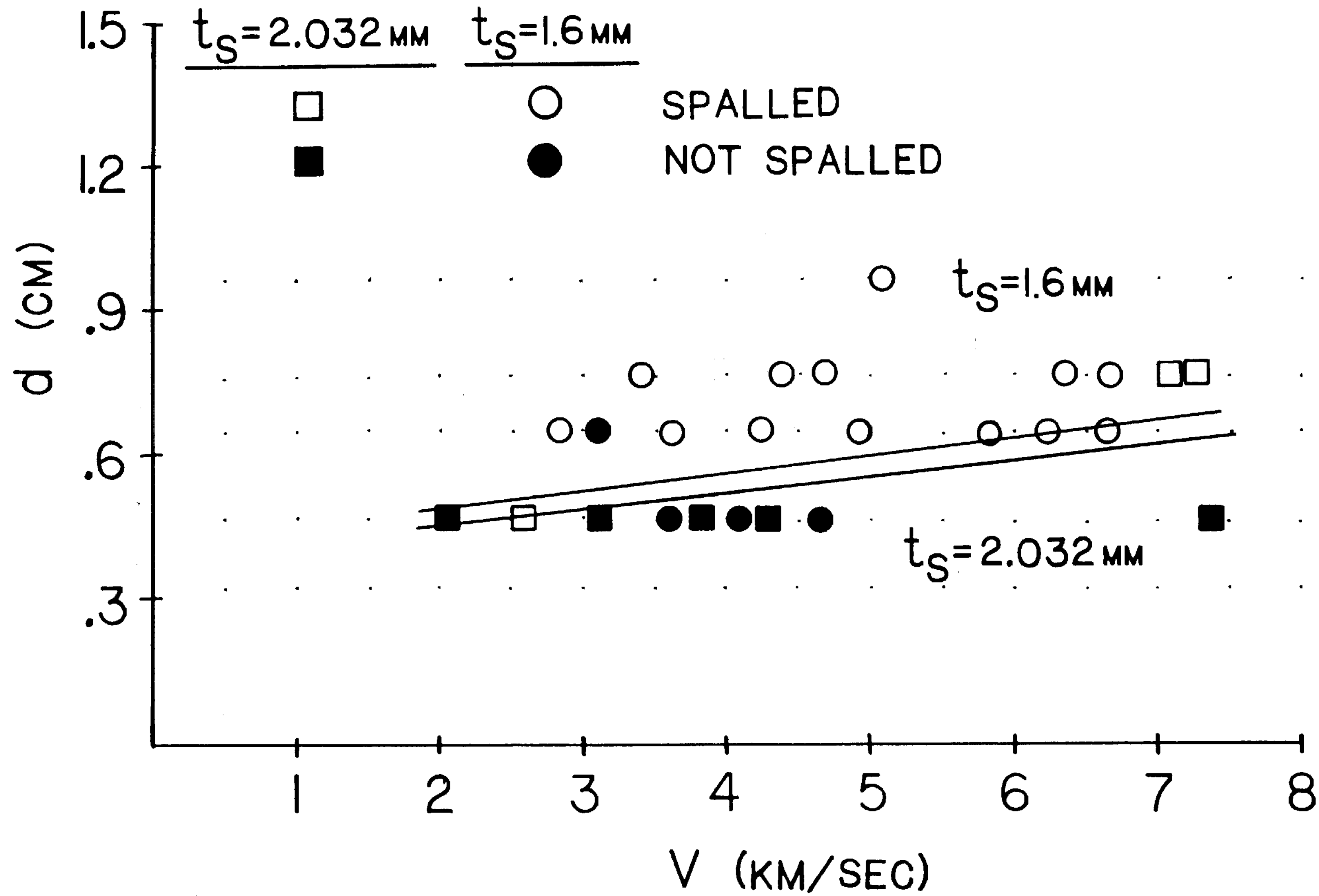

Figure 3.6 Spall Function, t_w=3.175 mm, θ=0°, S=10.16 cm, Without MLI, t_s=2.032 mm and t_s=1.6 mm

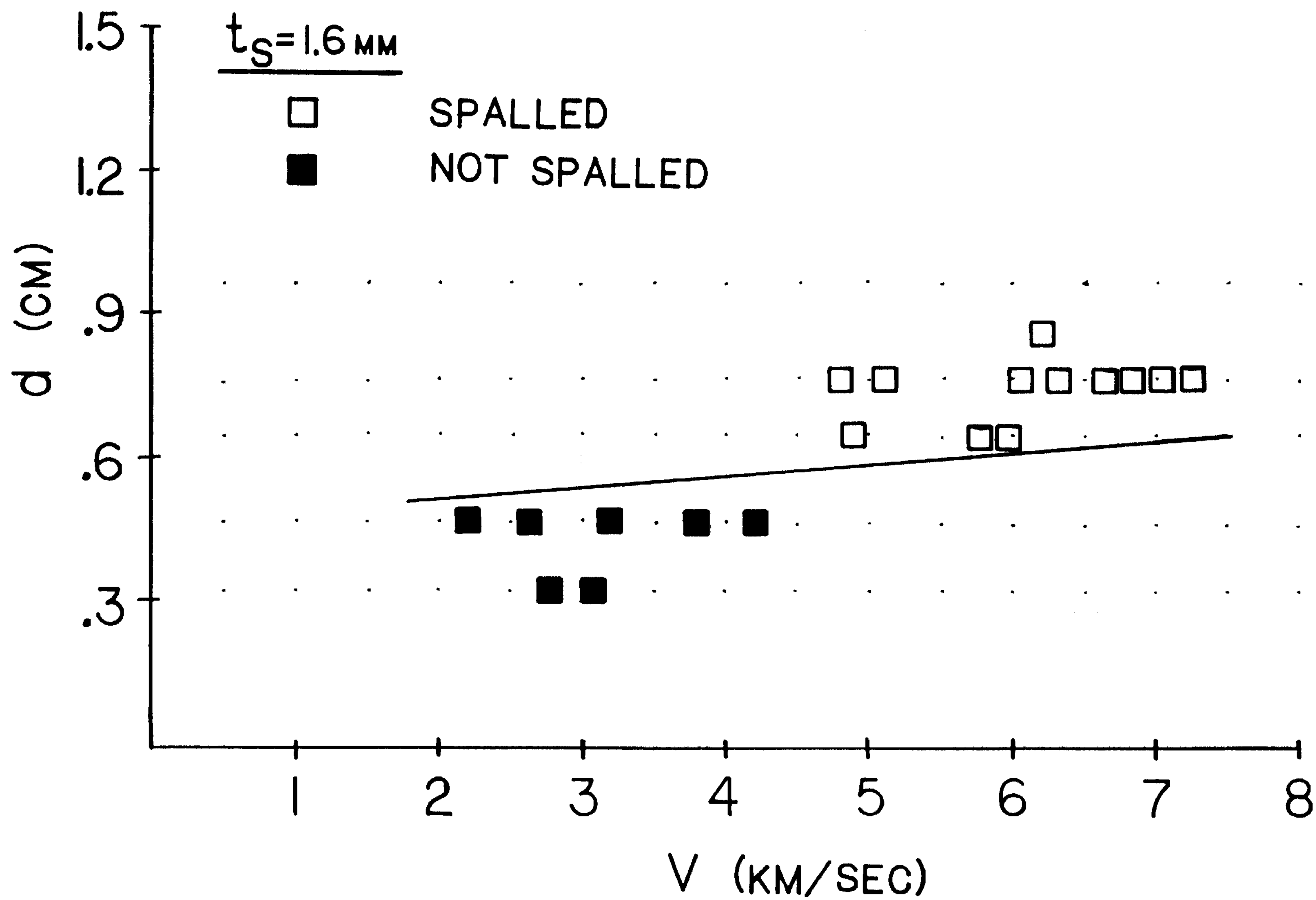

Figure 3.7 Spall Function, t_w=3.175 mm, θ=0°, S=15.24 cm, Without MLI, t_s=1.6 mm

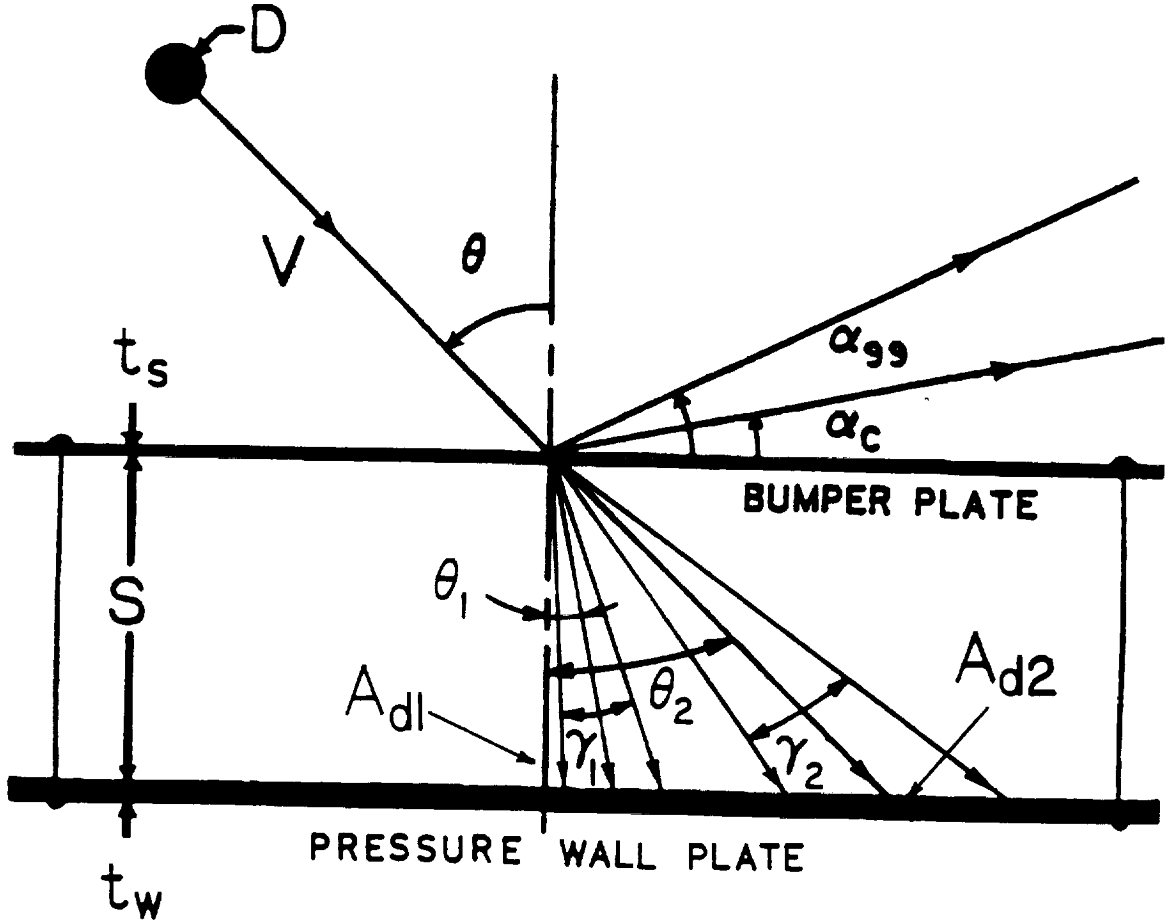

Figure 3.8 Oblique Impact of a Dual-Wall Structure

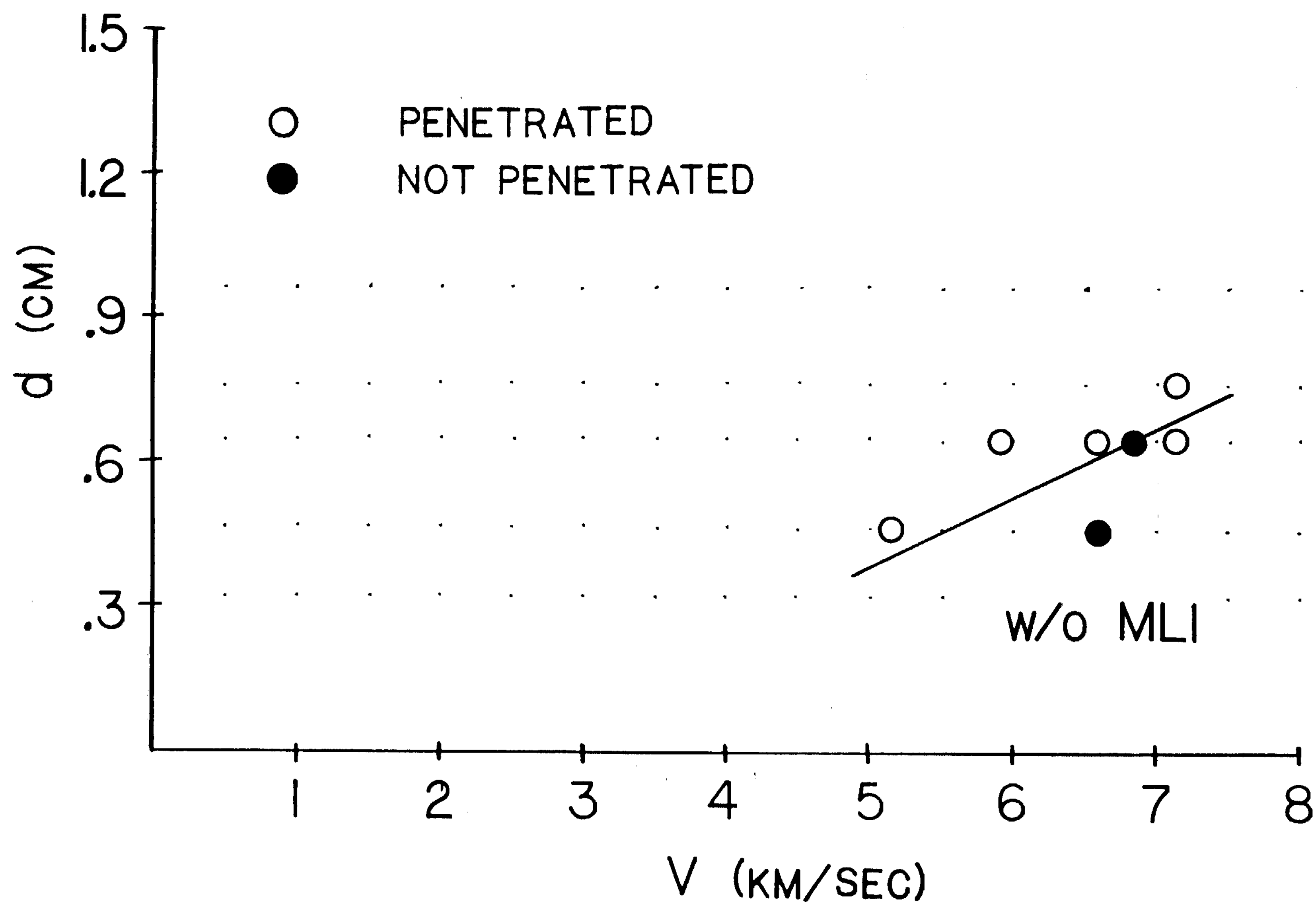

Figure 3.9 Penetration Function, t_s=1.6 mm, t_w=3.175 mm, θ=30°, S=10.16 cm, Without MLI

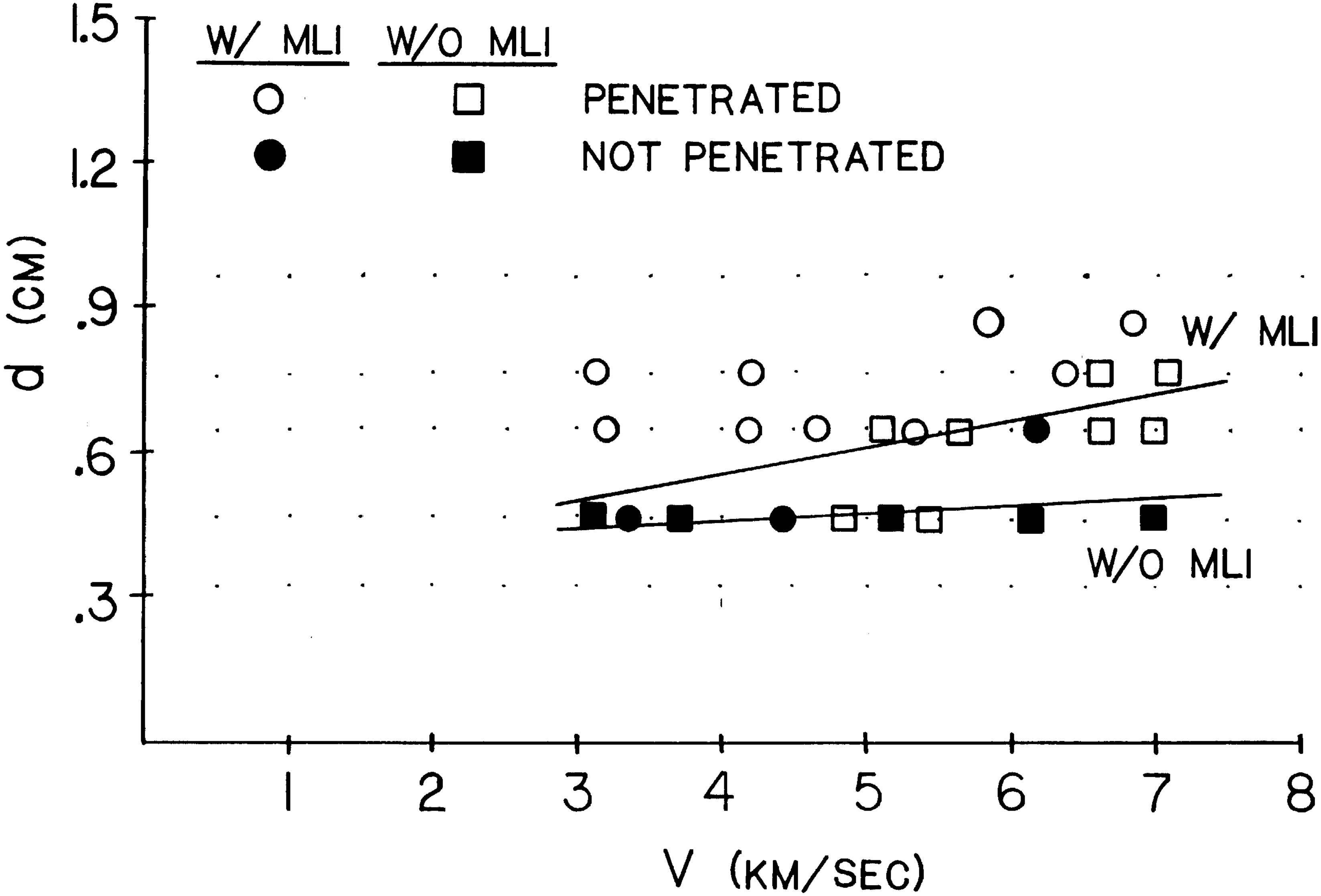

Figure 3.10 Penetration Function, t_s=1.6 mm, t_w=3.175 mm, θ=45°, S=10.16 cm, With and Without MLI

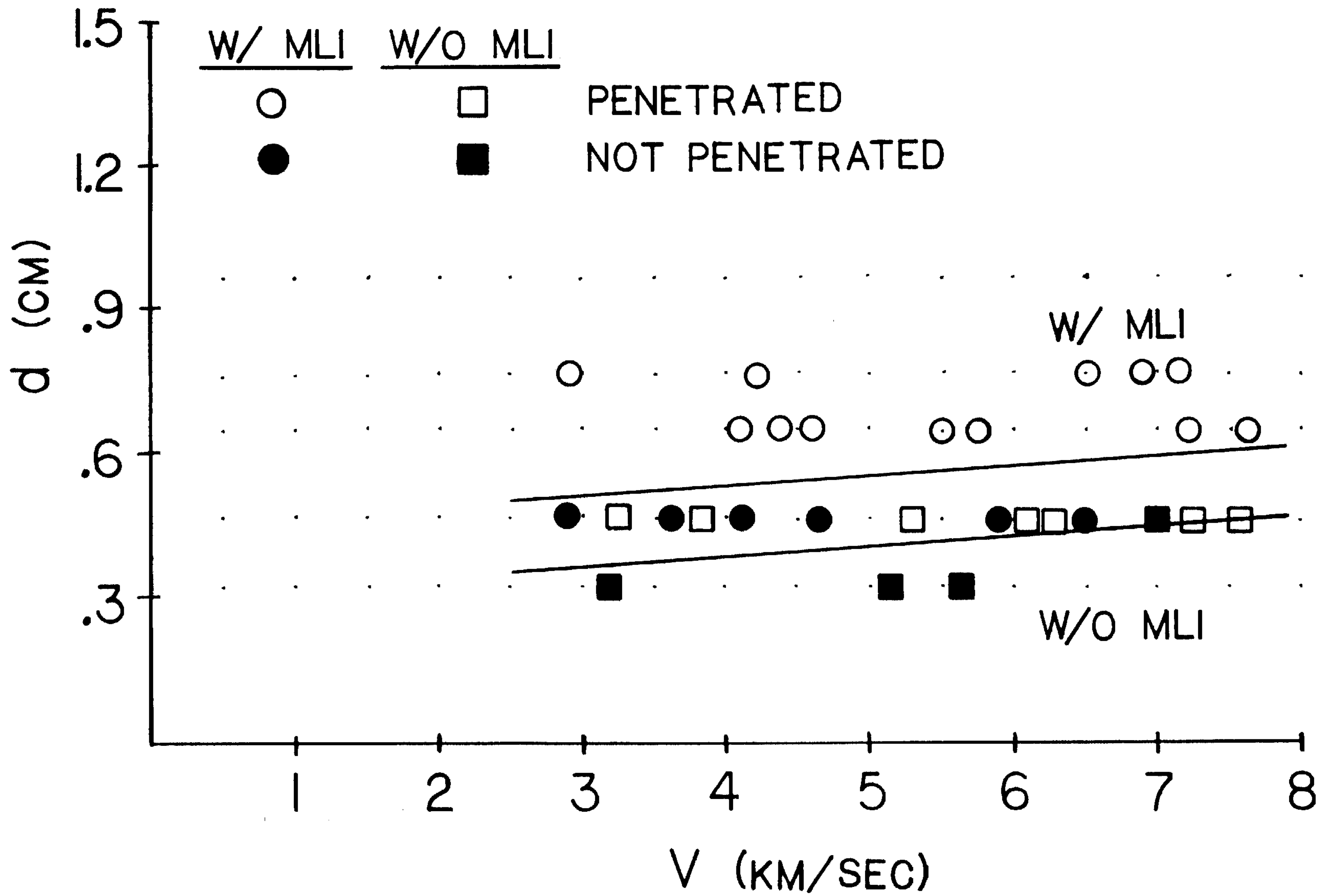

Figure 3.11 Penetration Function, t_s=1.016 mm, t_w=3.175 mm, θ=45^o, S=10.16 cm, With and Without MLI

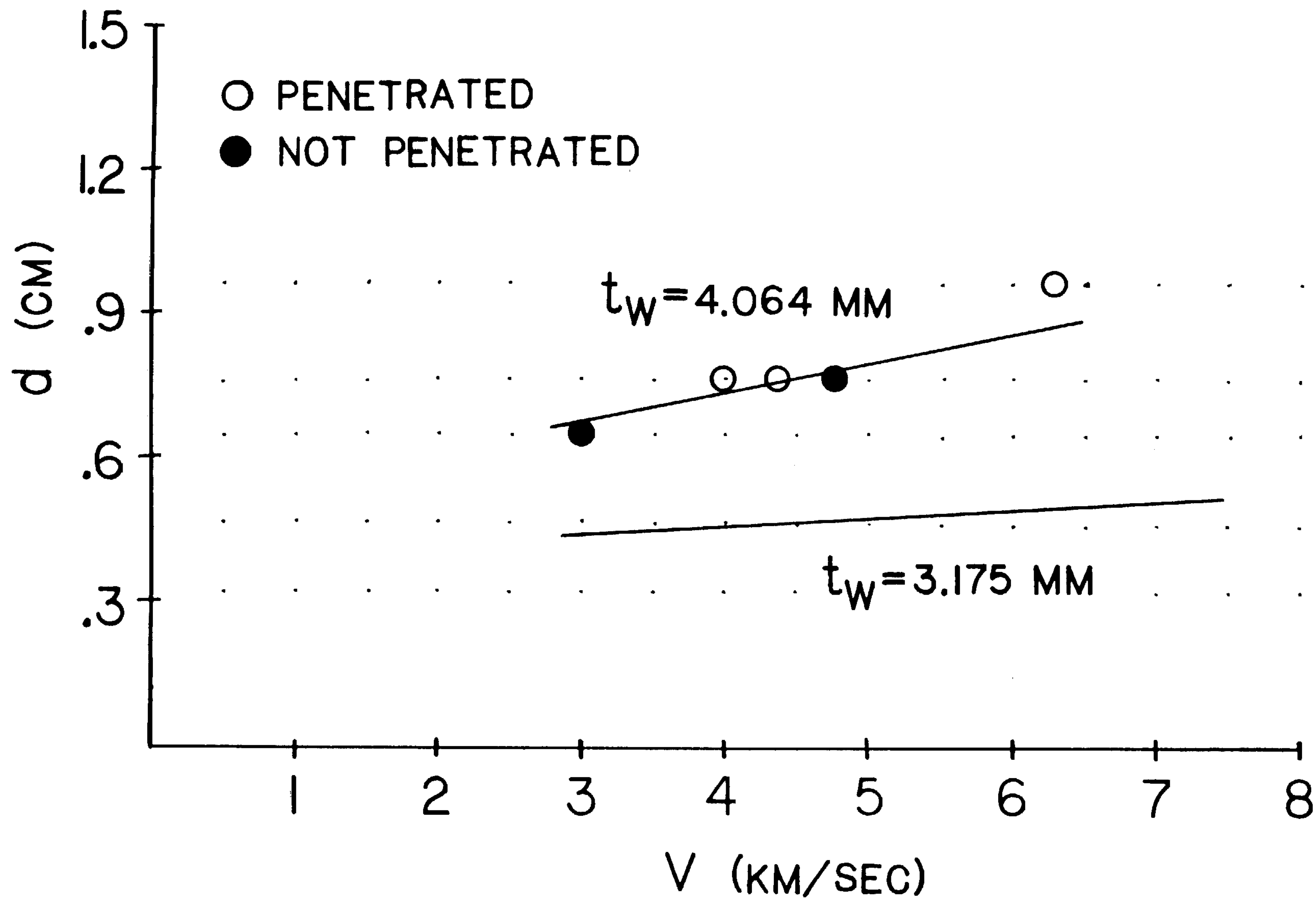

Figure 3.12 Penetration Function, t_s=1.6 mm, θ=45°, S=10.16 cm With MLI, t_w=4.064 mm and t_w=3.175 mm

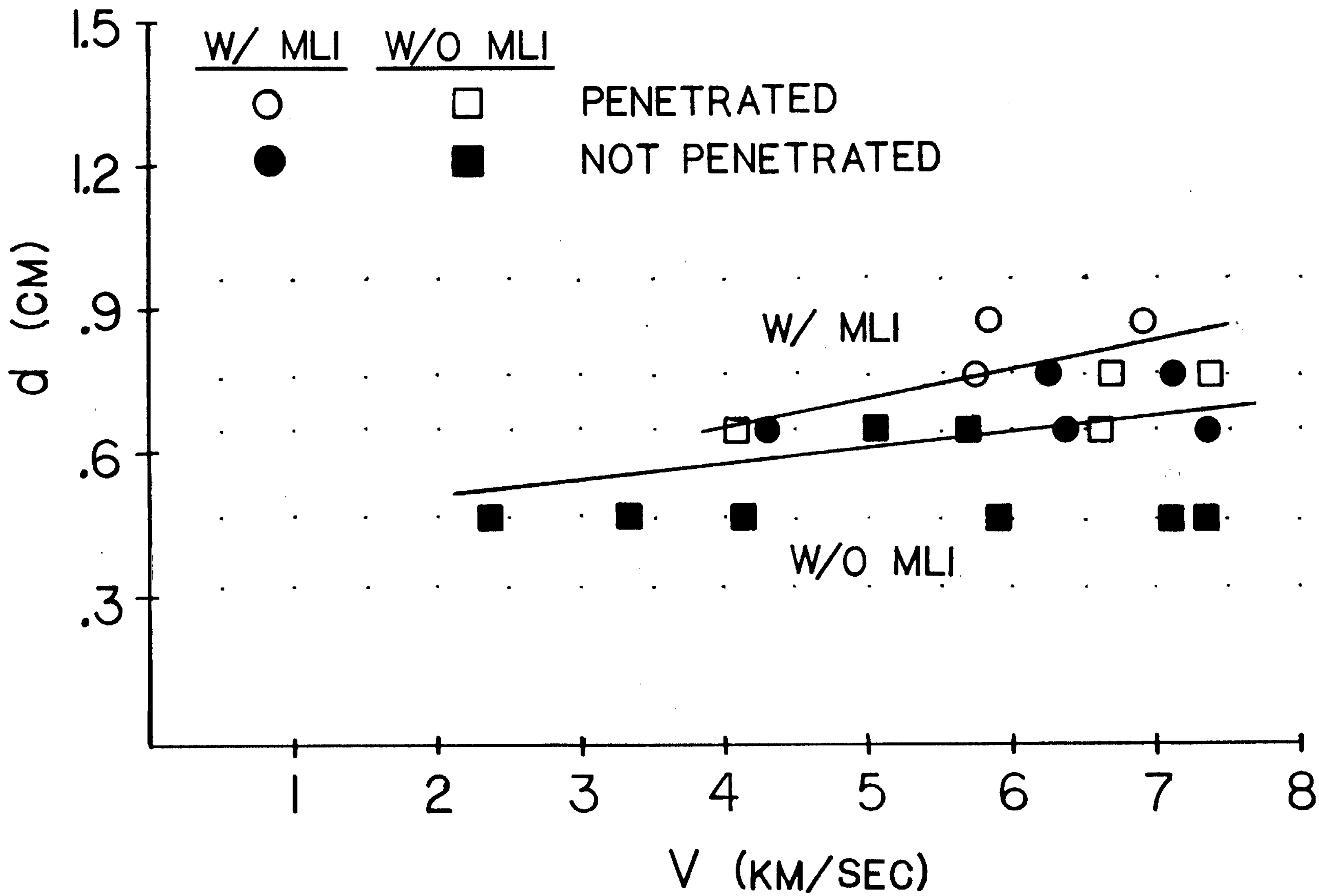

Figure 3.13 Penetration Function, t_s=1.6 mm, t_w=3.175 mm, θ=65°, S=10.16 cm, With and Without MLI

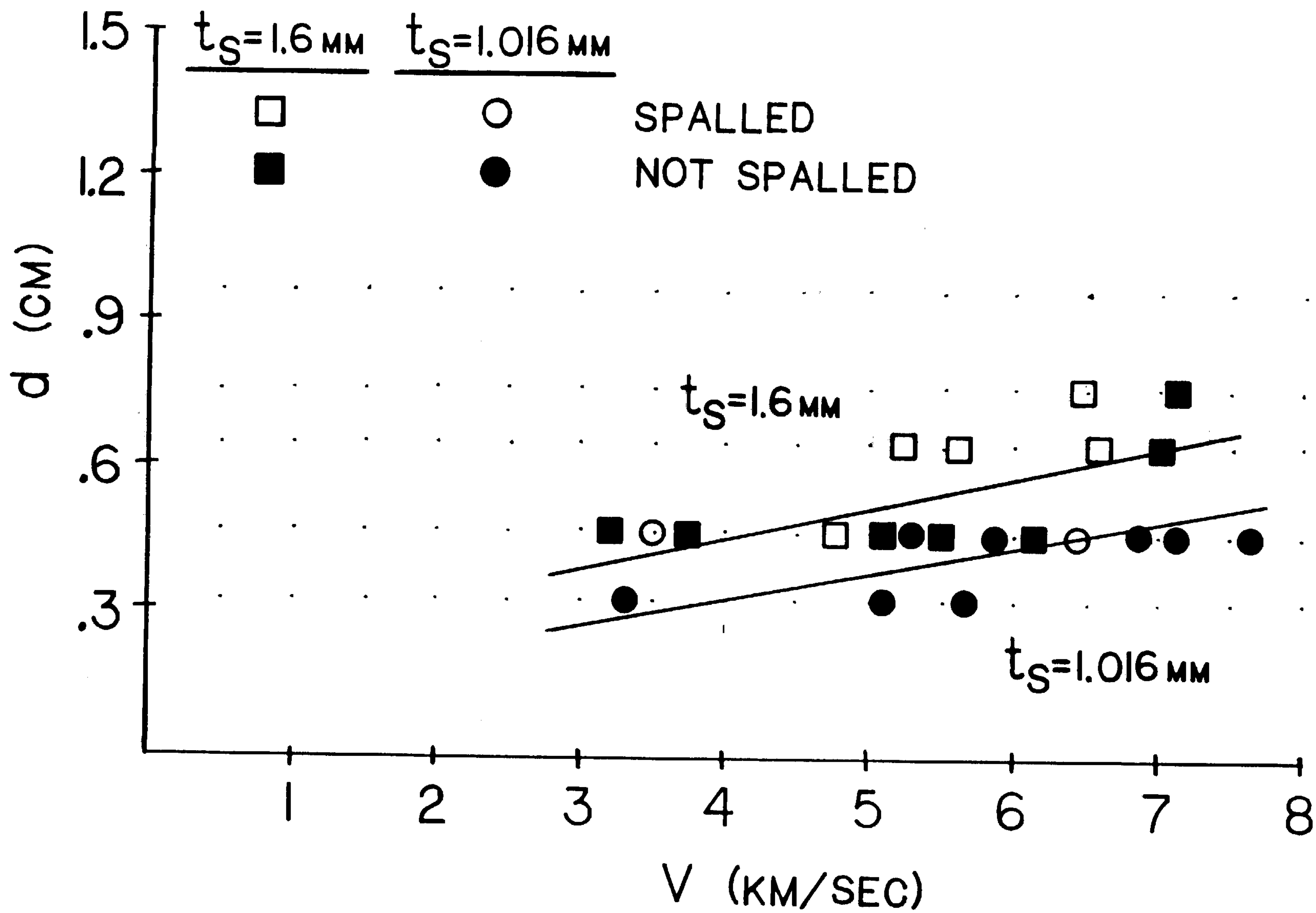

Figure 3.14 Spall Function, t_w=3.175 mm, θ=45°, S=10.16 cm, Without MLI, t_s=1.6 mm and t_s=1.016 mm

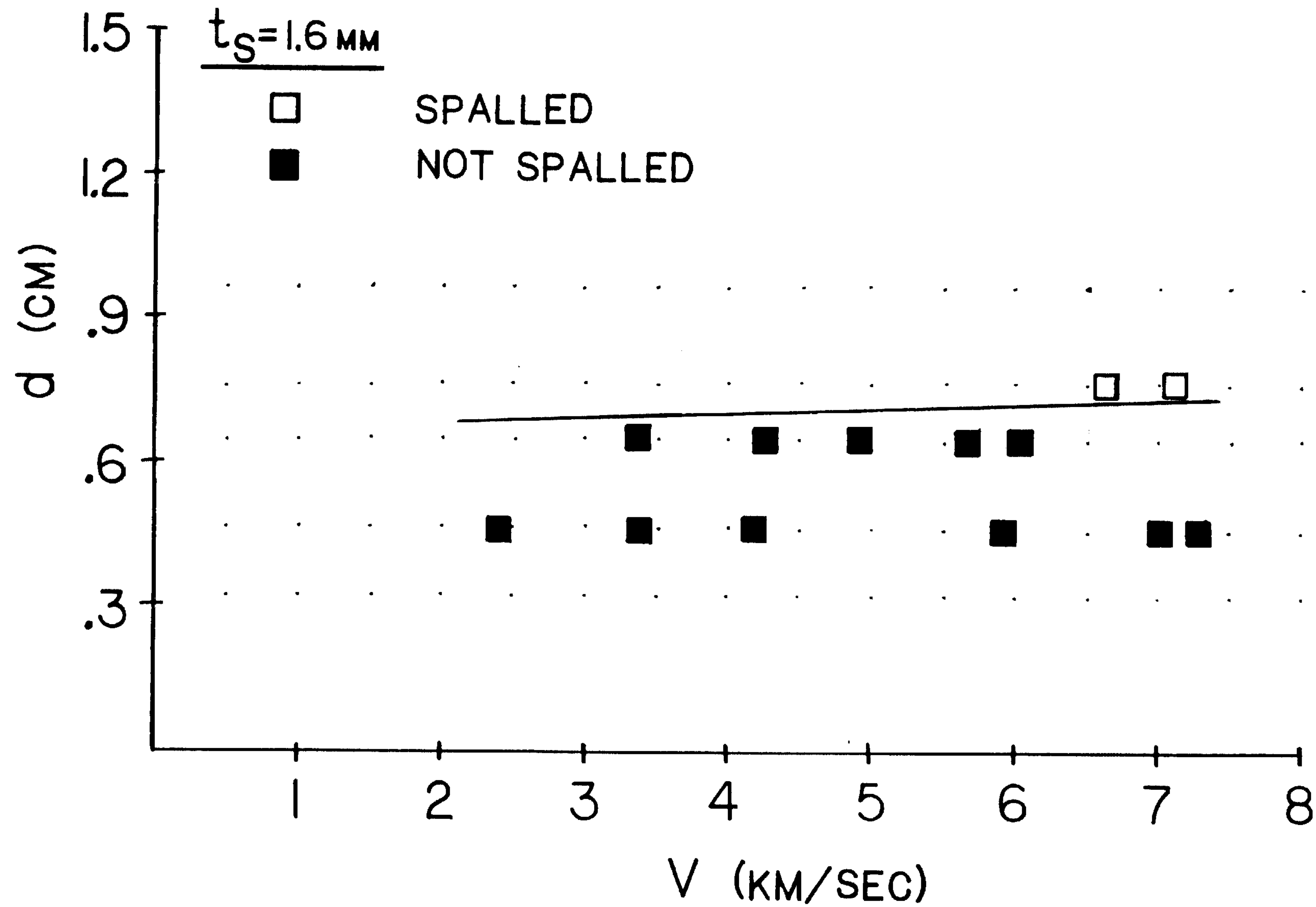

Figure 3.15 Spall Function, t_w=3.175 mm, θ=65°, S=10.16 cm, Without MLI, t_s=1.6 mm

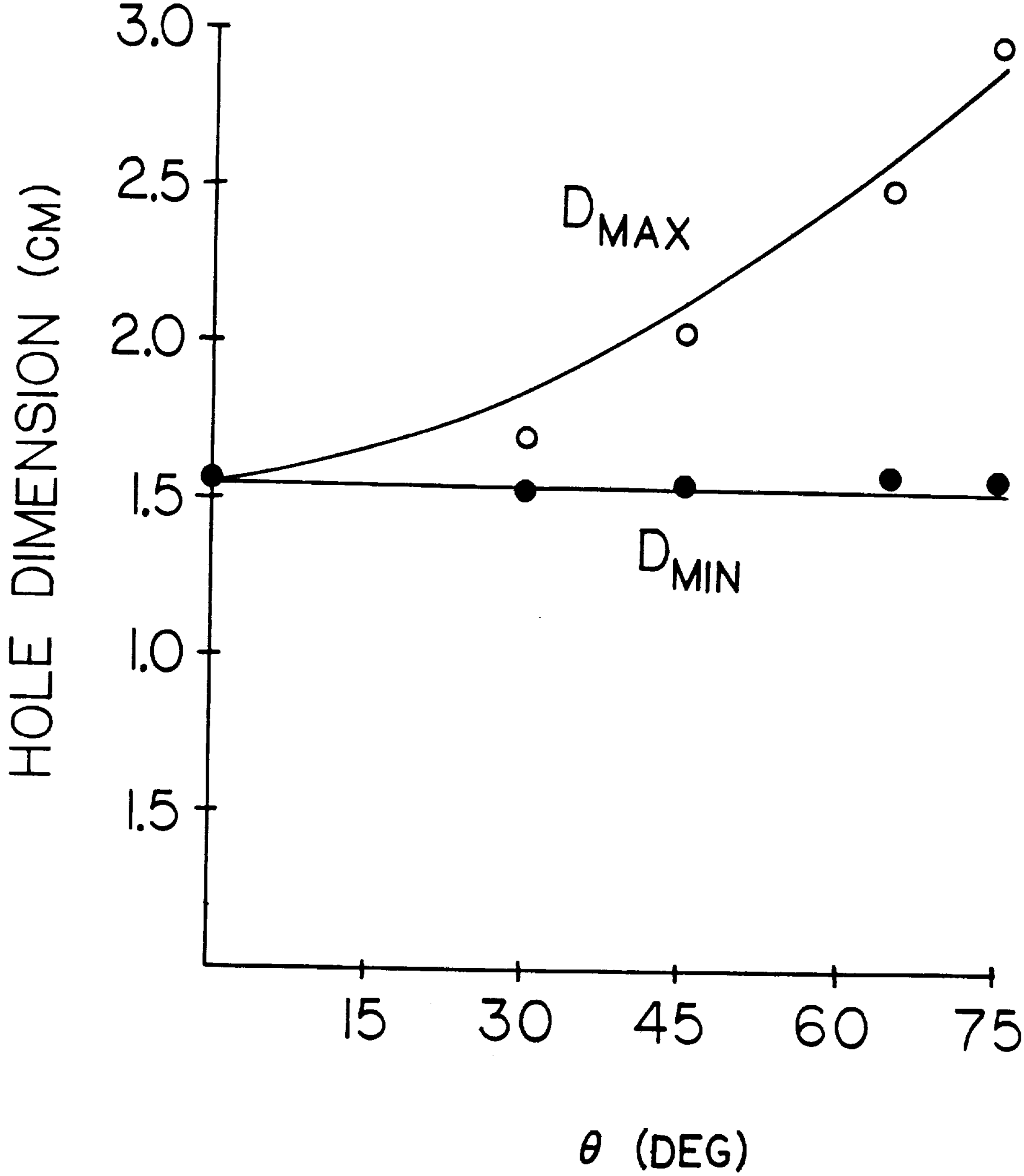

Figure 3.16 Comparison of Hole Dimension Data and Regression Equation Predictions, d=0.795 cm, V=6.5 km/sec

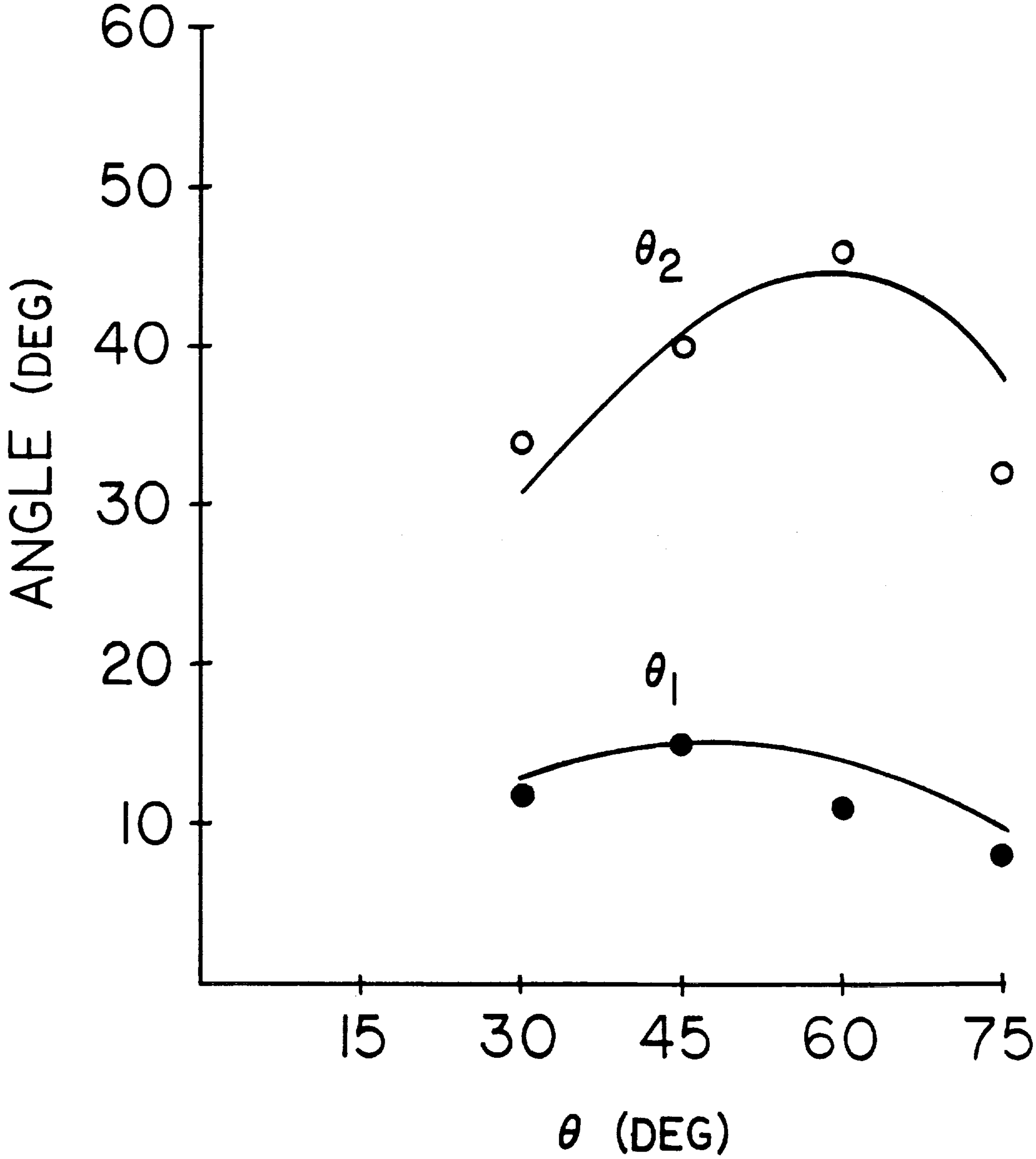

Figure 3.17 Comparison of Debris Cloud Trajectory Data and Regression Equation Predictions, d=0.795 cm, V=6.5 km/sec

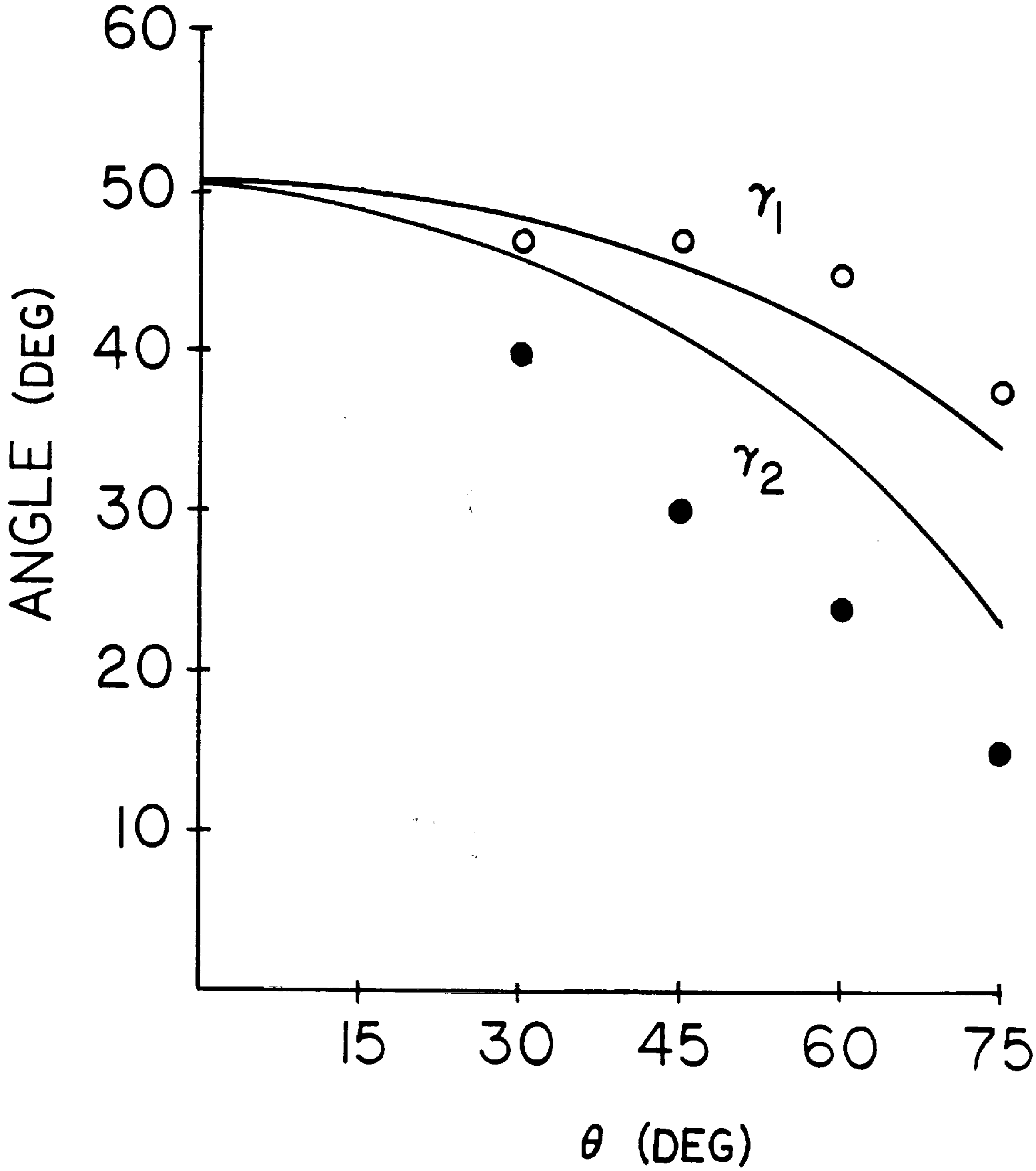

Figure 3.18 Comparison of Debris Cloud Cone Angle Data and Regression Equation Predictions, d=0.795 cm, V=6.5 km/sec

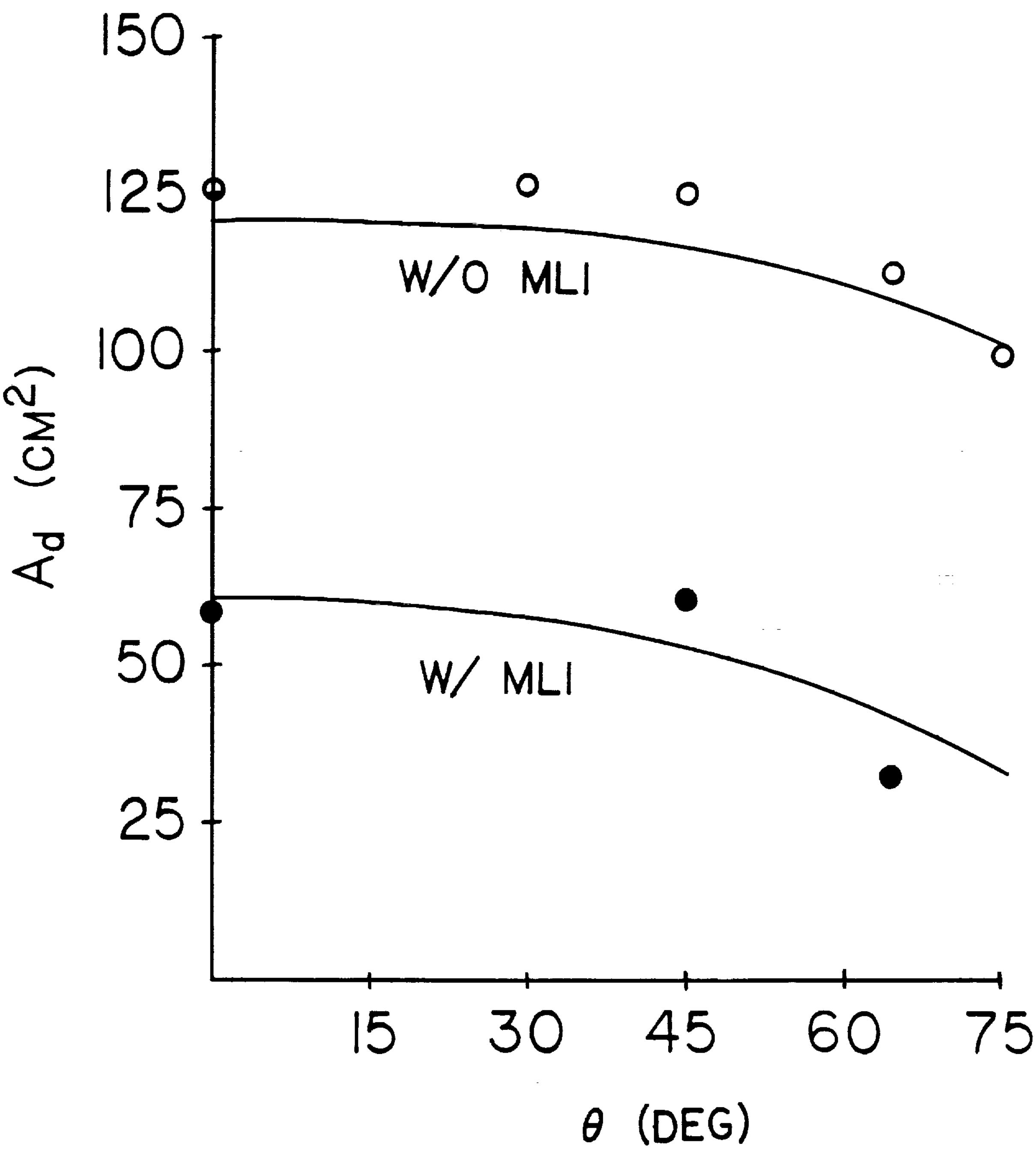

Figure 3.19 Comparison of Pressure Wall Damage Area Data and Regression Equation Predictions, d=0.795 cm, V=6.5 km/sec

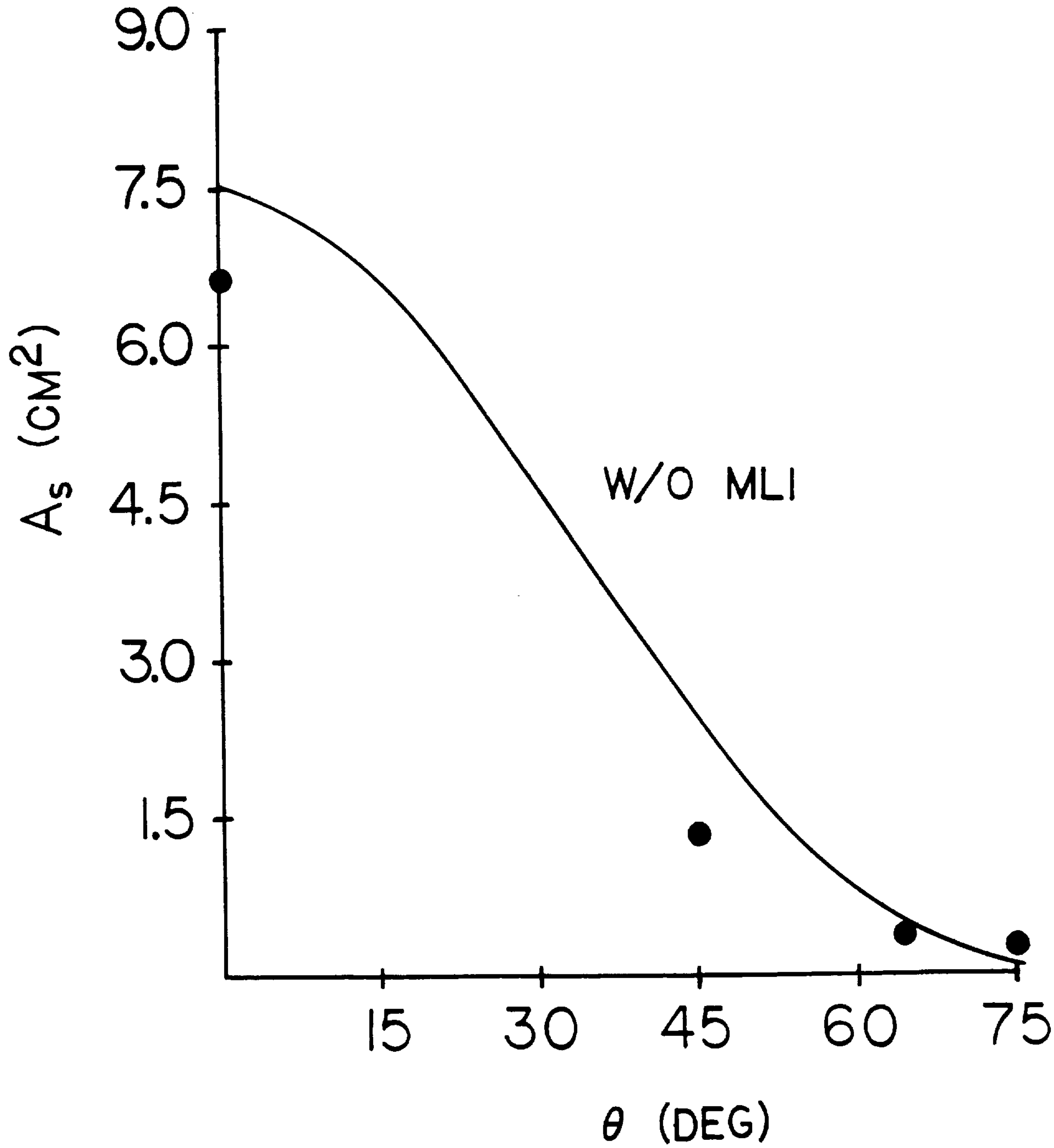

Figure 3.20 Comparison of Pressure Wall Spall Area Data and Regression Equation Predictions, d=0.795 cm, V=6.5 km/sec

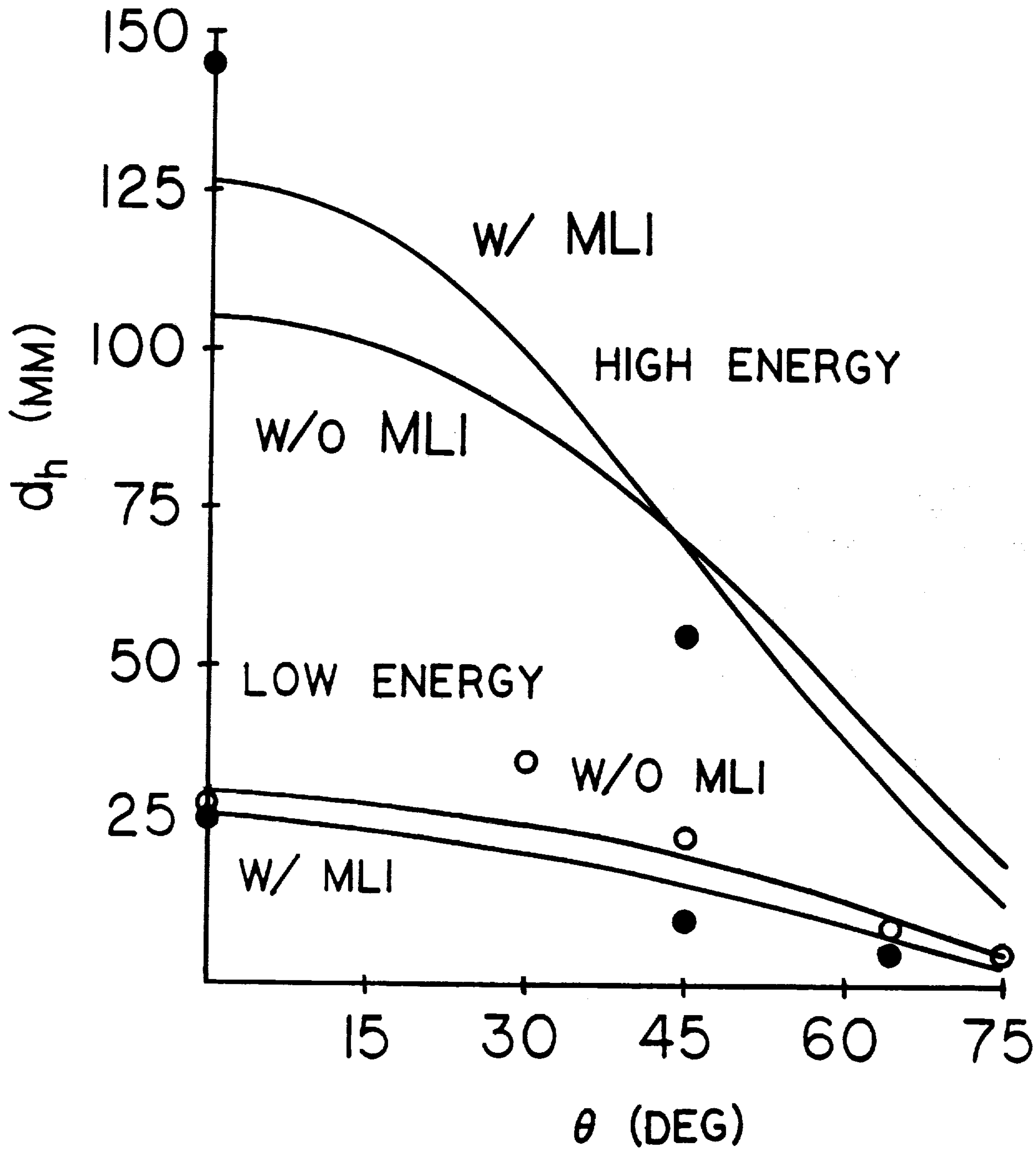

Figure 3.21 Comparison of Pressure Wall Hole Diameter Data and Regression Equation Predictions, Low Impact Energy (d=0.795 cm, V=6.5 km/sec) and High Impact Energy (d=1.27 cm, V=7.0 km/sec)

SECTION FOUR -- HYPERVELOCITY IMPACT OF DUAL-WALL STRUCTURES WITH CERAMIC AND COMPOSITE BUMPER PLATES

4.1 Introduction

In the majority of previous studies of the hypervelocity impact response of dual-wall, the bumper and structural wall were typically made from high-strength metallic materials, such as aluminum or steel. With the advent of many new high-strength composite and ceramic materials and their proliferation in aircraft applications, it has become necessary to evaluate their potential for use in long-duration space and aerospace structural systems. One aspect of materials evaluation for use in space and aerospace structural systems is the analysis of their response to hypervelocity impact loadings. Unfortunately, information on hypervelocity impact of composite and ceramic materials is scarce because work in this area has just begun [4.1]. A recent phenomenological investigation of the damage sustained by thick single-panel graphite/epoxy specimens under hypervelocity projectile impact showed that panel damage was a combination of multiple delamination and breakage of the fiber and matrix materials [4.2]. However, the use of composite and ceramic materials in multi-wall structural systems has yet to be addressed.

This Section presents the results of an investigation into the response of dual-wall systems with composite and ceramic bumpers under normal hypervelocity projectile impact loadings. Test results for dual-wall specimens employing three different fiber-reinforced composite materials and one ceramic material are reviewed qualitatively and quantitatively. Impact damage is characterized according to the extent of penetration, crater, and spall damage in the structural system. The analysis indicates that the extent of damage can be written as a function of the geometric and material properties of the projectile/dual-wall structural system. These functions can be used to perform parameter sensitivity studies and to evaluate hypothetical design configurations. The damage in the composite and ceramic material specimens is also compared to the damage in geometrically similar aluminum specimens caused by hypervelocity projectiles with similar impact energies. This comparative analysis, together with the overall composite and ceramic system impact response analysis, is used to determine the advantages and disadvantages of employing composite and ceramic materials in structural wall systems for long-duration spacecraft.

4.2 Hypervelocity Impact Test Parameters

In each test, a projectile of diameter d and velocity V impacted a bumper plate of thickness t_s along a trajectory perpendicular to the plane of the bumper plate (see Figure 4.1). The projectile shattered upon impact and formed a hole of diameter D in the bumper plate. Secondary projectile and bumper plate debris fragments created during the impact were sprayed upon a pressure wall plate of thickness t_w located a distance S behind the bumper plate. These secondary debris impacts created an area of damage A_d on the pressure wall plate; the angle γ is the cone angle of the secondary debris fragment cloud and represents the spread of the debris fragments. Occasionally, the impacts of the secondary debris fragments resulted in the creation of spall fragments ejected from the rear side of the pressure wall plate. In these instances, the total spalled area on the rear surface is denoted by A_s.

The conditions of the impact tests were chosen to simulate space debris impact of light-weight space structures as closely as possible, and still remain within the realm of experimental feasibility. Kessler [4.3] states that the average mass density for pieces of orbital debris less than 10 mm in diameter is approximately 2.8 gm/cm^3, which is approximately the same as that of aluminum. Although it is anticipated that the shape of the impacting projectile will affect the formation and spread of secondary debris particles [4.4], spherical projectiles were used in the test program to maintain repeatability and consistency. Thus, the testing was conducted with solid spherical 1100 aluminum projectiles with diameters ranging from 4.75 mm to 8.89 mm. The velocities of the impacting projectiles ranged from 3.43 to 7.40 km/sec.

A total of 24 aluminum, 12 composite, and 3 ceramic structural systems were used to study and evaluate the penetration resistance of dual-wall systems with composite and ceramic bumpers. In the composite systems, the bumper plates were made of a fiber reinforced composite material while the pressure wall plates were made of 2219-T87 aluminum. The composite materials used as bumper plates were Kevlar 49 and IM6/3501-6 graphite/epoxy. In the ceramic systems, the bumper plates were made of 3 layers of 0.635 mm thick alumina (Al_2O_3) fastened together with Crest 7450 adhesive; the pressure wall plates were made of 2219-T87 aluminum. In the aluminum systems, the bumper and the pressure wall plates were made of 6061-T6 and 2219-T87 aluminum, respectively. The thicknesses of the aluminum bumper plates were chosen so that they would have approximately the same areal density as the composite and ceramic material plates, that is, for example,

$$t_{s,aluminum} = (\rho_{composite}/\rho_{aluminum}) t_{s,composite} \tag{4.1}$$

The mechanical properties and the laminae lay-up of the composite and ceramic material bumper plates are given in Tables 4.1 and 4.2, respectively.

Additional test parameters are given in Tables 4.3 and 4.4. The results of the hypervelocity impact test firings are given in Tables 4.5 and 4.6; column entries of '----' indicate that penetration and/or spall of the pressure wall plate did not occur. A complete set of photographs that show the differences in pressure wall response between the Kevlar, graphite/epoxy, and aluminum systems may be found in Reference 4.5. Detailed post-test analyses of the damaged test specimens revealed many interesting features and characteristics of composite materials hypervelocity impact response.

4.3 Hypervelocity Impact Response of Kevlar Systems

4.3.1 Bumper Plate Damage Analysis

The impact damage in the Kevlar bumper plates typically consisted of a circular hole and large areas of delamination on the front and rear surfaces of the plates. Although the edge of the hole was usually frayed, its roundness was evident nonetheless. The delamination area of the front surface extended far beyond the the vicinity of the hole and was approximately twice as large as the delamination area of the rear surface. On both surfaces, the delamination was generally restricted to the outer layers, with the peeling in the direction of the surface laminate fibers. These observations are similar to those made in a previous study of the hypervelocity impact response of thick graphite/epoxy panels [4.2].

4.3.2 Pressure Wall Plate Damage Analysis

In Tables 4.7 and 4.8, penetration characteristics are summarized for test shots grouped according to both geometric and impact energy similarity. Table 4.7 shows results for impact energies below 2,000 joules (the 'low impact energy regime') while Table 4.8 shows results for energies greater than 10,000 joules (the 'high impact energy regime'). A penetration function for certain Kevlar systems in the low and high impact energy regimes and the corresponding aluminum systems is shown in Figure 4.2. Penetration functions for impact conditions and system geometries different than those for which the penetration function in Figure 4.2 was drawn can be constructed only after additional impact testing has been performed. Using Tables 4.7,4.8 and the detailed penetration data in Tables 4.5 and 4.6, a comparison of penetration response characteristics was performed.

In the low impact energy regime, the pressure wall plate damage areas of the Kevlar systems were highly concentrated and consisted of either a single hole (a penetrating impact) or a single crater (a non-penetrating impact). The damage areas in similar aluminum systems were more wide-spread and contained numerous small holes and/or craters. Among the high energy impacts, for a 101.6 mm stand-off distance, penetration of the pressure wall plates occurred in the Kevlar as well as in the aluminum systems. The damage areas on the pressure wall plates of both structural systems were observed to be similar in size (Tables 4.5,4.6). The similarity in penetration response of the Kevlar and aluminum systems is evident in Figure 4.2 where only one penetration function has been drawn for both, the Kevlar and aluminum system penetration data. However, when the wall spacing was increased to 152.4 mm, the Kevlar systems were penetrated while the corresponding aluminum systems were not. Furthermore, at this stand-off distance, pressure wall plate damage areas in the aluminum systems were significantly larger than those in the Kevlar systems.

These differences in response characteristics between the aluminum and

Kevlar systems indicate that aluminum bumpers are generally more effective in spreading out the secondary debris that is created by the initial projectile impact on the bumper plate, especially for impact energies above 10,000 joules. The concentration of the debris clouds and the resultant small damage areas on the pressure wall plates in the Kevlar systems can be explained in part by a mismatch in shock impedance between the Kevlar bumper plates and the aluminum projectiles [4.6]. The shock waves in the projectile and the bumper plate created by the initial impact interacted in a manner that prevented the complete break-up of the projectile. As a result, the dispersion of the secondary projectile and bumper plate fragments also decreased. An increased probability of pressure wall plate penetration also resulted from the increased concentration of the secondary debris fragment clouds.

It is interesting to note that the reverse sides of the pressure wall plates of the Kevlar systems did not exhibit any spall at either stand-off distance, while those of the aluminum systems exhibited significant spalling at both stand-off distances. This increased tendency for spall in the aluminum specimens is a direct consequence of the wider areal distribution of the impulse delivered by the secondary debris fragment cloud. The impulse delivered to the pressure wall plate in the Kevlar systems is more concentrated and therefore serves to penetrate the plate rather than cause spall.

4.3.3 Regression Analysis of Damage Data

A standard multiple linear regression analysis of the Kevlar 49 hole dimension data was performed to obtain an equation for hole diameter as a function the impact parameters and the material and geometric parameters of the bumper plate with the following result:

$$D/d = 1.923(V/C)^{0.968}(t_s/d)^{0.218} + 1.04 \qquad (4.2)$$

where $C = \sqrt{E_1/\rho}$; E_1 is the uni-directional ply modulus in the fiber direction, and ρ is the mass density of the bumper plate material. The average error of this equation was calculated to be 0.001% with a standard deviation of 4.824% and a correlation coefficient $R^2 = 0.873$. These values imply that equation (4.2) is a fairly good fit to the experimental hole diameter data. It is interesting to note that the velocity dependence in equation (4.2) is approximately the same as that in the equation of hole diameter in aluminum plates subjected to normal hypervelocity projectile impact.

Using the data in Tables 4.5 and 4.6, the following equations were obtained for cone angle, pressure wall damage area, pressure wall hole diameter in the event of a penetration, and pressure wall rear side spall area if spall occurs, as functions of the geometric, material, and impact parameters of the Kevlar 49 dual-wall systems.

Cone Angle

$$\cos\gamma = 0.332(V/C)^{-1.053}(t_s/d)^{-0.599} \qquad (4.3)$$

Pressure Wall Damage Area

$$A_d/A_p = 817.79(V/C)^{1.253}(t_s/d)^{0.679}(S/d)^{-0.158} \qquad (4.4)$$

Pressure Wall Hole Diameter

$$d_h/d = 5.836(V/C)^{2.171}(t_s/d)^{0.139}(S/d)^{0.155} \qquad (4.5)$$

where $A_p = \pi d^2/4$, and d_h is the equivalent hole diameter of the total penetrated area. The average errors, standard deviations, and correlation coefficients for equations (4.3-4.5) are given in Table 4.9. Based on the data in Table 4.9, it is evident that equations (4.3-4.5) fit the experimental data fairly well. It is noted that equations (4.2-4.5) are valid only for normal impacts of spherical aluminum projectiles on Kevlar 49 dual-wall specimens of similar lay-up and construction and for impact velocities between 3.4 and 7.4 km/sec.

It is also noted that a curve such as the one in Figure 4.2 must first be consulted to determine whether or not pressure wall penetration will occur in a dual-wall system with a Kevlar bumper plate as a result of a particular normal hypervelocity impact. If penetration will indeed occur, then equation (4.5) may be used to estimate the equivalent diameter of the resulting hole in the pressure wall. Additionally, since equations (4.2-4.5) are based on a relatively small number of tests, additional testing is recommended for further verification, or modification if necessary, of these equations.

4.4 Hypervelocity Impact of Graphite/Epoxy Systems

To determine if there would be a difference in resistance to pressure wall plate penetration between dual-wall specimens with bumper plates made of Kevlar 49, aluminum 6061-T6, and graphite/epoxy, two high energy impact tests were conducted with IM6/3501-6 graphite/epoxy as the bumper plate material. A summary of the resulting penetration and spall characteristics for the graphite/epoxy and corresponding aluminum tests is presented in Table 4.10.

An examination of the damaged graphite/epoxy bumper plates revealed that, unlike the delamination in the Kevlar bumper plates, the impact-induced delamination on the front and rear surfaces of the graphite/epoxy plates were not very extensive. However, the delamination was primarily restricted to the outer layers of both surfaces and were in the general direction of the outer laminate fibers. The holes in the graphite/epoxy plates were also more clearly defined than those in the Kevlar plate impacts.

The damage areas on the pressure wall plates of the graphite/epoxy systems were more wide-spread diffuse than those of the Kevlar systems. Although the pressure wall plates in the graphite/epoxy systems were still penetrated by the secondary debris fragments, the penetrations consisted of several small holes or craters rather than a single large hole or crater as in the Kevlar systems. Additionally, even though pressure wall plate penetration occurred in both the graphite/epoxy and the corresponding aluminum systems, the equivalent hole diameters of the penetrated pressure wall plates of the graphite/epoxy systems were significantly larger than those in the corresponding aluminum systems. Thus, the penetrations in the graphite/epoxy systems were more 'critical' than those in similar aluminum systems. Had these been on-orbit impacts, the larger penetrated areas in the graphite/epoxy systems would have allowed air to escape from a pressurized module at a higher rate than would the penetrations in the corresponding aluminum systems.

It is also noted that the pressure wall plates in the aluminum systems also exhibited significant rear side spall whereas the pressure wall plates of the graphite/epoxy systems did not. As discussed previously, this response characteristic of aluminum dual-wall systems is a serious matter and deserves further investigation.

4.5 Hypervelocity Impact Response of Alumina Systems

Three high energy impact tests were conducted with three-ply alumina bumper plates to determine if there would be a difference in resistance to pressure wall plate penetration between dual-wall specimens with alumina bumper plate and dual-wall specimens with aluminum 6061-T6 bumper plates. A summary of the resulting penetration and spall characteristics for the alumina and corresponding aluminum tests is presented in Table 4.11. It is noted that although the pressure wall plate thickness in the aluminum tests 228C,D are greater than those of the alumina tests, the total areal densities of the alumina systems and the aluminum systems in tests 228C,D are within 2.5% of each other.

An examination of the alumina bumper plate holes revealed many irregularities in their size and shape. Although all three alumina test shots were similar in impact energy, the hole in one alumina bumper plate was round (140A), while the holes in the other two (140B,C) were jagged. This indicates that multi-ply alumina bumper plates have a tendency to fracture and tear near the site of impact as well as melt or fragment.

The damage areas on the pressure wall plates of the alumina systems were similar in magnitude to those of the aluminum systems. However, the equivalent hole diameters of the penetrated pressure wall plates of the alumina systems were significantly larger than those in the corresponding aluminum systems. Thus, in a manner similar to the Kevlar and graphite/epoxy system penetrations, the penetrations in the alumina systems were more 'critical' than those in corresponding aluminum systems. It is also noted that the pressure wall plates in both the alumina and the aluminum systems exhibited rear side spall whereas the pressure wall plates of the Kevlar and graphite/epoxy systems did not. As discussed previously, the tendency of aluminum dual-wall systems to exhibit rear side spall is a serious matter and is in need of further investigation.

4.6 Summary and Conclusions

Based on the observations made in the preceding sections, it is concluded that thin Kevlar 49 IM6/3501-6 graphite/epoxy, and alumina panels offer no advantage over equivalent aluminum 6061-T6 panels in reducing the penetration threat of hypervelocity projectiles. However, it must be noted that significant pressure wall plate spalling was observed in the alumina and the aluminum systems while no spalling was observed in either the Kevlar or the graphite/epoxy systems. It is becoming increasingly apparent that, because of the high speeds with which spall fragments can travel, impact-induced spall can be as deleterious to mission success and crew safety as an actual penetration. Naturally, the major difference between a spall event and a penetration event is the lack of a pressure leak in a spall event. However, the lethality of the high-speed spall fragments must not be overlooked.

4.7 References

4.1 B.G. Cour-Palais, "Hypervelocity Impact in Metals, Glass, and Composites", Int. J. Impact Engng., Vol. 5, pp. 221-237 (1987).

4.2 C.H. Yew, and R.B. Kendrick, "A Study of Damage in Composite Panels Produced by Hypervelocity Impact", Int. J. Impact Engng., Vol. 5, pp. 729-738 (1988).

4.3 D.J. Kessler, R.C. Reynolds, and P.D. Anz-Meador, Orbital Debris Environment for Spacecraft Designed to Operate in Low Earth Orbit, NASA TM-100471, Houston, Texas (1989).

4.4 R.H. Morrison, A Preliminary Investigation of Projectile Shape Effects in Hypervelocity Impact of a Double Sheet Structure, NASA TN D-6944, Washington, D.C. (1972)

4.5 W.P. Schonberg, "Hypervelocity Impact of Spaced Composite Material Structures", International Journal of Impact Engineering, Vol. 10, in press (1990).

4.6 A.R. Coronado, M.N. Gibbins, M.A. Wright, and P.H. Stern, Space Station Integrated Wall Design and Penetration Damage Control, D180-30550-1, Boeing Aerospace Co., Seattle, Washington (1987).

	Kevlar 49	IM6/3501-6	Alumina
E $(x10^9\ N/m^2)$	----	----	379.2
ν	----	----	.317
E_1 $(x10^9\ N/m^2)$	76.0	203.0	----
E_2 $(x10^9\ N/m^2)$	5.5	11.0	----
G_{12} $(x10^9\ N/m^2)$	2.3	8.3	----
ν_{12}	.340	.320	----
ν_{21}	.025	.017	----
ρ (kg/m^3)	1340	1541	3900

Table 4.1 Unidirectional Ply Properties of Kevlar 49 (67% fiber volume) IM6/3501-6 Graphite/Epoxy (63% fiber volume) and Alumina [courtesy of NASA/MSFC and MMA]

Panel ID Number	Material	Number of Plies	Thickness (mm)	Lamina Lay-up
C1	Kevlar 49	12	2.032	$[0,\pm60,\mp60,0]_s$
C2	Kevlar 49	18	2.921	$(0,\pm60,\mp60,0)_3$
C3	Kevlar 49	24	3.810	$[(0,\pm60,\mp60,0)_2]_s$
C4	Graphite/ Epoxy	24	3.810	$[(0,\pm60,\mp60,0)_2]_s$
C5	Alumina	3	1.905	----

Table 4.2 Geometric Properties of Composite and Ceramic Material Bumper Plates

Test Number	Bumper ID Number	V (km/s)	d (mm)	t_s (mm)	t_w (mm)	S (mm)
			Kevlar 49			
103	C1	4.62	4.75	2.032	3.175	101.6
103A	C3	3.52	4.75	3.810	3.175	101.6
103B	C3	3.43	4.75	3.810	3.175	101.6
103C	C3	3.84	4.75	3.810	3.175	101.6
1031	C3	4.24	4.75	3.810	3.175	101.6
104	C3	6.72	7.62	3.810	3.175	101.6
104A	C3	6.65	7.62	3.810	3.175	101.6
104B	C3	7.01	7.62	3.810	3.175	101.6
1221	C2	7.15	7.62	2.921	3.175	152.4
1222	C2	7.40	7.62	2.921	3.175	152.4
			IM6/3501-6 Graphite/Epoxy			
177A	C4	6.91	6.35	3.810	3.175	101.6
177B	C4	7.38	6.35	3.810	3.175	101.6
			Alumina			
140A	C5	6.37	6.35	1.905	3.175	101.6
140B	C5	7.23	6.35	1.905	3.175	101.6
140C	C5	6.85	6.35	1.905	3.175	101.6

Table 4.3 Test Parameters for Composite and Ceramic Systems

Test Number	V (km/s)	d (mm)	t_s (mm)	t_w (mm)	S (mm)
P05	6.90	6.35	1.600	3.175	101.6
P06A	6.95	6.35	1.600	3.175	101.6
P16E	6.78	7.62	1.600	3.175	152.4
P16G	7.18	7.62	1.600	3.175	152.4
P20B	6.98	7.62	1.600	3.175	152.4
P20C	6.63	7.62	1.600	3.175	152.4
P21	6.63	7.62	1.600	3.175	101.6
P21A	6.47	7.62	1.600	3.175	101.6
P27	4.53	4.75	1.600	3.175	101.6
P27A	3.87	4.75	1.600	3.175	101.6
P27B	4.15	4.75	1.600	3.175	101.6
P33	7.21	6.35	1.016	3.175	101.6
P34	6.80	6.35	1.600	2.540	101.6
101	3.09	4.75	2.032	3.175	101.6
101A	3.96	4.75	2.032	3.175	101.6
101B	4.27	4.75	2.032	3.175	101.6
107	6.80	8.89	2.032	4.445	101.6
107A	6.74	8.89	2.032	5.080	101.6
107B	6.82	8.89	2.032	5.715	101.6
109B	3.61	4.75	2.032	3.175	101.6
228C	6.96	6.35	0.813	4.775	101.6
228D	6.95	6.35	0.813	4.775	101.6
EH3A	6.64	7.95	1.600	3.175	101.6
EH6C	6.58	7.95	1.600	3.175	101.6

Table 4.4 Test Parameters for Aluminum Systems

Test Number	D (mm)	γ (deg)	A_d (cm^2)	d_h (mm)	A_s (cm^2)
			Kevlar 49		
103	9.271	37.9	31.68	13.538	----
103A	9.677	34.1	30.39	8.103	----
103B	9.423	30.7	24.52	8.103	----
103C	9.271	26.7	26.71	----	----
1031	9.093	43.6	51.87	----	----
104	20.193	56.5	139.68	48.387	----
104A	19.685	64.0	126.64	50.063	----
104B	19.050	61.0	145.68	46.660	----
1221	19.558	40.8	102.58	54.458	----
1222	20.193	43.1	114.32	61.874	----
			IM6/3501-6 Graphite/Epoxy		
177A	15.596	49.4	81.03	11.075	----
177B	15.191	55.4	85.16	13.716	----
			Alumina		
140A	22.301	45.60	57.72	7.645	0.619
140B	33.096	57.31	97.21	----	----
140C	35.712	53.10	81.07	7.010	0.832

Table 4.5 Hypervelocity Impact Test Results for Composite and Ceramic Systems

Test Number	D (mm)	γ (deg)	A_d (cm^2)	d_h (mm)	A_s (cm^2)
P05	14.224	55.9	91.55	4.699	0.19
P06A	14.529	64.0	126.71	----	4.65
P16E	15.748	53.1	182.39	23.368	12.65
P16G	16.510	60.5	248.39	----	2.88
P20B	15.875	56.8	214.06	----	5.08
P20C	15.240	56.9	214.06	2.166	6.37
P21	15.875	63.9	126.64	28.804	5.29
P21A	14.300	58.1	102.58	33.782	----
P27	10.668	40.9	45.61	----	----
P27A	8.636	29.0	21.74	4.445	----
P27B	10.033	34.6	31.68	3.048	----
P33	13.005	64.0	126.64	crack	3.34
P34	14.122	64.0	153.29	10.363	2.68
101	10.135	28.1	20.25	6.655	----
101A	9.398	31.3	25.61	4.347	----
101B	14.224	52.8	81.03	----	----
107	19.050	66.5	139.61	15.434	12.13
107A	18.288	69.1	154.97	9.018	15.48
107B	19.050	66.5	139.68	crack	13.68
109B	10.160	44.2	62.06	----	----
228C	11.024	34.7	31.68	----	9.88
228D	11.201	33.4	29.16	2.642	2.86
EH3A	15.138	75.4	206.19	49.835	----
EH6C	17.475	63.7	126.64	31.979	----

Table 4.6 Hypervelocity Impact Test Results for Aluminum Systems

Test Number	Bumper Plate Material	Impact Energy (J)	Impact Momentum (kg-m/s)	Pressure Wall Plate	
				Penetrated?	Spalled?
103A	Kevlar	924.9	0.536	yes	no
109B	Aluminum	991.8	0.549	no	no
103B	Kevlar	895.3	0.522	yes	no
P27A	Aluminum	1139.8	0.589	yes	no
103C	Kevlar	1122.1	0.584	no	no
101A	Aluminum	1041.8	0.563	yes	no
P27B	Aluminum	1310.7	0.632	yes	no
1031	Kevlar	1368.1	0.645	no	no
101B	Aluminum	1387.5	0.650	no	no
103	Kevlar	1624.3	0.703	yes	no
P27	Aluminum	1561.7	0.689	no	no

Table 4.7 Penetration Comparison of Kevlar and Aluminum Systems (Impact Energy < 2,000 joules)

Stand Off Dist.	Test Number	Bumper Plate Material	Impact Energy (J)	Impact Momentum (kg-m/s)	Pressure Wall Plate	
					Penetrated?	Spalled?
101.6 mm	104B	Kevlar	15,441	4.405	yes	no
	EH6C/3A	Aluminum	15,733	4.739	yes	no
	P21	Aluminum	13,812	4.166	yes	yes
	104	Kevlar	14,274	4.236	yes	no
	104A	Kevlar	13,896	4.179	yes	no
	P21A	Aluminum	13,154	4.066	yes	no
152.4 mm	1221	Kevlar	16,064	4.493	yes	no
	P20B	Aluminum	15,309	4.386	no	yes
	P16G	Aluminum	16,199	4.512	no	yes
	1222	Kevlar	16,699	4.581	yes	no

Table 4.8 Penetration Comparison of Kevlar and Aluminum Systems (Impact Energy > 10,000 joules)

Regression Function	$\%\epsilon_{avg}$	$\sigma(\%)$	R^2
$\cos\gamma$	1.067	15.669	0.624
A_d/A_p	1.052	14.950	0.750
d_h/d	0.134	5.603	0.933

Table 4.9 Regression Analysis of Kevlar System Cone Angle and Pressure Wall Plate Damage Data, Error Summary

Test Number	Bumper Plate Material	Impact Energy (J)	Impact Momentum (kg-m/s)	Pressure Wall Plate	
				Penetrated?	Spalled?
P05	Aluminum	8657.4	2.509	yes	yes
177A	Graphite/Epoxy	8682.5	2.513	yes	no
177B	Graphite/Epoxy	9903.8	2.684	yes	no
P34	Aluminum	8408.2	2.473	yes	yes
P33	Aluminum	9452.7	2.622	crack	yes

Table 4.10 Penetration Comparison of Graphite/Epoxy and Aluminum Systems

Test Number	Bumper Plate Material	Impact Energy (J)	Impact Momentum (kg-m/s)	Pressure Wall Plate	
				Penetrated?	Spalled?
228C	Aluminum	8809	2.531	no	yes
228D	Aluminum	8041	2.418	yes	yes
140A	Alumina	7378	2.317	yes	yes
140B	Alumina	9505	2.629	no	no
140C	Alumina	8532	2.491	yes	yes
P05	Aluminum	8658	2.509	yes	yes
P06A	Aluminum	8783	2.528	no	yes

Table 4.11 Penetration Comparison of Alumina and Aluminum Systems

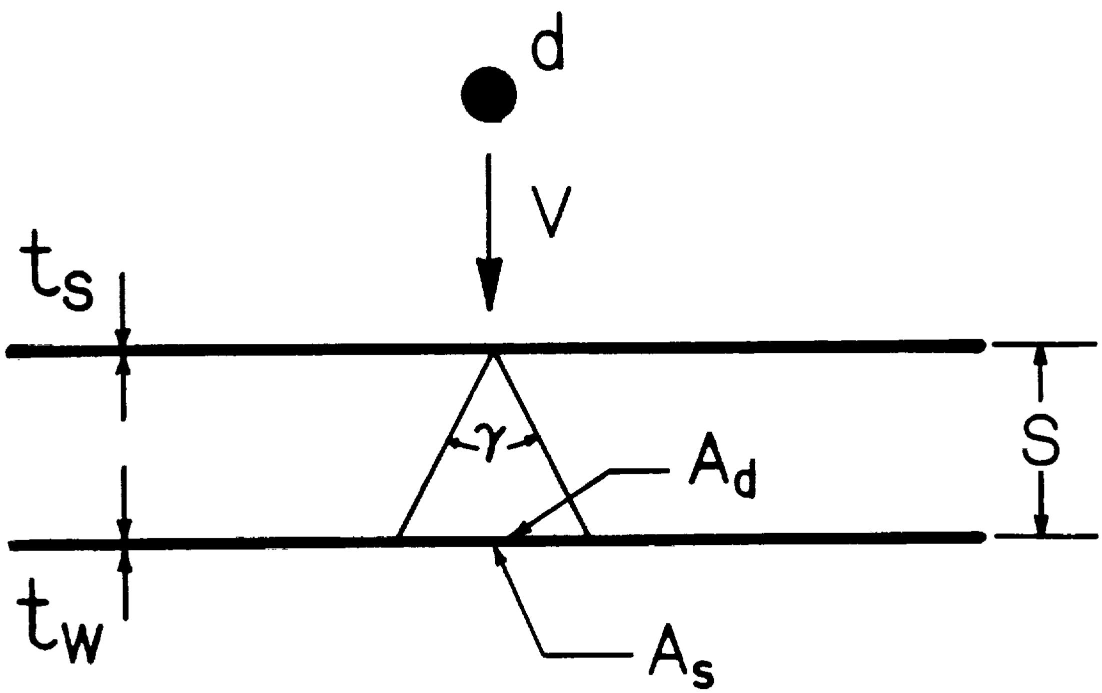

Figure 4.1 Normal Impact Test Configuration and Parameters

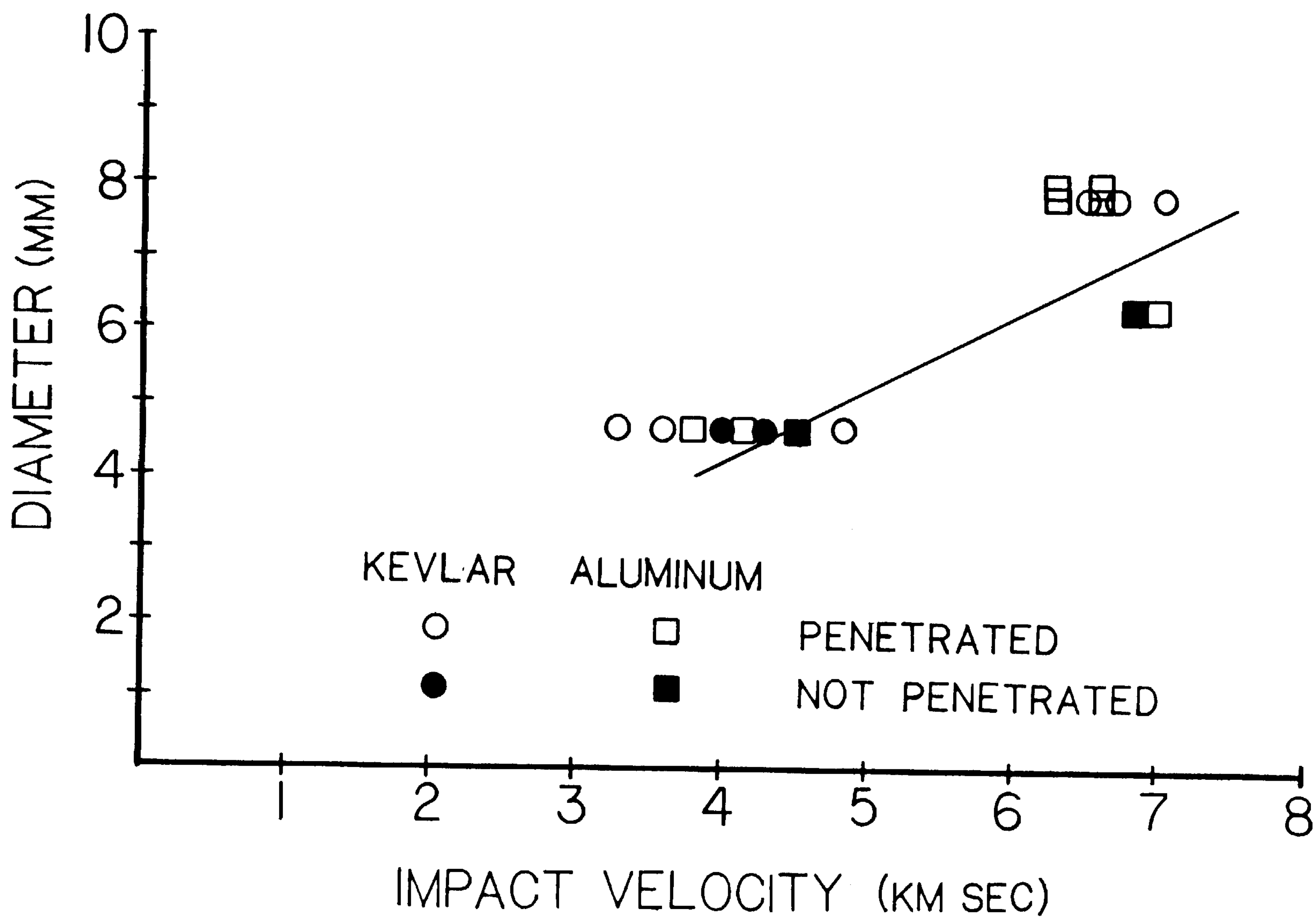

Figure 4.2 Penetration Function for Kevlar (t_s=3.81 mm) and Aluminum (t_s=1.6 mm) Dual-Wall Structures (t_w=3.175 mm, S=101.6 mm)

SECTION FIVE -- HYPERVELOCITY IMPACT RESPONSE OF SPACECRAFT WINDOW MATERIALS

5.1 Introduction

With the installation of windows for viewing as well as scientific purposes in spacecraft such as the Space Shuttle Orbiters and the Space Station Freedom, it has become necessary to study the response of window materials to hypervelocity projectile impact and to evaluate their degradation as a result of such impacts. Unfortunately, information on the hypervelocity impact response of window materials is relatively scarce (see, e.g. [5.1,5.2,5.3]).

This Section summarizes the results of an investigation into the response of window materials under hypervelocity projectile impact loadings. Two window materials of different hardness were considered in this study: Lexgard and glass. Several layers of Lexgard were glued together to form the single-panel Lexgard window test specimens. The glass window test specimens consisted of three panes separated by small distances. The impact damage to the Lexgard specimens is characterized according to the extent of surface damage, the extent of internal delamination, and the area of rear-side spall damage. The impact damage in the glass specimens is characterized according to the nature of the damage to each pane in the glass window system. A statistical analysis of the Lexgard impact test data indicates that the extent of the damage to the Lexgard specimens can be written as functions of the impact parameters of the original projectile and the geometric and material properties of the projectile/Lexgard window system. These empirical response functions can be used to perform parameter sensitivity studies and to evaluate hypothetical design applications and configurations.

5.2 Hypervelocity Impact Test Parameters

The conditions of the impact tests were chosen to simulate space debris impact of light-weight space structures as closely as possible, and still remain within the realm of experimental feasibility. Kessler, et.al., state that the average mass density for pieces of orbital debris less than 10 mm in diameter is approximately the same as that of aluminum [5.4]. Although it is anticipated that the shape of the impacting projectile will affect impact damage formation and propagation to some extent [5.5], spherical projectiles were used in the test program to maintain repeatability and consistency. Thus, the testing was conducted with solid spherical 1100 aluminum projectiles with diameters ranging from 3.175 mm to 9.525 mm. The velocities of the impacting projectiles ranged from 5.4 to 7.5 km/sec.

A total of 21 single-pane Lexgard specimens and 5 triple-pane glass specimens were used to study and evaluate the hypervelocity impact response of window materials. The Lexgard specimens were made from several 23 cm x 23 cm Lexgard sheets of varying thicknesses glued together (Figures 5.1a,b). The glass specimens consisted of three 15 cm x 15 cm panes separated by varying stand-off distances (Figure 5.2). In the glass specimens, the outer and inner panes were made from annealed soda lime and tempered Herculite II glass, respectively, while some middle panes were made from annealed soda lime glass and others from tempered Herculite II glass.

The mechanical properties of the window materials are given in Table 5.1; test parameters and configuration geometries for each window type are given in Tables 5.2, 5.3, and 5.4. The results of the hypervelocity impact test firings are given in Table 5.5 for the Lexgard specimens and in Table 5.7 for the glass specimens. Column entries of '----' in Table 5.5 indicate that penetration and/or spall of the Lexgard specimen did not occur. Table 5.6 contains a summary of the differences between experimental response characteristics and the response characteristics predicted using empirical equations derived from the experimental data. A complete set of photographs showing various response features of the Lexgard and triple-pane glass systems under hypervelocity impact can be found in Reference 5.6. Detailed analyses of the damaged test specimens revealed many interesting features and response characteristics of window materials under hypervelocity projectile impact loadings.

5.3 Hypervelocity Impact Response of Lexgard

5.3.1 Qualitative Damage Analysis

Two different window constructions were used to evaluate the response of Lexgard windows to hypervelocity projectile impact. One consisted of a 12.7 mm layer of Lexgard sandwiched in between two 3.175 mm Lexgard layers for a total specimen thickness t_w=19.05 mm (Figure 5.1a). The other contained an additional interior 12.7 mm layer for a total specimen thickness t_w=31.75 mm (Figure 5.1b). In each test, a projectile of diameter d and velocity V impacted a Lexgard window specimen along a trajectory perpendicular to the plane of the window (Figures 5.1a,b). The projectile shattered upon impact and created a series of shock waves that created an internal area of damage. This internal damage area was typically a circular area of delamination between the Lexgard layers. In some instances, front and rear surface petalling, as well as rear surface spall, resulted from shock wave interaction at the interface between a thin surface layer and a thick interior layer. Occasionally, penetration of the window specimen occurred as well. In these cases, the material surrounding the hole was melted and torn through the thickness of the specimen.

A summary of the damage to each of the Lexgard specimens can be found in Table 5.5 where D is the diameter of the hole in the specimen if penetration occured, A_d is the area of the internal damage region, and A_s is the area of rear surface spall if spall occured. Penetration functions for normal impact of both specimen types are shown in Figure 5.3 based on the penetration data in Table 5.5; a spall function for the normal impact of the thin Lexgard panels is shown in Figure 5.4. These curves can be used to determine if penetration or rear-surface spall will occur as a result of a particular high velocity impact. It is noted that the curves in Figures 5.3 and 5.4 are simply lines of demarcation between areas of penetration and no penetration and spall and no spall for the parameters indicated.

While rear surface spall occured frequently in the impact of the thin Lexgard specimens, it is interesting to note that rear surface spall did not occur in any of the thick specimens. Impact of the thick specimens resulted in either rear surface petalling without spall or in a 'ballooning' of the rear surface, also without spall. Additionally, the rear surface remained undamaged when a thick Lexgard specimen was impacted by the smaller projectiles; impact by the larger projectiles resulted in significant delamination between the two thick interior layers. Oblique impacts were observed to penetrate the thin specimens but not the thick specimens. At trajectory obliquities of 45° and 65°, the thin specimens were penetrated by 7.95 mm projectiles. However, the thick specimens were not penetrated at either trajectory obliquity, even though the projectile diameter was increased to 9.525 mm. Significant front and rear surface petalling and large areas of internal delamination were also observed in Lexgard specimens impacted by large obliquely incident projectiles.

5.3.2 Regression Analysis of Damage Data

A standard multiple linear regression analysis of the data in Table 5.5 was performed to obtain equations for hole diameter in the event of a penetration, internal damage area, and rear surface spall area if spall occurs as functions of geometric, material, and impact parameters.

Hole Diameter

$$D/d = 1.043(V/C)^{1.389}(t_w/d)^{-1.201} \quad , \theta = 0^o \tag{5.1}$$

Rear Spall Area

$$A_s/A_p = 0.000505(V/C)^{6.909}(t_w/d)^{0.946} \quad , \theta = 0^o \tag{5.2}$$

Damage Area

$$A_d/A_p = 39.04(V/C)^{1.390}\cos^{0.266}\theta(t_w/d)^{0.241} \tag{5.3}$$

where $C = \sqrt{E/\rho}$ and $A_p = \pi d^2/4$. The average errors, standard deviations, and correlation coefficients for equations (5.1-5.3) are given in Table 5.6. Based on the data in Table 5.6, it is evident that equations (5.1-5.3) fit the experimental data fairly well. It is noted that equations (5.1-5.3) are valid only for impacts of aluminum projectiles on Lexgard panels of similar lay-up and construction, and for impact velocities between 5.4 and 7.5 km/sec. Additionally, equations (5.1,5.2) are valid only for normal impacts while equation (5.3) may be used to calculate internal damage areas for normal and oblique impacts. Furthermore, before using equations (5.1) and (5.2), Figures 5.3 and 5.4 must be consulted to determine whether or not penetration or spall will occur as a result of a particular impact.

5.4 Hypervelocity Impact Response of Glass Systems

Two different configurations were used to study the response of triple-pane glass windows to hypervelocity projectile impact. The essential differences between the two systems were the thickness of the outer panes and the stand-off distance between the outer and middle panes (the 'outer stand-off distance'). In one triple-pane system, the outer pane thickness was 6.4 mm and the outer stand-off distance was 12.7 mm. In the other, the outer pane was 16 mm thick and the distance between the outer and middle pane was 50.8 mm. In both systems, the thicknesses of the middle and inner panes were 16 mm each and the spacing between the middle and inner panes was 12.7 mm.

A summary of the resulting damage to each pane in each test is presented in Table 5.7. For the purposes of this investigation, a glass window specimen was considered to be penetrated if the inner pane was cracked or shattered. A shattered pane is defined as a pane that disintegrates into smaller pieces upon impact. A cracked pane has numerous fractures, but remains intact after impact. Due to the small number of tests performed, it would be impossible and inappropriate to perform a regression analysis of the glass system damage data presented in Table 5.7. However, a qualitative analysis of the damage revealed many interesting features and characteristics of multi-pane window systems under hypervelocity impact.

The hypervelocity impact response of the triple-pane glass specimens was significantly different from that of the Lexgard test specimens. The damage in the glass panes was much more extensive due to their brittleness and low tensile strength. This allowed the shock-related stresses to overwhelm the material strengths for a longer period of time in the glass specimens than in the Lexgard test specimens [5.2]. In four of the glass tests, the outer pane was completely shattered and disintegrated. The thinner outer panes in Tests 18-1 and 18-2 were shattered into hundreds of pieces ranging from approximately 0.1 cm to 3 cm in diameter; the thicker outer panes in Tests 18-3 and 18-4 were shattered into several large chunks ranging from about 3.5 cm to 7.5 cm in diameter. In the fifth test, the outer pane was laminated and, as such, did not disintegrate upon impact. However, it was penetrated and sustained relatively large areas of spallation on both front and back surfaces. The middle panes in the specimens with the thick outer panes and the larger outer stand-off distance sustained no serious damage. The middle panes in the specimens with the thinner outer panes and the smaller outer stand-off distance were either cracked or shattered. The cracked middle panes contained numerous overlapping radial and concentric ring fractures. As such, their appearance strongly resembled that of a thick glass block subjected to a hypervelocity projectile impact [5.1]. The inner panes sustained no damage regardless of the thickness of the outer pane.

A more detailed examination of the damage sustained by each pane in the triple-pane glass window systems revealed that the systems with laminated panes faired better overall than did those systems without laminated panes. For example, in Test 18-2, the middle pane was laminated while in Test 18-1 it was not. Accordingly, the middle pane in Test 18-1 cracked in half while the middle pane in Test 18-2 merely sustained some cracks on the front surface and was not penetrated. Furthermore, lamination of the outer pane in Test 18-5 prevented its complete disintegration whereas the otherwise identical outer panes in Tests 18-1 and 18-2 were completely shattered under similar impacts.

Finally, the observed failures of the outer glass panes were compared against the predictions of the window penetration equations developed during the Apollo/Skylab era [5.3]:

$$p = 0.53\rho_p^{0.5}d_p^{1.06}V_p^{0.67} \tag{4}$$

$$t_c = 0.14V_p^{1.28}p \qquad\qquad t_s = 7p \tag{5a,b}$$

where ρ_p, d_p, V_p are the density (in gm/cm^3), diameter (in cm) and velocity (in km/sec) of the impacting projectile, ρ is the depth of penetration (in cm), t_c is the minimum thickness necessary to prevent through-cracks (in cm), and t_s is the minimum thickness needed to prevent rear-side spallation (in cm). Using these equations and the projectile parameters in Table 5.3, it was found that thicknesses on the order of 14 mm would be required to prevent through-cracks while glass blocks on the order of 64 mm thick would be required to prevent rear-side spall. Thus, it is not surprising that the thinner outer panes (in Tests 18-1 and 18-2) broke apart into hundreds of pieces while the thicker outer panes in Tests 18-3 and 18-4, which were fairly close to the thickness required to prevent through-cracking, broke apart into a relatively small number of pieces.

From these results, it can be concluded that both triple-pane glass window systems can withstand impacts of 3.175 mm diameter aluminum particles traveling at speeds of up to 6.6 km/sec. If such systems were used for spacecraft windows, it is unlikely that a pressure leak would occur due to an on-orbit impact of similar magnitude. If such an impact were to occur on a window system containing a thin outer pane placed at a small distance away from the middle pane, only the inner pane would be left to maintain the pressure seal. If the glass window system were to have a thin laminated outer pane or a thick outer pane placed at a relatively large distance from the middle plane, the middle pane would most likely remain undamaged and two window panes would be left to maintain the pressure seal. However, an on-orbit impact of a triple-pane glass window system with a thick outer pane would create large chunks of secondary debris which could subsequently be more damaging than the smaller secondary debris pieces created by the impact of a triple-pane window system with a thin outer pane. Lamination of both the outer and middle panes would reduce the potential for the creation of any glass debris fragments. In any case, the window would be rendered useless for viewing and scientific purposes and would necessitate the replacement of at least one pane of the window system.

5.5 Conclusions

An investigation of the hypervelocity impact response of spacecraft window materials has revealed many interesting features and response characteristics. Multi-layer Lexgard windows were found to sustain high levels of internal, penetration, and rear side spall damage as a result of normal and oblique hypervelocity impacts. The tendency of the Lexgard window panels to spall as a result of a hypervelocity impact is an area of major concern. Because of the high speeds with which spall fragments can travel, impact-induced spall can be as deleterious to mission success and crew safety as an actual penetration. The lethality of the high-speed spall fragments must not be overlooked.

Triple-pane glass window systems were found to be rather resilient under hypervelocity projectile impact loadings and did not sustain any penetration or spall damage of the inner-most window pane. Increasing the thickness of the outer pane served to reduce the number of fragments that formed when it shattered under impact; increasing the outer stand-off distance resulted in a significant decrease in the damage sustained by the middle window pane. Furthermore, it was found that laminating the outer and middle window panes prevented them from disintegrating upon impact. This is highly desirable in order that, in the event of an on-orbit glass window impact, the orbital environment does not become further contaminated by hundreds of glass debris fragments.

Based on the observations made during the course of this investigation, it is recommended that additional testing of multi-pane glass window systems be performed using large diameter projectiles and at oblique angles. Such testing would result in a more complete understanding of the growth of impact damage in glass window systems and in a more accurate prediction of the response of such systems in the event of an on-orbit impact.

5.6 References

5.1 R.E. Flaherty, "Impact Characteristics in Fused Silica", Proceedings of the AIAA Hypervelocity Impact Conference, AIAA Paper No. 69-367 (1969).

5.2 B.G. Cour-Palais, "Hypervelocity Impact in Metals, Glass, and Composites", Int. J. Impact Engng., Vol. 5, pp. 221-237 (1987).

5.3 B.G. Cour-Palais, "Hypervelocity Impact Investigations and Meteoroid Shielding Experience Related to Apollo and Skylab", Orbital Debris, NASA CP 2360, 1982, pp. 247-75.

5.4 D.J. Kessler, R.C. Reynolds, and P.D. Anz-Meador, Orbital Debris Environment for Spacecraft Designed to Operate in Low Earth Orbit, NASA TM 100471, Houston, Texas (1989).

5.5 R.H. Morrison, A Preliminary Investigation of Projectile Shape Effects in Hypervelocity Impact of a Double Sheet Structure, NASA TN D-6944, Washington, D.C. (1972)

5.6 W.P. Schonberg, "Response of Spacecraft Window Materials to Hypervelocity Projectile Impact", J. Spacecraft Rockets, Vol 27, in press (1990).

	Lexgard	Soda Lime Glass	Herculite II
E ($\times 10^9$ N/m^2)	2.47	70.4	75.9
ν	----	0.22	0.21
ρ (kg/m^3)	1150	2410	2464

Table 5.1 Mechanical Properties of Window Materials

Test Number	V (km/s)	θ	d (mm)	t_w (mm)
123-1	5.40	0	3.175	19.05
123-2	5.80	0	3.175	19.05
123-3	6.40	0	3.175	19.05
124-1	6.30	0	4.750	19.05
124-2	5.86	0	4.750	19.05
124-3	5.50	0	4.750	19.05
124-4	4.66	0	4.750	19.05
125A	5.27	0	6.350	19.05
125B	3.78	0	6.350	19.05
125C	3.23	0	6.350	19.05
126A	7.24	0	4.750	31.75
126B	7.46	0	4.750	31.75
127A	7.16	0	6.350	31.75
127B	7.41	0	6.350	31.75
129A	6.86	0	7.620	31.75
129B	6.45	0	7.620	31.75
129C	6.00	0	7.620	31.75
171A	6.60	45	9.525	31.75
172A	6.65	65	9.525	31.75
173A	6.91	45	7.950	19.05
174A	6.94	65	7.950	19.05

Table 5.2 Lexgard Impact Test Parameters

Test Number	V (km/s)	d (mm)	t_o (mm)	t_m (mm)	t_i (mm)	S_o (mm)	S_i (mm)
18-1	6.50	3.175	6.4	16.0	16.0	12.7	12.7
18-2	6.33	3.175	6.4	16.0	16.0	12.7	12.7
18-3	6.50	3.175	16.0	16.0	16.0	50.8	12.7
18-4	6.63	3.175	16.0	16.0	16.0	50.8	12.7
18-5	6.50	3.175	6.4	16.0	16.0	12.7	12.7

Table 5.3 Glass Impact Test Parameters

Test Number	Outer Pane	Middle Pane	Inner Pane
18-1	Soda Lime	Herculite II	Herculite II
18-2	Soda Lime	Laminated Herculite II	Herculite II
18-3	Soda Lime	Soda Lime	Herculite II
18-4	Soda Lime	Laminated Soda Lime	Herculite II
18-5	Laminated Soda Lime	Laminated Soda Lime	Herculite II

Table 5.4 Glass Window Pane Materials

Test Number	D (mm)	A_d (cm²)	A_s (cm²)
123-1	----	24.45	2.787
123-2	----	20.26	1.510
123-3	----	33.48	0.806
124-1	7.493	64.71	----
124-2	6.299	63.29	----
124-3	5.791	49.81	----
124-4	----	59.10	1.026
125A	10.414	113.42	----
125B	6.756	60.32	----
125C	----	51.81	----
126A	----	135.03	----
126B	----	109.42	----
127A	----	182.06	----
127B	----	188.39	----
129A	6.629	230.84	----
129B	----	159.61	----
129C	----	186.32	----
171A	----	387.93	----
172A	----	230.52	----
173A	45.7x53.3	153.29	----
174A	31.750	167.55	----

Table 5.5 Hypervelocity Impact Test Results for Lexgard Panels

Regression Function	$\%\epsilon_{avg}$	$\sigma(\%)$	R^2
D/d	0.038	3.045	0.971
A_s/A_p	10.658	62.233	0.827
A_d/A_p	1.280	16.402	0.804

Table 5.6 Regression Analysis of Lexgard Damage Data Error Summary

Test Number	Outer Pane	Middle Pane	Inner Pane	Penetrated?
18-1	Shattered; ≈100 fragments 0.1 to 2.5 cm	Shattered	No Damage	No
18-2	Shattered; ≈100 fragments 0.1 to 3.2 cm	Cracked No Penetration	No Damage	No
18-3	Shattered; 19 fragments 3.5 to 7.5 cm	Minor Pitting	No Damage	No
18-4	Shattered; 6 fragments 3.5 to 5.1 cm	Minor Pitting	No Damage	No
18-5	3.25 mm hole; 4.3 cm dia. spall on both surfaces; No Disintegration	Cracked No Penetration	No Damage	No

Table 5.7 Hypervelocity Impact Test Results for Glass Systems

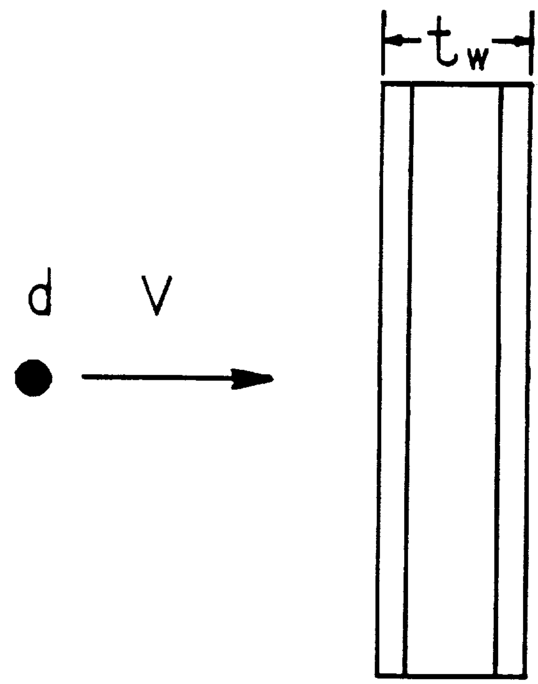

Figure 5.1a Thin Lexgard Window Test Specimen Configuration

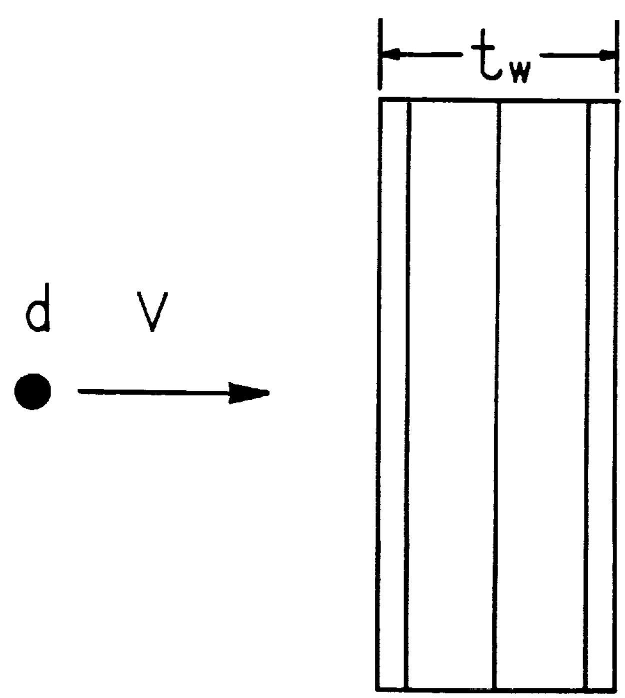

Figure 5.1b Thick Lexgard Window Test Specimen Configuration

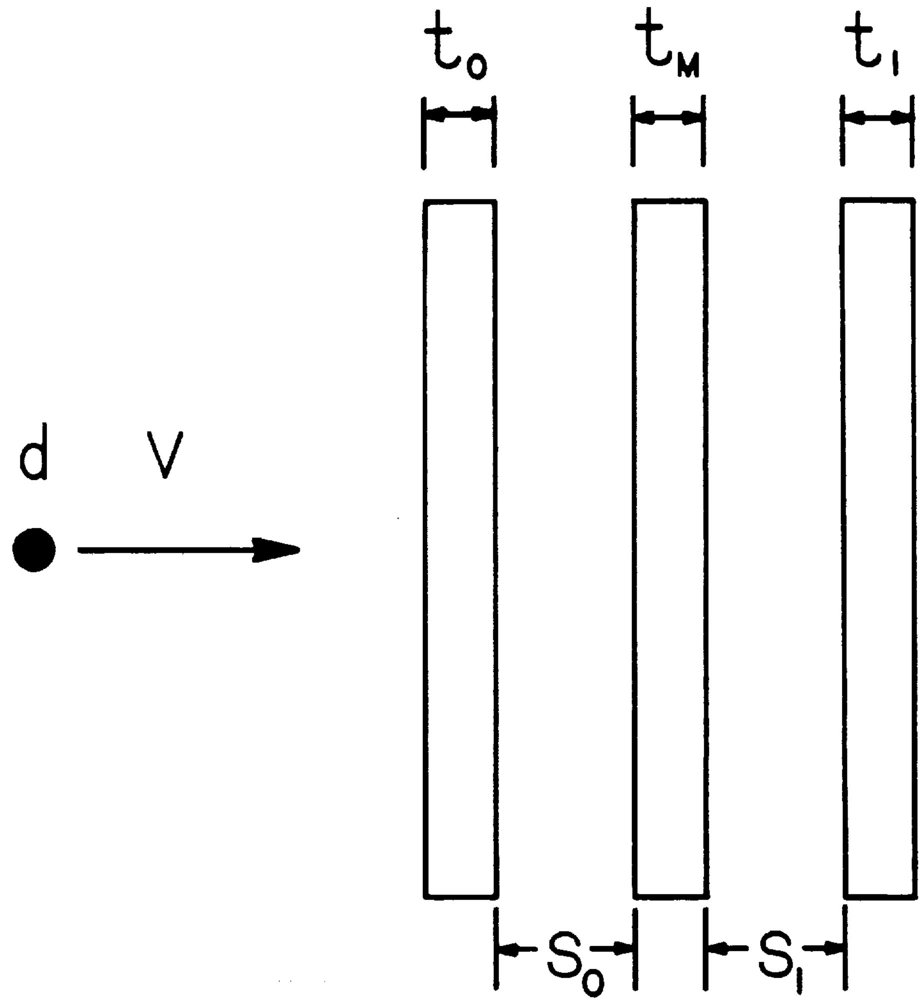

Figure 5.2 Triple Pane Glass Window Test Specimen Configuration

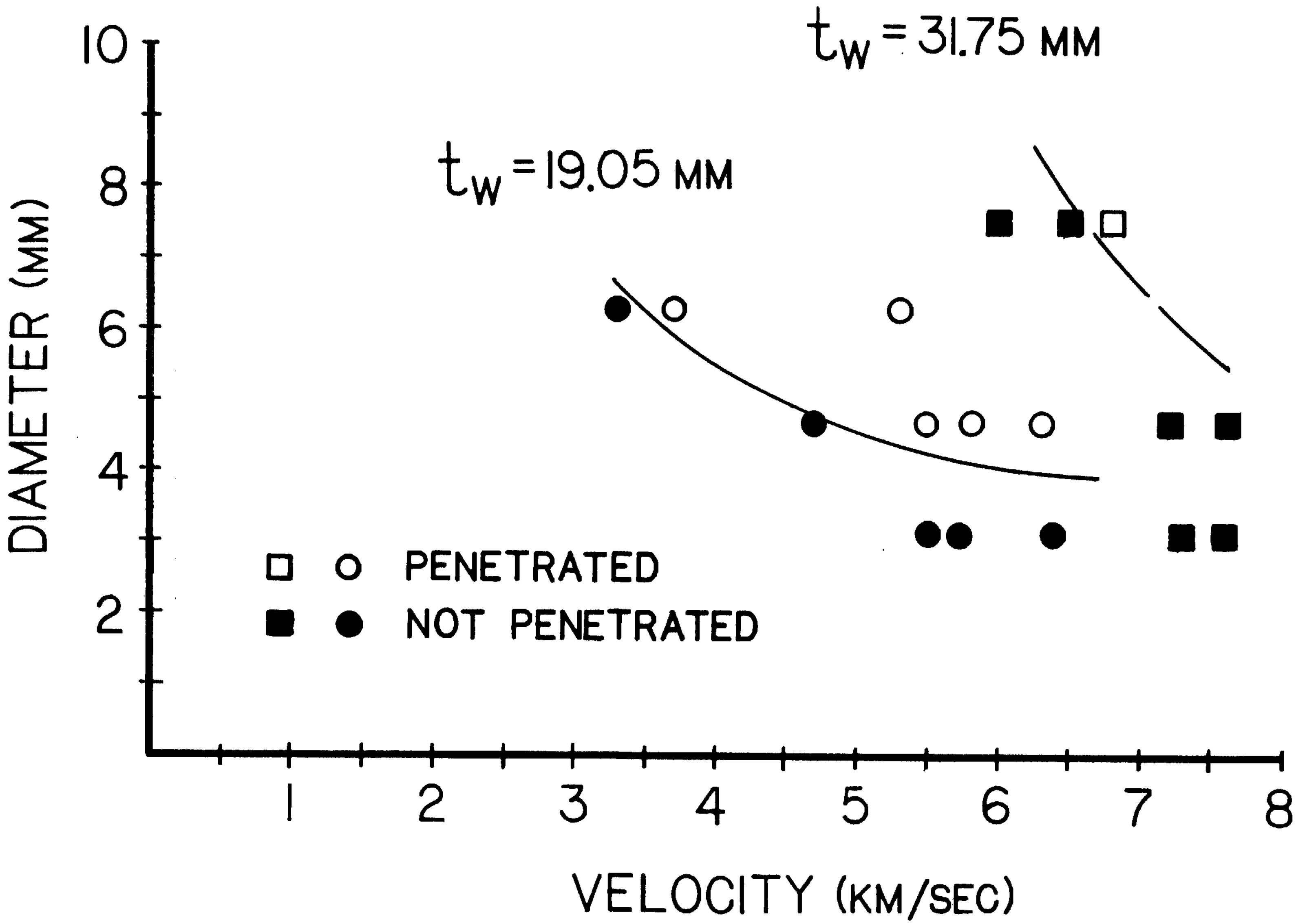

Figure 5.3 Penetration Functions for Lexgard Window Systems

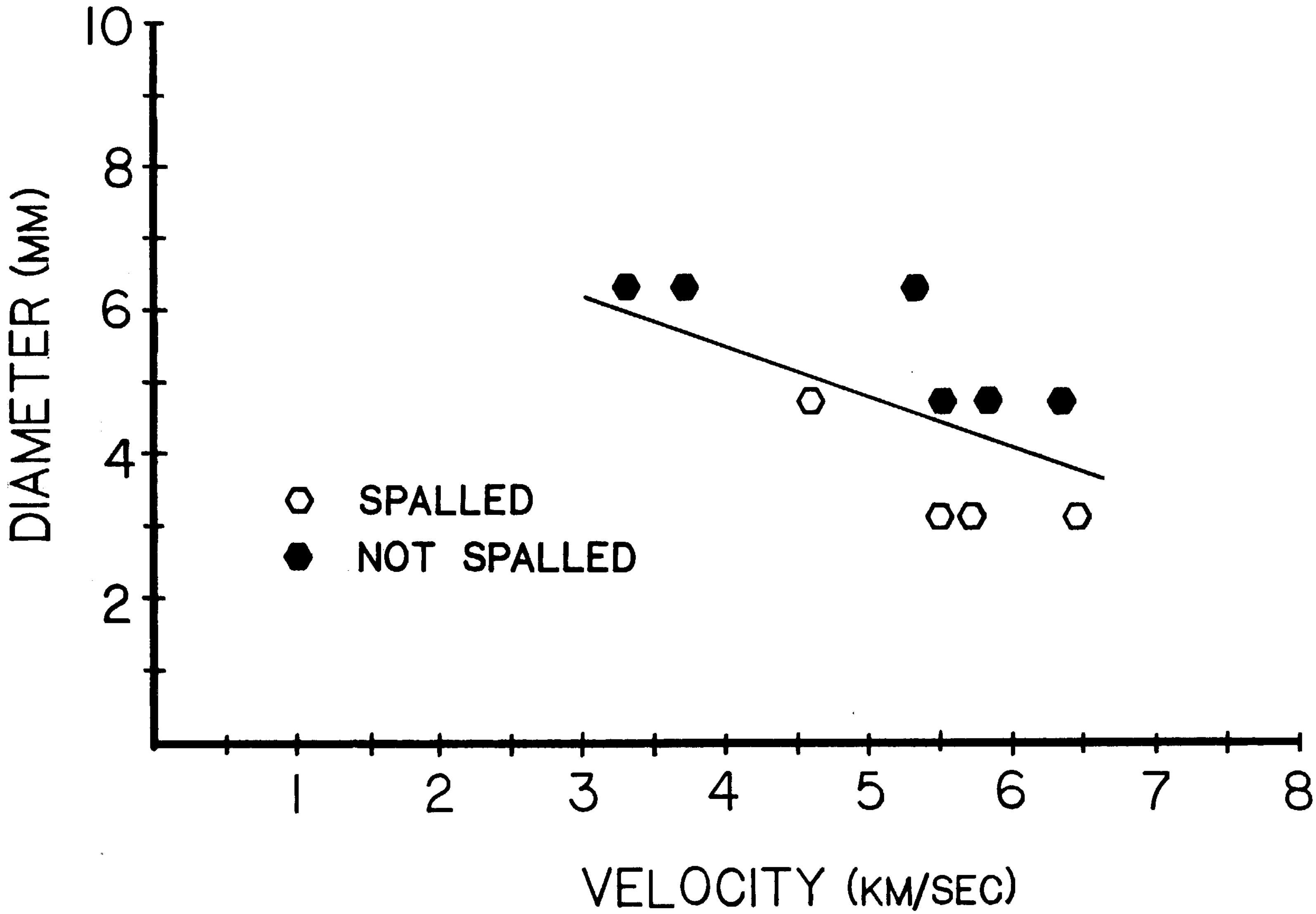

Figure 5.4 Spall Function for Thin Lexgard Window Systems

SECTION SIX -- HYPERVELOCITY IMPACT OF DUAL-WALL SYSTEMS WITH CORRUGATED BUMPERS

6.1 Introduction

In the majority of previous investigations of dual-wall structures under hypervelocity impact, the bumper plates were typically uniform in nature and made from a variety of metallic or composite materials. Dual-wall configurations were repeatedly shown to provide significant increases in protection against penetration by small high-speed projectiles over equivalent single-wall structures. However, the recent proliferation of large pieces of orbiting space debris has made it necessary to modify such systems so that they can resist penetration by projectiles with much higher impact energies. Novel design concepts that will possess increased levels of protection must be developed for spacecraft that are to be launched into the meteoroid and space debris environment.

This Section summarizes the results of an investigation in which a modified dual-wall structural system was tested for penetration by hypervelocity projectiles. In this modified system, the traditional uniform bumper was replaced by a corrugated bumper of equal weight. Impact test results for two different types of corrugated bumpers are reviewed qualitatively and quantitatively. Impact damage in the structural systems is characterized according to the extent of penetration, crater, and spall damage in the pressure wall plate as a result of the impact loadings. The impact damage in the specimens with corrugated bumper plates is compared to impact damage in specimens with uniform, monolithic bumpers of similar weight. This comparative analysis is used to determine the advantages and disadvantages of employing corrugated bumpers in structural wall systems for long-duration spacecraft.

6.2 Hypervelocity Impact Test Parameters

In each test, a projectile of diameter d and velocity V impacted a dual-wall test specimen along a trajectory inclined at an angle θ with respect to the outward normal of the test specimen bumper plate. Figure 6.1 illustrates the oblique impact of a dual-wall test specimen with a monolithic bumper plate (a 'monolithic bumper system') while Figure 6.2 shows the oblique impact of a dual-wall system with a corrugated bumper (a 'corrugated bumper system'). In Figure 6.2, the corrugated bumper is seen to consist of a series of corrugations sandwiched in between flat 'front' and 'rear' bumper plates, where the 'front' plate is that plate which is first struck by an incoming projectile.

In the monolithic bumper system impacts, the projectile was shattered and created a hole in the bumper plate. In the corrugated system impacts, a series of holes were created in the corrugations as the debris cloud containing projectile and bumper plate fragments spread out and moved through the corrugations. In both cases, the secondary debris fragments were sprayed upon a pressure wall plate of thickness t_w located a distance S behind the bumper. In the corrugated bumper systems, the distance S is measured from the pressure wall plate to the 'rear' plate of the corrugated bumper. In Figures 6.1 and 6.2, the angles θ_1 and θ_2 denote the trajectories of the centers of mass of the 'normal' and 'in-line' secondary debris fragments, respectively; the angles γ_1 and γ_2 represent the spread of these fragments. It is noted that the spread of the secondary debris clouds in the corrugated bumper systems began immediately so that by the time the debris cloud exited the rear of the bumper, a fair amount of spreading had already occured.

Therefore, the angles θ_1, θ_2 and γ_1, γ_2 for the corrugated bumper systems are measured from the impact site on the front plate and not from the debris cloud exit site on the rear plate. The impact of the secondary debris particles created 'normal' and 'in-line' areas of damage A_{d1} and A_{d2}, respectively, on the front surface of the pressure wall plate. In those tests where the path of the projectile was normal to the surface of the bumper plate (ie. $\theta=0^o$), the 'normal' and 'in-line' debris clouds overlapped in a single debris cloud whose center-of-mass trajectory was close to the inward normal of the test specimen bumper plate (ie. $\gamma_1 \simeq \gamma_2 = \gamma_n$ and $\theta_1 \simeq \theta_2 = \theta_n$). The damage areas also overlapped and combined to form a single area of damage A_d on the front surface of the pressure wall plate. Occasionally, the impacts of the secondary projectile and bumper plate fragments resulted in the creation of thin spall fragments ejected from the rear side of the pressure wall plate. In these cases, for both the normal and oblique impacts, the total spalled area on the rear surface is denoted by A_s.

The conditions of the impact tests were chosen to simulate space debris impacts of light-weight space structures as closely as possible, and still remain within the realm of experimental feasibility. Kessler, et.al., state that the average mass density for pieces of orbital debris less than 10 mm in diameter is approximately the same as that of aluminum [6.1]. Although it is anticipated that the shape of the impacting projectile will affect impact damage formation and propagation to some extent [6.2], spherical projectiles were used in the test program to maintain repeatability and consistency. Thus, the testing was conducted with solid spherical 1100 aluminum projectiles with diameters ranging from 6.35 mm to 9.53 mm. The velocities of the impacting projectiles ranged from 2.9 to 7.0 km/sec. To study the effects of trajectory obliquity on penetration, impact testing was performed at obliquities of 0^o and 45^o. Additionally, to simulate presence of thermal insulation in the spacecraft wall design, some of the tests were performed with MLI (multi-layer insulation) resting on the pressure wall plate.

A total of 18 structural systems with uniform monolithic bumper plates and 13 systems with corrugated bumper plates were used to study and evaluate the penetration resistance of dual-wall systems with corrugated bumpers. In both systems, the bumper and pressure wall plates were made from 6061-T6 and 2219-T87 aluminum, respectively. Two different types of corrugated bumper plates were used: one consisted of 'deep' corrugations with a rise angle $\alpha=53^o$; the other consisted of 'shallow' corrugations with a rise angle of $\alpha=20^o$ (see Figure 6.3). Detailed geometric parameter values for the corrugated bumpers are presented in Table 6.1. The parameters correspond to the dimensions of the repeating element of a corrugated bumper as shown in Figure 3. The thicknesses of the monolithic bumper plates were chosen such that the monolithic and corrugated bumper plates had similar areal densities. The corrugated bumper plates were calculated to have areal densities of approximately 0.456 gm/cm^2; therefore, dual-wall systems with monolithic bumper plates 1.6 mm thick were used for comparison. The MLI consisted of 30 layers of 0.5 mil kapton aluminized on one side and 29 layers of Dacron mesh between each kapton layer. Additionally, 1 layer of beta-cloth (coated s-glass) was added on the side nearest the bumper plate for durability. The areal density of this combination was calculated to be approximately 0.107 gm/cm^2 [6.3]. Additional test parameters and configuration geometries are given in Tables 6.2 and 6.3 for the tests with corrugated and monolithic bumper plates, respectively.

The results of the hypervelocity impact test firings are given in Tables 6.4 and 6.5 for the systems with corrugated and monolithic bumper plates, respectively. In Tables 6.4 and 6.5, column entries of '----' indicate that certain phenomena, such as pressure wall plate penetration, front surface damage, or rear surface spall, did not occur. Additionally, in Tables 6.4 and 6.5, d_h is the equivalent hole diameter of all the holes in the pressure wall plate in the event of pressure wall plate penetration. Penetration characteristics are summarized in Tables 6.6 and 6.7 for test shots grouped according to both geometric and impact energy similarity. Table 6.6 presents response summaries for the normal shots; Table 6.7a presents a summary of response characteristics for oblique shots with low impact energy (ie. lower than 10,000 joules) while Table 6.7b presents a summary for oblique shots with high impact energy (ie. greater than 10,000 joules). In Tables 6.7a and 6.7b, the superscript '1' indicates that the penetration or spall is in the 'normal' damage area while the superscript '2' indicates that 'in-line' penetration or spall has occured. Penetration functions for the structural systems under oblique impact are presented in Figure 6.4. Photographs showing the response of corrugated bumper systems to hypervelocity projectile impact can be found in Reference 6.4. Detailed analyses of the damaged test specimens revealed many interesting features and response characteristics of dual-wall structures with corrugated bumpers under hypervelocity projectile impact loadings.

6.3 Hypervelocity Impact Response of Dual-Wall Systems With Corrugated Bumpers

6.3.1 Bumper Damage Analysis

The impact damage in the monolithic bumper plates consisted of either a circular or an elliptical hole, depending on the trajectory obliquity. As the trajectory obliquity was increased from 0^{o} to 45^{o}, the hole became noticeably elongated. In the tests with the corrugated bumper plates, as the debris cloud containing projectile and bumper fragments moved through the corrugations, a significant number of the debris fragments were trapped within the corrugations and did not exit the rear bumper panel. Therefore, the amount of energy imparted to the pressure wall plate by the debris fragment clouds in the tests with the corrugated bumpers was much lower than that imparted to the pressure wall by the debris clouds in the tests with monolithic bumper plates.

6.3.2 Pressure Wall Plate Damage Analysis

In Tables 6.6 and 6.7, penetration characteristics are summarized for test shots grouped according to geometric and impact energy similarity. Penetration functions for the structural systems with shallow corrugated bumpers and the corresponding systems with traditional monolithic bumper plates are shown in Figure 6.4. Using Tables 6.4 through 6.7 and the penetration functions in Figure 6.4, a comparison of penetration response characteristics is performed.

According to Tables 6.4a and 6.5a, in the normal impact tests, the pressure wall plate damage areas of the systems with monolithic bumper plates were much larger than those in the corresponding dual-wall systems with corrugated bumper plates. The secondary debris cloud cone angles in the monolithic bumper system impacts were also larger than those in the corresponding corrugated bumper system impacts. In Table 6.6, pressure wall plate penetration is seen to occur in all three corrugated bumper systems and in almost all of the systems with monolithic bumper plates. Although the likelihood of penetration under normal impact appears to be the same for both type of systems, it is important to note that the reverse sides of the pressure wall plates of the corrugated bumper systems did not exhibit any spall, while those of the monolithic bumper systems exhibited significant rear-side spalling. This increased tendency for spall in the monolithic bumper specimens is a direct consequence of the wider areal distribution of the impulse delivered by the secondary debris fragment cloud. While the impulse delivered to the pressure wall plate in the corrugated bumper systems appeared to be more concentrated, the smaller damage areas are actually due to the fewer number of debris particles in the secondary debris clouds. This resulted in a decreased tendency for rear-side spall in the corrugated bumper systems.

Under oblique impact in the presence of MLI, neither system exhibited rear-side spallation of the pressure wall plate. However, this is probably a function of the presence of the MLI rather than the obliquity of impact. In a previous investigation of oblique hypervelocity impact, it was found that rear-side pressure wall plate spall could occur in dual-wall systems under oblique as well as normal impact [6.3]. Penetration of the pressure wall plate was found to occur in all but three of the systems with monolithic bumpers. However, only three of the corrugated bumper systems sustained pressure wall plate penetration. Furthermore, the equivalent hole diameters of the pressure wall plates in the penetrated corrugated bumper systems were much smaller than the equivalent hole diameters of the penetrated pressure wall plates in the corresponding monolithic bumper systems. Thus, while pressure wall plate penetration under oblique impact was possible in both types of systems, it occured with a much lower frequency and was much less severe in the systems with corrugated bumpers than in the monolithic bumper systems. In addition, in both types of systems, whenever pressure wall plate penetration occured under a 45^{o} impact, it occured in the 'in-line' damage area. This is consistent with the results of a previous investigation of oblique hypervelocity impact phenomena [6.5] in which it was observed that the more severe damage to the pressure wall plate of a dual-wall system under a 45^{o} impact was caused by the 'in-line' secondary debris fragments.

The increased protection against pressure wall plate penetration under oblique impact provided by the shallow corrugated bumpers as compared to the corresponding monolithic bumpers is also evident in Figure 6.4. The area between the two penetration functions represents those 45^{o} impacts that would penetrate a pressure wall plate protected by a monolithic bumper but would not penetrate a pressure wall plate protected by a shallow corrugated bumper similar in design to the ones used in this study.

In Tables 6.4b and 6.5b it can be seen that the total damage on the front surfaces of the pressure wall plates in the corrugated bumper systems under oblique impact were also generally smaller than those in the corresponding systems with monolithic bumpers. However, it is again noted that the smaller damage areas in the corrugated bumper systems were not due to a concentration of the debris clouds, but rather, as discussed previously, were due to the decrease in the quantity of bumper and projectile debris fragments that constituted the debris cloud and eventually struck the pressure wall plate.

Finally, it is noted that in approximately half of the corrugated bumper systems under oblique impact, there was absolutely no damage to the pressure wall plate along the 'normal' debris trajectory. This phenomenon occured only once in the dual-wall systems with monolithic bumpers. Since the MLI was present in both types of systems, it would appear that the corrugated bumpers absorbed a significant portion of 'normally' directed energy. This feature would serve to further lessen the likelihood of pressure wall plate penetration and would also reduce the magnitude of front surface damage on the pressure wall plates.

6.4 Summary and Conclusions

An investigation of the hypervelocity impact response of dual-wall structures with corrugated and monolithic bumpers has revealed many interesting response characteristics. Based on the observations made during the course of this study, it appears that a significant increase in protection against penetration by hypervelocity projectiles can be achieved if the traditional monolithic bumper in a dual-wall configuration is replaced with a corrugated bumper of equal or near-equal weight. In the specimens with corrugated bumpers, the frequency of pressure wall plate penetration was significantly lower than in corresponding specimens with monolithic bumper plates. Additionally, the damage area on the pressure wall plates was significantly decreased when a monolithic bumper plate was replaced with an equal-weight corrugated bumper plate. Use of corrugated bumper plates also decreased the possibility of pressure wall plate rear-side spall, especially under normal impact. The tendency for pressure wall plates in dual-wall specimens with traditional, monolithic bumpers to exhibit rear-side spall is a major area of concern because of the high speeds with which spall fragments can travel.

6.5 References

6.1 D.J. Kessler, R.C. Reynolds, and P.D. Anz-Meador, Orbital Debris Environment for Spacecraft Designed to Operate in Low Earth Orbit, NASA TM-100471, Houston, Texas (1989).

6.2 R.H. Morrison, A Preliminary Investigation of Projectile Shape Effects in Hypervelocity Impact of a Double Sheet Structure, NASA TN D-6944, Washington, D.C. (1972).

6.3 A.R. Coronado, M.N. Gibbins, M.A. Wright, and P.H. Stern, Space Station Integrated Wall Design and Penetration Damage Control, D180-30550-1, Boeing Aerospace Co., Seattle, Washington (1987).

6.4 R.J. Tullos and W.P. Schonberg, "Spacecraft Wall Design for Increased Protection Against Penetration by Space Debris Impacts", AIAA Paper No. 90-3663, Proc. Space Programs and Technologies Conference 1990, Huntsville, Alabama, September (1990).

6.5 W.P. Schonberg and R.A. Taylor, "Penetration and Ricochet Phenomena in Oblique Hypervelocity Impact", AIAA Journal, Vol. 27, pp. 639-646 (1989).

	Corrugation Type No. 1	Corrugation Type No. 2
α	53^{o}	20^{o}
h	19.0	25.4
t_1	0.508	0.803
t_2	0.508	0.508
t_3	0.508	0.508
d_1	7.938	3.175
d_2	44.450	146.050
d_3	15.875	6.350

Table 6.1 Geometric Parameters for Corrugated Bumpers (all lengths and thicknesses in mm)

Test Number	Rise Angle	V (km/s)	θ (deg)	d (mm)	MLI?	t_w (mm)	S (mm)
145A	53^{o}	5.40	0^{o}	6.35	N	3.175	101.6
145B	53^{o}	4.38	0^{o}	6.35	N	3.175	101.6
145C	53^{o}	3.79	0^{o}	6.35	N	3.175	101.6
307	20^{o}	2.96	45^{o}	6.35	Y	3.175	101.6
308	20^{o}	4.42	45^{o}	6.35	Y	3.175	101.6
309	20^{o}	4.60	45^{o}	7.95	Y	3.175	101.6
309B	20^{o}	4.86	45^{o}	7.95	Y	3.175	101.6
309R	20^{o}	4.56	45^{o}	7.95	Y	3.175	101.6
310	20^{o}	5.73	45^{o}	7.95	Y	3.175	101.6
310R	20^{o}	5.78	45^{o}	7.95	Y	3.175	101.6
311	20^{o}	5.29	45^{o}	9.53	Y	3.175	101.6
312	20^{o}	6.08	45^{o}	9.53	Y	3.175	101.6
312B	20^{o}	6.52	45^{o}	9.53	Y	3.175	101.6

Table 6.2 Test Parameters for Corrugated Bumper Systems

Test Number	V (km/s)	θ (deg)	d (mm)	MLI?	t_s (mm)	t_w (mm)	S (mm)
EHSS2B	5.88	0^o	6.35	N	1.60	3.175	101.6
P03	4.90	0^o	6.35	N	1.60	3.175	101.6
P04	4.95	0^o	6.35	N	1.60	3.175	101.6
PT4A	3.64	0^o	6.35	N	1.60	3.175	101.6
PT4B	4.26	0^o	6.35	N	1.60	3.175	101.6
002B	6.54	45^o	7.95	Y	1.60	3.175	101.6
205A	4.16	45^o	6.35	Y	1.60	3.175	101.6
205B	4.61	45^o	6.35	Y	1.60	3.175	101.6
205C	5.30	45^o	6.35	Y	1.60	3.175	101.6
205D	6.30	45^o	6.35	Y	1.60	3.175	101.6
205E	3.15	45^o	6.35	Y	1.60	3.175	101.6
211B	5.87	45^o	8.89	Y	1.60	3.175	101.6
211D	6.97	45^o	8.89	Y	1.60	3.175	101.6
212B	6.27	45^o	7.62	Y	1.60	3.175	101.6
230A	4.41	45^o	4.75	Y	1.60	3.175	101.6
230B	3.23	45^o	4.75	Y	1.60	3.175	101.6
320	3.08	45^o	7.95	Y	1.60	3.175	101.6
325	4.25	45^o	7.95	Y	1.60	3.175	101.6

Table 6.3 Test Parameters for Monolithic Bumper Systems

Test Number	θ_n (deg)	γ_n (deg)	A_d (cm^2)	d_h (mm)	A_s (cm^2)
145A	1.5	26.6	25.67	2.87	----
145B	0.2	24.8	22.06	2.28	----
145C	1.6	33.5	41.87	7.29	----

Table 6.4a Impact Test Results for Corrugated Bumper Systems, Normal Impact

Test Number	θ_1 (deg)	θ_2 (deg)	γ_1 (deg)	γ_2 (deg)	A_{d1} (cm^2)	A_{d2} (cm^2)	d_h (mm)	A_{s2} (cm^2)
307	----	40.7	----	3.3	0.0	1.29	----	----
308	28.4	38.7	13.2	7.4	9.55	6.39	----	----
309	20.3	37.6	13.7	13.0	7.94	17.81	2.98	----
309B	13.5	33.8	5.5	12.8	1.29	13.36	----	----
309R	16.7	38.7	15.3	5.3	11.42	2.84	----	----
310	----	35.6	----	6.7	0.0	3.87	----	----
310R	32.6	49.8	20.5	2.4	25.68	1.29	----	----
311	12.0	39.7	22.1	8.7	20.25	7.94	18.67	----
312	----	42.0	----	10.7	0.0	14.52	----	----
312B	----	21.8	----	22.8	0.0	25.68	15.37	----

Table 6.4b Impact Test Results for Corrugated Bumper Systems, Oblique Impact

Test Number	θ_n (deg)	γ_n (deg)	A_d (cm^2)	d_h (mm)	A_{s2} (cm^2)
EHSS2B	0.0	47.3	62.06	----	5.19
P03	1.4	48.4	81.03	9.09	3.44
P04	0.7	48.1	64.58	7.72	1.97
PT4A	6.9	49.1	64.58	16.01	3.94
PT4B	1.4	57.5	69.48	6.35	0.26

Table 6.5a Impact Test Results for Monolithic Bumper Systems, Normal Impact

Test Number	θ_1 (deg)	θ_2 (deg)	γ_1 (deg)	γ_2 (deg)	A_{d1} (cm^2)	A_{d2} (cm^2)	d_h (mm)	A_{s2} (cm^2)
002B	4.3	37.3	12.7	12.3	3.87	9.55	4.90	----
205A	9.9	41.2	32.3	10.8	28.58	7.94	2.44	----
205B	12.7	40.4	23.3	14.1	15.55	17.81	4.37	----
205C	19.3	37.9	15.9	12.1	7.92	9.58	16.94	----
205D	8.5	35.7	17.4	9.2	7.92	5.10	----	----
205E	8.5	37.3	14.0	4.5	5.10	1.29	8.79	----
211B	7.1	40.2	22.6	16.2	13.35	22.83	21.21	----
211D	----	40.2	----	11.8	0.0	11.42	38.18	----
212B	5.4	38.0	14.1	15.9	5.10	17.80	15.75	----
230A	5.7	42.5	20.9	3.0	11.42	0.71	----	----
230B	7.1	40.1	7.1	6.8	1.29	3.87	----	----
320	5.7	39.1	19.7	12.2	9.55	11.42	crack	----
325	11.3	41.2	27.7	10.9	20.26	7.94	14.17	----

Table 6.5b Impact Test Results for Monolithic Bumper Systems, Oblique Impact

Test Number	Bumper Type	Impact Energy (J)	Pressure Wall Plate	
			Penetrated?	Spalled?
145A	Corrugated	5302	yes	no
EHSS2B	Monolithic	6287	no	yes
145B	Corrugated	3489	yes	no
PT4B	Monolithic	3300	yes	yes
P-03	Monolithic	4366	yes	yes
P-04	Monolithic	4456	yes	yes
145C	Corrugated	2612	yes	no
PT4A	Monolithic	2409	yes	yes

Table 6.6 Penetration Comparison of Corrugated and Monolithic Bumper Systems Under Normal Impact

Test Number	Bumper Type	Impact Energy (J)	Pressure Wall Plate Penetrated?	Pressure Wall Plate Spalled?
307	Corrugated	1593	no	no
205E	Monolithic	1804	yes[2]	no
308	Corrugated	3552	no	no
205A	Monolithic	3147	yes[2]	no
205B	Monolithic	3864	yes[2]	no
309	Corrugated	7551	yes[2]	no
309B	Corrugated	8429	no	no
309R	Corrugated	7420	no	no
325	Monolithic	6446	yes[2]	no

Table 6.7a Penetration Comparison of Corrugated and Monolithic Bumper Systems Under Oblique Impact, Impact Energy < 10,000 joules

Test Number	Bumper Type	Impact Energy (J)	Pressure Wall Plate	
			Penetrated?	Spalled?
310	Corrugated	11,716	no	no
310R	Corrugated	11,922	no	no
002B	Monolithic	15,264	yes[2]	no
211B	Monolithic	17,193	yes[2]	no
212B	Monolithic	12,353	yes[2]	no
311	Corrugated	24,221	yes[2]	no
312	Corrugated	22,687	no	no
312B	Corrugated	26,089	yes[2]	no
211D	Monolithic	24,240	yes[2]	no

Table 6.7b Penetration Comparison of Corrugated and Monolithic Bumper Systems Under Oblique Impact, Impact Energy > 10,000 joules

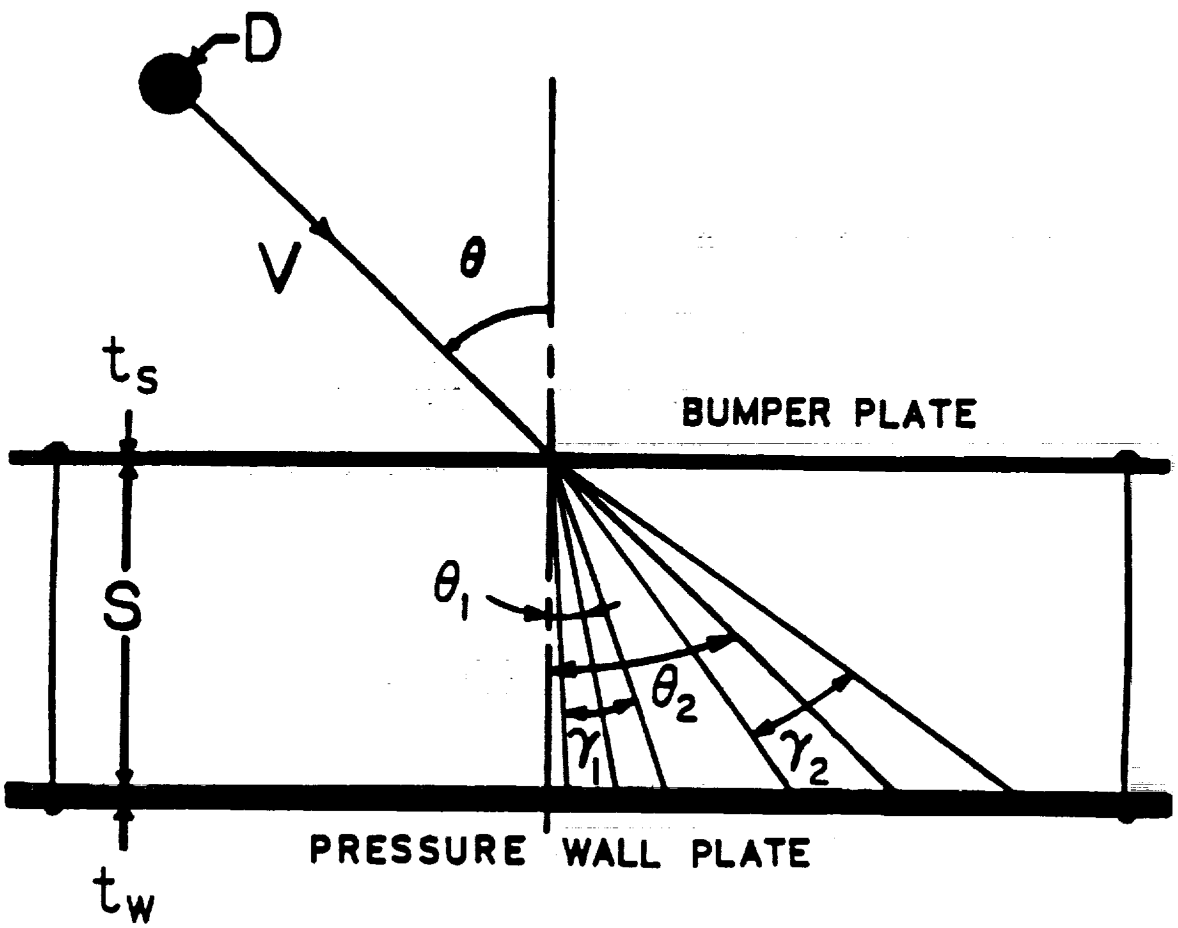

Figure 6.1 Impact Test Configuration and Parameters, Monolithic Bumper System

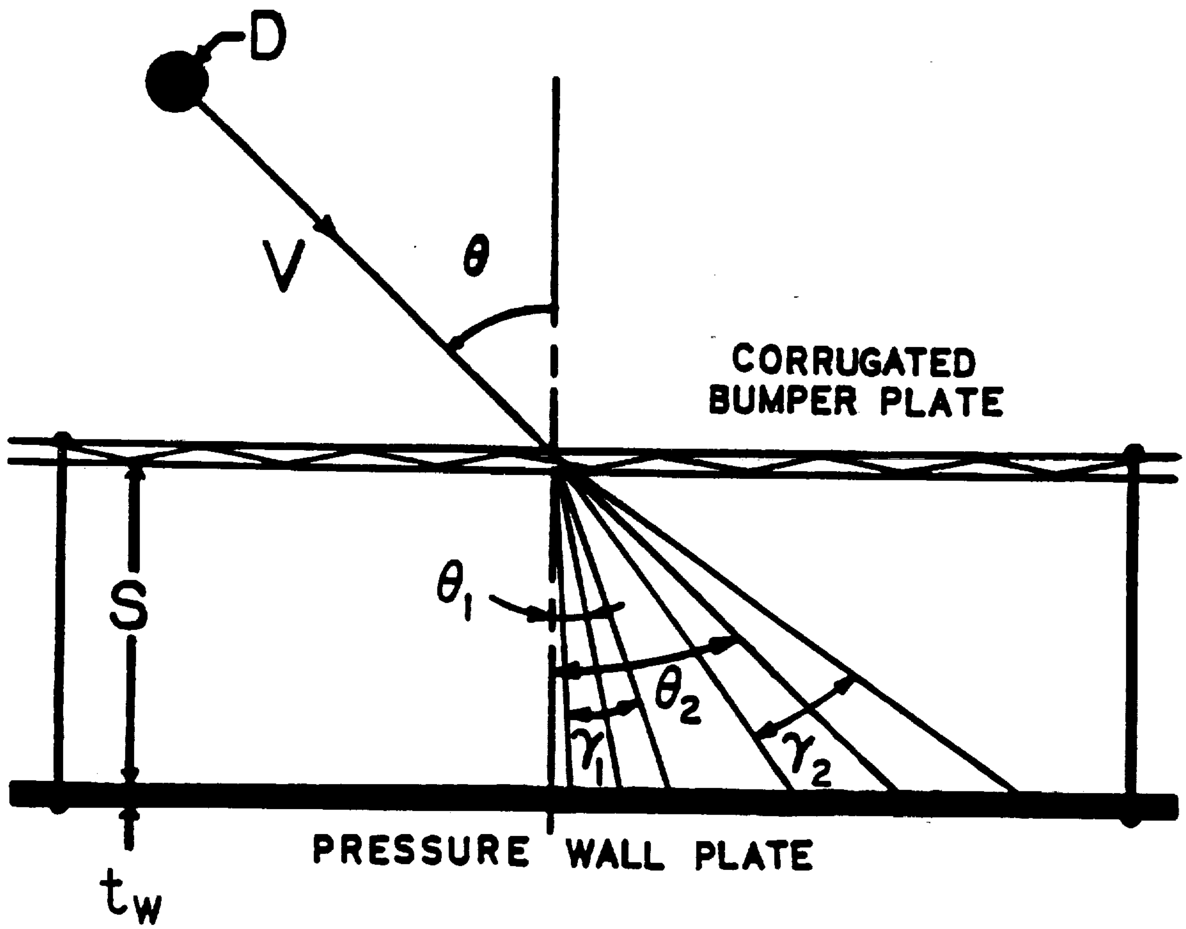

Figure 6.2 Impact Test Configuration and Parameters, Corrugated Bumper System

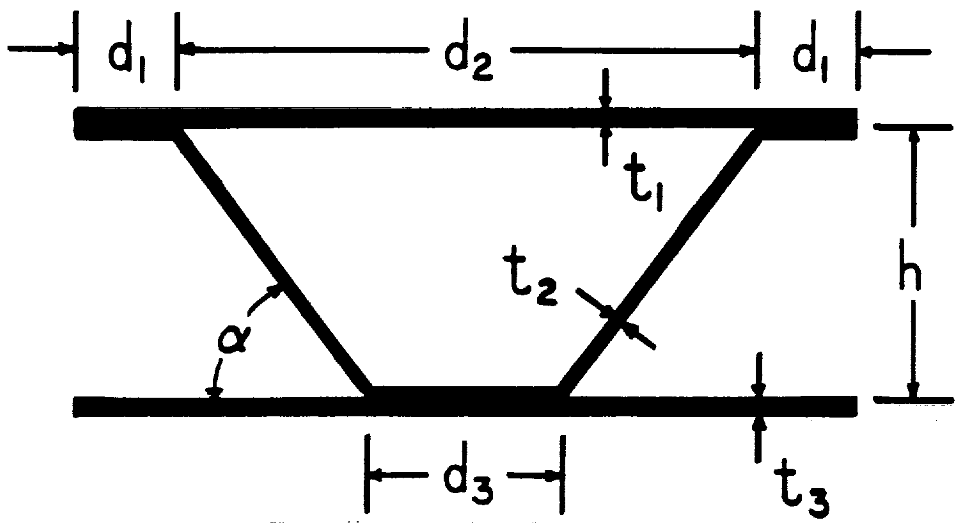

Figure 6.3 Corrugated Bumper Repeating Element

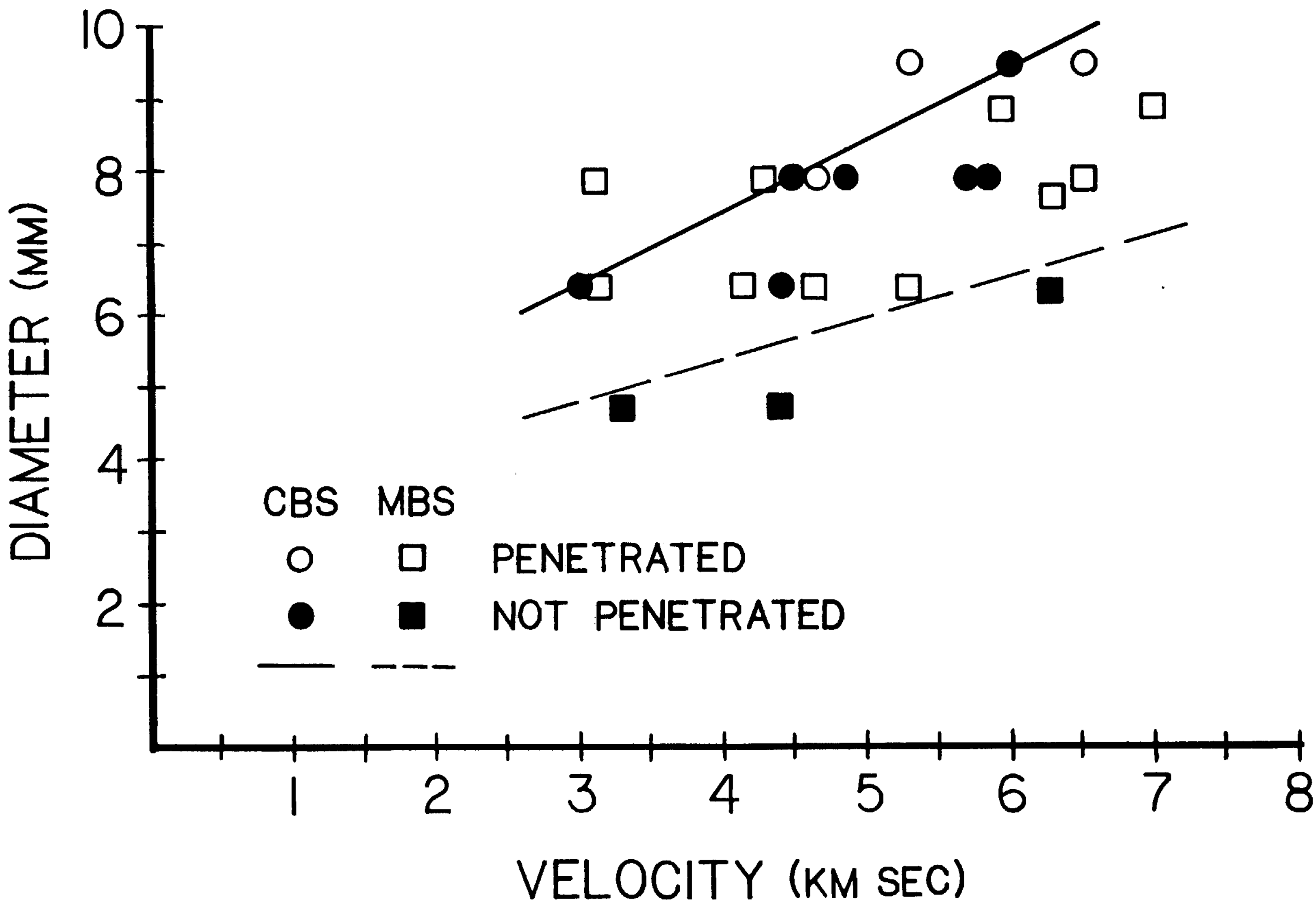

Figure 6.4 Penetration Functions for Corrugated and Monolithic Bumper Systems With MLI (CBS and MBS, respectively) for θ=45^{o} and α=20^{o}

SECTION SEVEN -- PROJECTILE SHAPE AND MATERIAL EFFECTS IN HYPERVELOCITY IMPACT OF DUAL-WALL STRUCTURES

7.1 Introduction

In the majority of the previous investigations of dual-wall structures under hypervelocity impact, spherical aluminum projectiles have been used in order to maintain repeatability and consistency during the test program. However, it has become evident that meteoroids and pieces of orbital space debris are far from spherical in shape. In addition, the densities of the various kinds of meteoroids (icy, stony, iron) are also significantly different from the densities of the various kind of orbital debris that exist in near-earth orbit (plastic, metallic, etc.). Unfortunately, hypervelocity impact testing of dual-wall structures with non-spherical, non-aluminum projectiles has been very limited in scope and was often included as a small part of a much larger test program that, for the most part, employed spherical aluminum projectiles. The following paragraph summarizes the results obtained in recent non-spherical, non-aluminum projectile impact testing of dual-wall structures.

Wallace, Vinson, and Kornhauser [7.1] tested dual-wall structures under impact by cylindrical steel, aluminum, and titanium and found that the steel impacts were more damaging than the impacts by aluminum projectiles with similar impact energy. This was also found to be true for spherical steel and aluminum projectiles in a series of tests performed by Maiden and McMillan [7.2]. Lundeberg, Lee, and Burch [7.3] tested dual-wall structures against impact by spherical and cylindrical aluminum, pyrex, and lexan projectiles. However, their study was directed primarily towards the determination of an optimum filler material for a dual-wall structure under a variety of impact conditions rather than comparing the effects of projectile shape and material on structural response. As such, the majority of their testing was performed with spherical projectiles with only a few cylindrical tests performed for comparison purposes. Arenz [7.4] found that the optimum total thickness required to prevent the penetration of an aluminum dual-wall structure impacted by lightweight syntactic foam projectiles was one-tenth of the optimum total thickness required when the same dual-wall structure was impacted by heavier aluminum projectiles. Gehring, Christman, and McMillan [7.5] used spherical aluminum, pyrex, and steel projectiles in their test program, but their main objective was to study the differences in target response caused by differences in target material properties and geometry. In a recent study of the effect of projectile properties on target cratering, Williams and Persechino [7.6] found that the effect of projectile density on shielded target damage was much higher than that on unshielded targets for equal mass projectiles. They reasoned that this was to be expected since the dense projectiles had a smaller cross-section and, as such, interacted with less shield material than did low density projectiles of equal mass. In addition, Williams and Persechino observed that spherical projectiles produced twice as much crater volume in shielded targets as did other projectiles with equal impact velocities and for equal values of encountered shield material.

Although it is impossible to design a spacecraft that will be resistant to impact penetration for all possible projectile shapes, velocities, and materials, in order to be able to design the best impact-resistant structure, it is important to understand the differences in impact response due to differences in projectile shape and material. This Section summarizes the results of an investigation into the effects of projectile shape and material on the hypervelocity impact response of aluminum dual-wall structural systems. Impact test results for two different projectile geometries and three different projectile materials are reviewed qualitatively and quantitatively. Impact damage in the structural systems is characterized according to the extent of penetration, crater, and spall damage in the structure as a result of the impact loadings. These characteristics are used to gain an insight into the effects of projectile material and shape on the response of aluminum dual-wall structures.

7.2 Hypervelocity Impact Test Parameters

Spherical and cylindrical projectiles of equal mass were fired at various velocities at aluminum dual-wall test specimens along trajectories inclined at various angles with respect to the outward normal of the test specimen bumper plates (Figure 7.1 shows the impact of a shperical projectile). Upon impact, the projectile was shattered and created a hole in the bumper plate. The secondary debris fragments created were sprayed upon a pressure wall plate of thickness t_w located a distance S behind the bumper. In Figure 7.1, the angles θ_1 and θ_2 denote the trajectories of the centers of mass of the 'normal' and 'in-line' secondary debris fragments, respectively; the angles γ_1 and γ_2 represent the spread of these fragments. The impact of the secondary debris particles created 'normal' and 'in-line' areas of damage A_{d1} and A_{d2}, respectively, on the front surface of the pressure wall plate. In those tests where the path of the projectile was normal to the surface of the bumper plate (ie. $\theta=0^o$), the 'normal' and 'in-line' debris clouds overlapped in a single debris cloud whose center-of-mass trajectory was close to the inward normal of the test specimen bumper plate (ie. $\gamma_1 \simeq \gamma_2 = \gamma_n$ and $\theta_1 \simeq \theta_2 = \theta_n$). The damage areas also overlapped and combined to form a single area of damage A_d on the front surface of the pressure wall plate. Occasionally, the impacts of the secondary projectile and bumper plate fragments resulted in the creation of thin spall fragments ejected from the rear side of the pressure wall plate. In these cases, for both the normal and oblique impacts, the total spalled area on the rear surface is denoted by A_s.

The conditions of the impact tests were chosen to simulate space debris impacts of light-weight space structures as closely as possible, and still remain within the realm of experimental feasibility. Two different projectile shapes (spherical and cylindrical) and three different materials of varying densities (lexan, aluminum, and steel) were used to examine the effect of projectile shape and material on the damage sustained by aluminum dual-wall systems under hypervelocity projectile impact. The length-to-diameter (L/D) ratios of the cylindrical projectiles were kept constant and equal to one. As such, the impacts of the cylindrical and spherical projectiles can be said to model the impacts of 'chunky' pieces of orbital debris.

The average mass density of pieces of orbital debris less than 10 mm in diameter is nearly that of aluminum [7.1,7.7]; the average mass density of stony meteoroids is approximately 0.5 gm/cm^3 [7.8]. In addition, iron meteoroids, which are much less numerous than stony meteoroids, are estimated to have a density of approximately 8.31 gm/cm^3 [7.1,7.8]. Thus, a lexan projectile, with a density of 1.25 gm/cm^3, could represent the impact of an icy meteoroid or a lighter piece of debris while a steel projectile, with a density of 7.83 gm/cm^3, could represent an iron meteoroid or a heavier piece of debris. Additional material properties of the projectiles used in the test program are provided in Table 7.1. The diameters of the spherical projectiles ranged from 6.35 mm to 9.525 mm; the diameters of the cylindrical projectiles ranged in value from 5.08 mm to 9.525 mm. The velocities of the impacting projectiles ranged from 2.9 to 7.4 km/sec. To study the effects of trajectory obliquity on penetration, impact testing was performed at obliquities of 0^o, 45^o, and 65^o. Additionally, to simulate presence of thermal insulation in the spacecraft wall design, some of the tests were performed with MLI (multi-layer insulation) resting on the pressure wall plate.

A total of 40 tests were performed with a variety of dual-wall structural systems to study and evaluate the effects of projectile shape and material on hypervelocity impact response. Included in these tests were 13 tests with cylindrical projectiles, 22 tests with spherical projectiles, and 5 tests with non-aluminum projectiles; one of these tests was performed with a non-metallic (lexan) cylindrical projectile. In all of the tests, the bumper and pressure wall plates were made from 6061-T6 and 2219-T87 aluminum, respectively. Two bumper plate thicknesses were used in the test program: 1.016 mm and 1.6 mm. The thicknesses of the pressure wall plates were kept constant at 3.175 mm. With the exception of one test in which the spacing was 15.24 cm, the spacing between the bumper plate and the pressure wall plate was kept constant at 10.16 cm. The MLI consisted of 30 layers of 0.5 mil kapton aluminized on one side and 29 layers of Dacron mesh, one layer between each kapton layer. Additionally, 1 layer of beta-cloth (coated s-glass) was added on the side nearest the bumper plate for durability. The areal density of this combination was calculated to be approximately 0.107 gm/cm^2 [7.9]. Additional test parameters and configuration geometries are given in Tables 7.2,7.3, and 7.4 for the tests with cylindrical, spherical, and non-aluminum projectiles, respectively.

The results of the hypervelocity impact test firings are given in Tables 7.5 through 7.10. Tables 7.5a,b and 7.6a,b present the results for the normal and oblique cylindrical and spherical projectile impact tests, respectively; Tables 7.7a,b present a summary of the penetration characteristics for the cylindrical and spherical impact tests. In Tables 7.7a,b, tests are grouped according to both geometric and impact energy similarity; the superscript '2' indicates that 'in-line' penetration or spall has occured. Table 7.8 presents the results for the non-aluminum projectile impact tests; penetration characteristics for the lexan and steel impact tests are summarized and compared against corresponding aluminum impact test results in Tables 7.9 and 7.10, respectively. The results of the test with the cylindrical lexan projectile are presented in Tables 7.5a,7.7a,7.8, and 7.9 to allow for comparison with other cylindrical and lexan test results. In Tables 7.5 through 7.10, column entries of '----' indicate that certain phenomena, such as pressure wall plate penetration, front surface damage, or rear surface spall, did not occur; additionally, d_h is the equivalent single hole diameter of all the holes in the pressure wall plate in the event of pressure wall plate penetration. Detailed analyses of the damaged test specimens revealed many interesting features and response characteristics of dual-wall structures under hypervelocity projectile impact loadings.

7.3 Effect of Projectile Shape on Impact Response

7.3.1 Bumper Plate Damage Analysis

The interaction of the impacting projectile with the bumper plate is an important factor in predicting the extent of the damage sustained by the pressure wall plate due to secondary debris impact. The impact of spherical and cylindrical projectiles on the bumper plates produced well-defined holes. Normal impacts by spherical projectiles resulted in circular holes while oblique impacts produced elliptical holes. Cylindrical projectile impact resulted in elliptical holes, regardless of the impact angle. This was probably due to a slight pitch of the projectile during its flight through the gun barrel which prevented it from hitting the bumper end on. A multiple linear regression analysis of the minimum and maximum bumper plate hole dimension data for cylindrical projectile impact resulted in the following hole dimension predictor equations:

$$D_{min}/d = 2.309(V/C)^{0.302}(t_s/d)^{0.561}\cos^{-0.177}\theta + 1.0 \tag{7.1}$$

$$D_{max}/d = 8.323(V/C)^{0.617}(t_s/d)^{1.639}e^{1.664\theta} + 1.4 \tag{7.2}$$

where $C=\sqrt{E/\rho}$ is the speed of sound in the bumper plate material and θ is in radians. Corresponding equations for spherical projectile impact were developed and presented previously in Section Three. The average errors, standard deviations, and correlation coefficients for these equations are given in the second, third, and fourth column, respectively, of Table 7.11. It can be seen from Table 7.11 that the equations are a fairly good fit to the experimental hole dimension data. However, it is noted that equations (7.1) and (7.2) are valid only for aluminum cylindrical projectiles with L/D=1, and for $0^o<\theta<65^o$, 2.95<V<7.15 km/sec, and $0.152<t_s/d<0.315$.

7.3.2 Pressure Wall Plate Damage Analysis

Examination of the damaged pressure wall plates revealed that certain damage characteristics were common to both spherical and cylindrical projectile impact. These general observations are similar to the results described in several previous investigations of oblique hypervelocity impact [7.9-7.14]. The various kinds of pressure wall plate damage shown in the photographs in References 7.9-7.12 are typical of the damage sustained by the pressure wall plates in this investigation.

1) In the normal impact tests without MLI, regardless of the shape of the projectile, the pressure wall plate damage areas were usually centered in an oval pattern beneath the bumper plate impact site. The damage area consisted of numerous craters and scars from impacting aluminum debris particles and vapor.

2) In the oblique impact tests without MLI, there were usually two damage areas instead of the single one found in the normal impact tests. One area was along a trajectory that was close to the normal between the bumper plate and the pressure wall plate. This 'normal' damage area was typically smaller and more cratered than the 'in-line' damage area. The 'in-line' damage area was more disperse and contained craters that were oblong due to the oblique trajectories of the impacting debris.

3) In the normal tests with MLI, the pressure wall plate damage areas were much smaller than those in similar tests without MLI. However, the equivalent diameter of the pressure wall plate hole in the tests with MLI was sometimes much larger than the diameter of the pressure wall plate hole in the tests without MLI. In these cases, the remains of the MLI appeared as if the MLI had exploded when it was impacted by the secondary debris cloud. The pressure wall plate in these tests was typically cracked in half or severely petalled. This was especially true for the tests with large projectile diameters (ie. greater than 7.5 mm) and high speeds of

impact (ie. greater than 6 km/sec). This potential for intermediate insulating material to explode upon impact has also been observed in a previous investigation of hypervelocity impact [7.3]. It is evident that extreme care must be taken in the selection of an appropriate insulating material for the walls of a dual-wall space structure in order to ensure that is does not explode in the event of an on-orbit impact by a large meteoroid or a large piece of space debris.

4) In the oblique tests with MLI, for a projectile diameter and velocity that penetrated the pressure wall plate when the original angle of obliquity was $\theta=45^{\circ}$, the pressure wall plate was not penetrated when the obliquity was $\theta=65^{\circ}$. In all of the penetrated specimens, the penetration occured along the 'in-line' secondary debris trajectory.

The effects of different projectile shapes became apparent upon examination of the extent and severity of the damage sustained by the pressure wall plates. In the tests with spherical projectiles, the total pressure wall damage areas were, on the average, approximately two to three times as large as the damage areas caused by cylindrical projectiles with similar impact energies, especially when the impact energy exceeded 10,000 joules (see Tables 7.5a,b and 7.6a,b). This is not surprising since the debris clouds for cylindrical projectile impact have been shown to be concentrated near the flight axis while the debris clouds resulting from a spherical projectile impact have been shown to resemble a diverging bubble [7.15].

A comparison of pressure wall plate penetrations revealed that under normal and oblique impact of dual-wall aluminum structures with a stand-off distance of 10.16 cm, the cylindrical projectiles penetrated the pressure wall plate just as often as did spherical projectiles with similar impact energies (see Tables 7.7a,b). With the exception of Test No. EH4A in which the pressure wall plate was cracked in half, the equivalent single hole diameters of the multiple holes in the penetrated pressure wall plates were also approximately equal. Thus, it would appear that, for a 10.16 stand-off distance, the penetrating power of cylindrical projectiles with L/D=1 is similar to that of spherical projectiles with similar impact energies. When the stand-off distance was increased from 10.16 cm to 15.24 cm, the pressure wall plate was not penetrated in the spherical projectile impact test (P16G). In the test with the cylindrical projectile (P18RV), the pressure wall plate was still penetrated at the larger stand-off distance and the equivalent hole diameter was slightly larger than at the smaller stand-off distance. This indicates that the secondary debris cloud in the cylindrical projectile impact contained solid as well as melted fragments. Changing the stand-off distance from 10.16 cm to 15.24 cm would not be expected to decrease the penetration potential of the solid debris fragments. The stand-off distance between the bumper plate and the pressure wall plate in an aluminum dual-wall structure would have to be increased significantly beyond 10.16 cm if the defeat of normally-incident non-spherical projectiles is of primary concern.

Because of the scarcity of pressure wall hole diameter, damage area, and spall area data for cylindrical projectile impact, a regression analysis was performed only for the debris cloud center-of-mass trajectory data. Corresponding equations for spherical projectile impact were presented previously in Section Three. Using the data in Tables 7.5a,b, the following equations were obtained for the trajectories of the centers-of-mass of the 'normal' and 'in-line' debris clouds under normal and oblique cylindrical projectile impact as functions of the geometric, material, and impact parameters of the dual-wall systems:

$$\tan \theta_1 = 0.2216\mathrm{x}10^{-8}(V/C)^{-1.710}(t_s/d)^{-11.557}\cos^{3.318}\theta \qquad (7.3)$$

$$\tan \theta_2 = 0.2536\mathrm{x}10^{-7}(V/C)^{-2.570}(t_s/d)^{-9.952}\cos^{1.088}\theta \qquad (7.4)$$

These equations can be used to estimate the locations of the 'normal' and 'in-line' pressure wall damage areas and can also be used to determine whether the debris clouds will overlap (if $\theta_1 \approx \theta_2$) or will separate (if $\theta_2 > \theta_1$). The average errors, standard deviations, and correlation coefficients for equations (7.3) and (7.4) are given in Table 7.11. Based on the data in Table 7.11, it is evident that equations (7.3) and (7.4) fit the data fairly well. It is again noted that equations (7.3) and (7.4) are valid only for aluminum cylindrical projectiles with L/D=1, and for $0^\circ < \theta < 65^\circ$, $2.95 < V < 6.90$ km/sec, and $0.152 < t_s/d < 0.315$.

In previous investigations in which MLI was included in a dual-wall structural configuration, it was found that the magnitudes of the pressure wall damage areas decreased dramatically as compared to those in structural systems without MLI (see, e.g., [7.9]). A review of the damage area data in Table 7.5b shows that, in the 45° cylindrical projectile impact tests, the MLI was able to completely absorb the energy of the 'normal' debris particles, thereby preventing the formation of the 'normal' pressure wall plate damage areas (note the non-existence of A_{d1} in Tests 223A,B,C in Table 7.5b). The ability of the MLI to neutralize the 'normal' debris particles can be attributed to one of the factors that distinguishes oblique projectile impact from normal projectile impact. In the oblique impact of a cylindrical projectile with a relatively small angle of obliquity, the shock pressures generated in the projectile exist for a shorter amount of time and are lower in magnitude than the shock pressures created in a spherical projectile under similar impact conditions. As a result, in the 45^{o} cylindrical projectile impacts, relatively little projectile break-up occurred. Although a weaker 'normal' debris cloud was undoubtedly created, the majority of the debris particles were concentrated in the 'in-line' debris cloud. As a result, the particles in the 'in-line' debris cloud penetrated the protective MLI layer, created an area of damage on, and in some cases penetrated through, the pressure wall plate. However, in the 65^{o} cylindrical impact tests, a larger portion of the projectile interacted with the bumper plate. This resulted in more projectile fragmentation and in a larger fraction of the debris particle energy being apportioned to the 'normal' debris cloud. As a result, each debris clouds possessed enough energy to penetrate the MLI and create 'normal' and 'in-line' pressure wall plate damage areas.

A comparison of the occurrence of spall on the reverse side of the pressure wall revealed the following.

1) Under normal impact conditions, spherical projectiles produced spall more frequently than normal impacts by cylindrical projectiles with similar impact energies, especially when the impact energies exceeded 10,000 joules (Table 7.7a). This can be explained by the fact the spherical projectiles produced larger damage areas on the pressure wall plates than did the cylindrical projectiles with similar impact energies. The more concentrated loads imparted to the pressure wall plates by the debris clouds created in cylindrical projectile impact served to penetrate the pressure wall plate rather than cause it to spall.

2) When the impact was normal and the impact energy was low, the presence of MLI served to diminish the size of the spall area. It would seem that in these cases the MLI absorbed a portion of the projectile and bumper plate debris particles and dissipated the associated impact energy. The weakened impulse was then unable to create internal stress waves with amplitudes high enough to cause the plate to spall.

3) Under oblique impact, a significant portion of the initial impact energy was diverted away from the pressure wall plate in the form of ricochet debris. In addition, the partitioning of the secondary debris clouds into two debris clouds further reduced the concentration of the energy directed towards the pressure wall plate. These two factors combined to significantly reduce the possibility of rear-side spall for oblique impacts, regardless of whether or not MLI was present in the structural system.

4) When the stand-off distance between the bumper plate and the pressure-wall plate was increased from 10.16 cm to 15.24 cm, under cylindrical projectile impact, spallation no longer accompanied pressure wall plate penetration. In addition, the pressure wall plate damage area and the equivalent hole diameter were similar in size (Table 7.5a). For spherical projectile impact, increasing the stand-off distance from 10.16 cm to 15.24 cm decreased the area of rear-side spall by a factor of two (Table 7.6a). Thus, the increase in the stand-off distance did not have a significant effect on structural response under cylindrical projectile impact; a much larger stand-off distance would be needed to mitigate the deleterious effects that accompany normal cylindrical projectile impact on aluminum dual-wall structures.

Finally, the impact of the cylindrical lexan projectile was found to be more damaging than the impact by a spherical aluminum projectile with similar impact energy. This agrees with results obtained previously [7.3] and is possibly due to the fact that the secondary debris cloud formed as a result of the cylindrical lexan projectile impact applied a stronger pressure pulse over a larger area of the pressure wall plate than did the debris cloud formed in the impact of the spherical projectile. In addition, this pressure pulse was applied over a larger area in the lexan projectile impact than in the aluminum projectile impact (note the relative magnitudes of γ_n and A_d for Test Nos. 225D and T2-16).

7.4 Effect of Projectile Material on Impact Response

An examination of the relative sizes of the pressure wall plate damage areas revealed that the lexan and aluminum projectiles produced the largest damage areas on the pressure wall plates while steel projectiles produced the smallest damage areas (Tables 7.6a,7.8). Although the lexan and aluminum projectiles produced damage areas of similar size, the major difference between the pressure wall plate damage due to lexan impact and the damage due to aluminum projectile impact lies in the number of pressure wall craters and holes. Lexan projectile impact resulted in sparse cratering of the pressure wall plate while the impact of aluminum projectiles with similar impact energies resulted in damage areas that were packed with deep overlapping craters and holes. This sparse pressure wall cratering under non-aluminum projectile impact was also observed in a previous study of hypervelocity projectile impact using pyrex projectiles [7.3].

The damage areas created by steel projectile impacts were four to five times as small as those created by aluminum impacts (Tables 7.6a,7.8). The fact that steel projectile impact produces more concentrated damage was also observed in a previous impact investigation [7.2]. This is probably due to the fact that the shock waves created in the steel projectiles as a result of the impact did not heat the steel to a temperature that would be high enough to cause it to melt and be dispersed over a large area. In addition, the secondary debris fragments formed by the steel projectile impacts penetrated deeper into the pressure wall plate than did those fragments formed by either aluminum or lexan projectile impact (see also [7.1]). This is to be expected since the debris clouds formed in steel projectile impact contained steel fragments as well as aluminum bumper fragments. Since penetration depth has been shown to be proportional to a positive power of particle density (see, e.g. [7.16]), the steel fragments formed during steel projectile impacts penetrated the pressure wall plate deeper than did the less dense debris fragments formed during aluminum or lexan projectile impact.

Penetration of the pressure wall plate did not occur in any of the lexan projectile impact tests; however, penetration did occur in all of the corresponding aluminum impact tests (Table 7.9). This would indicate that, for a given spacing, the ballistic limit thickness required for aluminum projectiles would be greater than that required for the lighter lexan projectiles. This qualitatively agrees with the results obtained in a previous investigation using non-aluminum projectiles [7.4]. The steel projectiles penetrated the pressure wall plates in both tests as did the corresponding aluminum projectiles (Table 7.10). The holes in the penetrated pressure wall plates for the steel and aluminum projectile impacts were similar in size and were accompanied by spallation of the material surrounding the holes on the rear side of the pressure wall plate. However, it is noted that the spall areas due to aluminum projectile impact were significantly smaller than the spall areas due to steel projectile impact (Table 7.6a,7.8).

In two previous investigations of hypervelocity impact, it was found that the areas of spall under aluminum projectile impact were larger than the spall areas due to steel projectile impact and that the spallation occured without penetration of the pressure wall plates in the dual-wall test specimens [7.2,7.5]. However, in these previous studies, the stand-off distance between the bumper plate and the pressure wall plate was only 5.08 cm, which is half of the stand-off distance used in the tests for this portion of the current investigation. In addition, the bumper plate material in the previous study was nickel, whereas the bumper plate material in the current investigation is aluminum. Since the interaction of the projectile with the bumper plate determines the state of the material in the secondary debris cloud (ie. solid or melted fragments, vapor, etc.) and the stand-off distance determines how much time is available for the debris cloud to spread out before it impacts the pressure wall plate, these differences in test specimen bumper material and geometry can cause significant differences in structural response.

7.5 Summary and Conclusions

An investigation of the effects of projectile shape and material on the hypervelocity impact response of aluminum dual-wall structures has been successfully performed. It was found that spherical projectiles damaged a larger area of the pressure wall plate than did cylindrical projectiles with similar impact energies. Both types of projectiles were observed to possess a similar potential for pressure wall plate penetration under similar impact conditions. This made it difficult to determine which shape was more lethal from a penetration standpoint. A moderate increase in the stand-off distance in a dual-wall structure did not appear to have a significant affect on structural response under cylindrical projectile impact. However, since only one test was performed at a larger stand-off distance, more testing is clearly needed to fully explore the effects of spacing on impact response under both, cylindrical and spherical projectile impact. The density of an impacting projectile was found to be directly related to the nature and extent of damage inflicted upon the pressure wall plate. The less dense projectiles produce larger damage areas with minimal penetration, while the more dense projectiles produce deeper and more concentrated damage. Based on the evidence obtained during the course of this investigation, it is recommended that more testing be performed for a larger variety of projectile shapes and materials at different velocities to more fully understand the effect of projectile shape and material on the impact damage in dual-wall space structures.

7.6 References

7.1 R.R. Wallace, J.R. Vinson, and M. Kornhauser, "Effects of Hypervelocity Particles on Shielded Structures", ARS Journal, pp. 1231-1237 (1962).

7.2 C.J. Maiden and A.R. McMillan, "An Investigation of the Protection Afforded a Spacecraft by a Thin Shield", AIAA Journal, Vol. 2, pp. 1992-1998 (1964).

7.3 J.F. Lundeberg, D.H. Lee, and G.T. Burch, "Impact Penetration of Manned Space Stations", J. Spacecraft, Vol. 3, pp. 182-187 (1966).

7.4 R.J. Arenz, "Projectile Size and Density Effects on Hypervelocity Penetration", J. Spacecraft, Vol. 6, pp. 1319-1321 (1969).

7.5 J.W. Gehring, D.R. Christman, and A.R. McMillan, "Experimental Studies Concerning the Meteoroid Hazard to Aerospace Materials and Structures", J. Spacecraft, Vol. 2, pp. 731-737 (1965).

7.6 A.E. Williams and M.A. Persechino, "The Effect of Projectile Porperties on Target Cratering", Int. J. Impact Engng., Vol. 5, pp. 709-728 (1987).

7.7 D.J. Kessler, R.C. Reynolds, and P.D. Anz-Meador, Orbital Debris Environment for Spacecraft Designed to Operate in Low Earth Orbit, NASA TM 100471, Houston, Texas (1989).

7.8 D. Rodriguez, Meteoroid Shielding for Space Vehicles, Aerospace Engineering, 20-66, December (1960).

7.9 A.R. Coronado, M.N. Gibbins, M.A. Wright, and P.H. Stern, Space Station Integrated Wall Design and Penetration Damage Control, D180-30550-1, Boeing Aerospace Co., Seattle, Washington (1987).

7.10 W.P. Schonberg and R.A. Taylor, "Penetration and Ricochet Phenomena in Oblique Hypervelocity Impact", AIAA Journal, Vol. 2, pp. 639-646 (1989).

7.11 W.P. Schonberg, "Hypervelocity Impact Penetration Phenomena in Aluminum Space Structures", J. Aero. Engng., Vol. 5, in press (1990).

7.12 W.P. Schonberg, "Hypervelocity Impact Response of Spaced Composite Material Structures", Int. J. Impact Engng., Vol. 10, in press (1990).

7.13 C.J. Maiden, J.W. Gehring, and A.R. McMillan, Investigation of Fundamental Mechanism of Damage to Thin Targets by Hypervelocity Projectiles, GM-DRL-TR-63-225, General Motors Defense Research Laboratory, Santa Barbara, California (1963).

7.14 J.F. Lundeberg, P.H. Stern, and R.J. Bristow, Meteoroid Protection for Spacecraft Structures, NASA CR-54201 (1065)

7.15 R.H. Morrison, A Preliminary Investigation of Projectile Shape Effects in Hypervelocity Impact of a Double Sheet Structure, NASA TN D-6944, Washington, D.C. (1972).

7.16 J.L. Summers, Investigation of High Speed Impact - Regions of Impact and Impact at Oblique Angles, NASA D-94 (1959).

Property	Lexan	Aluminum	Steel
ρ (km/m^3)	1150	2768	7833
E (x10^9 N/m^2)	2.47	68	200
ν	----	0.35	0.30

Table 7.1 Projectile Material Properties

Test No.	V (km/s)	d (mm)	θ (deg)	t_s (mm)	t_w (mm)	S (cm)	MLI
223A	6.58	6.655	45	1.016	3.175	10.16	Y
223B	6.75	6.655	45	1.016	3.175	10.16	Y
223C	5.67	6.655	45	1.016	3.175	10.16	Y
224A	6.49	6.655	65	1.016	3.175	10.16	Y
224B	4.80	6.655	65	1.016	3.175	10.16	Y
224C	3.70	6.655	65	1.016	3.175	10.16	Y
225D[1]	6.41	9.525	0	1.016	3.175	10.16	N
P18RV	7.12	6.655	0	1.600	3.175	15.24	N
P22	5.09	6.655	0	1.600	3.175	10.16	N
P22A	6.16	6.655	0	1.600	3.175	10.16	Y
P22B	6.89	6.655	0	1.600	3.175	10.16	N
T2-13	2.98	5.080	0	1.600	3.175	10.16	Y
T2-14	3.89	5.080	0	1.016	3.175	10.16	Y

[1]Lexan Projectile

Table 7.2 Test Parameters for Cylindrical Projectile Tests

Test No.	V (km/s)	d (mm)	θ (deg)	t_s (mm)	t_w (mm)	S (cm)	MLI
003A	6.54	7.950	45	1.016	3.175	10.16	Y
203A	4.79	7.620	65	1.016	3.175	10.16	Y
203B	3.65	7.620	65	1.016	3.175	10.16	Y
203E	6.72	7.620	65	1.016	3.175	10.16	Y
203F	3.05	8.890	65	1.016	3.175	10.16	Y
337	6.90	7.950	45	1.016	3.175	10.16	Y
EH3A	6.64	7.950	0	1.600	3.175	10.16	N
EH4A	6.13	7.950	0	1.600	3.175	10.16	Y
EHSS6C	6.64	7.950	0	1.600	3.175	10.16	N
P03	4.90	6.350	0	1.600	3.175	10.16	N
P07	2.93	6.350	0	1.600	3.175	10.16	Y
P08	2.96	6.350	0	1.600	3.175	10.16	Y
P16G	7.18	7.620	0	1.600	3.175	15.24	N
P21	6.63	7.620	0	1.600	3.175	10.16	N
P21A	6.47	7.620	0	1.600	3.175	10.16	N
P21C	6.60	7.620	0	1.600	3.175	10.16	Y
P33B	4.85	6.350	0	1.016	3.175	10.16	Y
PT4B	4.26	6.350	0	1.600	3.175	10.16	N
PT6A	4.29	7.950	0	1.016	3.175	10.16	N
T2-6	4.62	7.950	0	1.016	3.175	10.16	N
T2-6A	4.64	7.950	0	1.600	3.175	10.16	N
T2-16	5.41	9.525	0	1.016	3.175	10.16	N

Table 7.3 Test Parameters for Spherical Projectile Tests

Test No.	V (km/s)	d (mm)	θ (deg)	t_s (mm)	t_w (mm)	S (cm)	MLI	Projectile Material
225A	5.80	8.890	0	1.016	3.175	10.16	N	Lexan
225B	4.85	8.890	0	1.016	3.175	10.16	N	Lexan
225C	4.28	8.890	0	1.016	3.175	10.16	N	Lexan
225D[1]	6.41	9.525	0	1.016	3.175	10.16	N	Lexan
146A	6.95	3.175	0	1.600	3.175	10.16	N	Steel
146B	7.35	3.175	0	1.600	3.175	10.16	N	Steel

[1]Cylindrical Projectile

Table 7.4 Test Parameters for Non-Aluminum Projectile Tests

Test No.	D_{min} (cm)	D_{max} (cm)	θ_n (deg)	γ_n (deg)	A_d (cm²)	d_h (mm)	A_s (cm²)
225D[1]	1.750	1.750	3.6	73.7	182.58	56.4	----
P18RV	1.367	1.626	0.2	37.3	82.29	29.7	----
P22	1.450	1.478	2.9	40.6	44.84	39.1	21.35
P22A	1.369	1.529	1.4	27.3	19.23	44.2	----
P22B	1.450	1.707	0.6	51.9	76.97	23.4	10.45
T2-13	1.019	1.100	9.0	24.6	15.55	3.8	----
T2-14	0.955	0.991	5.3	26.9	20.25	3.6	----

[1]Lexan Projectile

Table 7.5a Test Results for Normal Cylindrical Impact Tests

Test No.	D_{min} (cm)	D_{max} (cm)	θ_1 (deg)	θ_2 (deg)	γ_1 (deg)	γ_2 (deg)	A_{d1} (cm²)	A_{d2} (cm²)	d_h (mm)	A_{s2} (cm²)
223A	1.326	1.826	----	49.1	----	8.1	----	17.74	5.33	----
223B	1.232	2.034	----	54.6	----	6.4	----	7.94	10.67	----
223C	1.250	1.753	----	53.2	----	7.5	----	11.42	12.70	----
224A	1.412	2.949	17.4	36.9	14.9	18.1	6.38	22.90	----	----
224B	1.227	2.799	16.7	58.9	18.0	4.6	9.55	6.38	----	----
224C	1.229	2.565	27.7	67.6	30.0	3.1	34.90	13.35	----	----

Table 7.5b Test Results for Oblique Cylindrical Impact Tests

Test No.	D (cm)	θ_n (deg)	γ_n (deg)	A_d (cm²)	d_h (mm)	A_s (cm²)
EH3A	1.514	3.3	76.9	206.19	49.78	7.09
EH4A	1.483	1.7	80.3	230.84	(1)	----
EHSS6C	1.588	3.6	63.7	126.64	32.00	5.42
P03	1.247	1.4	53.1	81.09	9.14	3.42
P07	1.066	0.7	19.7	9.81	9.14	----
P08	1.092	0.0	28.0	20.26	9.91	2.13
P16G	1.651	0.5	60.5	248.39	----	2.90
P21	1.032	1.9	63.9	126.64	28.63	5.29
P21A	1.430	1.7	58.1	102.58	33.78	1.23
P21C	1.529	0.3	17.5	7.68	----	----
P33B	1.196	2.7	26.7	18.32	21.08	----
PT4B	1.270	1.4	57.5	98.13	6.35	2.58
PT6A	1.278	3.6	50.2	61.74	27.18	0.65
T2-6	1.196	1.7	39.6	41.87	23.37	14.83
T2-6A	1.547	1.9	57.3	96.97	26.42	5.48
T2-16	1.278	8.9	24.7	66.58	41.15	----

(1) Severe Pressure Wall Plate Cracking and Petalling

Table 7.6a Test Results for Normal Spherical Impact Tests

Test No.	D_{min} (cm)	D_{max} (cm)	θ_1 (deg)	θ_2 (deg)	γ_1 (deg)	γ_2 (deg)	A_{d1} (cm²)	A_{d2} (cm²)	d_h (mm)	A_s (cm²)
003A	1.321	1.897	----	41.6	----	25.5	----	62.06	34.29	----
203A	1.283	2.383	11.3	56.8	22.8	6.6	15.55	13.35	----	----
203B	1.212	2.189	21.8	60.3	30.2	1.8	31.68	1.29	----	----
203E	1.481	2.964	14.0	56.3	30.9	13.9	27.68	57.74	----	----
203F	1.273	2.408	18.9	55.2	26.5	6.4	22.90	9.54	----	----
337	1.328	1.958	----	40.5	----	19.8	----	41.87	21.84	----

Table 7.6b Test Results for Oblique Spherical Impact Tests

Table 7.7a Comparison of Cylindrical and Spherical Normal Test Results

Test No.	Projectile Shape	Energy (J)	Pressure Wall Plate Penetrated?	Pressure Wall Plate Spalled?
Impact Energy < 10,000 J				
T2-13	Cylindrical	1240	yes	no
P07	Spherical	1561	yes	no
P08	Spherical	1593	yes	yes
T2-14	Cylindrical	2060	yes	no
P33B	Spherical	4270	yes	no
P22	Cylindrical	8134	yes	yes
T2-6A	Spherical	7650	yes	yes
Impact Energy > 10,000 J				
P22A	Cylindrical	11913	yes	no
EH4A	Spherical	13410	yes	no
P21C	Spherical	13687	no	no
P22B	Cylindrical	14904	yes	yes
EH3A	Spherical	15734	yes	yes
EHSS6C	Spherical	15734	yes	yes
P21	Spherical	13812	yes	yes
P21A	Spherical	13153	yes	yes
P18RV	Cylindrical	15916	yes	no
P16G	Spherical	16199	no	yes
225D[1]	Cylindrical	17368	yes	no
T2-16	Spherical	12371	yes	no

[1]Lexan Projectile

Test No.	Projectile Shape	Energy (J)	Pressure Wall Plate Penetrated?	Pressure Wall Plate Spalled?
		Oblique Impact, $\theta=45^{o}$		
223A	Cylindrical	13593	yes[2]	no
223B	Cylindrical	14304	yes[2]	no
223C	Cylindrical	10093	yes[2]	no
003A	Spherical	15263	yes[2]	no
337	Spherical	16990	yes[2]	no
		Oblique Impact, $\theta=65^{o}$		
224A	Cylindrical	13224	no	no
203E	Spherical	14189	no	no
224B	Cylindrical	7233	no	no
203A	Spherical	7210	no	no
224C	Cylindrical	4298	no	no
203B	Spherical	4186	no	no
203F	Spherical	4641	no	no

Table 7.7b Comparison of Cylindrical and Spherical Oblique Test Results

Test No.	D (cm)	θ_n (deg)	γ_n (deg)	A_d (cm^2)	d_h (mm)	A_s (cm^2)
			Steel Projectiles			
146A	0.876	0.6	28.9	21.48	32.93	7.61
146B	0.889	3.4	29.9	22.58	7.11	11.61
			Lexan Projectiles			
225A	1.344	0.0	50.2	71.23	----	0.26
225B	1.288	0.0	45.1	56.00	----	----
225C	1.273	1.9	44.2	53.54	----	----
225D[1]	1.750	3.6	73.7	182.58	56.39	----

[1]Cylindrical Projectile

Table 7.8 Test Results for Non-Aluminum Impact Tests

Test No.	Projectile Material	Energy (J)	Pressure Wall Plate Penetrated?	Pressure Wall Plate Spalled?
225A	Lexan	7708	no	yes
T2-6	Aluminum	7617	yes	yes
225B	Lexan	5390	no	no
225C	Lexan	4197	no	no
PT6A	Aluminum	6567	yes	yes
225D	Lexan	17368	yes	no
T2-16	Aluminum	12371	yes	no

[1]Cylindrical Projectile

Table 7.9 Comparison of Aluminum and Lexan Impact Test Results

Test No.	Projectile Material	Energy (J)	Pressure Wall Plate Penetrated?	Pressure Wall Plate Spalled?
146A	Steel	3174	yes	yes
PT4B	Aluminum	3299	yes	yes
146B	Steel	3549	yes	yes
P03	Aluminum	4366	yes	yes

Table 7.10 Comparison of Aluminum and Steel Results

Eqn. No.	ϵ_{avg}(%)	σ(%)	$100R^2$
D_{min}/d	0.001	3.75	67.3
D_{max}/d	0.001	6.82	93.7
$\tan\theta_1$	4.745	35.05	96.9
$\tan\theta_2$	3.052	27.93	98.5

Table 7.11 Regression Equations, Error Summary

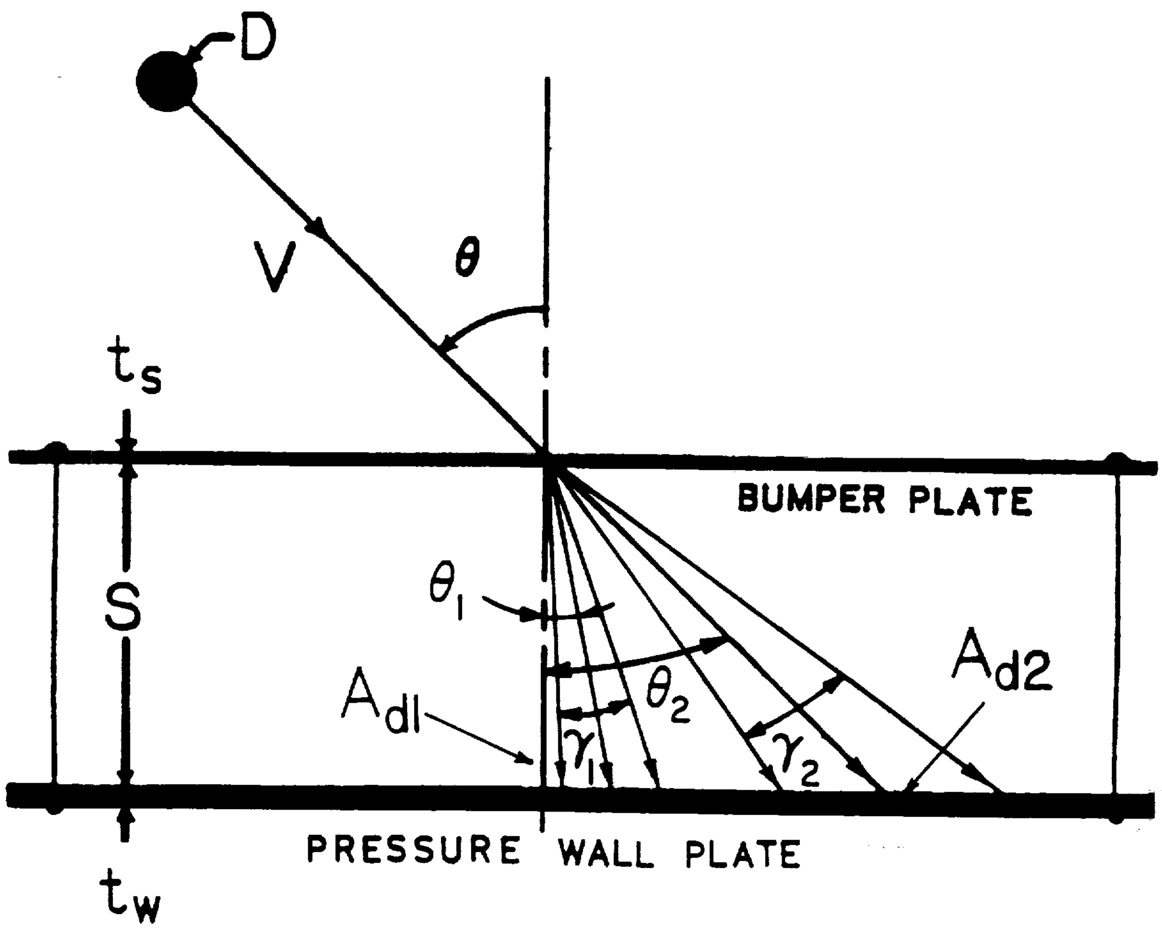

Figure 7.1 Oblique Impact of a Spherical Projectile on a Dual-Wall Structure

SECTION EIGHT -- HYPERVELOCITY IMPACT RESPONSE OF MULTI-BUMPER STRUCTURES

8.1 Introduction

Interestingly enough, one of the first investigations into the effectiveness of multi-bumper structures in reducing the penetration threat of high-speed meteoroids concluded that, for a constant weight structure, the use of more than one bumper within a given total spacing will actually increase the vulnerability of the spacecraft wall to hypervelocity impacts [8.1-8.3]. However, the analytical technique used to arrive at this conclusion was predicated on the assumption that the projectile and bumper debris clouds were vaporous and, as such, delivered a blast-loading to the pressure wall of the multi-bumper structure. Therefore, the conclusion that more than one bumper decreases penetration resistance may only be valid for meteoroid impacts in which the impact velocity can exceed 30 km/sec and vaporization will undoubtedly occur. In the case of orbital debris, the impact velocities are much lower (on the order of 12 km/sec) and it is more likely that the resultant debris clouds will consist mainly of fragmented bumper and projectile material. As such, a blast loading analysis is inappropriate and the resulting conclusion is invalid for space debris impacts.

Richardson [8.4] showed that dual aluminum bumpers at relatively large stand-off distances, i.e. 30 cm and greater, were capable of reducing pressure wall damage by as much as 60% over single aluminum bumpers with equivalent overall thickness. Test were also performed on dual-bumper systems in which the outer and inner bumpers were an aluminum mesh and a solid aluminum plate, respectively [8.5]. Again these dual-bumper systems proved to be more efficient in reducing pressure wall damage than similar weight single-bumper systems. Cour-Palais showed that there is a distinct advantage in using two back-up sheets instead of a single pressure wall of equal or greater weight in reducing the penetration threat of high speed projectiles [8.6,8.7].

This Section presents the results of an investigation into the response of single and multi-bumper structural systems under normal and oblique hypervelocity projectile impact loadings. Test results for multi-bumper specimens are reviewed for a variety of geometric configurations and impact parameters. Impact damage is characterized according to the nature and extent of penetration, crater, and spall damage in the structural system. The damage in the multi-bumper specimens is compared to the damage in similar weight single-bumper specimens caused by hypervelocity projectiles with similar impact energies. This comparative analysis is used to determine the advantages of employing multi-bumper structural systems as a means of increasing the protection of long-duration spacecraft against penetration by high speed meteoroid and space debris impacts.

8.2 Hypervelocity Impact Test Parameters

In each test, a projectile of diameter d and velocity V impacted one or more bumper plates along a trajectory inclined at an angle θ with respect to the outward normal of the test specimen bumper plate. Figure 8.1 illustrates the oblique impact of a single-bumper test specimen while Figure 8.2 shows the oblique impact of a dual-bumper system. In the single-bumper system tests, the projectile and a portion of the bumper plate surrounding the impact site shattered upon impact. In the multiple-bumper system tests, projectile and bumper plate fragments formed as a result of the impact on the first bumper plate moved through the remaining bumper plates creating additional secondary debris. In both cases, the projectile and bumper plate fragments eventually struck the pressure wall plate of thickness t_w located a distance S behind the front bumper plate. The thicknesses of the bumper plates in the single-bumper systems, t_s, were chosen to have the same total thickness as the n bumper plates in the multi bumper systems, that is,

$$t_s = t_{s1} + t_{s2} + \ldots + t_{sn} \quad (8.1)$$

In addition, the total stand-off distances in the single-bumper systems were chosen to be equal to the sum of the intermediate stand-off distances in the corresponding multi-bumper systems, that is,

$$S = S_1 + S_2 + \ldots + S_n \quad (8.2)$$

In the multi-bumper systems, a subscript of '1' refers to the bumper thickness or spacing that is farthest from the pressure wall plate while an 'n' refers to the bumper thickness or spacing that is closest. The impact of the secondary debris particles created 'normal' and 'in-line' areas of damage, A_{d1} and A_{d2}, respectively, on the front surface of the pressure wall plate. It is believed that the majority of the 'normal' secondary debris particles are bumper plate fragments while the majority of the 'in-line' debris particles are projectile fragments [8.8,8.9]. In those tests where the path of the projectile was normal to the surface of the bumper plate (ie. $\theta=0^o$), the damage areas overlapped and combined to form a single area of damage A_d on the front surface of the pressure wall plate. Occasionally, the impacts of the secondary projectile and bumper plate fragments resulted in the creation of thin spall fragments ejected from the rear side of the pressure wall plate. In these cases, for both the normal and oblique impacts, the total spalled area on the rear surface is denoted by A_s.

The conditions of the impact tests were chosen to simulate space debris impact of light-weight space structures as closely as possible, and still remain within the realm of experimental feasibility. Kessler et.al. [8.10] state that the average mass density for pieces of orbital debris less than 10 mm in diameter is approximately 2.8 gm/cm^3, which is approximately that of aluminum. Although it is known that the shape of the impacting projectile will affect the formation and spread of secondary debris particles [8.11], spherical projectiles were used in the test program to maintain repeatability and consistency. Thus, the testing was conducted with solid spherical 1100 aluminum projectiles with diameters ranging from 6.35 mm to 12.7 mm. The velocities of the impacting projectiles ranged from 3.2 to 7.34 km/sec. To study the effects of trajectory obliquity on penetration, impact testing was performed at obliquities of 0^o and 45^o. Additionally, to simulate the presence of thermal insulation in the spacecraft wall design, some tests were performed with MLI (multi-layer insulation) resting on the pressure wall plate. It is noted that the MLI was merely taped on to the pressure wall plate without being pulled taut. This enabled the layers within the MLI to act individually and not as a single unit.

A total of 61 structural systems with multiple bumpers and 19 single-bumper systems were used to study and evaluate the penetration resistance of multi-bumper systems. In both systems, the bumper and pressure wall plates were made from 6061-T6 and 2219-T87 aluminum, respectively; in all cases, the pressure wall plate thickness was kept constant at 3.175 mm. The MLI consisted of 30 layers of 0.5 mil kapton aluminized on one side and 29 layers of Dacron mesh, one layer between each kapton layer. Additionally, one layer of beta-cloth (coated s-glass) was added on the side nearest the bumper plate for durability. The areal density of this combination was calculated to be approximately 0.107 gm/cm^2 [8.12]. Additional test parameters and configuration geometries are given in Tables 8.1 through 8.7. Table 8.1 gives the parameters for multi-walled configurations with more than 2 bumper plates. Tables 8.2 and 8.3 give the test parameters for normal impact tests on dual-bumper specimens with total stand-off distances equal to and greater than 10.16 cm, respectively. Table 8.4 gives the impact test parameters for normal impact tests on single-bumper specimens. Table 8.5 gives the impact test parameters for the normal impact tests for the dual- and single-bumper specimens in which MLI was included. The impact test parameters for oblique impact tests on dual- and single-bumper specimens are given in Tables 8.6 and 8.7, respectively.

The results of the normal hypervelocity impact tests are given in Tables 8.8-8.10 for the multi-bumper systems without MLI; Table 8.11 gives the results of the normal hypervelocity impact tests for systems with single bumpers without MLI. Table 8.12 gives the test results for dual-bumper and single-bumper systems with MLI. Table 8.13 gives the 'normal' and 'in-line' pressure wall damage for the oblique impact tests. It is noted that in Tables 8.8-8.13, entries of '----' indicate that certain phenomena, such as pressure wall penetration, front surface damage, or rear surface spall, did not occur. Additionally, d_h is the equivalent single hole diameter of all the holes in the pressure wall plate in the event of pressure wall penetration. Penetration characteristics for normal and oblique shots are summarized and compared in Tables 8.14-8.16 and in Table 8.18, respectively. In these tables, the test shots grouped according to both geometric and impact energy similarity. Table 8.17 presents a summary and a comparison of the penetration characteristics for the normal tests which contained MLI.

Detailed analysis of the damaged test specimens revealed many interesting features and response characteristics of multi-bumper structures under hypervelocity projectile impact loadings. Finally, Figure 8.3 presents a comparison of the penetration functions for some of the dual-bumper and single-bumper systems considered in this investigation.

8.3 Hypervelocity Impact Response of Multi-Bumper Systems

8.3.1 Bumper Plate Damage Analysis

In the normal impact tests, the impact damage in the outer-most bumper plate of the multi-bumper systems typically consisted of a circular hole with a diameter larger than that of the projectile which struck the plate. Under 45^{o} impact, the impact damage in the outer-most bumper typically consisted of an elliptical hole whose maximum dimension was aligned with the projection of the flight path of the impacting projectile on the surface of the bumper plate. For both the normal and the 45^{o} impacts, the remaining bumper plates consisted of jagged holes that were increasingly larger in each successive plate. Although the edges of these holes were usually frayed, their roundness was evident nonetheless. The jaggedness of the holes is probably the result of a clear penetration by vaporous and molten secondary debris particles being followed by impulsive loads from the slower moving solid and molten debris fragments.

8.3.2 Pressure Wall Plate Damage Analysis

In Tables 8.14-8.18, penetration characteristics for single- and multiple-bumper systems are summarized for tests grouped according to geometric and impact energy similarity. In general, for both normal and oblique impact, under similar impact conditions, the multi-bumper systems sustained less damage than did corresponding single-bumper systems. Impact response characteristics for dual- and multi-bumper systems are described below and are compared to those in corresponding single-bumper systems first for normal impact and then for oblique impact.

In general, under normal impact, dual- and multi-bumper systems were more resistant to pressure wall plate penetration than corresponding single-bumper systems under similar impact conditions. For example, in Figure 8.3, the penetration function for normally impacted dual-bumper systems with S_1=2.54 cm, S_2=7.62 cm, t_s=1.6 mm, and S=10.16 cm is seen to be located above the penetration function for normally impacted single-bumper systems with the same total stand-off distance and bumper thickness, which is taken from Figure 3.2. The area between the two penetration functions represents projectile diameter and velocity combinations that would penetrate the single-bumper systems but would not penetrate the dual-bumper systems. It was also found that if pressure wall penetration occurred in a dual- or multi-bumper system and a corresponding single-bumper system, then the penetrated pressure wall plates in the single-bumper systems sustained larger equivalent single hole diameters than did the penetrated pressure wall plates in the corresponding multi-bumper systems (see Tables 8.9,8.10 and compare with Table 8.11). The increased penetration resistance of the dual-bumper specimens is due to the fact that the material in the debris cloud created by the impact of the projectile on the outer-most bumper plate is still traveling at relatively high speeds and is shocked again as it impacts the intermediate bumper plate. This results in further fragmentation of the debris cloud particles and a subsequent reduction in their penetration potential.

The pressure wall plate damage areas in the single-bumper systems were two to three times as large as those in the corresponding multi-bumper systems. The pressure wall plates in the single-bumper systems also demonstrated a greater tendency to undergo rear-side spallation under normal impact than did those in the corresponding multi-bumper systems under similar impact conditions. This is evident in Tables 8.9 and 8.10 where only four of the multi-bumper systems exhibited spall while in Table 8.11 it is seen that all of the single-bumper systems underwent rear-side spallation of the pressure wall plate. If a multi-bumper system did exhibit spall, the spall area was small compared to that in the single-bumper system (e.g. A_s=0.45 cm^2 for dual-bumper Test No. 175A while A_s=8.65 cm^2 for single-bumper Test No. P34B). A multi-bumper system is less likely to spall because the debris cloud pressure pulse that causes the shock wave to move through the pressure wall plate has been significantly reduced by the successive shocking of the particles in the debris cloud by the intermediate bumper plates.

In low energy impacts (ie. less than 10,000 joules) of dual-bumper systems, it was found that the systems with $S_1<S_2$ were less likely to be penetrated than otherwise equivalent systems in which $S_1>S_2$ (Table 8.14a and Table 8.15). However, in high energy impacts (ie. greater than 25,000 joules) of dual-bumper systems, it was found that systems with $S_1>S_2$ were less likely to be penetrated than otherwise equivalent systems in which $S_1<S_2$ (Table 8.14b and Tables 8.15,8.16). Under a high energy impact, dual-bumper systems in which $S_1>S_2$ are less likely to be penetrated than those with $S_1<S_2$ because if $S_1>S_2$, then the debris cloud has sufficient time to spread out before its high-speed particles impact the intermediate bumper plate and are shocked into further fragmentation. If the intermediate bumper plate is close to the outer-most bumper plate in a dual-bumper system under a high energy impact, then the debris cloud is still relatively concentrated when it impacts the intermediate bumper. Although some additional fragmentation will occur in this case, the debris cloud will still be in relatively concentrated when it leaves the intermediate bumper, which, in some systems, can result in an increased likelihood of pressure wall penetration.

Based on these observations, it would appear that there is an optimum location for the placement of the intermediate bumper plate depending on the energy of the impacting projectile, the geometry of the structural system (ie. t_s, S, and t_w), and the material properties of the bumper and pressure wall plates, and the energy of the impacting projectile. Because the optimum location depends on the energy of the the impacting projectile, a particular dual-bumper configuration may not be applicable over a wide range of impact conditions. The apparent difference in the optimum location of the intermediate bumper plate for low and high energy impacts is due to the action and interaction of two competing processes.

First, as the debris cloud moves toward the pressure wall plate, it spreads out radially. If $S_1>S_2$, then when the debris cloud impacts the intermediate bumper, its impulsive loading is distributed over a much larger area than if $S_1<S_2$. If $S_1<S_2$, then when the debris cloud impacts the intermediate bumper, it is still in a relatively concentrated form. It also follows that if $S_1>S_2$ and the debris cloud is diffuse when it impacts the intermediate bumper plate, then a larger portion of the debris particles will be absorbed by the intermediate bumper plate than if $S_1<S_2$ and the debris cloud were more condensed.

The second process is the shocking of the fragments in the debris cloud as they impact the intermediate bumper. The higher the stress levels in the intermediate bumper plate, the more shocking, and subsequently, the more debris cloud particle fragmentation and melting will occur. However, this additional fragmentation and melting can occur only if the stress levels are very high, that is, greater than the material strength of the intermediate bumper plate. According to the discussion in the preceding paragraph, if $S_1>S_2$, then a more diffuse load is applied to the intermediate bumper plate than when $S_1<S_2$. Thus, if $S_1>S_2$, then it is reasonable to assume that the stress levels in the intermediate bumper plate are lower and that the debris cloud particles are shocked less than if $S_1<S_2$, unless the debris cloud particles are traveling fast enough to individually create areas of high stress in the intermediate bumper plate.

This explains, in part, why fewer pressure wall plate penetrations occur in the high energy tests if $S_1>S_2$ and why fewer penetrations occur in the low energy tests if $S_1<S_2$. Apparently, in the high energy impacts, the debris particles are traveling fast enough so that they are individually shocked into fragmentation by the intermediate bumper plate. In these cases, the wider areal distributions of the debris clouds does not affect the shocking and fragmentation process. Furthermore, in the low velocity impacts, when $S_1<S_2$, the impacts of the concentrated debris clouds cause stress levels to rise sufficiently high so as to cause additional fragmentation of the debris cloud particles. If $S_1>S_2$ for a low energy impact, then the debris cloud would spread out and its particles, unless they were traveling slow enough so as to be stopped by the intermediate bumper plate, would pass through the intermediate bumper plate relatively unscathed. Similarly, if $S_1<S_2$ for a high energy impact, then the high-speed particles of the initial debris cloud would also pass through the intermediate bumper plate relatively undisturbed. In both of these alternative 'non-optimum' situations, penetration of the pressure wall plate would be possible.

As the stand-off distance was increased beyond 10.16 cm, it was found that the likelihood of pressure wall penetration in single-bumper systems steadily decreased. Only a few pressure wall penetrations occurred in single-bumper systems at stand-off distances greater than 20 cm, even at energy levels as high as 50,000 joules. When the stand-off distance was equal to 30.48 cm, the potential of pressure wall penetration in the single-bumper systems was roughly equal to that of similar dual-bumper systems with similar total stand-off distances (Table 8.14c). However, even at the large stand-off distances, the single-bumper systems exhibited significant amounts of rear-side pressure wall plate spallation whereas corresponding multi-bumper systems under similar impact conditions did not. The reason for this is that the multiple bumpers probably slow the fragments down to a velocity below the speed of sound in the pressure wall plate material. These slow moving fragments are less likely to cause spall than the faster fragments formed in single-bumper system impact.

It was also found that increasing the total stand-off distance by only 20% or 50% (e.g. from 10.16 cm to 15.24 cm) did not significantly affect the probability of pressure wall penetration in either the single- or the dual-bumper systems. In order to achieve a significant decline in the probability of pressure wall penetration, an increase in total stand-off distance on the order of 100% or 200% was needed (ie. from 10.16 cm to 20.32 cm or from 10.16 cm to 30.48 cm; see Table 8.15). Furthermore, it was found that increasing the number of intermediate bumper plates beyond two while maintaining the total stand-off distance S and the total bumper thickness t_s did not significantly affect the probability of pressure wall plate penetration in the multi-bumper systems at large stand-off distances (Table 8.16). This implies that not only is there an optimum location of an intermediate bumper within a given total spacing, but that there is also an optimum number of intermediate bumpers and an optimum total stand-off distance.

Although the number of tests with MLI was limited, certain trends were still evident. First, it was found that, under normal impact of single- and dual-bumper systems, the presence of MLI reduced the damage area on the pressure wall plate by as much as a factor of three or four (compare the values of A_d in Table 8.12 with those in Tables 8.9,8.11). Second, the presence of MLI also contributed to the reduction of the potential of pressure wall plates to undergo rear-side spallation.

Under oblique impact, the pressure wall plates in the single-bumper systems demonstrated a greater tendency to exhibit spall under the 'in-line' damage area than did the pressure wall plates in the corresponding dual-bumper systems under similar impact conditions (see Table 8.13). It was also found that the likelihood of pressure wall penetration in dual-bumper systems under oblique impact was only slightly less than that in corresponding single-bumper systems under similar impact conditions (Table 8.18). This is due to the fact that in the 45° impacts, the normal velocity components of the initial debris cloud particles are decreased to the low end of the hypervelocity regime. As a result of their lower velocities, the debris particles are not shocked to a pressure that is high enough to cause them to fragment as readily as the particles in a debris cloud that resulted from a normal impact. Since only minimal additional fragmentation occurs, the debris clouds move through the intermediate bumpers relatively undisturbed. However, since some additional fragmentation does occur, the probability of pressure wall penetration will decrease even if only by a small amount. In the event that pressure wall penetration occurred in both types of systems, the equivalent single hole diameter of the holes in the 'in-line' damage areas of pressure wall plates were, on the whole, larger in the single-bumper systems than in the multi-bumper systems (Table 13). Unlike normal impact, under oblique impact, the likelihood of pressure wall plate penetration in dual-bumper systems was approximately the same regardless of the position of the intermediate bumper relative to the outer bumper and the pressure wall plate (Table 8.18).

8.4 Summary and Conclusions

The recent proliferation of large pieces of orbital space debris has made it necessary to modify traditional penetration-resistant wall design for long-duration earth-orbiting spacecraft so that they can resist penetration by projectiles with much higher impact energies. One such modification is the replacement of a single bumper with two or more bumpers of equal weight. An investigation was performed to determine the advantages and disadvantages of using multi-bumper systems as a means of increasing the penetration resistance of long-duration spacecraft.

For normal impact, under similar impact conditions, multi-bumper systems were found to sustain less damage than corresponding single-bumper systems. The pressure wall plate damage areas and equivalent single-hole diameters in the single-bumper systems were significantly larger than those in corresponding multi-bumper systems. The pressure wall plates in normally-impacted single-bumper systems also demonstrated a greater tendency to undergo rear-side spallation than did those in corresponding normally-impacted dual- and multi-bumper systems. In high and low energy impacts of dual-bumper systems, it was found that pressure wall plate penetration was sensitive to the placement of the intermediate bumpers relative to the outer bumper plate and the pressure wall plate. Increasing the number of intermediate bumper plates beyond two while maintaining the total stand-off distance and the total bumper thickness of the structural system did not significantly alter pressure wall plate penetration. Under oblique impact, pressure wall penetration in dual-bumper systems was observed to be only slightly less than that in corresponding single-bumper systems under similar impact conditions. Unlike normal impact, under oblique impact, the likelihood of pressure wall plate penetration in dual-bumper systems was approximately the same regardless of the position of the intermediate bumper relative to the outer bumper and the pressure wall plate.

8.5 References

8.1 R.E. Sennett, "Effectiveness of Multisheet Structures for Meteroid Impact Protection", AIAA Journal, Vol. 6, pp. 942-943, 1968.

8.2 J.W. Gehring, "Engineering Considerations in Hypervelocity Impact", High-Velocity Impact Phenomena, R. Kinslow, ed., Academic Press (1970).

8.3 C.J. Maiden, J.W. Gehring, A.R. McMillan, and R.E. Sennett, Experimental Investigation of Simulated Meteoroid Damage to Various Spacecraft Structures, NASA TR 65-48 (1965).

8.4 A.J. Richardson and J.P. Sanders, "Development of Dual-Bumper Wall Construction for Advanced Spacecraft", J. Spacecraft, Vol. 9, pp. 448-

451 (1972).

8.5 E. Christiansen, Evaluation of Space Station Meteoroid/Debris Shielding Materials, Report No. 87-163, Eagle Engineering, Houston, Texas (1987).

8.6 B.G. Cour-Palais, "Space Vehicle Meteoroid Shielding Design", Proceedings of the Comet Halley Micrometeorid Hazard Workshop, N. Langdon, ed., ESA SP-153, Paris France, 85-92, 1979.

8.7 B.G. Cour-Palais, "Meteoriod Protection by Multi-Wall Structures", AIAA Paper No. 69-372, Proceedings of the AIAA Hypervelocity Impact Conference (1969).

8.8 W.P. Schonberg and R.A. Taylor, "Penetration and Ricochet Phenomena in Oblique Hypervelocity Impact", AIAA Journal, Vol. 27, pp. 639-646 (1989).

8.9 G.T. Burch, Multi-Plate Damage Study, AFATL-TR-67-116, Air Force Armament Laboratory, Eglin Air Force Base, Florida (1967).

8.10 D.J. Kessler, R.C. Reynolds, and P.D. Anz-Meador, Orbital Debris Environment for Spacecraft Designed to Operate in Low Earth Orbit, NASA TM 100471, Houston, Texas (1989).

8.11 R.H. Morrison, A Preliminary Investigation of Projectile Shape Effects in Hypervelocity Impact of a Double Sheet Structure, NASA TN D-6944, Washington, D.C. (1972).

8.12 A.R. Coronado, M.N. Gibbins, M.A. Wright, and P.H. Stern, Space Station Integrated Wall Design and Penetration Damage Control, D180-30550-1, Boeing Aerospace Co., Seattle, Washington (1987).

Table 8.1a Normal Impact Test Parameters, Multi-Bumper Systems, No MLI

Test No.	V (km/s)	d (mm)	t_s (mm)	Number of Bumpers	S (cm)	Impact Energy (J)
180A	6.41	9.53	4.064	4	17.78	24,902
180B	5.53	9.53	4.064	4	17.78	18,229
182A	6.30	9.53	4.064	4	17.78	24,204
188D	6.12	12.70	3.048	3	30.48	54,130
189C	5.87	12.70	3.048	6	30.48	50,125

Table 8.1b Intermediate Stand-off Distances, Multi-Bumper Systems

Test No.	S_1	S_2	S_3	S_4	S_5	S_6
180A	2.54	2.54	2.54	10.16	----	----
180B	2.54	2.54	2.54	10.16	----	----
182A	5.08	5.08	5.08	2.54	----	----
188D	10.16	10.16	10.16	----	----	----
189C	5.08	5.08	5.08	5.08	5.08	5.08

Table 8.1c Intermediate Bumper Thicknesses, Multi-Bumper Systems

Test No.	t_{s1}	t_{s2}	t_{s3}	t_{s4}	t_{s5}	t_{s6}
180A	1.016	1.016	1.016	1.016	----	----
180B	1.016	1.106	1.016	1.016	----	----
182A	1.106	1.016	1.106	1.016	----	----
188D	1.016	1.016	1.016	----	----	----
189C	0.508	0.508	0.508	0.508	0.508	0.508

Table 8.2 Normal Impact Test Parameters, Dual-Bumper Systems, S=10.16 cm, No MLI

Test No.	V (km/s)	d (mm)	t_s (mm)	t_{s1} (mm)	t_{s2} (mm)	S (cm)	S_1 (cm)	S_2 (cm)	Impact Energy (J)
115-1	4.40	6.35	1.626	0.813	0.813	10.16	2.54	7.62	3,520
115-2	4.06	6.35	1.626	0.813	0.813	10.16	2.54	7.62	2,997
115-3	3.82	6.35	1.626	0.813	0.813	10.16	2.54	7.62	2,653
117-1	4.09	6.35	1.626	0.813	0.813	10.16	5.08	5.08	3,042
117-2	4.17	6.35	1.626	0.813	0.813	10.16	5.08	5.08	3,425
118-1	4.40	6.35	1.626	0.813	0.813	10.16	7.62	2.54	3,520
118-2	4.49	6.35	1.626	0.813	0.813	10.16	7.62	2.54	4,492
118-3	4.52	6.35	1.626	0.813	0.813	10.16	7.62	2.54	3,715
130A	3.60	7.62	1.626	0.813	0.813	10.16	2.54	7.62	4,072
130B	4.85	7.62	1.626	0.813	0.813	10.16	2.54	7.62	7,391
130C	5.25	7.62	1.626	0.813	0.813	10.16	2.54	7.62	8,826
131A	4.60	6.35	2.413	1.600	0.813	10.16	7.62	2.54	3,848
131B	4.31	6.35	2.413	1.600	0.813	10.16	7.62	2.54	3,778
131C	4.64	6.35	2.413	1.600	0.813	10.16	7.62	2.54	3,814
152A	4.62	6.35	1.524	1.016	0.508	10.16	5.08	5.08	3,798
152B	3.63	6.35	1.524	1.016	0.508	10.16	5.08	5.08	2,396
153A	6.58	9.53	3.632	2.032	1.600	10.16	7.62	2.54	25,531
153B	6.92	9.53	3.632	2.032	1.600	10.16	7.62	2.54	29,049
158A	3.20	6.35	1.626	0.813	0.813	10.16	2.54	7.62	1,816
175A	6.99	6.35	1.626	0.813	0.813	10.16	1.35	8.81	8,733
175B	7.34	6.35	1.626	0.813	0.813	10.16	1.35	8.81	9,611
175C	7.30	6.35	1.626	0.813	0.813	10.16	1.35	8.81	9,690

Table 8.3 Normal Impact Test Parameters, Dual-Bumper Systems, S>10.16 cm, No MLI

Test No.	V (km/s)	d (mm)	t_s (mm)	t_{s1} (mm)	t_{s2} (mm)	S (cm)	S_1 (cm)	S_2 (cm)	Impact Energy (J)
176C	5.07	6.35	1.626	0.813	0.813	12.70	5.08	7.62	4,619
158B	3.21	6.35	1.626	0.813	0.813	15.24	2.54	12.70	1,839
160	6.50	9.53	1.626	0.813	0.813	15.24	2.54	12.70	25,849
179A	6.46	9.53	2.032	1.016	1.016	17.78	7.62	10.16	25,532
179B	6.70	9.53	2.032	1.016	1.016	17.78	7.62	10.16	27,467
181A	6.32	9.53	4.191	3.175	1.016	17.78	7.62	10.16	23,973
181B	5.52	9.53	4.191	3.175	1.016	17.78	7.62	10.16	18,632
167A	6.58	9.53	3.200	1.600	1.600	20.32	10.16	10.16	26,410
167B	6.66	9.53	3.200	1.600	1.600	20.32	10.16	10.16	26,895
187A	6.36	12.70	5.207	3.175	2.032	20.32	10.16	10.16	58,105
187B	6.02	12.70	5.207	3.175	2.032	20.32	10.16	10.16	52,021
191A	6.57	9.53	2.032	1.016	1.016	20.32	10.16	10.16	26,249
186A	6.07	12.70	5.207	3.175	2.032	30.48	10.16	20.32	53,246
186B	5.36	12.70	5.207	3.175	2.032	30.48	10.16	20.32	39,487
188A	5.72	12.70	5.207	3.175	2.032	30.48	20.32	10.16	46,274
188B	6.21	12.70	4.064	2.032	2.032	30.48	20.32	10.16	54,485
188C	6.06	12.70	4.064	3.175	1.016	30.48	20.32	10.16	52,544
188E	6.12	12.70	3.048	2.032	1.016	30.48	20.32	10.16	53,422

Table 8.4 Normal Impact Test Parameters, Single Bumper Systems, No MLI

Test No.	V (km/s)	d (mm)	t_s (mm)	S (cm)	Impact Energy (J)
213C	4.43	6.35	2.032	10.16	3,569
P03	4.90	6.35	1.600	10.16	4,366
P04	4.95	6.35	1.600	10.16	4,456
P34B	7.06	6.35	1.600	10.16	9,064
PT-4A	3.64	6.35	1.600	10.16	2,489
PT-4B	4.26	6.35	1.600	10.16	3,378
PT-8A	4.35	7.95	1.600	10.16	6,846
PT-8B	4.37	7.95	1.600	10.16	6,972
P35	6.69	8.89	1.600	15.24	22,332
184A	5.70	12.70	4.750	30.48	47,264
184B	5.28	12.70	4.750	30.48	41,793
189A	6.13	12.70	3.175	30.48	53,599
189B	6.10	12.70	3.175	30.48	54,130

Table 8.5 Normal Impact Test Parameters, Dual- and Single-Bumper Systems With MLI

Test No.	V (km/s)	d (mm)	No. Bump.	t_s (mm)	t_{s1} (mm)	t_{s2} (mm)	S (cm)	S_1 (cm)	S_2 (cm)	Impact Energy (J)
128A	4.10	6.35	2	1.626	0.813	0.813	10.16	2.54	7.62	3,441
128B	3.53	6.35	2	1.626	0.813	0.813	10.16	2.54	7.62	2,370
P12C	4.33	6.35	1	1.600	----	----	10.16	----	----	3,409
P12D	3.96	6.35	1	1.600	----	----	10.16	----	----	2,852

Table 8.6 Oblique Impact Test Parameters, Dual-Bumper Systems, No MLI, θ=45 deg

Test No.	V (km/s)	d (mm)	t_s (mm)	t_{s1} (mm)	t_{s2} (mm)	S (cm)	S_1 (cm)	S_2 (cm)	Impact Energy (J)
137A	4.86	6.35	1.626	0.813	0.813	10.16	7.62	2.54	4,474
137B	5.65	6.35	1.626	0.813	0.813	10.16	7.62	2.54	5,805
137C	6.16	6.35	1.626	0.813	0.813	10.16	7.62	2.54	6,990
137D	7.03	6.35	1.626	0.813	0.813	10.16	7.62	2.54	8,809
138A	6.52	6.35	1.626	0.813	0.813	10.16	7.62	2.54	13,317
138B	7.15	7.62	1.626	0.813	0.813	10.16	7.62	2.54	16,380
168A	5.54	6.35	1.626	0.813	0.813	10.16	9.44	0.72	5,461
168B	5.98	6.35	1.626	0.813	0.813	10.16	9.44	0.72	6,373
168C	6.67	6.35	1.626	0.813	0.813	10.16	9.44	0.72	7,997
168D	7.02	6.35	1.626	0.813	0.813	10.16	9.44	0.72	8,961
169A	6.87	6.35	1.626	0.813	0.813	10.16	9.76	0.40	6,532
169B	6.55	6.35	1.626	0.813	0.813	10.16	9.76	0.40	7,778
170A	6.52	6.35	1.626	0.813	0.813	10.16	8.81	1.35	7,636
170B	6.85	6.35	1.626	0.813	0.813	10.16	8.81	1.35	8,359

Table 8.7 Oblique Impact Test Parameters, Single-Bumper Systems, No MLI, θ=45 deg

Test No.	V (km/s)	d (mm)	t_s (mm)	S (cm)	Impact Energy (J)
002A	6.50	7.95	1.600	10.16	15,310
230C	5.18	6.35	1.600	10.16	4,842
230D	5.55	6.35	1.600	10.16	5,682
230E	6.57	6.35	1.600	10.16	7,969

Table 8.8 Test Results, Normal Impact, Multi-Bumper Systems, No MLI

Test No.	D_1 (cm)	D_2 (cm)	D_3 (cm)	D_4 (cm)	D_5 (cm)	D_6 (cm)	d_h (cm²)	A_d (cm)	A_s (cm²)
180A	1.422	4.369	9.220	13.360	----	----	----	53.52	----
180B	1.377	3.327	7.188	11.836	----	----	----	41.87	----
182A	1.415	5.055	11.760	5.055	----	----	----	17.81	----
188D	1.651	5.588	19.126	----	----	----	----	42.91	----
189C	1.420	9.881	14.580	19.279	cracked	22.047	18.29	32.32	----

Table 8.9 Test Results, Normal Impact, Dual-Bumper Systems, S=10.16 cm, No MLI

Test No.	D_1 (cm)	D_2 (cm)	d_h (mm)	A_d (cm^2)	A_s (cm^2)
115-1	0.978	2.583	----	38.06	----
115-2	0.894	2.167	----	35.05	----
115-3	0.907	1.953	4.85	38.29	----
117-1	0.973	3.683	----	13.16	----
117-2	0.925	2.700	1.02	14.28	----
118-1	0.965	3.683	3.73	6.46	----
118-2	0.942	3.480	----	38.32	----
118-3	1.011	3.830	crack	6.99	----
130A	1.026	2.217	10.72	25.81	----
130B	1.087	2.946	2.29	34.38	----
130C	1.123	3.462	3.56	34.78	----
131A	1.245	5.108	----	24.30	----
131B	1.130	3.345	10.24	20.47	----
131C	1.151	3.119	14.45	19.82	----
152A	1.069	3.475	----	16.24	----
152B	0.935	2.675	5.36	9.37	----
153A	1.905	1.270	60.96	93.68	----
153B	2.032	2.794	12.70	36.94	----
158A	0.782	1.824	5.21	13.61	----
175A	1.041	2.570	6.10	45.61	0.45
175B	1.052	2.433	2.05	30.41	0.06
175C	1.099	2.642	----	34.92	----

Table 8.10 Test Results, Normal Impact, Dual-Bumper Systems, S>10.16 cm, No MLI

Test No.	D_1 (cm)	D_2 (cm)	d_h (mm)	A_d (cm²)	A_s (cm²)
176C	0.940	3.688	----	34.92	0.01
158B	0.810	1.829	7.81	25.87	----
160	1.346	4.813	45.72	98.06	----
179A	1.397	5.080	84.07	241.94	----
179B	1.372	5.121	19.43	120.42	----
181A	2.283	9.550	----	62.06	----
181B	2.209	8.306	----	31.68	----
167A	1.951	8.555	----	36.13	----
167B	1.935	5.730	crack	61.72	----
187A	2.743	10.719	----	21.32	0.06
187B	2.743	9.347	----	36.33	----
191A	1.412	6.208	----	53.48	----
186A	2.667	10.160	----	61.35	----
186B	2.675	9.093	----	53.87	----
188A	2.743	11.463	----	46.52	----
188B	2.184	10.973	----	70.13	----
188C	2.746	16.535	----	114.32	----
188E	2.261	14.681	----	90.24	----

Table 8.11 Test Results, Normal Impact, Single-Bumper Systems, No MLI

Test No.	D (cm)	d_h (mm)	A_d (cm^2)	A_s (cm^2)
213C	1.217	6.86	71.23	3.19
P03	1.247	9.09	81.07	3.44
P04	1.247	7.72	64.58	1.97
P34B	1.448	25.65	80.97	8.65
PT-4A	1.016	16.00	69.48	3.94
PT-4B	1.270	6.35	98.13	2.58
PT-8A	1.244	46.99	81.42	6.19
PT-8B	1.270	37.34	85.23	1.42
P35	1.854	45.11	107.92	8.12
184A	3.200	----	622.26	0.13
184B	3.124	----	610.26	0.77
189A	2.946	23.88	394.19	1.30
189B	2.743	----	568.26	0.18

Table 8.12 Test Results, Normal Impact, Dual- and Single-Bumper Systems With MLI

Test No.	D_1 (cm)	D_2 (cm)	d_h (mm)	A_d (cm^2)	A_s (cm^2)
128A	0.960	2.262	----	9.37	----
128B	0.930	2.223	2.41	7.27	----
P12C	1.194	----	----	21.29	----
P12D	1.270	----	----	18.19	----

Table 8.13 Test Results, Oblique Impact, S=10.16 cm, No MLI

Test No.	$D_{1,min}$ (cm)	$D_{1,max}$ (cm)	D_2 (cm)	'Normal' Damage			'In-Line' Damage		
				d_h (mm)	A_d (cm^2)	A_s (cm^2)	d_h (mm)	A_d (cm^2)	A_s (cm^2)
				Multi-Bumper Systems					
137A	1.095	1.440	3.551	----	10.48	----	5.64	22.09	----
137B	1.064	1.409	3.769	----	12.48	----	6.07	20.57	----
137C	1.067	1.427	3.975	----	6.37	----	3.10	47.19	----
137D	1.069	1.549	3.782	----	6.84	----	6.35	16.26	0.76
138A	1.318	1.819	5.146	----	8.15	----	13.49	57.52	----
138B	1.298	1.697	5.250	----	8.92	----	12.27	55.45	----
168A	1.067	1.450	2.642	----	5.80	----	8.76	14.65	----
168B	1.052	1.527	2.462	----	6.82	----	10.52	25.11	----
168C	1.118	1.473	2.842	----	21.50	----	4.70	16.05	----
168D	1.227	1.557	2.710	----	26.11	----	----	29.68	----
169A	1.179	1.674	2.192	----	22.90	----	----	6.41	----
169B	1.166	1.621	1.696	----	41.87	----	4.95	21.81	----
170A	1.019	1.715	2.972	----	8.52	----	6.40	31.68	----
170B	1.080	1.572	2.819	2.16	25.65	----	----	15.52	----
				Single-Bumper Systems					
002A	1.560	2.024	----	----	45.61	----	27.97	91.21	1.31
230C	1.255	1.610	----	----	31.67	----	11.89	33.21	----
230D	1.336	1.631	----	2.591	34.25	----	12.78	36.94	0.15
230E	1.417	1.770	----	----	29.19	0.27	11.94	53.85	0.27

Table 8.14a Pressure Wall Damage Summary, Normal Impact, S=10.16 cm, Impact Energy < 10,000 Joules

Test No.	Stand-off Dist. (cm)	Impact Energy (J)	Pressure Wall Penetrated?	Pressure Wall Spalled?
		$t_s \simeq 1.6$ mm		
115-1	2.54 7.62	3,520	No	No
117-1	5.08 5.08	3,042	No	No
117-2	5.08 5.08	3,425	Yes	No
118-1	7.62 2.54	3,520	Yes	No
118-3	7.62 2.54	3,715	Yes	No
152A	5.08 5.08	3,798	No	No
PT-4B	10.16	3,378	Yes	Yes
118-2	7.62 2.54	4,492	No	No
130A	2.54 7.62	4,072	Yes	No
P03	10.16	4,366	Yes	Yes
P04	10.16	4,456	Yes	Yes
115-2	2.54 7.62	2,997	No	No
115-3	2.54 7.62	2,653	Yes	No
152B	5.08 5.08	2,396	Yes	No
158A	2.54 7.62	1,816	Yes	No
PT-4A	10.16	2,489	Yes	Yes
130B	2.54 7.62	7,391	Yes	No
PT-8A	10.16	6,846	Yes	Yes
PT-8B	10.16	6,972	Yes	Yes
130C	2.54,7.62	8,826	Yes	No
175A	1.35,8.81	8,733	Yes	Yes
175B	1.35,8.81	9,611	Yes	Yes
175C	1.35,8.81	9,690	No	No
P34B	10.16	9,064	Yes	Yes
		$t_s \simeq 2$ mm		
131A	7.62 2.54	3,848	No	No
131B	7.62 2.54	3,778	Yes	No
131C	7.62 2.54	3,814	Yes	No
213C	10.16	3,569	Yes	Yes

Table 8.14b Pressure Wall Damage Summary, Normal Impact, S=30.48 cm, Impact Energy > 25,000 joules

Test No.	Stand-off Dist. (cm)	Impact Energy (J)	Pressure Wall Penetrated?	Pressure Wall Spalled?
		$t_s \simeq 1.6$ mm, S = 15.4 cm		
160	2.54 12.70	25,849	Yes	No
P35	15.24	22,332	Yes	Yes
		$t_s \simeq 3$ mm, S = 30.48 cm		
188E	20.32 10.16	53,422	No	No
189A	30.48	53,599	Yes	Yes
189B	30.48	54,130	No	Yes
		$t_s \simeq 4.5$ mm, S = 30.48 cm		
186A	10.16 20.34	53,246	No	No
186B	10.16 20.34	39,487	No	No
188A	20.32 10.16	46,274	No	No
188B	20.32 10.16	54,485	No	No
188C	20.32 10.16	52,544	No	No
184A	30.48	47,264	No	Yes
184B	30.48	41,793	No	Yes

Table 8.15 Effect of Total Stand-off Distance and Total Bumper Thickness on Dual-Bumper System Response, Normal Impact

Test No.	Total Stand-off Dist. (cm)	Intermed. Stand-off Dist. (cm)	Impact Energy	Pressure Wall Penetrated?	Pressure Wall Spalled?
		$t_s \simeq 1.6$ mm			
118-2	10.16	7.62 2.54	4,492	No	No
130A	10.16	2.54 7.62	4,072	Yes	Yes
176C	12.70	5.08 7.62	4,619	No	Yes
158A	10.16	2.54 7.62	1,816	Yes	No
158B	15.24	2.54 12.70	1,839	Yes	No
		$t_s \simeq 2$ mm			
179A	17.78	7.62 10.16	25,532	Yes	No
179B	17.78	7.62 10.16	27,467	Yes	No
191A	20.32	10.16 10.16	26,249	No	No
		$t_s \simeq 3$ mm			
153A	10.16	7.62 2.54	25,531	Yes	No
153B	10.16	7.62 2.54	29,049	Yes	No
167A	20.32	10.16 10.16	26,410	No	No
167B	20.32	10.16 10.16	26,895	Yes	No
		$t_s \simeq 5$ mm			
187A	20.32	10.16 10.16	58,105	No	Yes
187B	20.32	10.16 10.16	52,021	No	No
186A	30.48	10.16 20.34	53,246	No	No

Table 8.16 Effect of Intermediate Spacing and Number of Intermediate Bumpers on Multi-Bumper System Response, Normal Impact

Test No.	Intermediate Stand-off Distances (cm)						Impact Energy (J)	Pressure Wall Penetrated?	Pressure Wall Spalled?
				$t_s \approx 4$ mm, $S = 17.78$ cm					
181A	7.62	10.16	----	----	----	----	23,973	No	No
181B	7.62	10.16	----	----	----	----	18,632	No	No
180A	2.54	2.54	2.54	10.16	----	----	24,902	No	No
180B	2.54	2.54	2.54	10.16	----	----	18,229	No	No
182A	5.08	5.08	5.08	2.54	----	----	24,204	No	No
				$t_s \approx 3$ mm, $S = 30.48$ cm					
188D	10.16	10.16	10.16	----	----	----	54,130	No	No
188E	20.32	10.16	----	----	----	----	53,422	No	No
189C	5.08	5.08	5.08	5.08	5.08	5.08	50,125	Yes	No

Table 8.17 Pressure Wall Damage Summary, Normal Impact, $t_s \simeq 1.6$ mm, S=10.16 cm, With MLI

Test No.	Stand-off Distances	Impact Energy (J)	Pressure Wall Penetrated?	Pressure Wall Spalled?
128A	2.54 7.62	3,441	No	No
P12C	10.16	3,409	No	No
128B	2.54 7.62	2,370	Yes	No
P12D	10.16	2,852	No	No

Table 8.18 Pressure Wall Damage Summary, Oblique Impact, $t_s \approx 1.6$ mm, S=10.16 cm

Test No.	Stand-off Dist. (cm)	Impact Energy	'Normal' Area Penetrated?	'Normal' Area Spalled?	'In-line' Area Penetrated?	'In-line' Area Spalled?
Impact Energy < 10,000 Joules						
137A	7.62 2.54	4,474	No	No	Yes	No
230C	10.16	4,842	No	No	Yes	No
137B	7.62 2.54	5,805	No	No	Yes	No
168A	9.44 0.72	5,461	No	No	Yes	No
230D	10.16	5,682	Yes	No	Yes	Yes
137C	7.62 2.54	6,990	No	No	Yes	No
137D	7.62 2.54	8,809	No	No	Yes	Yes
168B	9.44 0.72	6,373	No	No	Yes	No
168C	9.44 0.72	7,997	No	No	Yes	No
168D	9.44 0.72	8,961	No	No	No	No
169A	9.76 0.40	8,532	No	No	No	No
169B	9.76 0.40	7,778	No	No	Yes	No
170A	8.81 1.35	7,636	No	No	Yes	No
170B	8.81 1.35	8,359	Yes	No	No	No
230E	10.16	7,969	Yes	No	Yes	Yes
Impact Energy > 10,000 Joules						
138A	7.62 2.54	13,317	No	No	Yes	No
138B	7.62 2.54	16,380	No	No	Yes	No
002A	10.16	15,310	No	No	Yes	Yes

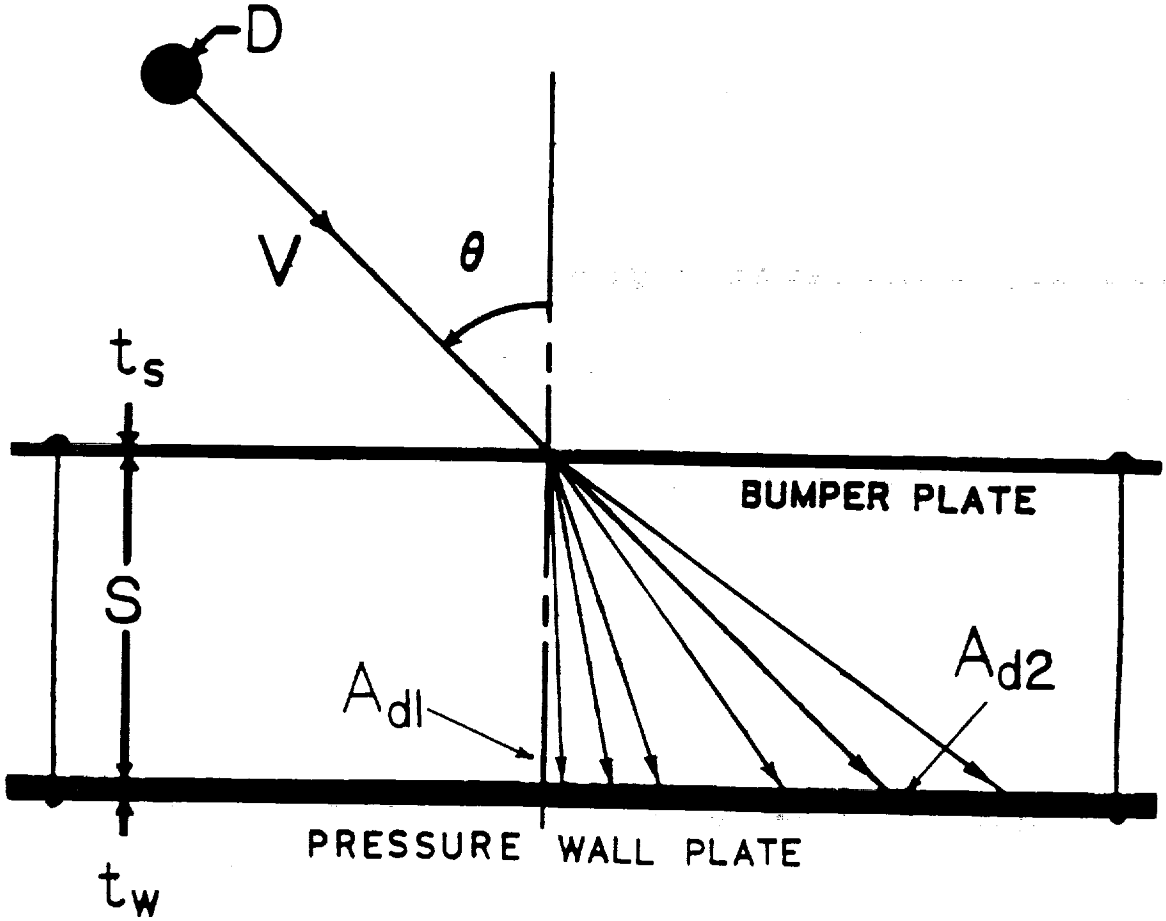

Figure 8.1 Oblique Impact of a Single-Bumper System

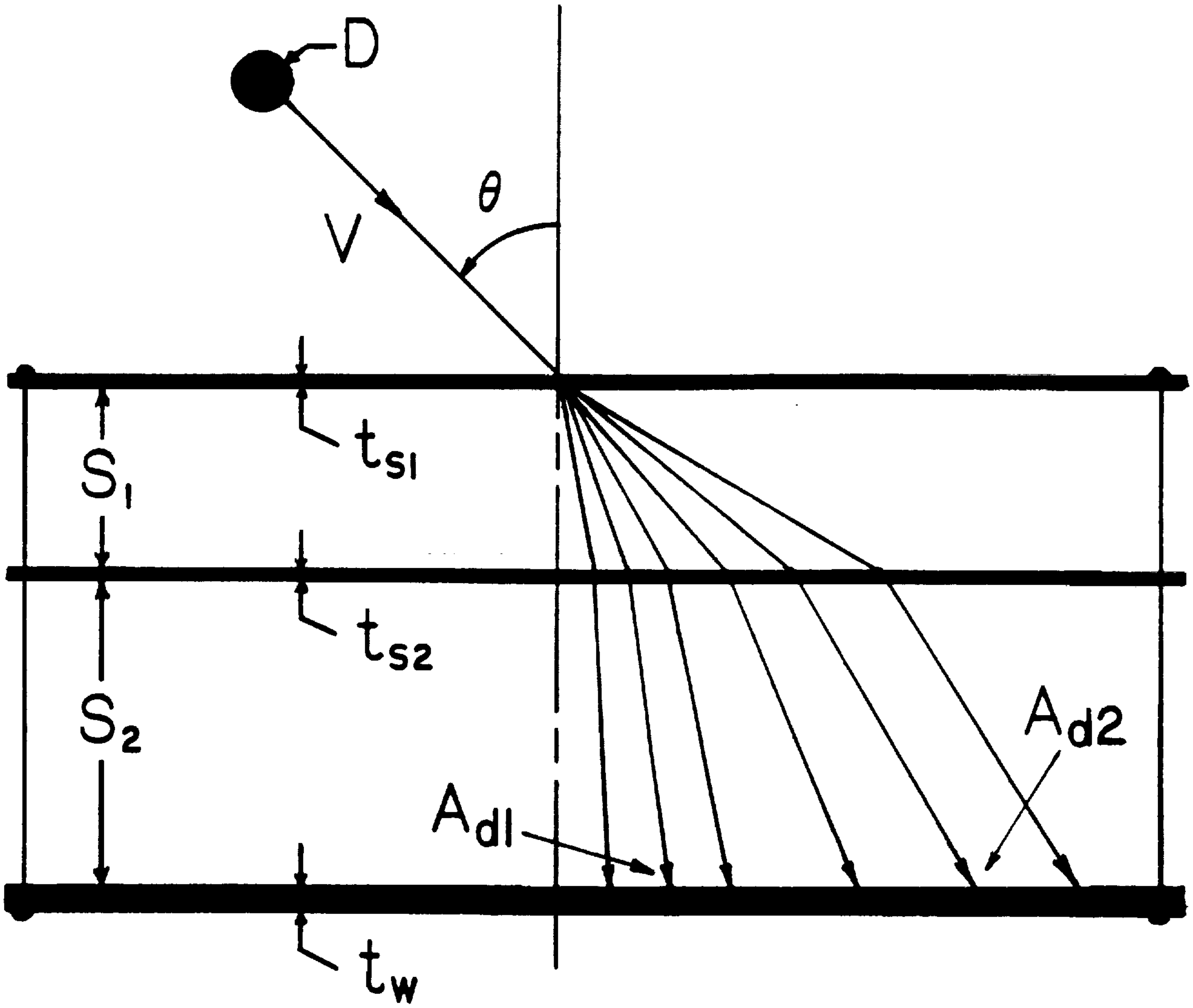

Figure 8.2 Oblique Impact of a Dual-Bumper System

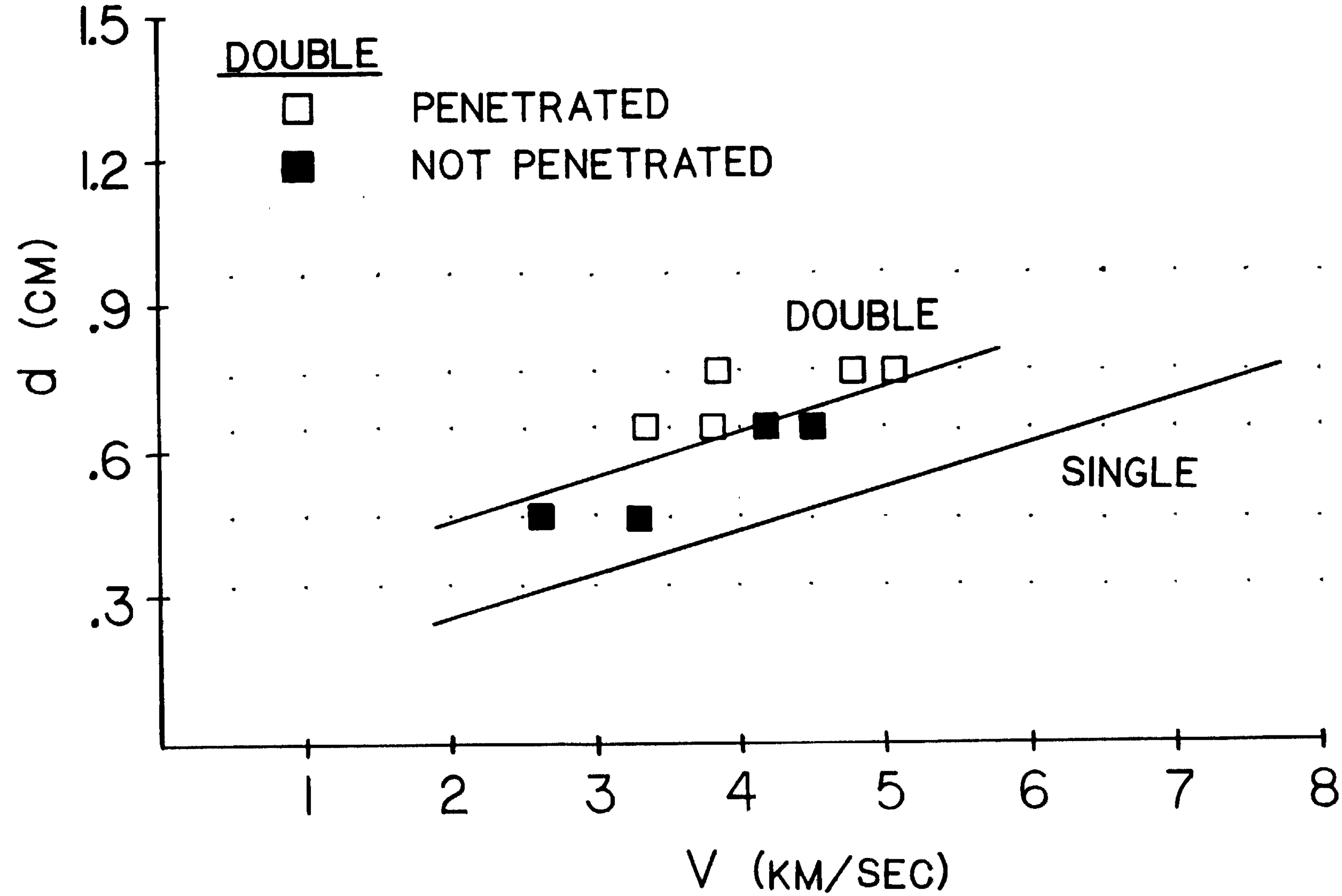

Figure 8.3 Penetration Functions for Normally Impacted Aluminum Dual-Bumper Systems (S_1=2.54 cm, S_2=7.62 cm) and Corresponding Single-Bumper Systems (t_s=1.6 mm, t_w=3.175 mm, S=10.16 cm)

SECTION NINE -- CONCLUSIONS AND RECOMMENDATIONS

9.1 Conclusions

An in-depth analysis of over 500 hypervelocity impact test specimens was performed in an effort to more fully understand the effects of the particulate space environment on the candidate materials, configurations, and support mechanisms of long-duration spacecraft. The analysis included the characterization of the effects of impact obliquity on pressure wall damage, the characterization of the potential of the rear side of the pressure wall to undergo spallation, the characterization of the effects of secondary and ricochet debris generated by oblique impacts, and the characterization of the effects of non-spherical and non-aluminum projectiles on pressure wall damage. Where possible, penetration curves and regression equations were developed to predict hypervelocity impact damage to dual-wall structural systems. A Hypervelocity Impact Damage Database was developed based on the test data obtained during the course of the various analyses that were performed.

In an investigation in which two composite materials and one ceramic material were used as bumper plate materials, it was found that thin Kevlar, graphite/epoxy, and alumina panels offer no significant advantage over equivalent aluminum 6061-T6 panels in reducing the penetration threat of hypervelocity projectiles. However, replacing monolithic aluminum bumpers with equal weight aluminum corrugated bumpers resulted in a significant increase in protection against pressure wall penetration by hypervelocity projectiles.

A study of multi-layer Lexgard windows under hypervelocity projectile impact revealed that such window systems sustained high levels of internal, penetration, and rear-side spall damage. On the other hand, triple-pane glass window systems were found to be rather resilient under hypervelocity projectile impact loadings and did not sustain any penetration or spall damage of the inner-most window pane.

An investigation of projectile shape and material effects on the impact response of aluminum dual-wall structures revealed that hypervelocity impacts by equal-weight spherical and cylindrical projectiles with L/D=1 at similar speeds resulted in similar levels of pressure wall penetration and crater damage. The density of the impacting projectile was found to be directly related to the nature and extent of damage inflicted to the pressure wall.

Finally, a study was performed to determine the advantages and disadvantages of using multi-bumper systems as a means of increasing the resistance of long-duration spacecraft to penetration by hypervelocity projectiles. It was found that multi-bumper systems sustained less damage than similar single-bumper systems. Front-side pressure wall damage areas, rear-side pressure wall spall areas, and single-hole diameters in penetrated pressure walls in the single-bumper systems were significantly larger than those in the corresponding multi-bumper systems.

9.2 Recommendations

An extensive program of hypervelocity impact testing and spacecraft materials evaluation has been underway at the NASA/Marshall Space Flight Center for over twenty years. However, additional testing is still required to more fully understand the various phenomena associated with the hypervelocity impact response of metallic and non-metallic materials that will be exposed to the meteoroid and space debris environment. It is imperative that more testing be performed using larger projectiles at higher impact velocities and at higher impact obliquities. Alternative bumper and pressure wall materials and configurations must be explored to provide the best protection possible to the crews of habitable spacecraft modules. Additionally, tests must be performed to study the effects of the composition and placement of thermal insulation, such as MLI, on the response of multi-wall structural systems. Perhaps alternative thermal insulation should be developed, preferably one without the damaging effects associated with MLI that were observed during the course of this investigation. Finally, tests with more tests with non-spherical and non-aluminum projectiles should be performed in order to more fully characterize different kinds of damage that can result from various projectile shapes and densities.

APPENDIX -- HYPERVELOCITY IMPACT DAMAGE DATABASE

An impact analysis of over 500 test specimens was performed to generate a Hypervelocity Impact Damage Database. The Database consists of 17 LOTUS files, which can be found on the floppy disk attached to this Report. A brief description of the Database, the various Database files, and a print-out of the Damage Database is presented in the following paragraphs.

The Hypervelocity Impact Damage Database developed during this investigation contains the following information (units are in parentheses):

1. Test number;
2. Bumper plate hole dimensions (in.);
3. Pressure wall equivalent hole diameter (in., if penetrated);
4. Pressure wall damage area (sq.in.);
5. Pressure wall spall area (sq.in., if spalled);
6. Debris cloud trajectory (θ_n, degrees);
7. Debris cloud spread (γ_n, degrees);
8. Diameters of the three largest holes in the pressure wall plate (in., if applicable);
9. Diameters and depths of the three largest craters on the pressure wall plate (in., if applicable);
10. Number of witness plates perforated (if applicable).

If the impact test was performed at a non-normal obliquity, then the information in items 3 through 9 is presented for both, the 'normal' and 'in-line' pressure wall plate damage areas.

In order to make the Damage Database more manageable, it has been split up into several small files, each of which contains the damage information from a similar group of tests. The following list presents the names of the LOTUS files and a description of their contents. Where feasible, the test numbers have also been included.

1. COMPOSITE.WK1 ... damage information for tests with composite and ceramic bumper plates (Test Nos. SS-103 through SS-104B, SS-122-1,SS-122-2, SS-140A through SS-140C, and, SS-177A and SS-177B);

2. LEXGARD.WK1 ..... damage information for window tests with multi-layer Lexgard panels (Test Nos. SS-123 through SS-129, and SS-171 through SS-174);

3. GLASS.WK1 .... damage information for window tests with multi-pane glass windows (Test Nos. SS-P-18-1 through SS-P-18-5);

4. CYLINDER.WK1 .... damage information for tests with cylindrical projectiles (Test Nos. SS-146A,B, and SS-225A through 225D);

5. NONALUM.WK1 ..... damage information for tests with non-aluminum projectiles;

6. NORDUAL.WK1 ..... damage information for normal impact tests on dual-bumper systems;

7. NORMUL.WK1 ...... damage information for normal impact tests on multi-bumper systems;

8. OBLDUAL.WK1 ..... damage information for oblique impact tests on dual-bumper systems;

9. NSERNMLI.WK1 .... damage information for normal and oblique impact tests with spherical aluminum projectiles on single-bumper aluminum systems without MLI (Test Nos. SS-001 through SS-231);

10. NSERYMLI.WK1 .... damage information for normal and oblique impact tests with spherical aluminum projectiles on single-bumper aluminum systems with MLI (Test Nos. SS-001 through SS-339);

11. EHSSMLIN.WK1 .... damage information for normal and oblique impact tests with spherical aluminum projectiles on single-bumper aluminum systems without MLI for the EH and EHSS test series (Test Nos. EH1A through EH1D and EHSS-1A through EHSS-8A);

12. EHMLIY.WK1 ...... damage information for normal and oblique impact tests with spherical aluminum projectiles on single-bumper aluminum systems with and without MLI for the EH, EHRP, MD, and PR-EH test series (Test Nos. EH2A through EH4B, EHRP-1 through EHRP-9, MD-Test-A,B,D, and PR-EH1 and PR-EH2);

13. PSERMLIN.WK1 .... damage information for normal impact tests

with spherical aluminum projectiles on single-bumper aluminum systems without MLI for the P test series (Test Nos. P-01 through P-35);

14. PSERMLIY.WK1 .... damage information for normal impact tests with spherical aluminum projectiles on single-bumper aluminum systems with MLI for the P test series (Test Nos. P-07 through P-35C);

15. TSERNMLI.WK1 .... damage information for normal impact tests with spherical aluminum projectiles on single-bumper aluminum systems without MLI for the T2 and PT test series (Test Nos. T2-2 through T2-20 and PT-4A through PT-8B);

16. TSERYMLI.WK1 .... damage information for normal impact tests with spherical aluminum projectiles on single-bumper aluminum systems with MLI for the T2 test series (Test Nos. T2-1 through T2-19B);

17. CORRBUMP.WK1 .... damage information for normal and oblique impact tests with spherical aluminum projectiles on aluminum systems with corrugated bumpers.

It is noted that this Hypervelocity Impact Damage Database must be used in conjunction with the MSFC/Boeing Phase B Test Parameter Database presented in Section 2.5.1. The MSFC/Boeing Database contains the material, geometric, and impact parameters for each test in the Hypervelocity Impact Damage Database. Specifically, the MSFC/Boeing Database contains the following parameter information:

1. Test number and date performed;
2. Projectile velocity, diameter, and shape;
3. Angle of obliquity;
4. Bumper plate(s) material(s) and thickness(es);
5. Pressure wall plate material and thickness;
6. Presence of MLI;
7. Stand-off distance;

Together, these two databases provide a wealth of information on the response of multi-sheet structures under normal and oblique hypervelocity projectile impact.

LOTUS FILE COMPOSITE.WK1

TEST NUMBER	BUMPER PLATE MATERIAL	BUMPER HOLE SIZE (IN.)	BACKWALL PENETRATED?	BACKWALL EQ. HOLE DIAMETER (IN.)	BACKWALL DAMAGE AREA (SQ. IN)	BACKWALL SPALLED?	BACKWALL SPALL AREA (SQ.IN.)	DEBRIS CLOUD TRAJECTORY (DEG)
103	KEVLAR	0.365	Yes	0.533	4.910	No	N.S.	1.720
103A	KEVLAR	0.381	Yes	0.319	4.710	No	N.S.	1.720
103B	KEVLAR	0.371	Yes	0.319	0.080	No	N.S.	1.720
103C	KEVLAR	0.365	No	N.P.	4.140	Yes	0.099	1.000
103-1	KEVLAR	0.358	No	N.P.	8.040	No	N.S.	0.000
104	KEVLAR	0.795	Yes	1.905	21.650	No	N.S.	1.430
104A	KEVLAR	0.775	Yes	1.971	19.630	No	N.S.	2.000
104B	KEVLAR	0.750	Yes	1.837	22.580	No	N.S.	3.580
122-1	KEVLAR	0.770	Yes	2.144	15.900	No	N.S.	3.530
122-2	KEVLAR	0.775	Yes	2.436	17.720	No	N.S.	0.000
140-A	ALUM.-OXIDE	0.602	Yes	0.300	8.950	Yes	0.096	0.000
140-B	ALUM.-OXIDE	1.303	No	N.P.	15.870	No	N.S.	0.000
140-C	ALUM.-OXIDE	1.406	Yes	0.276	12.560	Yes	0.129	0.000
177-A	GRAPHITE-EPOXY	0.614	Yes	0.436	12.560	No	N.S.	2.000
177-B	GRAPHITE-EPOXY	0.610	Yes	0.540	13.200	No	N.S.	1.000

DEBRIS CLOUD SPREAD (DEG)	HOLE NO. 1 DIAMETER (IN.)	HOLE NO. 2 DIAMETER (IN.)	HOLE NO. 3 DIAMETER (IN.)	CRATER NO. 1 DIA. (IN.)	CRATER NO. 1 DEPTH (IN.)	CRATER NO. 2 DIA. (IN.)	CRATER NO. 2 DEPTH (IN.)	CRATER NO. 3 DIA. (IN.)	CRATER NO. 3 DEPTH (IN.)
37.910									
34.050									
30.710									
26.690									
43.580				0.198	0.106	0.161	0.055	0.171	0.076
56.510									
64.010									
60.950									
40.760									
43.060									
45.600	0.195	0.164	0.124	0.175	0.169	0.142	0.114	0.156	0.095
57.320									
53.050	0.190	0.165	0.114						
49.440	0.200	0.166	0.164						
55.400									

LOTUS FILE LEXGARD.WK1

TEST NUMBER	WINDOW THICKNESS (IN.)	WINDOW PENETRATED?	WINDOW EQ. HOLE DIA. (IN.)	WINDOW INT. DAMAGE AREA (SQ. IN.)	WINDOW SPALLED?	WINDOW SPALL AREA (SQ. IN.)
123-1	0.750	No	N.P.	3.790	Yes	0.432
123-2	0.750	No	N.P.	3.140	Yes	0.234
123-3	0.750	No	N.P.	5.190	Yes	0.125
124-1	0.750	Yes	0.295	10.030	No	N.S.
124-2	0.750	Yes	0.248	9.810	No	N.S.
124-3	0.750	Yes	0.228	7.720	No	N.S.
124-4	0.750	No	N.P.	9.160	Yes	0.159
125-A	0.750	Yes	0.410	17.580	No	N.S.
125-B	0.750	Yes	0.266	9.350	No	N.S.
125-C	0.750	No	N.P.	8.030	No	N.S.
126-A	1.250	No	N.P.	20.930	No	N.S.
126-B	1.250	No	N.P.	16.960	No	N.S.
127-A	1.250	No	N.P.	28.220	Yes	0.380
127-A	1.250	No	N.P.	29.200	No	N.S.
129-A	1.250	Yes	0.261	35.780	No	N.S.
129-B	1.250	No	N.P.	24.740	No	N.S.
129-C	1.250	No	N.P.	28.880	Yes	1.180
171-A	1.250	No	N.P.	60.130	No	
172-A	1.250	No	N.P.	35.780	No	
173-A	0.750	Yes	1.943	23.760	No	
174-A	0.750	Yes	1.175	25.790	No	

LOTUS FILE GLASS.WK1

TEST NUMBER	MATERIAL	OUTER PANE PENETRATED	APPEARENCE	MATERIAL	MIDDLE PANE PENETRATED?	APPEARENCE	MATERIAL	INNER PANE PENETRATED?	APPEARENCE
18-1	SODA LIME	YES	SHATTERED	HERCULITE II	Yes	SHATTERED	HERCULITE II	No	No Damage
18-2	SODA LIME	YES	SHATTERED	LAM. HERCULITE	No	CRACKED	HERCULITE II	No	No Damage
18-3	SODA LIME	YES	SHATTERED	SODA LIME	No	MINOR PITTING	HERCULITE II	No	No Damage
18-4	SODA LIME	YES	SHATTERED	LAM. SODA LIME	No	MINOR PITTING	HERCULITE II	No	No Damage
18-5	LAM. SODA LIME	YES	HOLE (D=0.125")	LAM. SODA LIME	No	CRACKED	HERCULITE II	No	No Damage

LOTUS FILE CYLINDER.WK1

TEST NUMBER	BUMPER HOLE DMIN (IN.)	BUMPER HOLE DMAX (IN.)	BACKWALL PENETRATED?	BACKWALL EQ. HOLE DIAMETER (IN.)	BACKWALL DAMAGE AREA (SQ. IN.)	BACKWALL SPALLED?	BACKWALL SPALL AREA (SQ.IN.)	DEBRIS CLOUD TRAJECTORY (DEG)	DEBRIS CLOUD SPREAD (DEG)	HOLE NO. 1 DIAMETER (IN.)
225D1	0.689	0.689	YES	2.220	28.300	No	0.000	3.600	73.700	
P18RV	0.538	0.640	YES	1.169	12.755	No	0.000	0.200	37.300	1.167
P22	0.571	0.582	YES	1.539	6.950	Yes	3.309	2.900	40.600	1.539
P22A	0.539	0.602	YES	1.740	2.981	No	0.000	1.400	27.300	1.744
P22B	0.571	0.672	YES	0.921	11.930	Yes	1.620	0.300	51.900	0.821
T2-13	0.401	0.433	YES	0.150	2.410	No	0.000	9.000	24.600	0.148
T2-14	0.376	0.390	YES	0.142	3.139	No	0.000	5.300	26.900	0.140
223A	0.522	0.719	YES	0.210	0.000	No	0.000	N.D.	N.D.	
223B	0.485	0.801	YES	0.420	0.000	No	0.000	N.D.	N.D.	
223C	0.492	0.690	YES	0.500	0.000	No	0.000	N.D.	N.D.	
224A	0.556	1.161	NO	0.000	0.989	No	0.000	17.400	14.900	
224B	0.483	1.102	NO	0.000	1.480	No	0.000	16.700	18.000	
224C	0.484	1.010	NO	0.000	5.410	No	0.000	27.700	30.000	

HOLE NO. 2 DIAMETER (IN.)	HOLE NO. 3 DIAMETER (IN.)	CRATER NO. 1 DIA. (IN.)	CRATER NO. 1 DEPTH (IN.)	CRATER NO. 2 DIA. (IN.)	CRATER NO. 2 DEPTH (IN.)	CRATER NO. 3 DIA. (IN.)	CRATER NO. 3 DEPTH (IN.)	BACKWALL PENETRATED?	BACKWALL EQ. HOLE DIAMETER (IN.)	BACKWALL DAMAGE AREA (SQ. IN.)	BACKWALL SPALLED?	BACKWALL SPALL AREA (SQ.IN.)
0.096		0.159	0.099	0.140	0.096	0.150	0.070					
0.410												
		0.137	0.040	0.097	0.032	0.101	0.023					
		0.165	0.070	0.112	0.050	0.082	0.045					
									5.330	57.740		N.S.
									10.670	7.940		N.S.
									12.700	11.420		N.S.
		0.092	0.046	0.094	0.059	0.081	0.028		N.P.	22.900		N.S.
		0.074	0.034	0.119	0.020	0.070	0.024		N.P.	6.300		N.S.
		0.143	0.024	0.074	0.009	0.121	0.005		N.P.	13.350		N.S.

DEBRIS CLOUD TRAJECTORY (DEG)	DEBRIS CLOUD SPREAD (DEG)	HOLE NO. 1 DIA 1 (IN.)	HOLE NO. 1 DIA 2 (IN.)	HOLE NO. 2 DIA 1 (IN.)	HOLE NO. 2 DIA 2 (IN.)	HOLE NO. 3 DIA 1 (IN.)	HOLE NO. 3 DIA 2 (IN.)	CRATER NO. 1 DIA 1 (IN.)	CRATER NO. 1 DIA 2 (IN.)	CRATER NO. 1 DEPTH (IN.)	CRATER NO. 2 DIA 1 (IN.)	CRATER NO. 2 DIA 2 (IN.)	CRATER NO. 2 DEPTH (IN.)	CRATER NO. 3 DIA 1 (IN.)	CRATER NO. 3 DIA 2 (IN.)
49.100	10.100	0.210	0.206					0.131	0.128	0.070	0.234	0.114	0.074	0.121	0.061
54.600	6.400	0.261	0.193	0.330	0.230	0.249	0.170	0.189	0.090	0.142	0.153	0.097	0.155	0.168	0.085
53.200	7.500	0.437	0.393	0.271	0.202	0.181	0.139	0.195	0.130	0.154	0.198	0.120	0.106	0.240	0.146
36.900	18.100							0.104	0.098	0.060	0.071	0.069	0.011	0.061	0.055
58.900	4.600							0.292	0.257	0.041					
67.600	3.100							0.452	0.211	0.031	0.220	0.133	0.006	0.150	0.090

LOTUS FILE NONALUM.WK1

TEST NO.	PROJECTILE MATERIAL	BUMPER HOLE SIZE (IN.)	THETA (DEG)	GAMMA (DEG)	DAMAGE AREA (SQ.IN.)	PRESSURE WALL PENETRATED?	HOLE DIAMETER (MM)	PRESSURE WALL SPALLED?
146A	STEEL	0.345	0.600	28.900	3.329	yes	1.296	yes
146B	STEEL	0.350	3.400	29.900	3.500	yes	0.280	yes
225A	LEXAN	0.529	0.000	50.200	11.041	no	0.000	yes
225B	LEXAN	0.507	0.000	45.100	8.680	no	0.000	no
225C	LEXAN	0.501	1.900	44.200	8.299	no	0.000	no
225D	LEXAN	0.689	3.600	73.700	28.300	yes	2.220	no

SPALL AREA (CM2)	HOLE NO. 1 DIAMETER (IN.)	HOLE NO. 2 DIAMETER (IN.)	HOLE NO. 3 DIAMETER (IN.)	CRATER NO. 1 DIA. (IN.)	CRATER NO. 1 DEPTH (IN.)	CRATER NO. 2 DIA. (IN.)	CRATER NO. 2 DEPTH (IN.)	CRATER NO. 3 DIA. (IN.)	CRATER NO. 3 DEPTH (IN.)
1.180	0.572	0.062	0.052						
1.800	0.098	0.098	0.045						
0.040				0.090	0.067	0.085	0.064	0.081	0.057
0.000				0.135	0.089	0.112	0.086	0.125	0.083
0.000				0.078	0.073	0.076	0.064	0.090	0.063
0.000									

LOTUS FILE NORDUAL.WK1

TEST NUMBER	BUMPER PLATE MATERIAL	BUMPER #1 HOLE SIZE (IN.)	BUMPER #2 HOLE SIZE (IN.)	BACKWALL PENETRATED?	BACKWALL EQ. HOLE DIAMETER (IN.)	BACKWALL DAMAGE AREA (SQ. IN.)	BACKWALL SPALLED?	BACKWALL SPALL AREA (SQ.IN.)
115-1	ALUMINUM	0.381	1.017	NO		5.90	NO	
115-2	ALUMINUM	0.352	0.853	NO		5.43	NO	
115-3	ALUMINUM	0.357	0.769	YES	0.19	5.94	YES	
116-1	ALUMINUM	0.303	0.602	NO		0.52	NO	
116-2	ALUMINUM	0.260	0.350	NO		0.29	YES	0.01
117-1	ALUMINUM	0.383	1.498	NO		2.04	NO	
117-2	ALUMINUM	0.364	1.063	YES	0.04	2.21	NO	
118-1	ALUMINUM	0.380	1.450	YES	0.15	1.00	NO	
118-2	ALUMINUM	0.371	1.370	NO		5.94	NO	
118-3	ALUMINUM	0.398	1.508	YES	CRACK	1.08	NO	
119-1	ALUMINUM	0.409	0.624	YES	0.62	8.55	NO	
119-2	ALUMINUM	0.380	1.432	YES	0.97	2.53	NO	
119-3	ALUMINUM	0.375	1.538	YES	0.12	3.17	NO	
120-1	ALUMINUM/KEVLAR	0.469	2.000	NO		22.80	NO	
120-2	ALUMINUM/KEVLAR	0.438	1.500	NO		15.80	NO	
120-3	ALUMINUM/KEVLAR	0.406	0.750	NO		12.00	NO	
128A	ALUMINUM	0.378	1.034	NO		1.45	NO	
128B	ALUMINUM	0.366	0.875	YES	0.10	1.13	NO	
130A	ALUMINUM	0.404	0.873	YES	0.42	4.00	YES	
130B	ALUMINUM	0.428	1.160	YES	0.09	5.33	NO	
130C	ALUMINUM	0.422	1.363	YES	0.14	5.39	NO	
131A	ALUMINUM	0.490	2.011	NO		3.77	NO	
131B	ALUMINUM	0.445	1.317	YES	0.40	3.17	NO	
131C	ALUMINUM	0.453	1.228	YES	0.57	3.07	NO	
141A	ALUMINUM	0.564	1.706	YES		5.05	NO	
141B	ALUMINUM	0.531	1.860	NO		3.81	NO	
141C	ALUMINUM	0.555	1.988	NO		5.03	NO	
141D	ALUMINUM	0.625	2.605	NO		5.92	NO	
152A	ALUMINUM	0.421	1.368	NO		2.52	NO	
152B	ALUMINUM	0.368	1.053	YES	0.21	1.45	NO	
153A	ALUMINUM	0.750	1.500	YES	2.40	14.52	YES	
153B	ALUMINUM	0.800	1.100	YES	0.50	5.73	YES	1.70
158A	ALUMINUM	0.308	0.718	YES	0.21	2.11	NO	
158B	ALUMINUM	0.319	0.720	YES	0.31	4.01	NO	
159A	ALUMINUM	0.420	0.900	YES	0.27	6.61	NO	
159B	ALUMINUM	0.420	1.684	NO		7.31	NO	
160	ALUMINUM	0.530	1.895	YES	1.80	15.20	NO	
163A	ALUMINUM	0.650	2.490	NO		2.66	NO	
163B	ALUMINUM	0.601	1.898	NO		2.81	NO	
167A	ALUMINUM	0.768	3.368	NO		5.60	NO	
167B	ALUMINUM	0.762	2.256	YES	CRACK	9.57	NO	
175A	ALUMINUM	0.410	1.012	YES	0.24	7.07	YES	0.07
175B	ALUMINUM	0.414	0.958	YES	SMALL HOLES	4.71	YES	0.01
175C	ALUMINUM	0.433	1.040	NO		5.41	NO	
176A	ALUMINUM	0.400	1.821	NO		10.29	NO	
176B	ALUMINUM	0.383	1.295	NO		5.94	NO	
176C	ALUMINUM	0.370	1.452	NO		5.41	YES	VERY SMALL
176D	ALUMINUM	0.381	0.910	YES	0.27	2.41	NO	
179A	ALUMINUM	0.550	2.000	YES	3.31	37.50	NO	
179B	ALUMINUM	0.540	2.016	YES	0.77	18.67	NO	
181A	ALUMINUM	0.899	3.760	NO		9.62	NO	
181B	ALUMINUM	0.870	3.270	NO		4.91	NO	
186A	ALUMINUM	1.050	4.000	NO		9.51	NO	

ORIGINAL PAGE IS
OF POOR QUALITY

186B	ALUMINUM	1.053	3.580	NO	8.35	NO	
187A	ALUMINUM	1.080	4.220	NO	3.30	YES	0.01
187B	ALUMINUM	1.080	3.680	NO	5.68	NO	
188A	ALUMINUM	1.080	4.513	NO	7.21	NO	
188B	ALUMINUM	0.860	4.320	NO	10.87	NO	
188C	ALUMINUM	1.080	6.510	NO	17.72	NO	
188E	ALUMINUM	0.890	5.780	NO	13.99	NO	
191A	ALUMINUM	0.556	2.444	NO	8.29	NO	
192A	ALUMINUM	0.510	0.945	NO	1.23	NO	

HOLE NO. 1 DIAMETER (IN.)	HOLE NO. 2 DIAMETER (IN.)	HOLE NO. 3 DIAMETER (IN.)	CRATER NO. 1 DIA. (IN.)	CRATER NO. 1 DEPTH (IN.)	CRATER NO. 2 DIA. (IN.)	CRATER NO. 2 DEPTH (IN.)	CRATER NO. 3 DIA. (IN.)	CRATER NO. 3 DEPTH (IN.)	NO. WITNESS PLATES PENETRATED
			0.15	0.13	0.15	0.19	0.14	0.07	
0.191			0.17	0.12	0.16	0.10	0.14	0.14	1
			0.29	0.09					
			0.11	0.34					
0.040									0
0.147									0
			1.95	0.15					
0.010									0
0.624									1
0.973									2
1.210									1
			0.09	0.08	0.09	0.02	0.09	0.03	
0.095			0.13	0.08	0.12	0.04	0.11	0.09	0
0.422			0.21	0.05	0.17	0.03	0.16	0.07	1
0.070	0.059	0.032	0.14	0.08	0.14	0.08	0.13	0.07	0
0.124	0.065		0.13	0.05	0.12	0.09	0.11	0.09	0
0.403									0
0.569									1
			0.18	0.05	0.15	0.05	0.14	0.04	
			0.15	0.04	0.13	0.02	0.13	0.03	
			0.15	0.07	0.13	0.03	0.11	0.04	
0.211									0
2.400									4
0.500									1
0.205									1
0.310									2
0.200	0.150	0.100							2
1.800									4
0.010									1
0.240			0.19	0.16	0.16	0.13	0.16	0.17	0
0.010	0.010		0.14	0.13	0.14	0.06	0.14	0.13	0
			0.10	0.02	0.06	0.05	0.06	0.06	
			0.17	0.12	0.10	0.09	0.09	0.07	
			0.08	0.19					
0.268			0.24	0.10	0.16	0.15	0.11	0.08	0
3.131									0
0.765			0.13	0.10	0.11	0.07			2
			0.16	0.10	0.12	0.12	0.11	0.11	

0.27	0.04	0.22	0.02	0.20	0.04

LOTUS FILE NORMUL.WK1

TEST NUMBER	BUMPER PLATE MATERIAL	BUMPER #1 HOLE SIZE (IN.)	BUMPER #2 HOLE SIZE (IN.)	BUMPER #3 HOLE SIZE (IN.)	BUMPER #4 HOLE SIZE (IN.)	BUMPER #5 HOLE SIZE (IN.)	BUMPER #6 HOLE SIZE (IN.)	BACKWALL PENETRATED?	BACKWALL EQ. HOLE DIAMETER (IN.)	BACKWALL DAMAGE AREA (SQ. IN.)
180A	ALUMINUM	0.56	1.72	3.63	5.26			N		8.30
180B	ALUMINUM	0.54	1.31	2.83	4.66			N		6.49
182B	ALUMINUM	0.56	1.99	4.63	1.99			N		2.76
188D	ALUMINUM	0.65	2.20	7.53				N		6.65
189C	ALUMINUM	0.56	3.89	5.74	7.59	BUCKLED	8.68	Y	0.72	5.01
189D	ALUMINUM	0.65	2.16	6.38				Y	0.43	4.83
190A	ALUMINUM	0.47	1.14	1.98				Y	0.31	8.30
190B	ALUMINUM	0.51	2.00	4.38				N		1.77

BACKWALL SPALLED?	BACKWALL SPALL AREA (SQ.IN.)	HOLE NO. 1 DIAMETER (IN.)	HOLE NO. 2 DIAMETER (IN.)	HOLE NO. 3 DIAMETER (IN.)	CRATER NO. 1 DIA. (IN.)	CRATER NO. 1 DEPTH (IN.)	CRATER NO. 2 DIA. (IN.)	CRATER NO. 2 DEPTH (IN.)	CRATER NO. 3 DIA. (IN.)	CRATER NO. 3 DEPTH (IN.)	NO. WITNESS PLATES PENETRATED
N					0.20	0.04	0.13	0.03	0.11	0.02	
N											
N					0.08	0.03					
N											
N		0.72									2
N		0.43									1
N		0.28	0.13		0.22	0.11	0.16	0.07	0.14	0.08	2
N					0.11	0.04	0.01	0.07	0.09	0.07	

LOTUS FILE OBLDUAL.WK1

TEST NUMBER	BUMPER PLATE MATERIAL	BUMPER #1 HOLE DIA 1 (IN.)	BUMPER #1 HOLE DIA 2 (IN.)	BUMPER #2 HOL DIA (IN.)	BACKWALL PENETRATED?	BACKWALL EQ. HOLE DIAMETER (IN.)	NORMAL BACKWALL DAMAGE AREA (SQ. IN.)	BACKWALL SPALLED?	BACKWALL SPALL AREA (SQ.IN.)	HOLE NO. 1 DIA (IN.)	HOLE NO. 2 DIA (IN.)
137A	ALUMINUM	0.567	0.431	1.398	N		1.62	N			
137B	ALUMINUM	0.555	0.419	1.484	N		1.94	N			
137C	ALUMINUM	0.562	0.420	1.565	N		0.99	N			
137D	ALUMINUM	0.610	0.421	1.489	Y	0.250	1.06	N		0.200	0.150
138A	ALUMINUM	0.716	0.519	2.027	N		1.26	N			
138B	ALUMINUM	0.688	0.511	2.067	Y	0.081	1.38	N		0.024	
168A	ALUMINUM	0.571	0.420	1.040	N		0.90	N			
168B	ALUMINUM	0.061	0.414	1.040	N		1.06	N			
168C	ALUMINUM	0.580	0.440	1.119	N		3.33	N			
168D	ALUMINUM	0.613	0.442	1.067	N		4.05	N			
169A	ALUMINUM	0.659	0.464	0.863	N		3.55	N			
169B	ALUMINUM	0.638	0.459	0.899	N		6.49	N			
170A	ALUMINUM	0.675	0.401	1.170	N		1.32	N			
170B	ALUMINUM	0.619	0.425	1.110	Y	0.09	3.98	N		0.085	

ORIGINAL PAGE IS OF POOR QUALITY

HOLE NO. 3 DIA (IN.)	CRATER NO. 1 DIA (IN.)	CRATER NO. 1 DEPTH (IN.)	CRATER NO. 2 DIA 1 (IN.)	CRATER NO. 2 DEPTH (IN.)	CRATER NO. 3 DIA 1 (IN.)	CRATER NO. 3 DEPTH (IN.)	BACKWALL PENETRATED?	BACKWALL EQ. HOLE DIAMETER (IN.)	IN-LINE BACKWALL DAMAGE AREA (SQ. IN.)	BACKWALL SPALLED?	BACKWALL SPALL AREA (SQ.IN.)	HOLE NO. 1 DIA 1 (IN.)	HOLE NO. 1 DIA 2 (IN.)
	0.14	0.08	0.12	0.02	0.09	0.03	Y	0.22	3.42	N		0.19	
							Y	0.24	3.19	N		0.20	0.14
							Y	0.12	7.32	N		0.13	0.10
							N	0.25	2.52	Y	0.12		
	0.14	0.07	0.14	0.07	0.14	0.06	Y	0.53	0.92	N		0.60	0.31
							Y	0.48	0.60	N		0.57	0.24
							Y	0.35	2.27	N		0.27	0.27
							Y	0.41	3.89	N		0.53	0.26
							Y	0.19	2.49	N		0.21	0.16
	0.14	0.06	0.09	0.08	0.09	0.05	N		4.60	N			
	0.16	0.10	0.11	0.10	0.09	0.07	N		0.99	N			
	0.16	0.08	0.10	0.21	0.06	0.10	Y	0.20	3.30	N		0.27	0.31
	0.12	0.11	0.10	0.07	0.10	0.10	Y	0.25	4.91	N		0.24	0.16
							N		2.41	N			

ORIGINAL PAGE IS
OF POOR QUALITY

HOLE NO. 2		HOLE NO. 3		CRATER NO. 1			CRATER NO. 2			CRATER NO. 3			NO. WITNESS PLATES PENETRATED
DIA 1 (IN.)	DIA 2 (IN.)	DIA 1 (IN.)	DIA 2 (IN.)	DIA 1 (IN.)	DIA 2 (IN.)	DEPTH (IN.)	DIA 1 (IN.)	DIA 2 (IN.)	DEPTH (IN.)	DIA 1 (IN.)	DIA 2 (IN.)	DEPTH (IN.)	
0.11	0.08	0.07	0.05										1
0.15	0.12	0.12	0.09	0.18	0.13	0.08	0.15	0.12	0.08	0.15	0.12	0.05	1
0.05				0.22	0.17	0.14	0.21	0.13	0.16	0.17	0.17	0.12	0
													1
0.29	0.20	0.20	0.14	0.18	0.18	0.14	0.17	0.14	0.11	0.14	0.14	0.14	3
0.46	0.18	0.10	0.09	0.10	0.10	0.13							1
0.21	0.10	0.13	0.11										1
0.32	0.11												1
													0
				0.17	0.23	0.13	0.16	0.11	0.08	0.14	0.12	0.08	
0.14	0.14			0.27	0.20	0.15	0.25	0.17	0.10	0.24	0.16	0.12	2
0.19	0.14			0.14	0.19	0.19	0.14	0.12	0.06	0.09	0.10	0.06	1
				0.26	0.17	0.11	0.20	0.33	0.18	0.20	0.09	0.06	0

LOTUS FILE <u>NSERNMLI.WK1</u>

TEST NUMBER	BUMPER PLATE MATERIAL	BUMPER HOLE DIA 1 (IN.)	BUMPER HOLE DIA 2 (IN.)	BACKWALL PENETRATED?	BACKWALL EQ. HOLE DIAMETER (IN.)	BACKWALL DAMAGE AREA (SQ. IN.)	BACKWALL SPALLED?	BACKWALL SPALL AREA (SQ.IN.)
001A	ALUMINUM	0.825	0.658	YES	0.199	4.91	YES	0.04
002A	ALUMINUM	0.797	0.614	NO		7.07	NO	
101	ALUMINUM	0.399		YES	0.262	3.14	NO	
101A	ALUMINUM	0.370		YES	0.143	3.97	NO	
101B	ALUMINUM	0.560		NO		12.56	NO	
102	ALUMINUM	0.700		YES	0.030	33.18	YES	0.06
105	ALUMINUM	0.809	0.625	YES	0.417		NO	
105A	ALUMINUM	1.126	0.621	YES	0.312	5.03	NO	
105B	ALUMINUM	1.295	0.571	NO		1.21	NO	
106	ALUMINUM	0.931	0.766	NO		3.80	YES	0.10
106A	ALUMINUM	1.280	0.780	YES	0.368	9.84	NO	0.09
106B	ALUMINUM	1.772	0.645	NO		3.56	YES	0.13
106-1	ALUMINUM	1.140	0.740	YES	0.397	7.48	YES	0.10
106-2	ALUMINUM	1.530	0.625	NO		5.43	NO	
107	ALUMINUM	0.750		YES	0.608	21.64	YES	1.88
107A	ALUMINUM	0.720		YES	0.355	24.02	YES	2.40
107B	ALUMINUM	0.750		NO		21.65	YES	2.12
108	ALUMINUM	0.692		YES	0.224	44.30	YES	0.11
109	ALUMINUM	0.522		NO		19.64	NO	
109A	ALUMINUM	0.429		NO		13.85	NO	
109B	ALUMINUM	0.400		NO		9.62	NO	
109C	ALUMINUM	0.315		NO		1.12	YES	0.05
109D	ALUMINUM	0.319		NO		0.00	NO	
110	ALUMINUM	0.727		NO		13.36	YES	1.23
113	ALUMINUM	0.730	0.429	NO		2.99	NO	
113A	ALUMINUM	0.578	0.442	NO		4.37	NO	
114	ALUMINUM	0.869	0.598	NO		9.62	NO	
114B	ALUMINUM	0.628	0.514	NO		3.84	NO	
121-1	ALUMINUM	0.669		YES	0.041	27.39	YES	0.10
121-2	ALUMINUM	0.630		YES	0.650	18.67	YES	0.90
135A	ALUMINUM	0.598	0.506	NO		0.00	NO	
135B	ALUMINUM	0.647	0.564	NO		0.00	NO	
135C	ALUMINUM	0.556	0.516	NO		0.00	NO	
135D	ALUMINUM	0.561	0.521	NO		0.00	NO	
135E	ALUMINUM	0.620	0.567	NO		0.00	NO	
136A	ALUMINUM	0.720	0.550	NO		8.55	YES	0.06
136B	ALUMINUM	0.790	0.550	NO		7.35	YES	0.09
136C	ALUMINUM	0.670	0.530	NO		8.61	YES	0.06
139A	ALUMINUM	0.578		NO		10.32	YES	0.31
139B	ALUMINUM	0.541		YES	0.259	10.32	YES	0.25
142A	ALUMINUM	0.502		NO		53.69	NO	
143A	ALUMINUM	0.622		NO		58.92	NO	
143B	ALUMINUM	0.550		NO		58.92	NO	
144A	ALUMINUM	0.602		NO		9.62	YES	0.14
144B	ALUMINUM	0.548		YES	0.517	10.32	YES	0.32
144C	ALUMINUM	0.536		YES	0.184	8.30	YES	0.31
150A	ALUMINUM	0.712	0.563	NO		6.61	NO	
151A	ALUMINUM	0.723	0.631	NO		0.45	NO	
154A	ALUMINUM	0.546	0.429	NO		0.20	NO	
154B	ALUMINUM	0.482	0.372	NO		1.13	NO	
155A	ALUMINUM	0.571	0.519	YES	0.150		NO	
156A	ALUMINUM	0.751	0.429	NO		12.57	NO	
156B	ALUMINUM	0.630	0.442	NO		15.34	NO	

156C	ALUMINUM	0.630	0.428	NO		1.23	NO	
157A	ALUMINUM	0.680	0.537	NO		3.80	NO	
162A	ALUMINUM	0.550	0.466	NO		11.95	NO	
162B	ALUMINUM	0.455	0.389	YES	0.190	8.04	NO	
184A	ALUMINUM	1.260		NO		96.45	YES	0.02
184B	ALUMINUM	1.230		NO		94.59	YES	0.12
185A	ALUMINUM	1.260		YES	4.350	36.64	YES	5.07
189A	ALUMINUM	1.160		YES	0.940	61.10	YES	0.20
189B		1.080		NO		88.08	YES	0.03
202A	ALUMINUM	0.418		NO		2.07	NO	
202B	ALUMINUM	0.409	0.307	NO		1.77	NO	
202C	ALUMINUM	0.425	0.373	NO		4.43	NO	
202D	ALUMINUM	0.447	0.330	NO		1.23	NO	
202E	ALUMINUM	0.510	0.405	NO		0.00	NO	
202F	ALUMINUM	0.565	0.406	NO		0.00	NO	
204A	ALUMINUM	0.780	0.438	NO		2.41	NO	
204B	ALUMINUM	0.875	0.480	NO		1.77	NO	
204C	ALUMINUM	0.830	0.430	NO		2.76	NO	
204D	ALUMINUM	0.722	0.381	NO		5.94	NO	
206A	ALUMINUM	0.463	0.382	NO		3.98	NO	
206B	ALUMINUM	0.514	0.411	NO		3.55	NO	
206C	ALUMINUM	0.511	0.437	NO		5.41	NO	
206D	ALUMINUM	0.447	0.350	NO		4.43	NO	
206E	ALUMINUM	0.410	0.330	NO		5.43	NO	
206F	ALUMINUM	0.530	0.455	NO		3.46	NO	
208A	ALUMINUM	0.845	0.453	NO		24.85	NO	
208B	ALUMINUM	0.704	0.461	YES	0.117	7.07	NO	
208C	ALUMINUM	0.790	0.370	NO		6.74	NO	
208D	ALUMINUM	0.791	0.477	NO		5.73	NO	
208E	ALUMINUM	0.826	0.488	NO		0.79	NO	
213A	ALUMINUM	0.621		YES	0.212	10.32	YES	0.86
213B	ALUMINUM	0.617		NO		9.62	YES	1.13
213C	ALUMINUM	0.479		YES	0.270	11.04	YES	0.50
213D	ALUMINUM	0.526		NO		7.67	YES	0.14
214A	ALUMINUM	0.387		NO		21.65	YES	0.03
214B	ALUMINUM	0.404		YES	0.740	12.57	YES	0.58
214C	ALUMINUM	0.389		YES	0.102	9.62	YES	0.30
214D	ALUMINUM	0.370		NO		11.04	YES	0.35
215D	ALUMINUM	0.514		YES	0.259	4.91	NO	
216A	ALUMINUM	0.890	0.715	NO		4.43	NO	
216B	ALUMINUM	0.892	0.733	NO		3.98	NO	
216C	ALUMINUM	0.832	0.675	NO		3.55	NO	
217A	ALUMINUM	0.735	0.533	NO		8.95	NO	
217B	ALUMINUM	0.718	0.540	NO		16.80	NO	
217C	ALUMINUM	0.629	0.467	NO		7.67	NO	
217D	ALUMINUM	0.578	0.452	NO		3.98	NO	
217E	ALUMINUM	0.612	0.471	NO		7.67	NO	
222A	ALUMINUM	0.350	0.279	NO		1.48	NO	
222B	ALUMINUM	0.338	0.265	NO		1.23	NO	
222C	ALUMINUM	0.284	0.214	NO		2.07	NO	
228A	ALUMINUM	0.480		YES	1.000	11.46	YES	1.62
228B	ALUMINUM	0.496		YES	0.740	5.73	YES	2.30
228C	ALUMINUM	0.434		NO		4.91	YES	1.70
228D	ALUMINUM	0.441		YES	0.104	4.52	YES	0.51
230C	ALUMINUM	0.634	0.494	NO		4.91	NO	
230D	ALUMINUM	0.642	0.526	YES	0.102	5.31	NO	

230E	ALUMINUM	0.697	0.558	YES	0.179	4.52	NO	
231A	ALUMINUM	0.470	0.300	NO		4.45	NO	
231B	ALUMINUM	0.420	0.270	NO		8.00	NO	
231C	ALUMINUM	1.220	0.650	YES	0.160	10.75	YES	0.06
231D	ALUMINUM	1.020	0.650	YES	0.340	10.58	YES	0.06

DEBRIS CLOUD TRAJECTORY (DEG)	DEBRIS CLOUD SPREAD (DEG)	HOLE NO. 1 DIAMETER (IN.)	HOLE NO. 2 DIAMETER (IN.)	HOLE NO. 3 DIAMETER (IN.)	CRATER NO. 1 DIA. (IN.)	CRATER NO. 1 DEPTH (IN.)	CRATER NO. 2 DIA. (IN.)	CRATER NO. 2 DEPTH (IN.)	CRATER DIA. (IN.)
13.63	13.63	0.152	0.129		0.168	0.162	0.188	0.150	0.115
15.38	40.38				0.160	0.075	0.151	0.072	0.168
1.00	28.07	0.262							
0.86	31.26	0.143							
0.00	52.80				0.171	0.115	0.169	0.081	0.151
4.29	78.18	0.030							
		0.417							
10.07	21.38	0.203	0.182	0.152					
8.95	17.21								
4.00	30.57								
9.23	47.44	0.185	0.139	0.133	0.210	0.139	0.180	0.126	0.178
-1.00	-1.00								
11.31	41.37	0.169	0.159	0.138	0.187	0.146	0.204	0.145	0.216
-1.00	-1.00								
2.86	66.51	0.608							
3.72	69.10	0.355							
0.00	66.51								
2.81	34.31	0.200	0.100						
0.86	63.97								
3.01	55.30								
1.58	44.17				0.092	0.245	0.047	0.172	0.088
0.72	23.86								
2.15	54.55								
17.74	25.03								
6.84	32.46								
23.15	41.12								
4.86	30.68								
3.53	40.76	0.041			0.142	0.116	0.177	0.095	0.182
0.00	43.06	0.573	0.138	0.126	0.181	0.137	0.141	0.134	0.174
23.63	58.13								
22.17	52.84								
24.23	53.04								
26.57	53.30								
17.35	56.67								
11.31	43.94				0.208	0.133	0.149	0.095	0.116
10.07	42.39				0.155	0.125	0.200	0.106	0.184
11.03	44.42				0.175	0.094	0.169	0.088	0.145
14.04	45.82				0.223	0.139	0.191	0.112	0.140
0.00	48.80	0.238	0.103		0.213	0.142	0.157	0.135	0.294
2.36	54.55				0.134	0.063	0.141	0.056	0.125
2.29	56.79				0.171	0.113	0.163	0.085	0.145
1.50	56.82				0.195	0.057	0.192	0.053	0.122
1.58	47.26				0.228	0.107	0.090	0.084	0.210
7.13	46.04	0.403	0.323		0.148	0.121	0.107	0.105	0.174
1.86	44.19	0.137	0.123		0.351	0.131	0.110	0.073	0.089
8.53	39.60								
2.86	11.39								
7.13	7.02								
7.13	16.90								
		0.150							
26.57	47.06								
27.70	51.76								

8.53	17.86								
8.53	42.36								
20.56	68.74								
26.57	57.06	0.190							
1.62	49.52								
2.72	49.28								
0.57	59.12	4.350							
3.96	39.86	0.940							
1.29	47.58								
1.43	22.41				0.063	0.037	0.078	0.032	0.107
0.00	21.21				0.071	0.048	0.085	0.036	0.095
4.29	31.80				0.078	0.058	0.067	0.049	0.083
0.00	17.05				0.131	0.075	0.092	0.052	0.081
-1.00	-1.00								
33.02	27.35								
7.13	24.09				0.101	0.064	0.103	0.059	0.077
2.86	21.24				0.136	0.140	0.085	0.053	0.133
12.41	25.35				0.083	0.061	0.088	0.043	0.173
23.03	31.53				0.143	0.063	0.106	0.053	0.095
2.86	30.33				0.081	0.063	0.099	0.057	0.115
4.29	30.48				0.152	0.069	0.090	0.048	0.140
19.29	3.83				0.140	0.077	0.116	0.062	0.137
14.04	30.24				0.069	0.064	0.116	0.039	0.105
12.68	35.92				0.148	0.038	0.131	0.032	0.151
8.53	39.22				0.082	0.063	0.096	0.053	0.085
26.57	58.14				0.151	0.087	0.177	0.078	0.119
21.80	38.73	0.117			0.118	0.106	0.143	0.084	0.100
12.68	38.73				0.162	0.084	0.113	0.014	0.102
14.04	35.25								
9.93	39.73				0.175	0.147	0.129	0.113	0.097
0.00	48.44	0.212			0.178	0.116	0.113	0.103	0.157
2.86	48.26								
1.86	50.19	0.270			0.215	0.153	0.305	0.131	0.237
1.86	42.53				0.157	0.136	0.174	0.132	0.204
0.00	36.26				0.183	0.142	0.107	0.113	0.165
13.83	26.03	0.489	0.430	0.322	0.168	0.141	0.271	0.128	0.238
0.00	24.66	0.102			0.175	0.150	0.112	0.142	0.203
13.22	26.38				0.258	0.220	0.186	0.175	0.180
5.43	34.44	0.259			0.117	0.100	0.120	0.089	0.078
4.29	33.11				0.098	0.116	0.099	0.100	0.134
8.53	31.73				0.170	0.130	0.128	0.110	0.119
16.30	28.57				0.085	0.084	0.140	0.083	0.130
15.38	42.78				0.160	0.055	0.135	0.046	0.093
12.68	56.56								
20.56	38.30				0.070	0.066	0.111	0.062	0.074
20.56	27.81								
21.80	38.30				0.088	0.055	0.111	0.051	0.090
8.53	19.82				0.095	0.043	0.053	0.042	0.050
12.68	17.86				0.073	0.048	0.069	0.045	[illegible]
7.13	21.99				0.054	0.017	0.067	0.012	[illegible]
1.72	41.11	0.979	0.191		0.111	0.137	0.138	0.135	0.167
2.86	37.18	0.740			0.093	0.117	0.118	0.106	0.127
0.29	34.70				0.121	0.086	0.138	0.080	0.107
2.86	33.40	0.086	0.077		0.130	0.127	0.122	0.101	0.136
9.93	34.34				0.161	0.096	0.155	0.076	0.180
11.31	34.82	0.102			0.195	0.126	0.181	0.084	0.198

11.31	32.95	0.179			0.134	0.124	0.137	0.051	0.122
16.70	32.53								
13.36	1.36								
8.53	45.66	0.106	0.095	0.090	0.222	0.142	0.160	0.118	0.200
10.62	48.39	0.252	0.137	0.118	0.190	0.146	0.220	0.130	0.205

NO. 3 DEPTH (IN.)	BACKWALL PENETRATED?	BACKWALL EQ. HOLE DIAMETER (IN.)	BACKWALL DAMAGE AREA (SQ. IN.)	BACKWALL SPALLED?	BACKWALL SPALL AREA (SQ.IN.)	DEBRIS CLOUD TRAJECTORY (DEG)	DEBRIS CLOUD SPREAD (DEG)
0.137	YES	0.831	0.28	NO		37.78	16.10
0.063	YES	1.010	7.07	YES	0.20	39.95	24.36
0.071							
	YES	0.417		NO			
	YES	0.548	4.64	NO		46.80	20.71
	NO		1.04	NO		28.04	12.81
	YES	0.968	2.81	YES	0.17	37.95	15.69
0.117	YES	0.612	5.90	YES	0.09	48.37	19.32
	NO		0.00	NO		0.72	29.80
0.113	YES	0.426	11.58	YES	0.10	47.07	26.95
	NO		0.00	NO		1.58	36.26
0.170							
	NO		5.19	NO		42.38	20.40
	YES	0.397	3.30	NO		35.94	19.37
	NO		2.84	NO		51.12	10.84
	YES	0.376	2.52	NO		34.22	17.40
0.090							
0.102							
	YES	0.458	16.84	NO		23.63	58.13
	YES	0.071	15.07	YES	0.07	22.17	52.84
	YES	0.750	14.52	YES	0.75	24.23	53.04
	YES	0.957	15.21	NO		26.57	53.30
	YES	0.475	15.71	YES	0.30	17.35	56.67
0.076	YES	0.368	7.07	NO		43.53	20.92
0.053	NO		7.35	NO		41.83	23.54
0.068	YES	0.385	7.07	NO		38.22	24.25
0.107							
0.127							
0.500							
0.082							
0.029							
0.080							
0.090							
0.065							
	YES	0.489	6.61	NO		39.52	28.39
	YES	0.390	1.11	NO		34.61	11.74
	NO		4.15	NO		41.19	20.03
	YES	0.346	2.54	NO		45.71	13.32
	YES	0.269		NO			
	NO		0.00	NO		-1.00	-1.00
	NO		0.00	NO		-1.00	-1.00

	NO		0.00	NO		-1.00	-1.00
	NO		3.80	NO		35.94	21.25
	NO		11.95	NO		20.56	68.74
	NO		8.04	NO		26.57	57.06
0.016	YES	0.054	1.78	YES	0.04	35.94	13.31
0.022	YES	0.325	2.76	NO		39.52	15.81
0.028	YES	0.364	4.91	NO		39.95	20.05
0.026	YES	0.247	3.14	YES	0.08	41.19	16.88
	YES	0.124	9.62	NO		29.36	34.33
	YES	0.215	5.41	NO		-1.00	-1.00
0.058	YES	0.172	0.59	NO		44.78	22.14
0.049	NO		7.67	NO		47.86	24.48
0.038	NO		15.03	NO		55.77	23.88
0.038	NO		1.23	NO		54.70	6.04
0.040	YES	0.115	1.38	YES	0.12	37.78	11.53
0.046	NO		0.31	NO		37.78	5.50
0.059	YES	0.124	2.07	NO		44.27	12.73
0.034	NO		1.48	NO		38.66	11.98
0.026	NO		3.14	NO		38.66	17.59
0.050	NO		6.61	NO		30.96	26.57
0.040	NO		0.00	NO		-1.00	-1.00
0.060	NO		0.31	NO		50.77	3.50
0.010	NO		4.45	NO		52.43	14.34
	NO		5.68	NO		44.27	20.64
0.071	YES	0.164	11.79	NO		47.07	11.65
0.085							
0.129							
0.116							
0.112							
0.125							
0.128							
0.135							
0.085							
0.098	YES	1.155	6.49	NO		36.59	24.90
0.107	YES	0.916	7.67	NO		37.78	26.35
0.064	YES	0.299	3.55	YES	0.14	39.52	15.51
0.029	YES	0.765	13.36	YES	0.06	58.86	13.13
	YES	0.831	16.80	YES	0.08	59.35	16.56
0.044	YES	0.299	5.41	NO		56.31	10.70
	YES	0.355	4.43	YES	0.24	57.46	8.59
0.051	YES	0.564	19.64	YES	0.26	58.39	17.34
0.025	NO		1.48	NO		38.83	10.81
0.028	NO		0.60	NO		37.05	7.82
0.005	NO		0.20	NO		37.95	4.32
0.121							
0.081							
0.062							
0.098							
0.028	YES	0.468	5.15	NO		34.99	21.97
0.072	YES	0.503	5.73	YES	0.02	37.78	21.96

0.049	YES	0.470	8.35	YES	8.04	38.66	27.19
	NO		1.77	NO		34.70	14.55
	NO		0.00	NO		13.36	1.36
0.074	NO		7.07	NO		55.68	13.82
0.155	NO		7.65	NO		49.90	19.96

HOLE NO. 1 DIA 1 (IN.)	HOLE NO. 1 DIA 2 (IN.)	HOLE NO. 2 DIA 1 (IN.)	HOLE NO. 2 DIA 2 (IN.)	HOLE NO. 3 DIA 1 (IN.)	HOLE NO. 3 DIA 2 (IN.)	CRATER NO. 1 DIA 1 (IN.)	CRATER NO. 1 DIA 2 (IN.)	CRATER NO. 1 DEPTH (IN.)	CRATER NO. 2 DIA 1 (IN.)	CRATER NO. 2 DIA 2 (IN.)	CRATER NO. 2 DEPTH (IN.)
0.545	0.428	0.379	0.325	0.370	0.283	0.140	0.138	0.157	0.285	0.157	0.121
0.169	0.119	0.151	0.093	0.098	0.062	0.217	0.217	0.130	0.310	0.226	0.118
0.564	0.307										
0.456	0.304										
1.250	0.750										
0.640	0.437	0.354	0.233	0.200	0.162	0.196	0.185	0.096	0.192	0.160	0.083
0.313	0.213	0.290	0.271	0.190	0.190	0.276	0.195	0.084	0.227	0.151	0.069
0.513	0.308										
0.526	0.421	0.211	0.158								
0.630	0.276	0.177	0.157	0.118	0.079	0.195	0.166	0.131	0.153	0.120	0.079
0.071	0.071					0.145	0.145	0.110	0.157	0.157	0.102
0.750	0.750					0.235	0.196	0.106	0.116	0.116	0.091
0.957	0.957					0.145	0.145	0.089	0.144	0.144	0.088
0.475	0.475					0.098	0.098	0.079	0.109	0.109	0.064
0.316	0.232	0.295	0.211			0.235	0.125	0.105	0.160	0.160	0.104
						0.295	0.193	0.110	0.194	0.179	0.085
0.228	0.200	0.175	0.175	0.171	0.125	0.985	0.222	0.142	0.235	0.208	0.083
0.456	0.354	0.253	0.253	0.122	0.122						
0.320	0.320	0.220	0.220								
0.400	0.300										
0.200	0.200	0.100	0.100								

0.250	0.216					0.136	0.134	0.098	0.246	0.184	0.029
0.332	0.318					0.176	0.099	0.083	0.210	0.134	0.078
0.435	0.305					0.153	0.068	0.092	0.207	0.079	0.038
0.250	0.169	0.161	0.117			0.132	0.119	0.129	0.171	0.138	0.114
0.130	0.118					0.118	0.115	0.122	0.154	0.135	0.095
0.258	0.180					0.157	0.135	0.101	0.118	0.118	0.078
0.180	0.165					0.358	0.123	0.088	0.128	0.116	0.074
						0.102	0.095	0.058	0.137	0.115	0.057
						0.234	0.133	0.075	0.260	0.247	0.074
						0.268	0.228	0.065	0.251	0.065	0.058
0.125	0.105					0.135	0.101	0.086	0.139	0.089	0.081
						0.189	0.129	0.135	0.134	0.086	0.076
0.177	0.087					0.122	0.112	0.038	0.158	0.058	0.032
						0.238	0.145	0.072	0.383	0.160	0.065
						0.303	0.182	0.084	0.195	0.155	0.070
						0.098	0.090	0.069	0.152	0.074	0.062
						0.337	0.125	0.056	0.148	0.124	0.042
						0.212	0.141	0.126	0.182	0.119	0.030
0.172	0.157					0.227	0.194	0.121	0.145	0.180	0.078
1.388	0.913	0.281	0.235			0.257	0.250	0.187	0.309	0.117	0.126
0.916	0.916					0.157	0.148	0.141	0.205	0.149	0.128
0.313	0.286					0.220	0.122	0.226	0.386	0.259	0.187
1.113	0.471	0.190	0.177	0.174	0.160	0.303	0.189	0.205	0.441	0.279	0.150
1.091	0.483	0.347	0.269	0.298	0.240	0.235	0.218	0.193	0.213	0.185	0.152
0.328	0.273					0.261	0.205	0.141	0.170	0.136	0.130
0.490	0.257					0.372	0.294	0.245	0.391	0.263	0.151
0.485	0.257	0.319	0.274	0.293	0.257	0.235	0.215	0.205	0.467	0.285	0.199
						0.100	0.093	0.054	0.117	0.062	0.031
						0.071	0.051	0.035	0.065	0.048	0.034
						0.153	0.112	0.061	0.126	0.108	0.051
0.468	0.468					0.170	0.151	0.121	0.077	0.077	0.180
0.503	0.503					0.335	0.283	0.122	0.214	0.205	0.118

0.470	0.470	0.282	0.203	0.135	0.204	0.154	0.078
		0.259	0.145	0.135	0.195	0.136	0.067
		0.173	0.135	0.067	0.153	0.131	0.060

CRATER NO. 3 DIA 1 (IN.)	DIA 2 (IN.)	DEPTH (IN.)	NO. WITNESS PLATES PENETRATED
0.331	0.131	0.104	3
0.230	0.166	0.065	4
			2
			0
			0
			0
			1
			6
0.206	0.170	0.055	3
0.184	0.136	0.040	1
			3
			5
			0
			3
			3
			0
			2
0.087	0.087	0.079	2
0.100	0.100	0.098	1
0.127	0.127	0.029	2
0.109	0.109	0.072	2
0.108	0.108	0.056	0
0.230	0.187	0.085	1
0.195	0.163	0.072	
0.210	0.163	0.058	0
			1
			1
			1
			2
			0
			0
			0

			0
			2
			1
0.125	0.073	0.023	0
0.117	0.068	0.040	2
0.128	0.081	0.037	2
0.161	0.137	0.100	1
0.115	0.091	0.064	0
0.161	0.120	0.071	0
0.217	0.091	0.066	0
0.252	0.096	0.055	
0.153	0.146	0.029	
0.091	0.051	0.013	
0.112	0.075	0.058	1
0.162	0.092	0.059	
0.152	0.066	0.022	0
0.176	0.106	0.024	
0.194	0.160	0.028	
0.093	0.085	0.052	
0.199	0.070	0.013	0
0.172	0.134	0.027	
0.208	0.095	0.064	0
			3
			1
			1
			0
			1
0.286	0.149	0.107	4
0.262	0.169	0.109	4
0.254	0.204	0.164	1
0.188	0.163	0.112	4
0.428	0.240	0.138	4
0.230	0.152	0.095	1
0.251	0.208	0.142	1
0.216	0.166	0.149	2
0.095	0.058	0.030	
0.062	0.055	0.031	
0.086	0.054	0.006	
			4
			4
			1
0.175	0.116	0.057	3
0.244	0.195	0.184	2

0.189	0.151	0.057	1
0.176	0.153	0.056	0
0.193	0.159	0.053	0

LOTUS FILE NSERYMLI.WK1

TEST NUMBER	BUMPER PLATE MATERIAL	BUMPER HOLE DIA 1 (IN.)	BUMPER HOLE DIA 2 (IN.)	BACKWALL PENETRATED?	BACKWALL EQ. HOLE DIAMETER (IN.)	BACKWALL DAMAGE AREA (SQ. IN.)	BACKWALL SPALLED?	BACKWALL SPALL AREA (SQ.IN.)
001B	ALUMINUM	0.820	0.664	NO		0.20	NO	
002B	ALUMINUM	0.792	0.605	NO		0.60	NO	
003A	ALUMINUM	0.747	0.520	NO		0.00	NO	
004A	ALUMINUM	0.926	0.651	NO		6.07	NO	
102A	ALUMINUM	0.668		NO		10.99	NO	
102B	ALUMINUM	0.653		NO		7.74	NO	
102C	ALUMINUM	0.609		NO		7.40	NO	
102D	ALUMINUM	0.566		YES	0.200	7.16	NO	
201A	ALUMINUM	0.532	0.400	NO		0.44	NO	
201B	ALUMINUM	0.518	0.425	NO		0.44	NO	
201C	ALUMINUM	0.738	0.497	YES	0.151	0.20	NO	
201D	ALUMINUM	0.644	0.422	NO		0.00	NO	
203A	ALUMINUM	0.938	0.505	NO		2.41	NO	
203B	ALUMINUM	0.962	0.477	NO		4.91	NO	
203C	ALUMINUM	0.849	0.427	NO		9.62	NO	
203D	ALUMINUM	0.932	0.534	NO		0.79	NO	
203E	ALUMINUM	1.167	0.583	NO		3.98	NO	
203F	ALUMINUM	0.948	0.501	NO		3.55	NO	
203G	ALUMINUM	1.120	0.579	NO		6.34	NO	
205A	ALUMINUM	0.597	0.475	NO		4.43	NO	
205B	ALUMINUM	0.642	0.488	NO		2.41	NO	
205C	ALUMINUM	0.596	0.490	NO		1.23	NO	
205D	ALUMINUM	0.636	0.504	NO		1.23	NO	
205E	ALUMINUM	0.577	0.419	NO		0.79	NO	
207A	ALUMINUM	0.872	0.556	NO		0.30	NO	
207B	ALUMINUM	0.925	0.577	YES	0.140	4.43	YES	0.030
207C	ALUMINUM	1.001	0.615	NO		0.99	NO	
209A	ALUMINUM	0.686	0.437	NO		3.55	NO	
209B	ALUMINUM	0.847	0.506	NO		3.98	NO	
209D	ALUMINUM	0.773	0.557	NO		0.60	NO	
210B	ALUMINUM	1.196	0.666	YES	0.125	7.67	NO	
210D	ALUMINUM	1.400	0.675	YES	0.222	4.43	NO	
211B	ALUMINUM	0.842	0.667	NO		2.07	NO	
211D	ALUMINUM	0.906	0.710	NO		0.00	NO	
212B	ALUMINUM	0.791	0.609	NO		0.79	NO	
215A	ALUMINUM	0.477		YES	0.565	7.07	NO	
215B	ALUMINUM	0.508		YES	0.327	4.43	NO	
215C	ALUMINUM	0.513		NO		5.94	NO	
218A	ALUMINUM	0.797	0.569	NO		0.00	NO	
218B	ALUMINUM	0.765	0.572	NO		0.00	NO	
218C	ALUMINUM	0.828	0.584	NO		0.00	NO	
221A	ALUMINUM	0.501	0.403	NO		1.23	NO	
221B	ALUMINUM	0.531	0.395	NO		0.79	NO	
221C	ALUMINUM	0.438	0.331	NO		0.79	NO	
221D	ALUMINUM	0.457	0.323	NO		0.31	NO	
226A	ALUMINUM	0.478	0.390	NO		2.76	NO	
226B	ALUMINUM	0.551	0.412	NO		0.00	NO	
226C	ALUMINUM	0.593	0.372	NO		0.00	NO	
227A	ALUMINUM	0.591	0.444	NO		0.00	NO	
227B	ALUMINUM	0.586	0.428	NO		0.00	NO	
229A	ALUMINUM	0.618		NO		3.98	NO	
229B	ALUMINUM	0.491		YES	0.482	4.43	NO	
229C	ALUMINUM	0.508		YES	0.300	4.43	YES	0.10

230A	ALUMINUM	0.467	0.386	NO	1.77	NO
230B	ALUMINUM	0.463	0.354	NO	0.20	NO
301	ALUMINUM	0.537	0.418	NO	1.48	NO
303	ALUMINUM	0.724	0.568	NO	2.07	NO
303A	ALUMINUM	0.743	0.525	NO	4.43	NO
303B	ALUMINUM	0.732	0.562	NO	3.17	NO
306	ALUMINUM	0.901	0.697	NO	3.98	NO
319	ALUMINUM	0.645	0.439	NO	0.44	NO
320	ALUMINUM	0.723	0.543	NO	1.48	NO
321	ALUMINUM	0.701	0.527	NO	1.77	NO
324	ALUMINUM	0.672	0.458	NO	1.23	NO
325	ALUMINUM	0.759	0.600	NO	3.14	NO
326	ALUMINUM	0.750	0.594	NO	2.07	NO
333	ALUMINUM	0.389	0.291	NO	0.00	NO
334	ALUMINUM	0.394	0.298	NO	0.00	NO
335	ALUMINUM	0.509	0.386	NO	0.79	NO
336	ALUMINUM	0.615	0.410	NO	0.00	NO
336A	ALUMINUM	0.562	0.444	NO	0.00	NO
337	ALUMINUM	0.771	0.523	NO	0.00	NO
338	ALUMINUM	0.876	0.569	NO	0.00	NO
339	ALUMINUM	0.853	0.593	NO	0.00	NO

DEBRIS CLOUD TRAJECTORY (DEG)	DEBRIS CLOUD SPREAD (DEG)	HOLE NO. 1 DIAMETER (IN.)	HOLE NO. 2 DIAMETER (IN.)	HOLE NO. 3 DIAMETER (IN.)	CRATER NO. 1 DIA. (IN.)	CRATER NO. 1 DEPTH (IN.)	CRATER NO. 2 DIA. (IN.)	CRATER NO. 2 DEPTH (IN.)	CRATER DIA. (IN.)
13.63	33.41				0.139	0.045	0.058	0.037	0.060
4.29	12.74								
-1.00	-1.00								
12.41	36.70								
-1.00	-1.00								
-1.00	-1.80								
-1.00	-1.00								
-1.00	-1.00	0.200							
15.38	9.47								
2.86	9.99								
0.00	7.15	0.151			0.108	0.102	0.119	0.084	0.083
-1.00	-1.00								
11.31	22.80				0.071	0.047	0.087	0.025	0.061
21.80	30.23				0.131	0.043	0.077	0.020	0.079
23.03	40.29				0.180	0.014	0.073	0.007	0.103
14.04	12.92				0.104	0.031	0.085	0.028	0.107
14.04	30.85				0.097	0.076	0.088	0.039	0.199
18.91	26.51				0.109	0.057	0.161	0.038	0.075
17.61	36.07								
9.93	32.28				0.085	0.039	0.100	0.037	0.092
12.68	23.23				0.075	0.047	0.088	0.044	0.090
19.29	15.90				0.191	0.093	0.098	0.042	0.100
8.53	17.35				0.107	0.026	0.057	0.018	0.075
5.71	14.04				0.108	0.050	0.104	0.041	0.107
25.41	41.65				0.168	0.081	0.139	0.080	0.109
15.38	32.28	0.140			0.124	0.115	0.170	0.104	0.151
1.43	17.05				0.142	0.049	0.106	0.049	0.095
14.04	28.00				0.099	0.072	0.102	0.059	0.170
19.29	32.58				0.088	0.074	0.110	0.048	0.108
7.13	12.48				0.126	0.102	0.127	0.080	0.139
14.04	40.25	0.125			0.180	0.080	0.115	0.060	0.124
12.68	32.53	0.172	0.141		0.202	0.075	0.112	0.060	0.099
7.13	22.64				0.062	0.034	0.045	0.023	0.078
-1.00	-1.00								
5.43	14.13				0.076	0.030	0.066	0.024	0.059
-1.00	-1.00	0.565			0.227	0.129	0.158	0.126	0.267
-1.00	-1.00	0.327			0.107	0.118	0.123	0.114	0.079
-1.00	-1.00				0.052	0.100	0.069	0.092	0.214
-1.00	-1.00								
-1.00	-1.00								
-1.00	-1.00								
18.00	16.13				0.030	0.025	0.071	0.020	0.061
7.13	14.17								
3.58	14.13				0.118	0.023	0.065	0.012	0.051
4.29	8.49				0.099	0.008	0.058	0.001	
1.43	26.69				0.091	0.049	0.090	0.040	0.068
-1.00	-1.00								
-1.00	-1.00								
-1.00	-1.00								
-1.00	-1.00								
-1.00	-1.00				0.094	0.074	0.093	0.066	0.075
-1.00	-1.00	0.482			0.194	0.073	0.128	0.044	0.133
-1.00	-1.00	0.300			0.258	0.136	0.330	0.130	0.227

5.71	20.87
7.13	7.06
8.81	18.79
8.95	22.64
14.04	26.13
8.53	27.30
5.71	30.75
11.31	9.75
5.71	19.67
7.13	20.87
11.31	18.13
11.31	27.68
7.13	22.50
-1.00	-1.00
-1.00	-1.00
11.31	13.84
-1.00	-1.00
-1.00	-1.00
-1.00	-1.00
-1.00	-1.00
-1.00	-1.00

0.143	0.006	0.080	0.005	0.114
0.112	0.015	0.102	0.012	
0.125	0.036	0.067	0.021	0.053
0.104	0.027	0.116	0.024	0.092
0.135	0.031	0.111	0.020	0.070
0.039	0.012	0.057	0.003	0.045
0.130	0.022	0.103	0.017	0.146
0.107	0.028	0.132	0.022	0.139
0.126	0.020	0.107	0.020	0.096
0.100	0.065	0.137	0.037	0.204

NO. 3 DEPTH (IN.)	BACKWALL PENETRATED?	BACKWALL EQ. HOLE DIAMETER (IN.)	BACKWALL DAMAGE AREA (SQ. IN.)	BACKWALL SPALLED?	BACKWALL SPALL AREA (SQ.IN.)	DEBRIS CLOUD TRAJECTORY (DEG)	DEBRIS CLOUD SPREAD (DEG)
0.014	YES	0.310	1.23	NO		38.04	10.80
	YES	0.193	1.48	NO		37.33	12.36
	YES	1.350	9.62	NO		41.59	25.51
	NO		0.00	NO		-1.00	-1.00
	YES	0.330	0.99	NO		41.99	8.76
	YES	0.468	0.99	NO		40.53	8.87
0.031	YES	0.126	0.44	NO		50.77	4.33
	YES	0.490	0.31	NO		42.38	4.78
0.017	NO		2.07	NO		56.75	6.55
0.019	NO		0.20	NO		60.33	1.80
0.003	NO		0.20	NO		60.26	1.76
0.020	NO		7.67	NO		51.62	13.78
0.032	NO		8.95	NO		56.31	13.88
0.027	NO		1.48	NO		55.18	6.39
	YES	0.153	4.60	NO		56.79	10.57
0.029	YES	0.096	1.23	NO		41.19	10.83
0.029	YES	0.172	2.76	NO		40.36	14.08
0.034	YES	0.667	1.48	NO		37.95	12.05
0.008	NO		0.79	NO		35.66	9.18
0.033	YES	0.346	0.20	NO		37.33	4.53
0.071	YES	0.143	0.44	NO		57.99	3.03
0.086	NO		0.31	NO		60.33	2.18
0.040	NO		8.94	NO		51.17	24.56
0.035	NO		0.20	NO		57.59	2.12
0.045	NO		0.00	NO		-1.00	-1.00
0.078	NO		1.77	NO		54.56	6.65
0.051	NO		0.99	NO		56.83	5.18
0.050	YES	0.224	8.30	NO		48.49	23.74
0.009	YES	0.835	3.54	NO		40.20	16.15
	YES	1.503	1.77	NO		40.20	11.84
0.011	YES	0.620	2.76	NO		38.04	15.98
0.119							
0.111							
0.065							
	YES	0.655	7.67	NO		61.67	8.94
	YES	0.698	2.41	NO		61.28	5.39
	YES	0.730	3.98	NO		59.46	7.58
0.012	NO		0.44	NO		32.01	6.97
	NO		0.60	NO		39.95	7.45
0.010	NO		0.31	NO		41.19	5.11
	NO		0.20	NO		40.94	4.39
0.033	YES	0.950	0.99	NO		51.17	6.29
	YES	0.470	1.77	NO		53.82	6.66
	YES	0.430	0.99	NO		53.97	5.32
	YES	0.480	2.41	NO		52.27	8.39
	YES	1.419	6.49	NO		52.70	14.41
0.062							
0.023							
0.127							

0.002	NO		0.11	NO	42.54	3.00
	NO		0.60	NO	40.11	6.75
	NO		0.31	NO	41.19	5.20
0.014	NO		2.41	NO	38.04	14.27
0.010	YES	0.617	0.44	NO	39.95	6.33
0.006	NO		1.48	NO	40.94	11.49
0.001	YES	2.092	9.62	NO	42.15	26.64
	YES	0.721	0.99	NO	42.38	8.65
0.016	YES	CRACK	1.77	NO	39.09	12.23
0.021	YES	0.305	0.99	NO	38.83	9.31
	YES	0.708	0.44	NO	41.59	6.02
0.016	YES	0.558	1.23	NO	37.78	10.88
0.029	YES	0.538	0.99	NO	39.95	9.11
	NO		0.11	NO	41.19	3.04
	NO		0.11	NO	36.59	3.56
	YES	0.384	2.07	NO	38.40	13.35
	YES	0.543	1.18	NO	43.53	9.54
	NO		1.77	NO	39.95	11.93
	YES	0.857	6.49	NO	40.53	19.81
	YES	1.273	1.77	NO	37.78	13.89
	YES	1.717	20.63	NO	40.20	35.08

HOLE NO. 1		HOLE NO. 2		HOLE NO. 3		CRATER NO. 1			CRATER NO. 2		
DIA 1 (IN.)	DIA 2 (IN.)	DIA 1 (IN.)	DIA 2 (IN.)	DIA 1 (IN.)	DIA 2 (IN.)	DIA 1 (IN.)	DIA 2 (IN.)	DEPTH (IN.)	DIA 1 (IN.)	DIA 2 (IN.)	DEPTH (IN.)
0.384	0.136	0.223	0.156	0.133	0.082	0.263	0.081	0.123	0.250	0.084	0.111
0.200	0.187					0.213	0.147	0.065	0.160	0.109	0.051
1.350	1.350										
0.402	0.271					0.334	0.203	0.204	0.179	0.169	0.126
0.511	0.462										
0.156	0.102					0.194	0.144	0.084	0.105	0.042	0.045
0.422	0.313	0.404	0.274								
						0.151	0.120	0.056	0.138	0.137	0.034
						0.275	0.263	0.126			
						0.500	0.308	0.065			
						0.209	0.108	0.041	0.143	0.083	0.033
						0.252	0.130	0.077	0.090	0.088	0.042
						0.297	0.287	0.203	0.477	0.306	0.156
0.108	0.108	0.108	0.108								
0.130	0.071					0.370	0.103	0.120	0.237	0.199	0.117
0.214	0.138					0.172	0.155	0.092	0.110	0.080	0.053
0.278	0.269	0.210	0.178	0.197	0.169	0.075	0.072	0.050	0.086	0.057	0.046
						0.208	0.107	0.089	0.238	0.097	0.081
0.348	0.345										
0.154	0.133										
						0.232	0.156	0.062	0.074	0.071	0.025
						0.139	0.077	0.036	0.115	0.038	0.022
						0.261	0.137	0.085	0.167	0.096	0.045
0.252	0.199					0.114	0.071	0.035	0.085	0.071	0.023
0.835	0.835					0.200	0.100	0.075	0.094	[illegible]	[illegible]
1.515	1.491					0.107	0.083	0.027	0.089	0.056	0.022
0.728	0.321	0.402	0.335	0.152	0.104	0.112	0.075	0.090	0.089	0.065	0.059
0.708	0.606					0.135	0.077	0.183	0.220	0.163	0.133
0.668	0.608	0.384	0.214								
1.216	0.439					0.382	0.241	0.111	0.390	0.206	0.097
						0.155	0.105	0.046	0.156	0.083	0.040
						0.175	0.089	0.030	0.066	0.052	0.015
						0.255	0.127	0.084	0.185	0.141	0.068
						0.409	0.198	0.133	0.148	0.075	0.013
0.478	0.409	0.163	0.138			0.247	0.141	0.186	0.173	0.131	0.179
0.775	0.285					0.165	0.101	0.109			
0.333	0.278	0.246	0.161	0.240	0.220	0.138	0.089	0.124	0.168	0.078	0.118
0.527	0.356	0.210	0.126	0.165	0.100	0.163	0.093	0.062	0.098	0.050	0.039
2.445	0.823										

0.673	0.565		
3.500	1.250		
1.015	0.512		
CRACK			
0.316	0.294		
0.829	0.605		
0.824	0.378		
0.693	0.418		
0.470	0.313		
0.718	0.410		
1.075	0.670	0.121	0.115
1.468	1.110		
1.717	1.717		

0.142	0.083	0.068	0.143	0.114	0.056
0.191	0.088	0.040	0.138	0.056	0.022
0.385	0.308	0.060	0.252	0.145	0.016
0.423	0.221	0.179	0.379	0.194	0.167
0.096	0.088	0.017			
0.472	0.326	0.257	0.383	0.380	0.248
0.137	0.103	0.040	0.111	0.045	0.033
0.462	0.313	0.138	0.251	0.152	0.077
0.256	0.159	0.117	0.092	0.080	0.035
0.419	0.186	0.173	0.101	0.095	0.080
0.313	0.211	0.098			
0.364	0.290	0.109			
0.265	0.112	0.161	0.081	0.064	0.068
0.183	0.119	0.185	0.195	0.159	0.116
0.101	0.058	0.055	0.148	0.083	0.048

CRATER NO. 3 DIA 1 (IN.)	DIA 2 (IN.)	DEPTH (IN.)	NO. WITNESS PLATES PENETRATED
0.111	0.069	0.090	0
0.202	0.098	0.047	0
			4
			0
0.118	0.094	0.040	1
			4
0.089	0.042	0.038	0
			3
0.133	0.083	0.020	
0.152	0.063	0.026	
0.060	0.053	0.005	
0.214	0.159	0.050	
			0
0.089	0.086	0.002	0
0.217	0.092	0.049	0
0.138	0.096	0.015	1
0.189	0.060	0.068	
			2
			0
0.129	0.085	0.015	
0.109	0.099	0.036	
0.077	0.075	0.020	0
0.232	0.094	0.039	4
0.105	0.081	0.011	4
0.087	0.068	0.049	2
			3
			1
0.293	0.235	0.055	4
			4
0.170	0.166	0.065	4
0.072	0.050	0.025	
0.102	0.091	0.008	
0.097	0.054	0.035	
			4
			4
0.081	0.063	0.032	2
0.143	0.070	0.031	3
			1
			2
			0

0.191	0.081	0.040	
0.310	0.218	0.150	
			2
0.339	0.232	0.188	
0.121	0.048	0.026	2
			4
0.222	0.134	0.055	0
			2
			4
0.171	0.070	0.015	1
0.150	0.134	0.031	3
0.330	0.262	0.054	1
			2
0.200	0.090	0.092	
			4
			2
			4

LOTUS FILE EHSSMLIN.WK1

TEST NUMBER	BUMPER PLATE MATERIAL	BUMPER HOLE DIA 1 (IN.)	BUMPER HOLE DIA 2 (IN.)	BACKWALL PENETRATED?	BACKWALL EQ. HOLE DIAMETER (IN.)	BACKWALL DAMAGE AREA (SQ. IN.)	BACKWALL SPALLED?	BACKWALL SPALL AREA (SQ.IN.)
EH1A	ALUMINUM	0.670	0.630	YES	1.51	19.63	NO	
EH1B	ALUMINUM	0.790	0.650	YES	0.89	11.04	NO	
EH1C	ALUMINUM	0.980	0.650	YES	0.01	10.64	YES	0.11
EH1D	ALUMINUM	1.420	0.570	YES	0.19	15.90	NO	
EHSS1A	ALUMINUM	0.557		NO		11.04	YES	0.97
EHSS1B	ALUMINUM	0.510		YES	0.58	11.79	YES	1.12
EHSS1C	ALUMINUM	0.518		YES	0.37	11.04	YES	1.24
EHSS2A	ALUMINUM	0.521		NO		8.30	YES	0.23
EHSS2B	ALUMINUM	0.480		NO		9.62	YES	0.81
EHSS3A	ALUMINUM	~~0.634~~	0.558	YES	0.24	9.62	YES	0.19
EHSS3B	ALUMINUM	0.614	0.583	YES	0.89	7.07	NO	
EHSS3C	ALUMINUM	0.542	0.491	YES	0.79	10.32	NO	
EHSS4A	ALUMINUM	0.747	0.573	NO		2.41	NO	
EHSS4B	ALUMINUM	0.697	0.563	NO		3.14	YES	0.05
EHSS4C	ALUMINUM	0.649	0.505	NO		6.49	YES	0.05
EHSS5A	ALUMINUM	0.522	0.478	YES	0.48	8.30	NO	
EHSS5B	ALUMINUM	0.556	0.493	YES	0.43	14.19	NO	
EHSS5C	ALUMINUM	0.857	0.478	YES	0.27	3.55	YES	0.04
EHSS5D	ALUMINUM	0.787	0.433	YES	0.19	3.98	NO	
EHSS6A	ALUMINUM	0.644		YES	0.31	13.36	YES	1.02
EHSS6B	ALUMINUM	0.578		YES	2.23	16.80	YES	0.05
EHSS6C	ALUMINUM	0.480		YES	1.26	19.63	YES	0.84
EHSS7A	ALUMINUM	0.822	0.656	NO		3.14	NO	
EHSS7B	ALUMINUM	0.860	0.667	NO		4.91	YES	0.26
EHSS8A	ALUMINUM	1.460	0.546	YES	0.43	6.49	YES	0.03

DEBRIS CLOUD TRAJECTORY (DEG)	DEBRIS CLOUD SPREAD (DEG)	HOLE NO. 1 DIAMETER (IN.)	HOLE NO. 2 DIAMETER (IN.)	HOLE NO. 3 DIAMETER (IN.)	CRATER NO. 1 DIA. (IN.)	CRATER NO. 1 DEPTH (IN.)	CRATER NO. 2 DIA. (IN.)	CRATER NO. 2 DEPTH (IN.)	CRATER DIA. (IN.)
24.82	60.51	1.513			0.190	0.076	0.122	0.068	0.193
10.90	47.26	0.887			0.141	0.111	0.141	0.093	0.199
9.93	46.80	0.010			0.135	0.072	0.150	0.070	0.139
4.29	56.80	0.142	0.132		0.224	0.139	0.185	0.137	0.273
1.72	50.19				0.112	0.085	0.085	0.072	0.080
0.36	52.19	0.427	0.392		0.159	0.146	0.169	0.132	0.119
0.00	50.19	0.184	0.179	0.140	0.122	0.145	0.134	0.127	0.120
0.36	44.19				0.098	0.073	0.084	0.073	0.089
0.00	47.26				0.161	0.146	0.121	0.128	0.079
23.27	41.80	0.173	0.162		0.205	0.151	0.195	0.129	0.127
22.66	35.23	0.873	15.000	0.092	0.163	0.132	0.106	0.129	0.096
28.48	40.13	0.790			0.127	0.148	0.154	0.137	0.191
8.53	24.36				0.070	0.075	0.104	0.074	0.110
16.04	26.73				0.086	0.096	0.131	0.085	0.094
16.04	36.39				0.134	0.152	0.141	0.125	0.127
21.80	41.18	0.289	0.265	0.197	0.099	0.120	0.110	0.108	0.128
25.17	51.39	0.362	0.180	0.160	0.166	0.152	0.160	0.130	0.149
9.93	29.43	0.270			0.102	0.097	0.115	0.093	0.097
21.80	29.53	0.160	0.103		0.145	0.114	0.155	0.077	0.097
0.00	54.41	0.310							
0.00	59.78	2.204	0.157	0.148	0.118	0.139	0.144	0.113	0.153
3.58	63.68	1.259							
12.68	25.28				0.114	0.116	0.128	0.103	0.099
23.03	33.10				0.102	0.091	0.172	0.075	0.118
10.62	38.31	0.363	0.207	0.120	0.118	0.124	0.164	0.117	0.116

NO. 3 DEPTH (IN.)	BACKWALL PENETRATED?	BACKWALL EQ. HOLE DIAMETER (IN.)	BACKWALL DAMAGE AREA (SQ. IN.)	BACKWALL SPALLED?	BACKWALL SPALL AREA (SQ.IN.)	DEBRIS CLOUD TRAJECTORY (DEG)	DEBRIS CLOUD SPREAD (DEG)
0.067	NO		0.00	NO		24.82	60.51
0.078	NO		0.00	NO		38.13	28.47
0.063	NO		6.61	NO		50.19	15.01
0.039	NO		0.00	NO		24.82	56.80
0.061							
0.117							
0.093							
0.064							
0.078							
0.115	NO		0.00	NO		23.27	41.80
0.123	NO		0.00	NO		22.66	35.23
0.068	NO		0.00	NO		28.48	40.13
0.045	YES	0.33	1.48	NO		39.95	11.06
0.065	YES	0.51	5.41	YES	0.02	37.05	19.95
0.109	YES	0.45	2.41	NO		43.30	5.69
0.106	NO		0.00	NO		21.80	41.18
0.119	NO		0.00	NO		25.17	51.39
0.085	NO		2.76	NO		63.72	5.10
0.052	NO		0.44	NO		58.39	3.04
0.074							
0.086	YES	0.90	3.55	NO		39.27	17.09
0.073	YES	0.96	2.07	NO		42.15	12.24
0.110	NO		0.00	NO		10.62	38.31

HOLE NO. 1		HOLE NO. 2		HOLE NO. 3		CRATER NO. 1			CRATER NO. 2		
DIA 1 (IN.)	DIA 2 (IN.)	DIA 1 (IN.)	DIA 2 (IN.)	DIA 1 (IN.)	DIA 2 (IN.)	DIA 1 (IN.)	DIA 2 (IN.)	DEPTH (IN.)	DIA 1 (IN.)	DIA 2 (IN.)	DEPTH (IN.)
						0.118	0.118	0.139	0.256	0.236	0.129
						0.200	0.159	0.084	0.142	0.142	0.056
0.391	0.231	0.154	0.113			0.289	0.149	0.153	0.268	0.126	0.132
0.460	0.210	0.300	0.288	0.250	0.187	0.210	0.136	0.152	0.146	0.115	0.130
0.341	0.273	0.319	0.224	0.208	0.199	0.244	0.137	0.168	0.223	0.128	0.146
						0.197	0.081	0.040	0.191	0.176	0.036
						0.225	0.107	0.055	0.180	0.070	0.051
1.318	0.548	0.226	0.156	0.226	0.142	0.287	0.169	0.142	0.210	0.156	0.131
1.463	0.600	0.152	0.128	0.140	0.130	0.215	0.147	0.128	0.145	0.112	0.061

CRATER NO. 3 DIA 1 (IN.)	DIA 2 (IN.)	DEPTH (IN.)	NO. WITNESS PLATES PENETRATED
0.177	0.177	0.121	
0.150	0.120	0.041	
			1
			1
0.190	0.126	0.120	0
0.163	0.102	0.110	2
0.274	0.131	0.090	1
0.137	0.074	0.005	
0.153	0.090	0.024	
			2
			2
			2
0.248	0.142	0.126	2
0.144	0.105	0.052	2

LOTUS FILE <u>EHMLIY.WK1</u>

TEST NUMBER	BUMPER PLATE MATERIAL	BUMPER HOLE DIA. 1 (IN.)	BUMPER HOLE DIA. 2 (IN.)	BACKWALL PENETRATED?	BACKWALL EQ. HOLE DIAMETER (IN.)	BACKWALL DAMAGE AREA (SQ. IN.)	BACKWALL SPALLED?	BACKWALL SPALL AREA (SQ.IN.)
EH1A	ALUMINUM	0.130	0.629	YES	0.198	14.52	NO	
EH1AA	ALUMINUM	1.319	0.629	YES	0.137	11.16	NO	
EH1AB	ALUMINUM	1.319	0.591	YES	0.195	16.62	NO	
EH1B	ALUMINUM	1.102	0.472	YES	0.171	10.75	NO	
EH1C	ALUMINUM	0.787	0.394	NO		6.61	NO	
EH2A	ALUMINUM	0.634		YES	2.505	17.87	NO	
EH2B	ALUMINUM	0.751		NO		4.91	NO	
EH2C	ALUMINUM	0.631		YES	0.410	2.76	NO	
EH2D	ALUMINUM	0.635		YES	1.516	7.74	NO	
EH2E	ALUMINUM	0.583		YES	2.710	8.95	NO	
EH3A	ALUMINUM	0.596		YES	1.962	31.96	YES	1.11
EH4A	ALUMINUM	0.584		YES	0.870	35.78	NO	
EH4B	ALUMINUM	0.645		YES	1.600	21.65	NO	
EHRP1	ALUMINUM	1.140	0.650	NO		14.52	NO	
EHRP2	ALUMINUM	1.300	0.630	NO		14.52	NO	
EHRP3	ALUMINUM	0.781	0.625	NO		6.49	NO	
EHRP4	ALUMINUM	0.813	0.563	NO		8.30	NO	
EHRP5	ALUMINUM	0.813	0.563	NO		4.43	NO	
EHRP6	ALUMINUM	0.782	0.551	NO		5.41	NO	
EHRP7	ALUMINUM	0.669	0.413	NO		5.94	NO	
EHRP8	ALUMINUM	0.594	0.438	YES	0.075	20.63	NO	
EHRP9	ALUMINUM	0.669	0.472	NO		15.71	NO	
MOTA	ALUMINUM	0.324		YES	0.320	0.15	NO	
MOTB	ALUMINUM	0.320		YES	0.420	1.47	NO	
MOTD	ALUMINUM	0.630		NO		6.83	NO	
PREH1	ALUMINUM	0.620		YES	1.100	25.97	NO	
PREH2	ALUMINUM	0.615		YES	1.990	25.97	NO	

DEBRIS CLOUD TRAJECTORY (DEG)	DEBRIS CLOUD SPREAD (DEG)	HOLE NO. 1 DIAMETER (IN.)	HOLE NO. 2 DIAMETER (IN.)	HOLE NO. 3 DIAMETER (IN.)	CRATER NO. 1 DIA. (IN.)	CRATER NO. 1 DEPTH (IN.)	CRATER NO. 2 DIA. (IN.)	CRATER NO. 2 DEPTH (IN.)	CRATER DIA. (IN.)
5.00	55.69	0.161	0.104	0.050	0.170	0.111	0.169	0.094	0.218
4.72	47.77	0.172	0.137		0.208	0.135	0.205	0.130	0.174
5.00	59.33	0.195			0.181	0.139	0.241	0.116	0.224
4.29	48.70	0.171			0.169	0.086	0.200	0.065	0.124
2.86	38.74				0.215	0.074	0.209	0.068	0.150
7.69	60.23	2.505							
0.00	34.71								
3.58	26.16	0.410							
7.83	41.67	1.516							
0.00	45.68	2.710							
3.29	76.88	1.962							
1.72	80.31	0.870			0.125	0.056	0.062	0.044	0.109
1.86	66.41	1.600							
11.31	56.23								
11.31	49.29								
8.81	34.98				0.120	0.068	0.160	0.057	0.115
12.95	44.78				0.190	0.137	0.142	0.114	0.117
1.86	33.13				0.130	0.059	0.100	0.049	0.121
9.93	36.08				0.180	0.139	0.175	0.095	0.125
22.17	31.25				0.150	0.075	0.115	0.055	0.125
10.62	57.60	0.075			0.150	0.060	0.126	0.058	0.180
7.13	50.31				0.173	0.102	0.137	0.059	0.151
12.13	6.02	0.320							
0.00	19.41	0.420							
3.01	40.39								
1.86	71.10	1.100							
0.00	71.72	1.990							

NO. 3 DEPTH (IN.)	BACKWALL PENETRATED?	BACKWALL EQ. HOLE DIAMETER (IN.)	BACKWALL DAMAGE AREA (SQ. IN.)	BACKWALL SPALLED?	BACKWALL SPALL AREA (SQ.IN.)	DEBRIS CLOUD TRAJECTORY (DEG)	DEBRIS CLOUD SPREAD (DEG)
0.083	NO		0.00	NO		22.05	55.69
0.129	NO		0.00	NO		22.17	47.77
0.108	NO		0.00	NO		19.93	59.33
0.053	NO		0.00	NO		21.80	48.70
0.039	NO		0.00	NO		20.56	38.74
0.034							
	NO		10.18	NO		46.40	24.15
	NO		9.62	NO		64.80	8.89
0.040	YES	1.004	7.07	NO		41.19	24.78
0.081	YES	0.347	11.05	NO		48.68	28.27
0.041	YES	0.341	7.07	NO		25.17	28.56
0.078	YES	0.425	20.03	YES	0.061	48.37	33.96
0.051	NO		2.07	NO		61.54	5.71
0.055	NO		0.00	NO		10.62	57.60
0.040	NO		0.00	NO		7.13	50.31

HOLE NO. 1		HOLE NO. 2		HOLE NO. 3		CRATER NO. 1			CRATER NO. 2		
DIA 1 (IN.)	DIA 2 (IN.)	DIA 1 (IN.)	DIA 2 (IN.)	DIA 1 (IN.)	DIA 2 (IN.)	DIA 1 (IN.)	DIA 2 (IN.)	DEPTH (IN.)	DIA 1 (IN.)	DIA 2 (IN.)	DEPTH (IN.)
1.004	1.004					0.225	0.175	0.140	0.200	0.188	0.139
0.276	0.157	0.276	0.157	0.197	0.118	0.117	0.102	0.092	0.156	0.112	0.090
0.276	0.217	0.197	0.177	0.146	0.146	0.156	0.156	0.116	0.195	0.185	0.116
0.472	0.197	0.201	0.177	0.157	0.130	0.242	0.200	0.139	0.165	0.150	0.127
						0.175	0.146	0.089	0.147	0.137	0.046

CRATER NO. 3 DIA 1 (IN.)	DIA 2 (IN.)	DEPTH (IN.)	NO. WITNESS PLATES PENETRATED
			1
			1
			0
			0
			1
			0
			0
			0
			2
			2
			2
0.185	0.170	0.139	2
0.228	0.152	0.070	0
0.125	0.125	0.062	1
0.160	0.160	0.076	1
0.113	0.113	0.029	
			0
			0
			0
			2
			2

LOTUS FILE PSERMLIN.WK1

TEST NUMBER	BACKWALL PENETRATED?	BACKWALL EQ. HOLE DIAMETER (IN.)	BACKWALL DAMAGE AREA (SQ. IN.)	BACKWALL SPALLED?	BACKWALL SPALL AREA (SQ.IN.)	DEBRIS CLOUD TRAJECTORY (DEG)	DEBRIS CLOUD SPREAD (DEG)
P-01	NO		0.14	YES	0.17	0.72	38.57
P-02	NO		0.40	NO		1.29	47.30
P-03	NO		0.36	YES	0.53	1.43	53.11
P-04	NO		0.30	YES	0.31	0.72	48.10
P-05	YES		14.19	YES	0.03	0.43	55.94
P-06A	NO		19.64	YES	0.72	4.15	64.01
P-13	YES	0.25	9.35	YES	0.29	3.05	32.08
P-13B	NO		8.04	YES	0.19	0.48	29.85
P-13C	YES	0.47	22.06	YES	0.49	0.57	47.64
P-14	YES	0.46	7.35	NO		0.38	28.61
P-14A	YES	0.19	8.25	NO		3.15	[illegible]
P-14B	NO		20.91	YES	0.05	3.24	46.42
P-14D	YES	0.15	4.91	NO		1.43	23.52
P-15	NO		2.78	NO		10.02	17.67
P-15A	NO			NO		8.62	
P-15C	NO			NO			
P-16	YES	1.21	21.24	YES	0.54	2.20	46.66
P-16A	YES	0.79	21.65	YES	0.49	0.95	47.26
P-16B	YES	0.94	13.66	YES	1.08	0.48	37.90
P-16C	YES	0.70	20.63	YES	2.03	3.15	46.27
P-16E	YES	0.92	28.27	YES	1.96	0.00	53.11
P-16G	NO		38.50	YES	0.45	0.48	60.47
P-17	YES	0.63	33.53	YES	1.43	0.00	20.04
P-20B	NO		33.18	YES	0.79	1.24	56.74
P-20C	YES	0.19	33.18	YES	0.98	0.76	56.92
P-21	YES	1.13	19.53	YES	0.82	1.86	63.97
P-21A	YES	1.33	15.90	YES	0.19	1.72	58.14
P-24C	YES	0.19	22.37	YES	0.48	0.67	47.91
P-24F	YES	0.19	25.80	YES	0.34	1.05	50.90
P-25	NO		8.50	NO		2.29	30.62
P-25A	NO		5.15	NO		10.85	11.98
P-25B	YES	0.31	0.00	NO		0.10	-2.96
P-25C	NO		1.47	NO		2.10	13.01
P-27	NO		7.07	NO		3.58	40.99
P-27A	YES	0.18	3.37	NO		1.86	29.01
P-27B	YES	0.12	4.91	NO		1.86	34.68
P-28	NO		1.63	NO		0.72	20.40
P-33	NO		19.63	YES	0.52	0.57	63.99
P-34	YES	0.41	23.76	YES	0.42	1.72	63.98
P-34B	YES	1.01	12.55	YES	1.34	0.72	53.13
P-35	YES	1.78	16.73	YES	1.26	2.39	41.97

HOLE NO. 1 DIAMETER (IN.)	HOLE NO. 2 DIAMETER (IN.)	HOLE NO. 3 DIAMETER (IN.)	CRATER NO. 1 DIA. (IN.)	CRATER NO. 1 DEPTH (IN.)	CRATER NO. 2 DIA. (IN.)	CRATER NO. 2 DEPTH (IN.)	CRATER NO. 3 DIA. (IN.)	CRATER NO. 3 DEPTH (IN.)	NO. WITNESS PLATES PENETRATED
0.185			0.145	0.118	0.180	0.102	0.109	0.090	0
0.247									0
0.470									2
0.365	0.244	0.134							1
0.194									1
0.154									0
1.080	0.220	0.220							2
0.786			0.155	0.124	0.133	0.080	0.140	0.069	2
0.940									1
0.695									1
0.920									0
0.630									2
0.204	0.174		0.139	0.114	0.148	0.105	0.155	0.072	1
1.134									2
1.330									3
0.110	0.110	0.110							0
0.110	0.110	0.110							1
0.310									2
			0.128	0.067	0.136	0.060	0.144	0.055	
0.175			0.219	0.141	0.241	0.105	0.154	0.103	0
0.120			0.199	0.142	0.103	0.118	0.215	0.106	0
0.408									0
0.950	0.290	0.190							0
1.766	0.126	0.084	0.241	0.127	0.190	0.112	0.130	0.091	1

LOTUS FILE PSERMLIY.WK1

TEST NUMBER	BUMPER PLATE MATERIAL	BUMPER HOLE SIZE (IN.)	BACKWALL PENETRATED?	BACKWALL EQ. HOLE DIAMETER (IN.)	BACKWALL DAMAGE AREA (SQ. IN.)	BACKWALL SPALLED?	BACKWALL SPALL AREA (SQ.IN.)	DEBRIS CLOUD TRAJECTORY (DEG)
P-7	ALUMINUM	0.42	YES	0.36	1.52	NO		0.72
P-8	ALUMINUM	0.43	YES	0.39	3.14	YES	0.33	0.00
P-9	ALUMINUM	0.52	NO		0.21	NO		0.00
P-10	ALUMINUM	0.51	NO		1.70	NO		0.00
P-11	ALUMINUM	0.51	NO		0.33	NO		0.57
P-12B	ALUMINUM	0.56	NO		0.97	NO		0.00
P-12C	ALUMINUM	0.47	NO		3.30	NO		1.43
P-12D	ALUMINUM	0.50	NO		2.82	NO		2.58
P-13D	ALUMINUM	0.56	NO		0.69	NO		1.53
P-13E	ALUMINUM	0.48	NO			NO		
P-14C	ALUMINUM	0.37	NO		4.60	NO		11.59
P-14E	ALUMINUM	0.33	YES	0.32	6.20	NO		1.24
P-14F	ALUMINUM	0.34	NO		4.55	NO		1.72
P-15B	ALUMINUM	0.20	NO		0.25	NO		7.22
P-16H	ALUMINUM	0.61	NO		2.38	NO		0.00
P-16J	ALUMINUM	0.62	NO		1.74	NO		0.00
P-16K	ALUMINUM	0.60	NO		1.00	NO		2.10
P-16L	ALUMINUM	0.57	NO		6.56	NO		1.81
P-16M	ALUMINUM	0.55	YES	0.53	8.87	NO		15.46
P-16N	ALUMINUM	0.51	YES	0.25		NO		
P-16P	ALUMINUM	0.57	YES	0.40	4.45	NO		1.15
P-20F	ALUMINUM	0.61	NO		8.15	NO		1.05
P-20G	ALUMINUM	0.51	YES	0.47	7.07	NO		0.95
P-20H	ALUMINUM	0.61	NO		6.21	YES	0.01	0.86
P-21B	ALUMINUM	0.66	NO		1.62	NO		0.57
P-21C	ALUMINUM	0.60	NO		1.19	NO		0.29
P-21D	ALUMINUM	0.59	YES	1.03	6.03	NO		1.29
P-24G	ALUMINUM	0.48	NO		3.31	NO		0.67
P-27C	ALUMINUM	0.36	NO		1.64	NO		1.00
P-27D	ALUMINUM	0.35	NO		1.69	NO		1.00
P-27E	ALUMINUM	0.34	NO		0.15	NO		0.43
P-27F	ALUMINUM	0.33	NO		0.22	NO		1.29
P-33B	ALUMINUM	0.47	YES	0.83	2.84	NO		2.72
P-33B-1	ALUMINUM	0.47	YES	0.20	2.84	YES	0.13	0.14
P-33C	ALUMINUM	0.44	NO		2.38	NO		0.00
P-34C	ALUMINUM	0.48	NO		4.52	NO		3.72
P-34C-1	ALUMINUM	0.46	YES	0.30	5.31	NO		3.29
P-34C-2	ALUMINUM	0.48	NO		5.31	NO		0.29
P-35B	ALUMINUM	0.62	NO		10.32	NO		0.00
P-35C	ALUMINUM	0.59	YES	SPLIT	SPLIT	NO		

DEBRIS CLOUD SPREAD (DEG)	HOLE NO. 1 DIAMETER (IN.)	HOLE NO. 2 DIAMETER (IN.)	HOLE NO. 3 DIAMETER (IN.)	CRATER NO. 1 DIA. (IN.)	CRATER NO. 1 DEPTH (IN.)	CRATER NO. 2 DIA. (IN.)	CRATER NO. 2 DEPTH (IN.)	CRATER NO. 3 DIA. (IN.)	CRATER NO. 3 DEPTH (IN.)
19.70	0.360								
28.00	0.390								
7.44									
20.81									
9.29									
15.73									
28.71									
26.58									
8.94									
21.78									
26.36	0.320								
22.43									
5.26									
16.49									
14.16									
10.74									
27.08									
9.64	0.320	0.210	0.210						
	0.250								
22.44	0.320	0.220	0.110						
30.04									
28.07	0.375	0.250	0.125						
26.33									
20.41									
17.47									
38.08	1.026								
19.48									
20.53									
20.68									
6.30									
7.44									
26.72	0.800	0.200	0.100						
26.69	0.200								
24.54									
33.35									
35.91	0.300								
35.98									
33.54				0.165	0.101	0.093	0.082	0.087	0.068
	SPLIT								

LOTUS FILE TSERNMLI.WK1

TEST NUMBER	BUMPER PLATE MATERIAL	BUMPER HOLE DIA. 1 (IN.)	BUMPER HOLE DIA. 2 (IN.)	BACKWALL PENETRATED?	BACKWALL EQ. HOLE DIAMETER (IN.)	BACKWALL DAMAGE AREA (SQ. IN.)	BACKWALL SPALLED?	BACKWALL SPALL AREA (SQ.IN.)
T2-2	ALUMINUM	0.307		YES	0.069	2.41	YES	0.06
T2-4	ALUMINUM	0.438		YES	0.538	7.67	YES	0.56
T2-6	ALUMINUM	0.471		YES	0.924	6.49	YES	2.03
T2-6A	ALUMINUM	0.609		YES	1.040	15.03	YES	0.86
T2-8	ALUMINUM	0.500		YES	1.150	7.80	YES	1.52
T2-10	ALUMINUM	0.307						
T2-11	ALUMINUM	0.541						
T2-12	ALUMINUM	0.531						
T2-16	ALUMINUM	0.530		YES	1.620	10.32	NO	
T2-18	ALUMINUM	0.696		YES	1.680	16.80	YES	0.34
T2-20	ALUMINUM	0.627		YES	0.596	21.65	YES	0.74
PT-4A	ALUMINUM	0.400		YES	0.630	10.77	YES	0.61
PT-4B	ALUMINUM	0.500		YES	0.250	15.21	YES	0.40
PT-4C	ALUMINUM	0.456		YES	0.396	5.25	YES	0.25
PT-6A	ALUMINUM	0.500		YES	1.060	9.57	NO	
PT-8A	ALUMINUM	0.490		YES	1.850	12.62	YES	0.96
PT-8B	ALUMINUM	0.500		YES	1.470	13.21	YES	0.22

ORIGINAL PAGE IS
OF POOR QUALITY

DEBRIS CLOUD TRAJECTORY (DEG)	DEBRIS CLOUD SPREAD (DEG)	HOLE NO. 1 DIAMETER (IN.)	HOLE NO. 2 DIAMETER (IN.)	HOLE NO. 3 DIAMETER (IN.)	CRATER NO. 1 DIA. (IN.)	CRATER NO. 1 DEPTH (IN.)	CRATER NO. 2 DIA. (IN.)	CRATER NO. 2 DEPTH (IN.)	CRATER NO. 3 DIA. (IN.)	CRATER NO. 3 DEPTH (IN.)
0.00	24.66	0.069			0.161	0.119	0.117	0.087	0.098	0.086
3.58	42.73	0.282	0.270	0.229	0.183	0.129	0.335	0.127	0.134	0.115
1.72	39.59	0.924			0.153	0.123	0.105	0.117	0.103	0.109
1.86	57.32	1.000	0.172	0.148	0.145	0.165	0.138	0.131	0.244	0.111
0.57	42.97	1.110	0.260	0.170						
0.95	40.11	1.610	0.125	0.081	0.108	0.131	0.131	0.117	0.170	0.10
3.58	60.11	1.590	0.420	0.151	0.127	0.164	0.132	0.127	0.128	0.119
1.86	66.40	0.430	0.299	0.208	0.152	0.163	0.119	0.146	0.154	0.130
6.98	49.11	0.490	0.290	0.200						
1.43	57.53	0.200	0.150							
1.72	35.85	0.396			0.109	0.112	0.142	0.101	0.162	0.084
3.58	50.19	1.070			0.160	0.116	0.125	0.109	0.145	0.103
2.00	53.22	1.850								
2.72	54.00	1.460	0.200							

LOTUS FILE TSERYMLI.WK1

TEST NUMBER	BUMPER PLATE MATERIAL	BUMPER HOLE DIA. 1 (IN.)	BUMPER HOLE DIA. 2 (IN.)	BACKWALL PENETRATED?	BACKWALL EQ. HOLE DIAMETER (IN.)	BACKWALL DAMAGE AREA (SQ. IN.)	BACKWALL SPALLED?	BACKWALL SPALL AREA (SQ.IN.)
T2-1	ALUMINUM	0.268		YES	0.281	0.31	NO	
T2-3	ALUMINUM	0.411		YES	0.160	2.76	NO	
T2-5	ALUMINUM	0.434		YES	0.840	5.41	NO	
T2-7	ALUMINUM	0.488		YES	0.564	7.67	NO	
T2-7A	ALUMINUM	0.547		YES	0.632	7.67	NO	
T2-15	ALUMINUM	0.522		YES	3.440	31.92	NO	
T2-17	ALUMINUM	0.608		YES	3.270	31.54	NO	
T2-19	ALUMINUM	0.576		NO		13.36	NO	
T2-19A	ALUMINUM	0.527		YES	0.499	8.30	NO	
T2-19B	ALUMINUM	0.474		YES	0.690	2.41	NO	

DEBRIS CLOUD TRAJECTORY (DEG)	DEBRIS CLOUD SPREAD (DEG)	HOLE NO. 1 DIAMETER (IN.)	HOLE NO. 2 DIAMETER (IN.)	HOLE NO. 3 DIAMETER (IN.)	CRATER NO. 1 DIA. (IN.)	CRATER NO. 1 DEPTH (IN.)	CRATER NO. 2 DIA. (IN.)	CRATER NO. 2 DEPTH (IN.)	CRATER NO. 3 DIA. (IN.)	CRATER NO. 3 DEPTH (IN.)
0.00	8.99	0.281			0.098	0.006				
7.13	26.16	0.160			0.174	0.071	0.070	0.040	0.138	0.015
1.72	36.26	0.840			0.103	0.020	0.044	0.015	0.099	0.011
3.58	42.07	0.564			0.132	0.067	0.104	0.052	0.097	0.048
1.72	42.60	0.632			0.189	0.102	0.096	0.057	0.174	0.048
1.86	77.14	3.440								
1.72	74.71	3.270			0.175	0.073	0.058	0.056	0.114	0.045
1.72	54.53				0.116	0.120	0.097	0.071	0.066	0.046
3.58	43.92	0.419	0.270		0.174	0.127	0.408	0.122	0.150	0.090
3.58	24.32	0.690			0.194	0.109	0.235	0.089	0.147	0.055

LOTUS FILE CORRBUMP.WK1

TEST NUMBER	BUMPER SIZE DN(IN.)	HOLE FRONT DX(IN.)	BUMPER SIZE DN(IN.)	HOLE BACK DX(IN.)	BACKWALL PENETRATED?	BACKWALL EQ. HOLE DIAMETER (IN.)	BACKWALL DAMAGE AREA (SQ. IN.)	BACKWALL SPALLED?	BACKWALL SPALL AREA (SQ.IN.)	DEBRIS CLOUD TRAJECTORY (DEG)
145A	0.332	0.332	1.500	2.375	YES	0.113	3.90	NO		1.45
145B	0.330	0.330	1.220	2.200	YES	0.090	3.42	NO		0.24
145C	0.292	0.292	1.500	1.875	YES	0.287	6.49	NO		1.57
307	0.349	0.484	1.000	1.500	NO			NO		
308	0.379	0.527	1.250	2.375	NO		1.40	NO		28.37
309	0.390	0.571	1.750	1.750	NO		1.23	NO		20.30
309-1	0.570	1.140	3.050	3.620	NO			NO		
309B	0.486	0.650	2.750	3.250	NO		0.20	NO		13.50
309R	0.492	0.563	1.500	2.000	NO		1.77	NO		16.70
310	0.494	0.725	3.500	4.000	NO			NO		
310R	0.406	0.621	1.500	2.000	NO		3.90	YES	0.010	32.62
311	0.546	0.808	4.500	4.750	NO		3.14	NO		12.95
312	0.600	1.000	3.700	3.900	NO			NO		
312B	0.553	0.830	3.500	3.750	NO			NO		

DEBRIS CLOUD SPREAD (DEG)	HOLE NO. 1 DIAMETER (IN.)	HOLE NO. 2 DIAMETER (IN.)	HOLE NO. 3 DIAMETER (IN.)	CRATER NO. 1 DIA. (IN.)	CRATER NO. 1 DEPTH (IN.)	CRATER NO. 2 DIA. (IN.)	CRATER NO. 2 DEPTH (IN.)	CRATER NO. 3 DIA. (IN.)	CRATER NO. 3 DEPTH (IN.)
26.63	0.113			0.123	0.136	0.143	0.117	0.100	0.107
24.81	0.090								
33.49	0.287			0.131	0.104	0.127	0.101	0.181	0.099
13.22									
13.69				0.069	0.042				
5.48				0.060	0.036	0.049	0.002		
15.26				0.074	0.003	0.049	0.001	0.062	0.006
20.54				0.258	0.136	0.118	0.072	0.096	0.041
22.12				0.100	0.079	0.096	0.034	0.063	0.027

BACKWALL PENETRATED?	BACKWALL EQ. HOLE DIAMETER (IN.)	BACKWALL DAMAGE AREA (SQ. IN.)	BACKWALL SPALLED?	BACKWALL SPALL AREA (SQ.IN.)	DEBRIS CLOUD TRAJECTORY (DEG)	DEBRIS CLOUD SPREAD (DEG)	HOLE NO. 1 DIA 1 (IN.)	DIA 2 (IN.)
NO		0.20	NO		40.70	3.29		
NO		0.99	NO		38.66	0.18		
YES	0.168	2.76	NO		37.60	13.03	0.110	0.127
NO								
NO		2.07	NO		33.82	12.79		
NO		0.44	NO		38.66	5.25		
NO		0.60	NO		35.90	6.70		
NO		0.20	NO		49.82	2.44		
YES	0.735	1.23	NO		39.69	22.12	0.322	0.322
NO		2.25	NO		41.99	10.73		
YES	0.605	3.98	NO		21.80	22.79	0.331	0.160

HOLE NO. 2 DIA 1 (IN.)	HOLE NO. 2 DIA 2 (IN.)	HOLE NO. 3 DIA 1 (IN.)	HOLE NO. 3 DIA 2 (IN.)	CRATER NO. 1 DIA 1 (IN.)	CRATER NO. 1 DIA 2 (IN.)	CRATER NO. 1 DEPTH (IN.)	CRATER NO. 2 DIA 1 (IN.)	CRATER NO. 2 DIA 2 (IN.)	CRATER NO. 2 DEPTH (IN.)	CRATER NO. 3 DIA 1 (IN.)	CRATER NO. 3 DIA 2 (IN.)	DEPTH (IN.)	NO. WITNESS PLATES PENETRATED
				0.197	0.189	0.092	0.109	0.064	0.006				
				0.102	0.115	0.085	0.101	0.111	0.076	0.176	0.126	0.061	
				0.149	0.169	0.059	0.090	0.084	0.068	0.144	0.152	0.046	
				0.195	0.113	0.081	0.191	0.137	0.044	0.257	0.170	0.050	
				0.100	0.070	0.074	0.105	0.022	0.007	0.080	0.070	0.002	
0.661	0.662			0.098	0.098	0.098	0.048	0.048	0.029	0.023	0.023	0.032	
0.593	0.461	0.141	0.159	0.156	0.101	0.046							

★U.S. GOVERNMENT PRINTING OFFICE:1991 .527-064/26008

NASA
National Aeronautics and Space Administration

Report Documentation Page

1. Report No. NASA CR-4343	2. Government Accession No.	3. Recipient's Catalog No.
4. Title and Subtitle Hypervelocity Impact Physics		5. Report Date January 1991
		6. Performing Organization Code
7. Author(s) William P. Schonberg, Alan J. Bean, and Kent Darzi		8. Performing Organization Report No.
		10. Work Unit No. M-655
9. Performing Organization Name and Address University of Alabama-Huntsville Department of Mechanical Engineering Huntsville, Alabama		11. Contract or Grant No. NAS8-36955/D.O. 16
12. Sponsoring Agency Name and Address National Aeronautics and Space Administration Washington, D.C. 20546-0001		13. Type of Report and Period Covered Final Contractor Report
		14. Sponsoring Agency Code

15. Supplementary Notes

Contract Monitor: Dr. Ann F. Whitaker, Materials and Processes Laboratory, Marshall Space Flight Center, AL 35812

16. Abstract

All large spacecraft are susceptible to impacts by meteoroids and orbiting space debris. These impacts occur at extremely high speeds and can damage flight-critical systems, which can in turn lead to catastrophic failure of the spacecraft. Therefore, the design of a spacecraft for a long-duration mission must take into account the possibility of such impacts and their effects on the spacecraft structure and on all of its exposed subsystem components.

The work performed under the contract consisted of applied research on the effects of meteoroid/space debris impacts on candidate materials, design configurations, and support mechanisms of long term space vehicles. Hypervelocity impact mechanics was used to analyze the damage that occurs when a space vehicle is impacted by a micrometeoroid or a space debris particle. An impact analysis of over 500 test specimens was performed to generate a hypervelocity impact damage database.

17. Key Words (Suggested by Author(s)) Hypervelocity, Space Debris, Meteoroid, Impact Testing, Light Gas Gun, Oblique Impact, Impact Damage, Space Structures	18. Distribution Statement Unclassified-Unlimited Subject Category: 18

19. Security Classif. (of this report)	20. Security Classif. (of this page)	21. No. of pages	22. Price
Unclassified	Unclassified	336	A15

NASA FORM 1626 OCT 86

For sale by the National Technical Information Service, Springfield, VA 22161-2171